1995

Development of sparsely reinforced elastomer sheets.

Rong. Pan
University of Windsor

DEVELOPMENT OF SPARSELY REINFORCED ELASTOMER SHEETS

By

Rong Pan

A Dissertation
Submitted to the Faculty of Graduate Studies and Research
Through the Engineering Materials Program of the
Department of Mechanical and Materials Engineering
In Partial Fulfilment of the Requirements for
the Degree of Doctor of Philosophy at the
University of Windsor

Windsor, Ontario, Canada
December, 1995

ISBN 0-612-11020-6

Name Rony Paz

Dissertation Abstracts International is arranged by broad, general subject categories. Please select the one subject which most nearly describes the content of your dissertation. Enter the corresponding four-digit code in the spaces provided.

Materials Science + Engineering

SUBJECT TERM

C 0 7 9 4

SUBJECT CODE

U·M·I

Subject Categories

THE HUMANITIES AND SOCIAL SCIENCES

COMMUNICATIONS AND THE ARTS

Architecture 0729
Art History 0377
Cinema 0900
Dance 0378
Fine Arts 0357
Information Science 0723
Journalism 0391
Library Science 0399
Mass Communications 0708
Music 0413
Speech Communication 0459
Theater 0465

EDUCATION

General 0515
Administration 0514
Adult and Continuing 0516
Agricultural 0517
Art 0273
Bilingual and Multicultural 0282
Business 0688
Community College 0275
Curriculum and Instruction 0727
Early Childhood 0518
Elementary 0524
Finance 0277
Guidance and Counseling 0519
Health 0680
Higher 0745
History of 0520
Home Economics 0278
Industrial 0521
Language and Literature 0279
Mathematics 0280
Music 0522
Philosophy of 0998
Physical 0523
Psychology 0525
Reading 0535
Religious 0527
Sciences 0714
Secondary 0533
Social Sciences 0534
Sociology of 0340
Special 0529
Teacher Training 0530
Technology 0710
Tests and Measurements 0288
Vocational 0747

LANGUAGE, LITERATURE AND LINGUISTICS

Language
- General 0679
- Ancient 0289
- Linguistics 0290
- Modern 0291

Literature
- General 0401
- Classical 0294
- Comparative 0295
- Medieval 0297
- Modern 0298
- African 0316
- American 0591
- Asian 0305
- Canadian (English) 0352
- Canadian (French) 0355
- English 0593
- Germanic 0311
- Latin American 0312
- Middle Eastern 0315
- Romance 0313
- Slavic and East European 0314

PHILOSOPHY, RELIGION AND THEOLOGY

Philosophy 0422
Religion
- General 0318
- Biblical Studies 0321
- Clergy 0319
- History of 0320
- Philosophy of 0322

Theology 0469

SOCIAL SCIENCES

American Studies 0323
Anthropology
- Archaeology 0324
- Cultural 0326
- Physical 0327

Business Administration
- General 0310
- Accounting 0272
- Banking 0770
- Management 0454
- Marketing 0338

Canadian Studies 0385
Economics
- General 0501
- Agricultural 0503
- Commerce-Business 0505
- Finance 0508
- History 0509
- Labor 0510
- Theory 0511

Folklore 0358
Geography 0366
Gerontology 0351
History
- General 0578
- Ancient 0579
- Medieval 0581
- Modern 0582
- Black 0328
- African 0331
- Asia, Australia and Oceania 0332
- Canadian 0334
- European 0335
- Latin American 0336
- Middle Eastern 0333
- United States 0337

History of Science 0585
Law 0398
Political Science
- General 0615
- International Law and Relations 0616
- Public Administration 0617

Recreation 0814
Social Work 0452
Sociology
- General 0626
- Criminology and Penology 0627
- Demography 0938
- Ethnic and Racial Studies 0631
- Individual and Family Studies 0628
- Industrial and Labor Relations 0629
- Public and Social Welfare 0630
- Social Structure and Development 0700
- Theory and Methods 0344

Transportation 0709
Urban and Regional Planning 0999
Women's Studies 0453

THE SCIENCES AND ENGINEERING

BIOLOGICAL SCIENCES

Agriculture
- General 0473
- Agronomy 0285
- Animal Culture and Nutrition 0475
- Animal Pathology 0476
- Food Science and Technology 0359
- Forestry and Wildlife 0478
- Plant Culture 0479
- Plant Pathology 0480
- Plant Physiology 0817
- Range Management 0777
- Wood Technology 0746

Biology
- General 0306
- Anatomy 0287
- Biostatistics 0308
- Botany 0309
- Cell 0379
- Ecology 0329
- Entomology 0353
- Genetics 0369
- Limnology 0793
- Microbiology 0410
- Molecular 0307
- Neuroscience 0317
- Oceanography 0416
- Physiology 0433
- Radiation 0821
- Veterinary Science 0778
- Zoology 0472

Biophysics
- General 0786
- Medical 0760

EARTH SCIENCES

Biogeochemistry 0425
Geochemistry 0996
Geodesy 0370
Geology 0372
Geophysics 0373
Hydrology 0388
Mineralogy 0411
Paleobotany 0345
Paleoecology 0426
Paleontology 0418
Paleozoology 0985
Palynology 0427
Physical Geography 0368
Physical Oceanography 0415

HEALTH AND ENVIRONMENTAL SCIENCES

Environmental Sciences 0768
Health Sciences
- General 0566
- Audiology 0300
- Chemotherapy 0992
- Dentistry 0567
- Education 0350
- Hospital Management 0769
- Human Development 0758
- Immunology 0982
- Medicine and Surgery 0564
- Mental Health 0347
- Nursing 0569
- Nutrition 0570
- Obstetrics and Gynecology 0380
- Occupational Health and Therapy 0354
- Ophthalmology 0381
- Pathology 0571
- Pharmacology 0419
- Pharmacy 0572
- Physical Therapy 0382
- Public Health 0573
- Radiology 0574
- Recreation 0575
- Speech Pathology 0460
- Toxicology 0383

Home Economics 0386

PHYSICAL SCIENCES

Pure Sciences

Chemistry
- General 0485
- Agricultural 0749
- Analytical 0486
- Biochemistry 0487
- Inorganic 0488
- Nuclear 0738
- Organic 0490
- Pharmaceutical 0491
- Physical 0494
- Polymer 0495
- Radiation 0754

Mathematics 0405
Physics
- General 0605
- Acoustics 0986
- Astronomy and Astrophysics 0606
- Atmospheric Science 0608
- Atomic 0748
- Electronics and Electricity 0607
- Elementary Particles and High Energy 0798
- Fluid and Plasma 0759
- Molecular 0609
- Nuclear 0610
- Optics 0752
- Radiation 0756
- Solid State 0611

Statistics 0463

Applied Sciences

Applied Mechanics 0346
Computer Science 0984
Engineering
- General 0537
- Aerospace 0538
- Agricultural 0539
- Automotive 0540
- Biomedical 0541
- Chemical 0542
- Civil 0543
- Electronics and Electrical 0544
- Heat and Thermodynamics 0348
- Hydraulic 0545
- Industrial 0546
- Marine 0547
- Materials Science 0794
- Mechanical 0548
- Metallurgy 0743
- Mining 0551
- Nuclear 0552
- Packaging 0549
- Petroleum 0765
- Sanitary and Municipal 0554
- System Science 0790

Geotechnology 0428
Operations Research 0796
Plastics Technology 0795
Textile Technology 0994

PSYCHOLOGY

General 0621
Behavioral 0384
Clinical 0622
Developmental 0620
Experimental 0623
Industrial 0624
Personality 0625
Physiological 0989
Psychobiology 0349
Psychometrics 0632
Social 0451

To My Parents:

Pingzhang Pan, Yongjing Zhang

ABSTRACT

Presently most road and railway vehicles designed to haul toxic or flammable liquids are built with a single shell tank construction. The transportation of hazardous liquids poses a problem if the vehicle hauling the liquid is involved in an accident. Loss of liquid can happen if the tank integrity is compromised. The current work is an attempt to develop a lightweight, relatively inexpensive, sparsely reinforced elastomer liner material to incorporate inside the containers, to contain leakage should the outer shell fail. The general design methodology is thus Fail-Safe Design. If this were designed properly to be an inexpensive easily replaceable disposable item, it could prevent significant liquid loss, and reduce subsequent clean-up costs.

Thermoplastic polyurethane (TPU) elastomer is chosen as an ideal candidate for at least one side of the sheet matrix material because of its high strength, tear resistance, puncture and cut resistance, abrasion resistance, chemical resistance, and generally good impermeability to fluids being transported. In this project, sparsely reinforced TPU elastomer composites have been developed. The TPU matrix was reinforced with webs of continuous fibers of various types and patterns, wherein the reinforcement serves as a load carrying structural element designed to resist both crack initiation and propagation. A unique thermoforming process technique has been designed specifically to produce the sparsely reinforced sheet material. Representative sheets of these materials have been studied for strength, toughness and different deformation behaviours by the means of tensile tests, tear tests, snag tests, slow puncture tests, and hydraulic bulge tests. A series of test apparatus have been designed and built for examining these mechanical properties.

Also, the effect of different reinforcements, web patterns and strand diameters on the mechanical properties has been investigated. The sparsely reinforced TPU composites produce outstanding tear strength, snagging resistance, and an increase in the elongation to failure in an ASTM Die-C type of tear test. The best material of those tested to date is TPU sheet reinforced sparsely with a web of extruded polyurethane fiber. The intersections of the polyurethane rod reinforcements are very effective crack arrestors.

ACKNOWLEDGEMENTS

The author wishes to express her sincere gratitude to Dr. D. F. Watt for his invaluable academic guidance, supervision and suggestions, financial support as well as his encouragement and confidence throughout all parts of this study.

She would like to express her thanks to the academic committee members: Dr. D. Northwood, Dr. C. C. St. Pierre, Dr. C. Zhang, University of Windsor, for their time, help, and guidance.

She also would like to express her thanks to the all the members of the Central Research Shop for the effort they made to build and set up all the experimental apparatus; to the faculty technicians Mr. John Robinson, Mr. Werner Beck, and Mr. Robert Tattersall for their technical advice and help, to Mr. Stephen Petrovcik for his photography assistance, to Mrs. Barbara L. Denomey and Mrs Barbara C. Carr for their secretarial assistance.

The author wishes to acknowledge Armando Sardanopoli, Mark Evans, and Paul Bury of the BASF Polyurethane Division in Wyandotte, Michigan for supplying materials, data and advice. She would also like to thank Cooley Inc. in Pawtucket, RI for supplying the polyester scrim material.

Finally the author wishes to acknowledge the financial support to this study from the Natural Science and Engineering Research Council of Canada (NSERC) through a NSERC Postgraduate Scholarship - PGS 4 (1992-1994), the Ministry of Universities and Colleges of Ontario through an Ontario Graduate Scholarship (1994 - 1995), and the Faculty of Graduate Studies and Research of University of Windsor through a Postgraduate Tuition Scholarship (1994 - 1995).

TABLE OF CONTENTS

LIST OF TABLES

LIST OF FIGURES

CHAPTER 1

INTRODUCTION

1.1. Scope of the Problems

The transportation of hazardous liquids poses a problem if the vehicle hauling the liquids is involved an accident.[1] Most these products are transported by one of three different modes: road, rail, or marine and inland waters. The general trend observed in transportation modes is that trucks tend to take the largest share, followed by rail, which is increasing in popularity only recently in the 1990's, and the remainder are taken by marine and inland water transport. The Canada-United States trade modal splits are outlined in Table 1-1. A preliminary collection of some statistical data of transportation splits has been made.[2] The data gathered were for marine, road and rail transport, but only the latter two will be discussed in this chapter.

The Canadian Government categorizes hazardous goods into the 9 classes listed in Table 1-2.[3] The most common of these in terms of tonnage shipped by road or rail is Class 3; flammable liquids. As an example of the scale of the problem, in Canada in 1986, 51.3 million tonnes of dangerous goods were transported, of which 63% were Class 3. A comparable figure for the transport of hazardous goods by road in the U.S. was 1.5 billion tonnes in 1982.[4,5] This does not include automotive gas tanks, and we do not see the adoption of elastomer liners as probable in automobile or small truck gas tanks.

In 1979, Transport Canada, an agency of the Canadian Government, established

"CANUTEC", the Canadian Transport Emergency Centre to provide advice to shippers 24 hours a day. They also compiled accident statistics. The sub-division of these by transportation mode and Class of Hazard are given in Table 1-3[6] for a typical fiscal year. While the total fraction of vehicles and rail cars releasing hazardous chemicals remains a very small percentage, the effects of a single release can be very serious, and expensive in terms of damage at the time of the accident, and in terms of later insurance coverage.

Accidents in the transportation of hazardous goods take their toll on people as well as the environment. It is desirable to find ways to lessen their effect. A lightweight, relatively inexpensive, sparsely reinforced elastomer sheet used as a type of liner material is a possible way to reduce the spills in a transportation accident. It would be incorporated inside the containers to contain leakage should the outer shell fail. If this were designed to be an easily replaceable disposable item, it could prevent significant liquid loss, and reduce subsequent clean-up costs.

1.2. Sparsely Reinforced Elastomer Sheets

1.2.1. General Fiber-Reinforced Polymer Composites[7, 8]

Fiber-reinforced polymer composite materials consist of fibers of high strength and modulus, embedded in or bonded to a matrix with distinct interfaces (boundary) between them. In this form, both fibers and matrix retain their physical and chemical identities, yet, they produce a combination of properties that cannot be achieved with either of the constituents acting alone. There are three basic elements in a fiber-reinforced composite: fiber, matrix, and the fiber matrix interface.

In general, fibers are the principal load-carrying members. They are the elements that provide resistance to breaking and bending under the applied load. The surrounding matrix keeps fibers in the desired location and orientation. The role of the matrix in a fiber-reinforced composite is (1) to transfer stresses between the fibers, (2) to provide a barrier against an adverse environment, and (3) to protect the surface of the fibers from mechanical abrasion. The matrix plays a minor role in the tensile load-carrying capacity of a composite structure. However, selection of a matrix has major influence on the interlaminar shear as well as the in-plane shear properties of the composite material. Thus, even though the fibers provide reinforcement for the matrix, the latter also serves a number of useful functions in fiber-reinforced composite materials.

The fiber-matrix interface is the critical factor that determines to what extent the potential properties of the composite will be achieved and maintained during use. Localized stresses are usually highest at or near the interface, which may be the point of premature failure of the composite. The interface must have appropriate chemical and physical features to provide the necessary load transfer from the matrix to the reinforcement. The interface also assists the matrix in protecting the fibers.

Favourable high stiffness to weight ratio, high strength, low density, excellent durability, and design flexibility are primary reasons that advanced fiber-reinforced polymer composites are used in many structural components in the aircraft, automotive, marine, and other industries. In many applications, these elements consist of thin laminae reinforced either unidirectionally or bidirectionally and assembled together to form a laminate. These components are generally subjected to bending and in-plane loadings.[9]

1.2.2. Sparsely Reinforced Elastomer Sheets

1.2.2.1. Sparse Reinforcement Elastomer Sheets

The idea of sparsely reinforced elastomer sheets is similar to the presence in nature of structures such as a spider's web, and the tensile action of animal skin which must have spurred man to develop tension systems for his use. A perfect example is the air supported roof in the Silver Dome in Pontiac, Michigan which is a membrane roof with predominantly tensile forces. The main load bearing element in the roof is steel cable.

It is common for a polymer composite that the role of the reinforcement is to increase the strength, and that this ordinarily causes a reduction in the ability of the composite to deform significantly before failure. The standard theory of fibre reinforcement also states that in order to achieve a real fiber reinforcement, a composite must have a certain minimum level of fiber (continuous) volume fraction given by:[10]

$$V_{min} = (\sigma_{mu} - \sigma_{m\varepsilon}) / (\sigma_{fu} + \sigma_{mu} - \sigma_{m\varepsilon}) \qquad (1\text{-}1)$$

or the ultimate strength of the material will be worse than that of the unreinforced matrix material. In equation (1-1) above, V_{min} is the critical minimum volume fraction of fibre reinforcement required to achieve strengthening, σ_{mu} is the ultimate strength of the unreinforced matrix, $\sigma_{m\varepsilon}$ is the stress that would be carried in the unreinforced matrix at a strain equal to the failure strain of the fibre, and σ_{fu} is the ultimate strength of the fibre in isolation from the matrix. The argument is that below this minimum volume fraction of reinforcement, the fibres are unable to contribute much to the strengthening before failure of the fibres will lead to premature failure of the composite as a whole.

The new work presented below challenges part of this conventional knowledge; sparsely reinforcing the elastomers leads to an improvement in the amount they will elongate before failure in a tear test. It is desirable that the materials should not only have a high strength and tear resistance, but also be able to withstand large deformations.

1.2.2.2. Design of Sparsely Reinforced Flexible Composites

(a) **Matrix material**. The objective is to develop a material which has good elongation and outstanding tear resistance. The matrix material must have good tear initiation resistance; the reinforcements are to act as a tear propagation arrester. If loaded locally, the matrix must be able to move so as to transfer the load to surrounding fillers before tearing. Thus, in order to obtain the maximum reinforcement benefit it is necessary to use matrices with a high ductility.[11] The main intrinsic property of elastomers is their ability to undergo large elastic deformation. Therefore, soft thermoplastic polyurethanes (TPU) were chosen as candidates for developing materials because they are inherently tough elastomers. TPU elastomers show high extension and tear resistance under tensile loads and have a good load-bearing capability. They are processable like thermoplastics which gives them design flexibility.

(b) **Reinforcements**. Two types of fibers are chosen as reinforcement materials. One is TPU-rod, which is extruded in 1 mm diameter fiber, using higher hardness TPU raw material. Another is carbon fibers with 1000 filaments (1K) or 3000 filaments (3K) per strand. The present report shows that favourable reinforcement effects occur whether or not the reinforcement is itself an elastomer, or if it is a stiff reinforcement like carbon

fiber. It is of interest to note that carbon fibers themselves are not stronger than glass fiber, but their modulus of elasticity is 3-5 times higher. The higher Young's modulus of composite filled with carbon fibers, compared with those filled with glass fibers (at same concentration), leads to situation where the fraction of load transmitted to the carbon fiber is higher, and this deceases the stresses borne by the matrix.[12]

1.3. Research Objectives

The objective of the present research is to envisage and develop a tough, strong, lightweight, inexpensive elastomer liner material with outstanding tear resistance which could be incorporated inside the containers, and possibly to ameliorate the effect of these accidents for all but Class 1, Class 7 and some parts of Class 9 types of materials.

To do this, sparsely reinforced urethane-based elastomer sheets are to be developed in which this flexible tough material is reinforced with webs of continuous fibers of various types and patterns. Generally, sheet polymers have good tear initiation resistance but relatively poor tear propagation resistance. So, the fibers incorporated act both as load bearing members and as crack arrestors. They also prevent local collapse or bulges, and they increase the kink resistance of the composites.

If a local penetration failure did occur, say by a needle or knife edge, then the webbing should act as a crack arrester to limit the propagation of the tear into the rest of the material. This was the original logic that led to the recognition of the need for this class of materials.

In order to create the sparsely reinforced sheet material, a thermoforming process

technique must be specially designed and developed. Then the sparsely reinforced TPU elastomer sheets have to be produced by this unique thermoforming method. Meanwhile, representative sheets of these materials should be studied for strength, toughness, and different deformation behaviour by the means of various tests such as tensile tests, tear tests, snag tests, slow puncture tests, hydraulic bulge tests, and large missile impact tests. A series of test apparatus have been designed and built for investigating these mechanical properties. Also, the effect of different reinforcements, web patterns and strand diameters on the mechanical properties should be considered.

A different aspect of the scope of the problem is the actual design and fabrication of a liner for a tanker-trailer or a railcar. It must be inexpensive and easy to install, and cause no interference with filling or draining the tank. The mating of the liner to these connector fittings will be a challenging problem for someone else. But it seems that someone should start somewhere, and so we have chosen to develop a material that would be suitable for such a liner. This work makes a modest start toward the development of such liners by testing models of candidate materials.

In this dissertation, the details of development of sparsely reinforced elastomer sheets are given in Chapter 3. In Chapter 4 to Chapter 8, the deformation behaviour of the sparsely reinforced elastomer sheets are discussed, and the conlusions related to this study are given in Chapter 9.

1.4. Anticipated Relevance of These Tests to Real Accidents

At this time we do not have detailed information on the modes in which the leaks

have occurred from tanks involved in accidents. We envisage the following possibilities:

(a) The Tank Splits Open Cleanly. The dynamic forces developed in the tank and the fluids during the accident cause the tank to tear relatively cleanly. This means that tensile stresses or bending moments, perhaps acting at welds, cause something close to a simple tensile failure such that an opened crack would allow the tank to leak fluid.

The tests most relevant here would be the bulge test for a large gap in the crack faces, and the tensile ductility for the case where the internal membrane sticks to the inner tank wall, perhaps for inertial reasons. Penetration resistance, tear initiation and propagation resistance would only be an issue if the crack opened out onto a sharp object.

(b) The Tank is Penetrated by a Sharp-edged Object. In the crash, the tank is raked along its side by some strong objects which fold the sharp broken edges of the torn tank inward onto the membrane. Alternatively the corner of something like an I-beam is driven into the tank wall. The coupler from one rail car penetrates the wall of the preceding tank car.

The slow penetration test results are a guide to resistance here, as is the snag test. The former, with the screwdriver indentor, allows the reinforcements (TPU rod or C fiber) to help support the load, as they would if the edge were not more ragged than a carpenter saw blade. The snag test is a dynamic test against the penetration by a sharp snagging point on a rough edge. It becomes relevant when the tank continues to move past a sharp edged intruding object. The tear resistance test is also relevant if the membrane is torn locally by the sharp edge, as this could determine the rate of fluid loss.

(c) The Tank is Penetrated by A Sharp-pointed Object. In the accident, the

tank falls onto an exposed rod or spike which pierces the tank wall.

Again the snag test and the slow penetration tests are the most relevant of the current tests. Another new test comprised of a sharp pick falling into sheet metal backed by the membrane full of fluid would be more representative for this type of failure mode.

(d) The Tank Filling or Drain Connections are Torn Off. There is no doubt that making suitable connections to the tank filling and drain connection points will be a big challenge in the detailed design of bladder inserts for liquid hauling vehicles. However, present rail-car standards have already required that these areas are armoured against being knocked loose during accidents. With trucks, the fill and drain points usually extend outside the general tank body, they appear to be vulnerable to being sheared off in an accident. If these connections are directly connected to an elastomer fitting, it is conceivable that they may be able to withstand larger displacements without loss of liquid than the welded connections now found on tanks. The details of such fill point to membrane connections remain to be worked out, but crash worthiness will have to be taken into account.

CHAPTER 2

LITERATURE REVIEW

As stated in Chapter 1, fibre-reinforced polymer composites are used primarily as structural components in various applications due to their high strength and high stiffness to weight ratio. According to conventional wisdom, the fibre volume percentage incorporated should be over a minimum (generally > 15%) to achieve the reinforcement effect. The sparsely reinforced elastomer composite challenges these conventional concepts. These elastomeric materials have better tensile strength and tear resistance at volume fractions much lower than 15%. It is desirable that the materials should not only have a high strength and tear resistance, but are also able to withstand large deformation. There is no literature directly related to sparsely reinforced materials. Therefore, it is necessary to give a general review on what is known about the components used in sparsely reinforced TPU elastomers, and an overview of conventional thermoplastic composites to help the reader to better understand in later chapters about the sparsely reinforced flexible materials and their functions.

2.1. Thermoplastic Polyurethane Elastomers

2.1.1. History Review

Thermoplastic polyurethane (TPU) elastomers are a member of the polyurethanes family of polymer. Pioneering polyurethane work was discovered by Otto Bayer and his coworkers of I. G. Farben industrie at Leverkusen, Germany (now Bayer AG) in 1937.[13]

Subsequently, the elastomer properties of polyurethane were recognized by DuPont and by ICI.[14, 15] By the 1940's polyurethane produced on an industrial scale.[16] Only in the late fifties was it found that essentially linear polyurethane elastomers based on 4,4'-diphenylmethane diisocynate could be processed like thermoplastics.[17, 18] This class of materials has become very important among the polymers because of their unique property of combining superior tear strength, high strength with high hardness and high modulus plus high elongation at break, and overall resistance to most types of aliphatic and aromatic fluids.

2.1.2. Morphology

2.1.2.1. Basic Components[19]

There are three fundamental ingredients in TPU: short-chain diols, long-chain diols, and diisocyanates. Generally, short-chain diols act as chain extender, which include ethylene glycol, 1,4-butanediol, 1,6-hexanediol, and so on. Long-chain diols can be categorized into polyester or polyether diols, which have a molecular weight 600-6000. Diisocyanates usually are 4,4'-diphenylmethane diisocyanate (MDI) produced by phosgenation of 4,4'-diphenylmethane diamine (MDA), 2,4- and 2,6-toluene diisocyanates (TDI) [isocynates with two or more NCO groups in the molecule are needed for the formation of polyurethanes]. Preferred diisocyanates are those having large molecular structural bulk resulting in interchain steric hindrance, and these have the highest levels of modulus, tear and tensile strengths.[20-22]

2.1.2.2. Structure of TPU[23-28]

Almost all TPUs are block copolymers of $(—AB—)_n$ type, where A and B are the hard and soft segments. The structure of TPU can be described as follows:

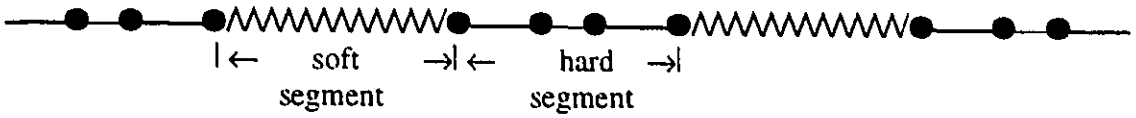

ΛΛΛΛ long chain diol, —— diisocyanate, — chain extender, ● urethane group

Urethane group: —NH—C—O—
‖
O

The soft-segments (1000-2000nm) usually are an amorphous phase, which consists of saturated aliphatic polyether or polyester long-chain diols. The long-chain diols interconnect two hard segments. The soft segments are quite mobile and are normally present in coiled formation, alternate with stiff oligourethane.

The hard segments (150nm) are formed by addition of the chain extender to the diisocyanate MDI, which is dispersed in the amorphous phase. Because the hard and soft segment are incompatible, the TPU exhibits a two-phase structure.[29] The hard segments have a tendency to aggregate and form crystalline domains. The crystallites provide reinforcement by acting as physical crosslink sites and as multifunction tie-down points for the soft segment blocks.

Crosslinks may be in the form of either covalent chemical bonds, or physical-chemical bonds plus some mechanical entanglement of the chains.[30] Hydrogen bonding of almost all NH groups occur in segmented polyurethanes between both urethane and urea groups and thus give the rigid domains.[31] Also, hydrogen bonding is considered to occur between these NH groups and the soft-segment oxygen atoms, C=O in polyester

and -COC-groups in polyether.

2.1.2.3. The Roles of Segments

In a typical TPU, the hard segments determine the hardness, modulus, tear strength, and upper use temperature. Being covalently coupled to the soft segments, hard segments inhibit plastic flow of the chains, thus creating elastomeric resiliency. The high modulus of TPUs is attributed to a two-phase microstructure.[22-37]

The soft segments form an elastomer matrix which accounts for the reversibly elastic, and high deformability properties of TPU. The long flexible soft segment largely controls the low temperature properties, the solvent resistance and the weather properties of TPU. The mobility of the molecular chains depends to a large extent on the chemical nature and chain length of the soft segment. In order to obtain good elastomeric properties, especially high impact resistance, the soft segment should be amorphous and possess a low glass transition temperature. The chemical composition and the molecular weight of long-chain diols greatly affect the extent of phase separation of the TPU. The higher the molecular weight and the longer the hydrocarbon chain length of the long-chain diols, the better the phase separation will be. Because of stronger hydrogen bonding, the phase mixing of a polyester-based TPU, is generally greater than that of a polyether-based TPU. The hard segment domains of polyether based tend to be larger and more complex than those found in polymers based on adipic acid polyesters. Polyester-based TPU has better physical properties, thermooxidative stability, and oil resistance. Polyether-based TPU exhibits better low temperature properties, hydrolytic

stability, and resistance to microbial attack at a similar hardness.[19, 23]

2.1.2.4. Morphology of Hard Segment Domains and Spherulite

Considerable efforts have been made to elucidate the nature of TPU hard segment domains. The hard segment domains were first observed as equiaxed grains of 3-50 nm diameter in solvent etched and iodine stained polyether or polyester/MDI/Butanediol-based urethane.[38] The ordered hard segment phase is thought to be composed of domains of thickness (dimension parallel to chain axis) equal to the hard segment length.[39] Harrell[40] showed that hard segment crystallization could occur for blocks as short as one unit for a piperazine-based urethane. Blackwell et al.[41–44] extensively studied the structure of hard segments in MDI/diol/polytetramethylene adipate polyurethane by X-ray diffraction, and was able to index the 11 observed reflections with a triclinic unit cell.

Hard segment domains can arrange into spherulite structures.[45, 46] Models for hard rich spherulite structure include both the possibility of radial as well as tangential oriented hard segment domain. Domain size apparently increased with increase in hard segment content as evidenced by sharpening of the WAXS reflections.[45, 46] The hard segment phase forms (para)-crystalline domains which are fibrillar in nature. The concentration of the hard segment is greatest at the centre of the largest spherulite suggesting the preferential agglomeration of molecules with the longest hard segment sequenced at the beginning of the phase separation process from solution.[47, 48] Spherulite have diameters from several thousands of nm up to about 20 μm.[46–49]

According to Chang, Wilkes, Minoura et al.[50, 51] in WAX diffraction of diamine-

extended polyurethanes, the peaks appearing at 9° - 28° of 2θ correspond to either supramolecular structure of bulk and or stress crystallized and paracrystalline soft segments, and vary with the nature of the chain extender. Thus it can be said that the peaks around 9° and 28° represent the formation of an overall ordered structure or at least stress-induced ordering of soft segments. The other important characteristic of WAX diffraction pattern of polyurethane also appears over a range of 2θ. This is attributed to the amorphous solution of the hard and soft segments to give an evenly distributed bulk.[52, 53] It was observed that with the increase in crystallinity, the intensity of the peaks increased along with the reduction in the span of halo.[54]

It is suggested that spherulite in TPU are formed from two separate sources: strain-induced crystallization and aggregation of rigid-segment domains.

2.1.2.5. Segmental Orientation Under Deformation

Infrared dichroism experiments [55-59] have shown that segmented polyurethanes undergo some degree of irreversible orientation, especially of the hard segments, at large strains. The soft segments may be readily oriented by an applied stress but return to the unoriented state when the stress is removed. The hard segments, however, show a more complex behaviour of orientation and relaxation. This behaviour is dependent on the magnitude of the applied stress, the molecular weight of the soft segments and the crystallinity of the hard segments.[60, 61]

X-ray studies[52, 62] have confirmed the process of strain-induced orientation and crystallization in polyurethane. Bonard et al[52, 63, 64] found that the soft segments oriented

into the direction of stretch, with strain-induced crystallization occurring at about 150% strain. Hard segment orientation was found to depend on whether the hard segment domain was partly crystalline or ordered in a paracrystalline state. The paracrystalline segments were found to orient transverse to the stretch direction at strain below 200%. At higher strains the hard segments became oriented into the stretch direction with increasing strain. This behaviour was explained by a model where the hard segment lamellae orient as a whole into the stretch direction at low strains. At higher strains, they break up and the hard segment themselves orient into the stretch direction. Soft segment force strands cause the hard segment lamellae to be rotated and oriented into the stretch direction. Estes[61] pointed out that upon stretching, the soft segments relaxed almost completely when the load was removed, while the hard segment orientation recovered only slightly. It was found that the hard segment orientation remained transverse in crystalline copolymer even at high elongation.

Polyurethane with partly crystalline hard segment domains had a much lower average orientation than those with non-crystalline domains. This effect was ascribed to the transverse (negative) orientation of the hard segments in partly crystalline domains. It was found that after a step increase in strain the orientation of the hard segments increase with time, while the soft segment orientation decreased. It was concluded that the decrease in the soft segment orientation was a result of the randomization of those segments due to an entropy driven stress relaxation. As soft segments relax, they exert a tension on the hard segments causing them to increase their orientation. The non-hydrogen bonded hard segment domains are more easily disrupted than the hydrogen

bonded polyurethanes, yet the system may be reinforced by a greater tendency to crystallize at high strains.[65]

Strain-induced crystallization of the soft segment matrix is largely irreversible[66] and leads to permanent deformation and a noticeable hysteresis effect. Once crystallization has occurred, the polymer becomes brittle. Subsequent energy placed into the system leads to the disruption of the soft segment crystallinity, crazing, bond breaking, crack initiation and propagation, and eventually the failure of the polymer as a tensile break.

2.1.2.6. Effects of Hard Segments on Mechanical and Thermal Properties

The thermo-mechanical properties of linear segmented polyurethane are substantially different from those of chemically crosslinked products. The polyurethane chains contain a large number of polar groups and, since the chains are not bound closely together by short covalent chemical bonds, these polar groups are free to align themselves and form very strong physical-chemical bonds. When mechanical forces are applied, temperature dependent changes in the orientation and mobility of structures within the hard segment domains can occur (plastic deformation, strain-induced softening). In this process, the initial hydrogen bonds are broken, and new, energetically more favourable hydrogen bonding takes place. It is very possible that soft segments will move through the hard segment domains. A change in superstructure occurs, causing an alignment in the direction of the movement (*Fig. 2-1*). The large number of these polar groups prevents the chains sliding over each other under an applied stress. Tension is more

evenly distributed, the individual bonds are less over stressed and, as a result, the resistance of the material to further stress is increased. This effect is utilized in the so-called thermal fixing process of elastomeric fibres. Furthermore, this effect contributes to the high tensile strength, elongation, tear strength and set values.[23]

Miller et al[67] have shown that the hard segment length distribution in TPUs will affect the stress and elongation at break as well as Young's modulus. Smith[68] indicated that the ultimate properties are closely related to the morphology of the TPU. The stress-strain curve of TPUs is generally believed to be affected by the hard segment to soft segment ratio, soft segment length, hard segment crystallinity, and susceptibility of the hard segment to reorientation and alignment. In a given polyurethane system, a good correction exists between the stress-strain properties and the content of the urethane hard segment. As the hard segment content increases, the Young's and secant moduli will also increase, whereas the elongation at break will decrease. Because the reorientation of the hard segment is time-dependent, the stress-strain curve will be affected by the extension rate. Temperature also affect the stress-strain curve of TPUs, as indicated by the work of Smith, in which the moduli of TPUs at a fixed strain decreased with increasing temperature.

The melting range of the hard segment domains determines the dimensional thermal stability of linear segmented polyurethanes. Generally, the melting range of the polymer can be related to the melting range of the hard segment. With increasing length of the hard segment, the melting range also rises.[69] Very irregular hard segment domains depress the melting range and hamper the soft segment chains. This results in glass

transition temperatures smeared towards higher temperature ranges.

Harrell[40] also reported that increasing the hard segment block length did not appreciably affect the degree of order with the hard segment domains though the melting point of the hard segment rich phase was raised. Narrowing of the hard segment size distribution increases modulus, tensile, and extension set drastically. Narrowing of the soft segment distribution causes a slight increase in modulus, a moderate increase in elongation and tensile, and a large increase in extension set.

2.1.3. Structure-Properties Relationship

2.1.3.1. Crosslinking and Deformation Behaviours in TPU Elastomer

The properties of TPU are related to segmented flexibility, chain entanglement, interchain forces and crosslinking. Both covalent and polar crosslinks contribute to the crosslink network and the modulus of polyurethane elastomers. The dependence of this modulus on temperature can be divided into contributions from a covalently linked network conforming to the statistical theory of rubber elasticity and contributions from secondary crosslinks which are assumed to have a temperature dependence governed by the Arrhenius type of temperature dependence.[70]

As the primary crosslinking decreases the contribution of secondary bonds to the modulus increases. For a given strain the stress reduces as the temperature rises due to melting of softening of domain structures which cease to function as physical crosslink sites. Tear strength and tensile strength also decrease as the temperature rises.

During deformation the crosslinking areas of TPUs undergo a certain

rearrangement which causes stress softening and leads to permanent deformation.[71-74] In addition to the effects mentioned above, physical interactions take place in the soft regions of the elastomers. Polydiols can usually be crystallized and are often solids at room temperature. Incorporation the polydiols into elastomers has the effect of slightly depressing the melting point and lowering the crystallization rate, so that in many cases an undeformed elastomer shows little or no crystallization. During extension, however, the molecules become parallel, and the crystallization is accelerated. Crystallization effects can improve tensile strength and tear resistance. The strains which occur during thermoforming can lead to crystallization during stretching of the materials used in the present study.

The tear resistance of TPUs is related to their hard segment content. A TPU with a high hard segment content normally has a high tear strength. The tear strength of ester-based TPUs are usually higher than those of ether-based TPUs of similar hardness.

Tensile strength, 300% modulus, and tear strength are substantially affected by the melting point T_m of the soft segment polyols. Melting points between 20 and 60°C are advantageous for two reasons: the tendency of the polymer to crystallize at room temperature is sufficiently suppressed and a certain stress induced crystallization already takes place, leading to some degree of consolidation. Increasing chain length of the soft segment, decreasing amounts of hard segments, as well as high linearity (low long chain branching) of the polyurethane favour crystallization. Since physical-chemical bonds are relatively easily broken at high temperatures, the properties of polyurethanes tend to decrease as the temperature increases.

2.1.3.2. Oil, Grease, Solvent and Chemical Resistance[19, 70, 75-79]

TPU exhibit excellent resistance to pure mineral oils (diesel oils) and greases. Some technical oils and greases can attack TPU at elevated temperatures due to the additives they may contain. Non-polar solvents such as hexane, heptane and paraffin oil have almost no effect on the polar polyurethanes. Even at high temperatures only a slight swelling may be observed.

Solvents may act differently on the hard and soft segments of the polymer. Solvents encapsulate the polymer molecules and break the intermolecular and intramolecular force, thus increasing the distance between the molecules of the polymer. As a result the polymer goes into the solution phase, where the chains are separated and float free.

TPU is stable in contact with petroleum hydrocarbons if they do not contain alcohol. In certain fluids the polyurethanes, like other rubbers, swell but when removed and allowed to dry out they return to their original dimensions. The effect of organic materials on polyurethanes is dependent upon the chemical groups present in these materials.

- Alcohols, acids, and ketones and esters tend to cause swelling and degradation, particularly at high temperatures.
- Aliphatic hydrocarbons and esters are generally inert, but aromatic hydrocarbon are more active and promote swelling at room temperature and gradual breakdown at higher temperatures. Up to service temperatures of about 50°C, polyurethane elastomers in contact with these organic fluids, or their grease, can be considered

as some of the most resistant materials available when the combined effects of oil or greases and weathering are encountered.

- Chlorinated solvents or aromatic components like toluene cause swelling and sometimes degradation. The tensile and tear strengths are reduced to about 25% of their initial values after 6 months' immersion in chloroform at room temperature. Methylene chloride causes even more rapid breakdown, whilst carbon tetrachloride and trichloroethylene are relatively inert, although swelling does occur. The degree of swelling is dependant on the structure of the polyurethane. Ester-types swell less than ether-types and hard polyurethanes swell less than soft ones.
- The resistance of polyurethane elastomers to immersion in water has been identified as relatively poor and is directly applicable to immersion in dilute solutions of inorganic materials in water. Provided the inorganic substance has no catalytic effect the solution can be expected to behave as pure water.
- Acidic or alkaline media accelerate hydrolytic attack and therefore solutions of salts of weak acids or bases are likely to degrade polyurethanes faster than water.
- As a generalization, it can be stated that, provided the PH of a solution lies between the value of 5.5 and 8, the action of the solution can be considered similar to the action of the water. At higher acidities or higher alkalinities it is advisable to test the effect of the particular solution. As would be expected, strong acids and bases attack polyurethane rapidly.

Good solvents for TPUs are dimethyformamide, tetrahydrofuran, n-methy

pyrrolidone, dimethylacetamide, and dimethylsulfoxide.[80]

If these materials are to be used as liquid containment liners, then the side in direct contact with the liquid should be impermeable to and non-reactive with the liquid to be contained.

2.1.3.3. Hydrolytic Stability[81, 82]

The effect of hydrolysis on the properties of TPUs is due to chain cleavage, with an accompanying reduction in average molecular weight. When the molecular weight of TPU is reduced to a critical value, cracks will develop on the surface of the TPU. These cracks are usually deep random cracks. With TPU elastomers the presence of —COC— and —COOC— groups in the main-chain structure results in these materials inevitably undergoing some degree of hydrolytic attack in the course of time. The relative hydrolytic stability of three principal linear polyol series used in synthesizing urethane elastomers can be ranked in the following order :

polyether > polycaprolactone > polyester
(highest stability → lowest stability)

In general it is true that the longer the hydrocarbon chain of the glycol portion of a polyglycol adipatre the more resistant is the polyester to hydrolysis.

2.2. Carbon Fibres[83-86]

2.2.1. Introduction

The term carbon fibre is a generic one representing a family of fibres.[87] The

element carbon has two low-density allotropes, namely graphite and diamond. Ideal monocrystalline graphite is composed of planar layers of hexagonal structure stacked in either an ABAB sequence (hexagonal lattice, *Fig. 2-2*) or in an ABCABC sequence (rhombohedral).[88] The distance between the planes 0.34 nm is large compared with that between the adjacent atoms in a plane 0.142 nm (*Fig. 2-2b*). The planar networks are comprised of hexagonal rings of carbon atoms bonded by the stabilizing, strong hybrid $sp^2=\pi$ bonding which generates the high modulus and theoretical tensile strength of the fibre. The weak van der Waals type bond between the neighbouring layers produces a low shear modulus and cross-plane Young's modulus that is detrimental to fibre properties.[89]

Structurally, carbon fibres contain a blend of amorphous carbon and graphitic carbon. Their high tensile modulus results from the graphite form. Carbon in the graphite form is highly anisotropic with a Young's modulus in the layer plane being equal to about 1000 GPa while that along the c axis is equal to about 35 GPa. Since graphite is the stable form of carbon at room temperature, any useful graphite fibre must either be a single crystal with layer planes parallel to the fibre axis, or else a polycrystal of very high preferred orientation. Consequently, carbon fibre has a very high degree of preferred orientation of hexagonal planes along the fibre axis.

Carbon Fibre Conversion Processes. All continuous carbon fibres produced to date have started with organic precursors that were subsequently converted to carbon fibres. Three different precursor materials are used at present to produce carbon fibres: rayon, polyacrylonitrile (PAN), and isotropic and liquid crystalline pitches. Each

precursor category requires a different processing technique but generally the precursor-to-carbon-fibre fabrication process involves the following sequences: stabilization, carbonization, graphitization (optional), surface treatments, application of sizing or finishes, and spooling. *Figure 2-3* shows schematically what must be accomplished in converting an all-carbon backbone polymer into an ordered carbon fibre.[90]

2.2.2. Properties

Chemical Properties.[91] Carbon fibres are relatively inert to most chemicals and resistant to corrosion under ambient conditions. In general, carbon/graphite fibres are resistant to common alkaline solutions at all concentrations and temperatures, and to the aqueous solutions of most inorganic salts up to their boiling point. Immersion of carbon fibre in the following reagents showed no significant loss in tensile strength or modulus at 50°C:50%v/v HCl acid, H_2SO_4 acid, and nitric acid; 50% w/v NaOH solution; 50% w/w hypophosphorous acid; and orthophosphoric acid. Carbon fibres are not affected by moisture, atmosphere, solvents, and weak acid at room temperature.[92]

The surface of carbon fibres is subject to attack by strong oxidizing agents and halogens, especially at elevated temperatures. The fibres react with most molten metals (aluminum and titanium) and must be protected by a barrier coating. Carbon fibres are not wet by molten metals and are difficult to wet with resins, especially the higher modulus fibres.

Sizing of fibres with epoxy, thermoplastics or other resins serves as a protective coating to prevent fibre abrasion, improve handleability and possibly to provide a

compatible interface. The sizing may improve the wetting of the fibre by matrix resins but not necessarily improve the bond strength between the resin and fibre.[93]

Bulk Properties. The density of the carbon fibre varies in the range of 1.6-2.2 $g.cm^{-3}$, which is about 80 to 94% and 86 to 100% of theoretical for PAN- and Pitch-based fibres respectively. The diameters of carbon fibres are in the range of 4 to 10 μm.

Mechanical Properties. The main types of high-performance materials are usually divided into three classes, designated as high-modulus, high strength, and type A or type III fibres. Typical properties of these materials and the recently developed ultrahigh-modulus and ultrahigh-strength materials are shown in *Fig. 2-1*. The modulus of carbon fibre depends on the degree of perfection of alignment, heat treatment temperature, and defects between and within the crystallites.[94]

Carbon fibres increase in modulus by about 10% when highly loaded. However, the fibres show complete eleastic recovery upon unloading and do not appear to degrade because of mechanical fatigue or show stress rupture at temperatures below 2000°C. The moduli and strength of carbon fibres are essentially constant up to a temperature of 1000°C for fibres given a higher heat treatment temperature. There is a drop of about 30% in modulus at 1900°C. Above 2200°C, creep becomes appreciable.

2.3. Thermoplastic Composites

2.3.1. Thermoplastic Resin Systems

Most thermoplastics can be used as matrices in polymer composites, from simple filled injection molding compounds, through reinforced thermoplastic molding and

stamping materials, to advanced structural composites. The latter have a relatively high proportion of reinforcing fibre, 60 vol%, and which are normally in a continuous unidirectional or woven form in a high-performance thermoplastic resin matrix.

Historically, reinforced thermoplastic composites have been limited to short-fibre compounds for injection and compression molding applications. However, maximum reinforcing benefit is generally achieved by long-fibre reinforcements, which are widely used in the thermoset industry. It is clear that the best possible property profile will be derived from the highest loading of the longest fibre, provided that each fibre is fully wetted by a resin of adequate stiffness to prevent buckling of the fibres when subjected to compressive loading. Long-fibre reinforced thermoplastic composites have not been widely used primarily due to limitation in the development of processing technology. In recent years, significant progress has been made in combining thermoplastic resins with continuous-fibre reinforcement.

2.3.2. Architecture of Fibres

Thermoplastic composites containing long fibre reinforcement can be divided into two broad categories, those containing long fibres in the form of a random mat and those containing continuous fibres in unidirectional or fabric forms.[95]

Fibre reinforcement constitutes the structural backbone of a composite. The architecture of the textile preform, or the fibre orientation and the level of structural integrity, determine the fibre packing density and the translation efficiency of fibre properties to the composite structure.[96] On the basis of structural integrity, fibre linearity,

and continuity, fibre architecture or structural reinforcement was classified into four categories: discrete, continuous, planar interlaced (2-D) and fully integrated (3-D) systems. Fukuta et al.[97] classified textile structural reinforcements according to the axis of fibre or yarn introduction and geometric dimension as shown in *Fig. 2-2*.

2.3.3. Fabrication of thermoplastic composites[98]

Product forms of thermoplastics can be classified as preimpregnated, in which the fibres are completely wetted and fully impregnated by the resin, forming a continuous phase, or postimpregnated, in which the fibres and resin are merely in close physical juxtaposition and can move interdependently until fused during later processing. The products obtained by combining the continuous reinforcing fibres and thermoplastic polymer matrices are usually referred to as prepreg materials. A prepreg material contains a multitude of reinforcing fibre filaments impregnated with the polymer resin. Resins that can be converted to film, powder, or a fibrous form can be applied to both preimpregnated and postpregnated systems.

The fabrication process for thermoplastics involves melting, consolidating, shaping, and solidifying. In preimpregnated or postpreimpregnated forms, fusing plies to make a finished part requires simply heating to the melting point, applying contact pressure, and cooling to solidify.

2.3.4. Basic Mechanics of Fibre Reinforced Polymer Matrix Composites

As fibre-reinforced composites are microscopically inhomogeneous and

nonisotropic (orthotropic), the mechanics of fibre reinforced composites are far more complex than the conventional materials. The matrix holds the fibres together and transmits the applied load to the fibres. Thus, transfer of the applied load to the fibre occurs by means of the shear strain in the matrix. The basic assumptions in describing fibre/matrix interactions in a unidirectional lamina owing to tensile and compressive loading areas follows:[99]

1. Fibres are uniformly distributed throughout the matrix.
2. Perfect bonding exists between fibres and matrix and the Poisson ratios of the two elements are the same.
3. The matrix is free voids.
4. Applied loads are either parallel to or normal to the fibre direction.
5. The lamina is initially in a stress-free state.
6. Both fibres and matrix behaves as linearly elastic materials.

For continuous parallel fibres, according to above assumptions, we can write

$$\begin{aligned} \varepsilon_f &= \varepsilon_m = \varepsilon_c \\ \sigma_f &= E_f \varepsilon_f = E_f \varepsilon_c \\ \sigma_m &= E_m \varepsilon_m = E_m \varepsilon_c \end{aligned} \qquad (2\text{-}2)$$

where the subscripts f, m and c represent fibre, matrix, and composite, respectively and σ, ε, and E are stress, strain, and Young's modulus. The total tensile force P applied on the composite lamina is shared by the fibre and matrix so that

$$P = P_f + P_m \tag{2-3}$$

Then the equation, called the rule of mixtures, for Young's modulus in the fibre direction is given as:

$$E_L = E_f v_f + E_m(1-v_f) \tag{2-4}$$

and

$$\begin{aligned} \sigma_c &= \sigma_f v_f + \sigma_m v_m \\ &= \sigma_f v_f + \sigma_m(1 - v_f) \end{aligned} \tag{2-5}$$

where v is volume. Equation (2-4) shows that the composite longitudinal modulus is intermediate between the fibre and matrix moduli.

The fraction of load carried by fibres in unidirectional continuous fibre lamina is

$$\frac{P_f}{P_c} = \frac{\sigma_f v_f}{\sigma_f v_f + \sigma_m(1-v_f)} = \frac{E_f v_f}{E_f v_f + E_m(1-v_f)} \tag{2-6}$$

From Equation (2-6), we can see that fibre is main load-bearing element. The fibre load fraction can be increased by increasing the fibre volume fraction. Although cylindrical fibre can be theoretically packed to almost 90% volume fraction, the practical limit is close to approximately 80%. Over this limit, the matrix will not be able to wet the fibres.

The mechanical properties of fibre reinforced material depend critically upon the fibre length distribution, fibre orientation distribution and interfacial shear strength. In particular, the fibre-matrix interfacial shear strength is one of the most important parameters in controlling the toughness and the strength of a composite material.[100]

In PMCs, frictional slip usually takes place between fibres and polymers. In

addition, the effect of poor interfacial adhesion must be considered, since this is common with inert fibres such as carbon fibres. The effect of poor adhesion will affect the onset of slip, i.e. the slip point.

2.3.5. Improving Interfacial Bonding in Carbon Fibre Composites

As mentioned above, the interface between the carbon fibre and resin plays an important role in determining the performance of carbon fibre reinforced PMCs. It is evident that the majority of the carbon fibre surface atoms must bond to the resin through low energy interactions such as dispersion, dipole-dipole, dipole-induced dipole, electrostatic, π-bonding, hydrogen bonding, or donor acceptor interactions. Therefore, much effort has been made to improve the surface bonding characteristic of carbon fibre.

Ehburge and Donnet[101] point out that there are two principle ways of improving interfacial bonding in carbon composites: (a) increase the fibre surface roughness, and thus the interfacial area, and (b) increase the surface reactivity.

The methods used in surface treatment of carbon fibre can be classified into: (a) oxidative treatment (b) chemical vapour deposition. The results of oxidation treatment increase the fibre surface area, the number of oxygen-containing surface groups (—C=O and —C—O— configurations) and effect the removal of the original weakly bonded layer of surface defects. Chemical vapour deposition treatment improves the fibre resin adhesion by depositing more active forms of carbon.

2.4. Thermoplastic Polyurethane Composites[102-117]

TPU composites are used in the many applications requiring high impact resistance, higher flexural modulus and strength, and ease of processing on conventional injection molding machines. TPU composites for structural reaction injection molding (SRIM) show low molding pressures and fast molding cycles. The significance of fibre reinforced thermoplastic polyurethane to the plastic industry is the potential to provide the beneficial properties of TPU with improved tensile strength and modulus, flexural strength and modulus, without sacrificing a substantial amount of impact strength. To date, TPU composites are reinforced by various fibres such as glass fibres, Kevlar fibres, and Nylon fibres. Reinforcing materials may take the form of short chopped fibre, continuous strand mats, fleece mats or roving fabric, dependent on requirements. In the most application, glass fibres are the reinforcement fibres of choice. Molded parts with very high stiffness are achieved by reinforcing with carbon fibres. Reinforcement fibre content is generally over 20%, and up to 80% by weight. TPU elastomers have the potential to extend their mechanical properties to a new and higher magnitude depending on amount of reinforcements incorporated and the application.

Arena[114] reported glass fibre reinforced TPU can be used as large exterior body parts such as bumpers, side door panels and rocker panels due to their excellent combination of stiffness and impact strength and a high heat distortion temperature. Mechanical properties such as stiffness and impact properties depend on the concentration of glass fibre and the shore hardness of the TPU matrix. Also, the impact properties are dependent both on flexibility and tear strength. With respect to tear strength, it shows an

increase when the glass fibre content is over 25 wt%. Optimum value for tear strength are obtained at high concentrations of small diameter glass fibres. As expected, at higher glass fibre concentration and shore hardness the multiaxial (falling dart) impact strength decrease.

Kutty[103-105] has reported on the mechanical properties of short Kevlar (aramid) fibre filled millable thermoplastic polyurethane. Rheological and stress relaxation behaviour of short Kevlar aramid fibre-thermoplastic polyurethane composites have also been determined. The authors stated that for loading in the longitudinal direction, the majority of fibres are in a direction perpendicular to the direction of propagation of fracture, and that the fibres can arrest or deflect the advancing tear, thereby delaying the failure. In this process the stress concentration at the fibre-matrix interface becomes so high that the fibres are pulled out of the matrix on failure. In the transverse direction, the fibres, being oriented parallel to the direction of the advancing tear, are not effective in giving hindrance to or arresting the propagation of fracture. Thus, the tear propagates through the fibre-matrix interface.

As mentioned above, TPU composites have been used in structural applications to replace metal parts such as bumper beams, knee bolsters, door panels and leaf springs. To date, there is no literature related to the investigation of sparsely reinforced thermoplastic polyurethane elastomers. As well, the processing technology for making sparsely reinforced TPU elastomer is different from traditional thermoplastic composites. So, considerable effort has been required to develop this new material and process.

CHAPTER 3

DEVELOPMENT OF SPARSELY REINFORCED ELASTOMER SHEETS BY THERMOFORMING

3.1. Thermoforming

3.1.1. Brief Introduction

Thermoforming is a generic term encompassing many techniques for producing plastic articles from flat sheet. It is one of the oldest processes of shaping plastic items. It dates back to the end of the last century, when the celluloid-blowing process was developed. However, sheet forming was restricted to a few applications with acrylics and cellulosics, and was of little importance in comparison to compression or injection molding. A chronology of the early development of thermoforming in plastic is given in Table 3-1.[118, 119] Modern thermoforming began about 50 years ago. The development of vacuum forming, the improvement of machinery, and the introduction of new thermoplastics has made sheet forming the fastest-growing processing method for thermoplastics.[120, 121]

Advantages. Thermoforming offers processing advantages over competitive processes such as blow molding, injection molding, injection blow molding, and rotational molding due to a relatively low forming pressure, and its low pressure-type tooling.

Since the molds are subjected relatively low forces, molds can be made of relatively inexpensive materials and mold fabrication time is very short which gives low mold and machinery costs. It provides, in particular, an economic way of fabricating large parts using single surface sheet, and producing parts with multiple layer sheet material or high strength reinforcement composites. Parts with very small thickness-to area ratio can be fabricated. For thin-wall parts, fabrication time is extremely short, making the process very economical for high volume production.[122]

Some disadvantages include the need to start with extruded sheet materials instead of the cheaper resin and the fact that thermoformed objects often have to be trimmed. The amount of scrap generated in the trimming operation frequently determines the economics of thermoforming against other processes like injection molding or rotational molding.

Application. Thermoforming is widely used for either the rapid production of small parts such as cups using multicavity molds, or the relatively slow production of large parts. Applications range from 6.5 m boats to suitcases, from business machine housings to door liners for refrigerators. The major markets are listed in Table 3-2[123]

3.1.2. The Basic Concept of Thermoforming

The basic thermoforming processing steps are clamping, heating, shaping, cooling and trimming. It consists of holding the thermoplastic sheet by around its perimeter, exposing the captured sheet to heat, heating it to its softening point, and pressing the hot and pliable sheet against the contours of a mold. The required pressure is supplied either

mechanically, hydraulically, pneumatically, or by vacuum. The formed sheet is removed from the mold after cooling. The forming cycle is then considered complete. Today, there are three basic methods of thermoforming: vacuum forming, pressure forming (compressed air), and mechanical forming. They can be subdivided into more than twenty modified methods.[124, 125] There are three types of mold configurations: male mold, female mold, and matched mold.

Vacuum Forming.[126] The vacuum-forming process relies on the heated plastic sheet's self-sealing ability and trapped air space evacuation by vacuum. As the air is removed from the enclosed cavity, it causes a pressure reduction on that side of the sheet, thus allowing the natural atmospheric pressure to fill the cavity and force the heated plastic sheet into the evacuated space, as shown in *Fig. 3-1*. Vacuum forming can basically qualify as pressure forming, using the natural atmospheric pressure to accomplish the forming task.

Classification of Thermoformed Sheets. Thermoformed sheets are loosely categorized as thin-gage (sheet thickness less than 0.25 mm) and thick-gage (sheet thickness greater than 0.25 mm). Thick-gage sheet can be further divided into medium-weight sheet (0.25 to 1.5 mm) and heavy-gage sheet (greater than 1.5 mm).

Choice of vacuum thermoforming technique. Vacuum forming processing was chosen for this project based on economics. In other cases, where a shape with a large surface area and relatively thin walls is needed, sheet forming may be the only process that is technically feasible.

Elastollan 1185A type TPU elastomer sheet supplied by BASF is used as matrix

material. TPU elastomer sheets are reversible with heat despite their effective crosslink and extension links, which is a state called "virtual crosslink". This permits their thermoforming applications.[127-129] In principle, thermoplastic polymers of sufficient molecular weight are suitable for thermoforming since, while the sheet is being heated, they are strong enough so that they do not sag excessively before the vacuum or pressure is applied.

3.1.3 Heating Sheet

3.1.3.1. Basic Ways of Heating Sheets

There are three basic heating methods used in the thermoforming process: contact heating (where a heated plate is placed against the sheet), forced convection hot air ovens, and radiant heating. Heating with radiant energy essentially uses infrared-light spectrum wavelengths. Infrared radiant heating is the most popular heating method in the field of thermoforming. The thermal radiation wavelength range is normally from about 0.1μm to 100μm. Near-infrared is 0.7μm to 3μm and far-infrared is 3μm to 20μm or more. The important wavelength range for most radiant thermoforming processes is about 0.3μm to about 20μm.[122]

Common heaters used in convection industry are Nichrome spiral wires, steel rod heaters, quartz tube heaters, ceramic plates with embedded resistance wires, and steel plates that reradiate combustion energy from gas flames.[123] Thermoformer radiant heaters emit energy in the infrared region, with the peak wavelength depending upon the radian heater temperature. The temperature of the emitting surface of the most flexible heater

should adjustable from 150 to 700°C (300-1300°F), where the radiated infrared waves vary from 6.8 to 2.97 μm.[130] Nearly all thermoforming heaters function in the far infrared wavelength band of 2.5 μm to 10 μm. The heater temperature range for this peak infrared wavelength is 886 to 16°C. The best efficiency (at wavelengths of 3.00 to 3.50 μm) comes when the heater glows "cherry red". Most plastic sheet that is thermoformed requires an emitter temperature of 510-643°C(950-1190°F).

In thermoforming, the two basic energy sources used for heating thermoplastic sheets are gas and electricity.[126] When gas is used as the heat energy source, the gas is usually burned in a controlled manner. More than 90% of thermoforming processing uses electric power to heat the thermoplastic sheet. The electrical energy is converted into heat when electricity is run through a high resistance wire.

3.1.3.2. Infrared Absorption Spectrum

An infrared spectrum is obtained when a sample absorbs radiation in the region of the electromagnetic spectrum known as the infrared. There are two main factors that contribute to absorption within solids: electronic excitation and bond vibrations. In reality, molecular bonds are constantly stretching and bending, lengthening and contracting. For certain wavelengths, the energy in infrared light corresponds exactly to the amount needed to increase certain molecular motions of a sample. For infrared radiation, if the frequency of the radiation matches the natural vibration of the molecule, there occurs a net transfer of energy to the molecule that results in a change in the amplitude of the molecular vibrations. Because each light frequency absorbed by the

molecule corresponds to a specific bond vibration, if the sample is irradiated with energy of many different wavelengths and determine which wavelengths are absorbed and which pass through, the absorption spectrum of the compound can be determined.[131, 132] The most efficient heater would be one rich in the natural frequency wavelengths.

3.1.3.3. Heat Transfer Modes

There are three components one has to consider when dealing with radiative transfer in semi-transparent materials: reflection, absorption and transmission. These three components of the irradiation should add up to the irradiation. *Fig. 3-2.*[133]

The fractions reflected, absorbed and transmitted are dependent upon wavelength, ie. they are spectral in nature, and on the angle of incidence. Absorption in a material is function of "α", the absorption coefficient, (which is wavelength dependent) and the thickness "x" of the material. This is mathematically stated by Beer-Lambert's law:[133]

$$I_{\lambda,x}=I_{\lambda,o}\, e^{(-\alpha x)} \qquad (3\text{-}1)$$

where $I_{\lambda,o}$ is intensity of the radiation at the surface which is not reflected, and $I_{\lambda,x}$ is the intensity at depth x after absorption.

In order to understand radiative heat transfer within a semi-transparent material (such as TPU), a unit volume located in the interior of the material is considered. The unit volume could be experiencing two processes simultaneously. First of all, it could be emitting radiation to the surrounding region. However, it could also be absorbing radiation emitted from the surrounding region. In other words, radiative heat transfer within a semi-transparent material is the result of the interaction of the simultaneous

emission and absorption of radiation throughout the volume. Some of the radiation emitted in the interior may reach the surface where it is observed as emission, with the rest being absorbed on its way to the surface. Hence, it should be clear that emission is a volume phenomena for materials. Therefore, the overall emissivity of a semi-transparent material is a function of the temperature distribution within the material.[134]

3.1.3.4. IR Absorption in the Polymers

As to the intensity of far infrared absorption bands, polymers can be classified roughly into three groups. The first group includes molecules containing heavy polar atoms. Examples are halogenated polyhydrocarbons and silicones. These compounds have polar bonds and give rise to very strong absorption bands. Their spectra are in the long IR wavelength region. The second group comprises practically all compounds with less heavy and polar heteroatoms such as oxygen and nitrogen. Aromatic structures are also included in this group. Examples are polyesters, polyethers, phenolic resins, amino and amido resins, and polyhydrocarbons. These compounds give rise to absorption bands of medium intensity. The third group consists of compounds having only structures of low polarity. Examples are aliphatic polyhydrocarbons of all kinds. These molecules usually have only weak absorption bands in the far infrared.[135]

3.1.3.5. Infrared Spectrum of TPU

TPU shows strong absorption in the IR region. A list of the wavelengths of the most intensive absorption bands of chemical groupings present in polyurethane is given

in Table 3-3.[136] The carbonyl stretching region occurs at 5.5-6.0 μm in the infrared. Polyurethane with —NH—CO—O— group should exhibit spectral similaries to amides as well as esters. This is true for the rocksalt range where the carbonyl band found in urethanes absorbs near 1724 cm^{-1} and amide II band at 1540 cm^{-1}. The amide I band of the urethanes (C=O) occurs at a different frequency from the C=O stretching vibration of other compounds such as the dimer and trimer. The amide I band comprises five individual components at 1740, 1730, 1725, 1713 and 1702 cm^{-1}.[137] An infrared spectrum of TPU 1185A used in thermoforming is shown in *Fig. 3-3*. The efficiency of absorption of the radiation by semi-transparent polymers depends upon matching the radiant source peak wavelength to the primary absorption wavelengths of the polymer.

3.2. Thermoforming Equipment Design

A single station, vacuum thermoforming process was chosen for development of sparsely reinforced TPU elastomer sheets. The thermoforming equipment designed for this experimental work includes heating equipment, mold, vacuum system, clamps, valves and sealing.

3.2.1. Heating Equipment

A single stage, movable thermoformer was designed and constructed as shown in *Fig. 3-4*. It is composed of heater, variacs (variable transformer), furnace frame, and thermal insulating materials. The radiant heating method was adapted in this thermoforming process. The energy density which can be transferred by infrared radiation

from the heat source to the plastic sheet depends on many variables.

Nichrome spiral resistance wire was used as heating element. The resistance heater emits energy into the far-infrared region and still has sufficient energy density for all plastic heating. The surface temperature of radiant heaters can range between 315 to 700°C (600°F and 1300°F). The wires are embedded in refractory bricks. The arrangement of heating elements is presented in *Fig. 3-5*. Fourteen pieces of resistance wire are divided into three groups: left, centre, and right. Each brick contains two wire strands. The left and right groups is two bricks wide and centre group has three bricks. Each group has the same power of 1.67 KW, but the left and right group has only two bricks so the area of the centre group has lower power density than the left and right groups. This is to correct for the higher intensity that would occur in the centre portion if the emitter intensity was uniform. The total heating area is 0.756 m x 0.914 m, and the effective heating area is 0.66 m x 0.838 m. The total power is 5 Kw at 220 V. The electrical current input of three groups is controlled through three variacs adjusted individually to uniformly heat the sheet. The furnace is enclosed using glass-cotton board with aluminium foil liner to reduce the heat loss, and to stop air drafts.

3.2.2. Mold

Regardless of the materials used, every mold must have certain features. Provisions must be made for clamping the sheet against the mold surface. Vent or vacuum holes must be provided in those areas into which the sheet is drawn last. The mold surface must remain relatively nonadhesive during sheet contact and static-free after

the sheet is removed. The mold surface should also be sufficiently hard to retain its shape and texture for its lifetime. The mold must not change in dimensions either during fabrication or during storage. The material should be relatively free from chemical and moisture attack.

Mold materials. The choice of material depends primarily upon the quantity and quality of formed items to be produced. For the experimental short runs used on the current project, wood was chosen as a material to make the mold.

Mold design. The mold was designed as a female mold. The mold system consists multiple layers as described in *Fig. 3-6*. The vacuum holes (12.7 mm in diameter) were drilled through the vacuum frame, and copper pipes were embedded inside of these holes to connect with the vacuum system. The vacuum holes were arranged to ensure the sheet would be drawn down uniformly and quickly. The middle layer frame with nails (mesh frame) was for winding reinforcements. An insert plate specially designed was put into the middle layer frame to keep good contact between the TPU sheets and fiber when the second layer of sheet was forming (mold arrangement for second side sheet forming as shown in *Fig. 3-6b*). The top is the main mold body with the sheet clamp frame, which is removable. The bottom mold plate was placed on a wooden board of the mold station which was supported by an aluminum frame. All part of the mold frames and top mold were separable. Standard wood filling techniques were used to remove surface defects to ensure good sealing. The radiated surface of the mold was protected by temperature-resistant alumina fiber blanket covered with aluminum foil, which was also good for releasing the TPU sheet after forming. Sponge rubber weather

stripping and TPU elastomer strips were used as airtight sealing materials between each layer of the wooden mold frame parts.

3.2.3. Vacuum System

The vacuum system is composed of a vacuum pump, valves, and vacuum pipes. With a vacuum on one side, the maximum pressure available is the atmospheric pressure of 101.3 KPa (14.7 psia). For most forming processes, only a fraction of this pressure is needed. The magnitude of the forming force is established by the difference in the air pressure acting upon each side of the sheet. The air between the mold and the sheet has to be evacuated very rapidly. In order to achieve the rapid vacuum and necessary pressure to properly thermoform, it is essential to have a vacuum pump with a rated capacity delivering a vacuum of about 711.2 mm (28 in.) of mercury.[124] The pump should be of the high-capacity type rather than the high-vacuum type. Many kinds of vacuum pumps can be used. Rotary, piston, diaphragm, eccentric rotor type vacuum pumps, all establish a good vacuum but are less capable of evacuating a large volume of air quickly. Here, a GAST 23 series rotary vane type oilless vacuum pump (0523-V191Q-G582DX) was chosen for this vacuum system. Rotary vane oilless vacuum pump air compressors are designed for general vacuum requirements up to 689 mmHg (27 in. Hg) continuous duty as well as low pressure requirements up to 68.9 KPa (10 psi).

Vacuum ports. Proper air evacuation assists material flow in the desired direction and in uniform wall thickness. In general, deep corners require intensified evacuation to ensure the draw of material into corners. Large, flat surfaces require the least evacuation.

To quickly remove the bulk of the air, a few large ports (1/4" diameter) were used. The distribution of vacuum ports in the vacuum frame is shown in *Fig. 3-6a*. The location of the vacuum holes is critical in forming of the plastic. This arrangement ensures the sheet draws uniformly to the bottom along the wall of mold. If the placement of the vacuum ports is too central in the cavity, the partially formed plastic can cover the holes, sealing them off, rendering further forming impossible. Air pockets will then be trapped in the cavity. The rate of forming depends on the total cross-sectional area of all air vents, and the flow through them.

3.2.4. Air Redistribution Plate

This plate was specially designed by the author to avoid turbulent air flow which was disturbing the ordered web patterns when the air was rapidly evacuated from the space between the mold and the sheet. It is an intermediate mold plate inserted inside the vacuum frame and between the vacuum frame and the reinforcement meshes used when forming the first layer of TPU sheet (*Fig. 3-6a*). The holes of the air redistribution plate are designed to be distributed over the entire surface. When the vacuum is applied, the air flow has to redistribute its path and pass through these many tiny holes before leaving. Therefore, the plate plays a key role in uniformly evacuating air over whole plate surface, and keeping reinforcement meshes in place. The plate is 1 mm thick aluminum with which the polymer does not stick, making for easy demolding of the thermoformed TPU sheet. Several trials have found that aluminum plate is better than the stainless steel plate for demolding. The section of the holes have a cone shape in

order to evacuate air fast. The fine side of the holes faces the reinforcements. The size of the air holes should be small enough not to leave any mark on the formed TPU sheet, and also to prevent the TPU sheet or fibres sucking into the holes of the plate so that it would stick on the plate.

3.2.5. Air Escape Channels

Air escape channels are designed for releasing part of expanded warm air in the mold cavity to prevent the TPU sheet from bulging upward during the heating stage. The amount of air volume to escape should be equal to the amount of air volume expansion as the temperature increases to the forming temperature. According to the ideal gas equation at constant pressure:

$$\Delta V = V_1\left(\frac{T_2}{T_1} - 1\right) \qquad (3-2)$$

where ΔV the amount of air volume expansion, V_1 is the cavity of the mold, T_1 is room temperature, and T_2 is the forming temperature. A few of small holes were drilled through the mold wall. The holes were opened when heating, and were sealed as soon as vacuum was applied.

3.2.6. Clamps

C-type clamps are specially designed to clamp maximum distance of 33 cm (13") between the clamp frame and the wooden board of the mold station. For sheet heating, as well as for the forming process, the plastic sheet must be restrained firmly between the

clamp frame and the top of the mold. The mold segments were all pressed tightly together by six C-clamps which were uniformly placed along the edges of the clamp frame as shown in *Fig. 3-4*.

3.3. Thermoforming Temperature Determination

3.3.1. Forming Temperature

This is the temperature that the sheet should reach for proper forming conditions under normal circumstances. Thermoplastic sheet can be vacuum-drawn over a range of temperatures. The normal forming temperature is determined by heating the sheet to the highest temperature. The lowest forming temperature is that at which a square box with fairly sharp and distinguished corners can be drawn from the sheet without whitening or other visible disadvantage; the upper limit forming temperature is that at which the sheets either get so soft and fluid that they sag in the clamping frame by their own weight or change their appearance, or scorch owing to degradation. It is crucial to ensure that the sheet stays below this temperature. For best results, thermoplastic sheets should be heated uniformly to prevent internal stress.

3.3.2. DSC Curve of TPU

By the means of thermal analysis, differential scanning calorimetry (DSC) directly measures endothermic or exothermic behaviour of a material as a function of temperature and provides valuable information about the thermal properties a sample under investigation such as heat of cure, glass-transition temperature, melting point, etc.[138]

In the DSC scans, TPU samples ware heated to 250°C (**first scan**), then quenched with liquid nitrogen to -150°C, and scanned a **second time** up to 250°C.[139] In some of the first scans there is a broad, shallow endotherm at about 75°C. This transition is believed to be due to the volatilization of moisture picked up by the plaque as it sat at ambient temperature and humidity, since it is not present on the second scan.

The DSC curve for the TPU sheet used for thermoforming sparsely reinforced sheet is shown in *Fig. 3-7.* The first endotherm around -37.38°C indicates the glass transition (Tg) of the soft segment followed by the crystallization of the soft segment showing the exotherm. The next endotherm is the hard segment disruption (melting) around 162°C to 200°C. The small endotherm centred at approximately 70°C is attributed to the disruption of domains with limited short-range order.[140, 141] The lower useful operating temperature is limited by the glass transitional temperature T_g of the flexible polyester or polyether soft segment which is always well below normal ambient temperature. The upper operating temperature limit depends mainly on the softening point of the hard segment. The upper limit is influenced mostly by the breaking of interchain hydrogen bonds at temperature above 110°C.[142] Although TPU can exhibit a wide rubbery plateau, ranging from about -40 to about 100°C, this plateau region might be not suitable for thermoforming because materials must flow in order to be shaped irreversibly. TPU will flow only when the hard segment is softened or melted, which takes places some 150 - 200°C above T_g.[143] Therefore, the thermoforming temperature should be controlled around endotherm temperature range (155° to 180°C) of the hard segment according to the DSC curve for TPU.

3.3.3. Sagging

In the thermoforming, sagging could be used as a clue for determining the thermoforming. There are two causes for sagging in heated sheets: thermal expansion and melt flow.[124] Thermal expansion occurs in all non-oriented sheets being heated from room temperature to the forming temperature, and is about 1 to 2% in all directions. Since the sheet is firmly restrained on all four sides by the clamping frames, this growth must appear as sag. Melt flow sagging can occur in a thermoplastic sheet when the viscosity of the resin becomes excessively low at the forming temperature and the sheet begins to droop because of its own weight.

3.3.4. Experimental

As reference from the DSC of TPU, the thermoforming temperature of TPU sheet was determined experimentally by measuring the temperature and observing the appearance and sagging change of TPU sheet during heating.

The approximate sheet surface temperature was estimated with an infrared thermometer (Model OS-760). The infrared thermometer can provide precise temperature measurements in the range of 50° to 700°C on a digital display. The IR sensing head is a wide band IR radiation sensor that utilizes precise mirror optics and a unique filter. It can be used as an IR pyrometer for non-contact measurement of IR radiation. In the testing, the IR sensing head was aimed at three reference circles on TPU sheet (named left, centre, and right), and the temperature was recorded. The temperature range measured was from room temperature to the temperature where TPU sheet drooping was

apparent. The temperature measurements are presented in *Fig. 3-8*. The temperature distribution over the TPU surface was quite uniform. The forming temperature was found to be around 160 to 180°C, closely matching the temperature given by DSC of Elastollan 1185A TPU.

In the present work, a reference forming temperature was also obtained experimentally by a thermocouple attached to the bottom surface of the air redistribution plate. Generally, the vacuum forming could be applied when the temperature of the plate reached 60°C to 65°C.

In the experiment, sagging and changing of TPU sheet appearance were also used as indicators of readiness for thermoforming. Between the time of the cold sheet exposure and the resulting sag, there are changes in the sheet that can be observed. The sheet's response to heat was observed to follow the sequences:

1. As soon as the plastic is exposed to the heat, various temperature levels are created within the plastic and the first changes can be observed. The partially heated plastic will go through a wavelike movement. The reaction of the plastic sheet to the heat may come in such pronounced levels that the sheet shows an immediate but temporary sag. The sag rapidly disappears with further heating. The temporary condition should not be confused with materials displaying an immediate and permanent sag condition.
2. As the sheet is further exposed to the heat, its normal reaction causes it to tighten up. This tightening gives the sheet the appearance of well-stretched-out material, almost like the skin surface of a drum. In this state, knowledge of the changing

temperature conditions is vital to successful heating. As the sheet became transparent, it was close to the lower limit of forming temperature.

3. A definite sag will then appear in the heated sheet. At this point, the sheet is heated and softened to the point where its ability to support itself is reduced and the sheet will yield to gravity. The softened TPU sheet will start to sag. When the centre part of the sheet was gradually drooping down about 50 to 80 mm, it was an approximate time for thermoforming. The heating process usually took about 8 to 10 minutes. The forming process took a few seconds.

3.4. Thermoforming Sparsely Reinforced Elastomer Sheets

3.4.1. Material Preparation

3.4.1.1. TPU Sheets

TPU sheet pretreatment. In order to guarantee optimum product performance in the finished part and also prevent surface defects, the water content of Elastollan must be maintained at less than 0.1%. All TPU products should be predried before processing. A chemical reaction occurs during processing of TPU products if exposure to moisture is allowed at a processing temperature between 180 to 220°C for Elastollan TPUs, there is actually a chemical reaction. During this reaction, two things occur. Carbon dioxide (CO_2) gas is released and the properties of the finished product are diminished. After drying, the products should be used within 30-45 minutes. BASF recommends the following drying schedules for Elastollan TPU:

Elastollan Hardness	Drying Period	Drying Temperature
Up to 90 Shore A	2-4 hours	80 to 90°C (175 to 195°F)
Harder than 95 Shore A	2-4 hours	90 to 105°C (195 to 220°F)

Thickness measurement. The thickness of the TPU sheet was checked using a low pressure digimatic indicator before thermoforming. After thermoforming, a circle grid analysis method[144] was applied to determine the thickness of thermoformed TPU sheet. This was done in the following steps. The circles, 19 mm diameter, were drawn on the sheet using a template before thermoforming. The thermoforming process is a biaxial stretching process, so the area change of the circles can be measured using a Mylar film with graduated diverging lines (*Fig. 3-9*). This film is placed over the ellipse and shifted until the diverging lines straddle the major axis of the ellipse. The percent stretch can be read directly from the film. The film is next turned 90 degrees to measure the minor strain. The amount of biaxial stretching is frequently expressed as a percentage increase in linear directions: lengthwise and transverse. It may also be defined as an area increase by thickness reduction, according to the formula:

$$Per\ cent\ stretch = 100\left(\sqrt{\frac{t_o}{t_f}} - 1\right) \qquad (3-3)$$

where t_o initial thickness, t_f final thickness. The details follow.

A correlation between the thinning out of the sheet during the drawing operation and the biaxial stretching in linear direction may be calculated from the following

formula:[145]

$$e_{eng} = Engineering\ Strain = \frac{L_f - L_o}{L_o} \tag{3-4}$$

$$\Delta = \frac{\Delta V}{V} = \frac{(1+e_x)\,(1+e_y)\,(1+e_z)\,dxdydz - dxdydz)}{dxdydz} \tag{3-5}$$

$$\Delta = (1+e_x)(1+e_y)(1+e_z) - 1 \tag{3-6}$$

Since the volume change is zero for plastic deformation,

$$\Delta+1 = 0+1 = (1+e_x)(1+e_y)(1+e_z) \tag{3-7}$$

$$(1+e_z) = 1/(1+e_x)(1+e_y) \tag{3-8}$$

so

$$t_f = \frac{t_o}{\left(1+\frac{L_f-L_o}{L_o}\right)\left(1+\frac{W_f-W_o}{W_o}\right)} \tag{3-9}$$

or

$$t_f = \frac{t_o}{\left(\frac{L_f}{L_o}\right)\left(\frac{W_f}{W_o}\right)} \tag{3-10}$$

so for a circle:

$$t_f = \frac{t_o D_o^2}{D_{long} D_{short}} \tag{3-11}$$

where t_o initial thickness, t_f final thickness, L_f final length, L_o initial length, W_f final width, W_o initial width. D_o initial circle diameter, D_{long} major axis of ellipse, D_{short} minor axis of ellipse. The area of an ellipse is πab.

3.4.1.2. Reinforcement

TPU-rod. TPU-rod was extruded into fiber using a slightly higher hardness 1195A TPU raw material. The properties are listed in Table 3-4a. The fiber has a diameter of 1 mm. Two types of TPU-rod were extruded; solid and hollow.

Carbon Fibres. Two types of carbon fibres were used; 1K and 3K per strand (1K means 1000 fibres/strand). The properties of the carbon fibres are presented in Table 3-4b. It was found in the experimental trials that the carbon fiber had to be bundled together to prevent the blowing of the strand into individual filaments when the vacuum was applied. So the following method[146-149] was used as a pretreatment of the carbon fibres. The apparatus specially designed for treating carbon fibres is shown in *Fig. 3-10.* A solvent coating process was adapted to prepreg the fibres. Solvent coating is typically accomplished by immersing the fiber strand into a bath containing a solvent and resin mixture, then the fiber is routed through the bath and is dried in a one pass heating zone. The carbon fiber coating is made of the TPU pellets which were dissolved into a solvent THF. Resin content was controlled by adjusting the solvent-resin ratio. The drying step reduced volatiles and drew together and dried the resin so that the towpreg would not adhere to itself during unspooling later in the treatment process. *Figure 3-11* shows carbon fiber before coating, and after coating. The filaments of coated carbon fiber strand adhere well together. Coating increases the flexibility of the carbon fibres. Loose uncoated fibers kink easily but in the coated strand, they support each other. The coated carbon fibres were easy to handle when winding meshes, and kept the mesh patterns in place during forming. They also achieved better bonding with the TPU matrix sheets,

which is important in their performance as crack arrestors.

3.4.1.3. Reinforcement Meshes

The reinforcement was arranged into different patterns before being put into the mold. The middle mold frame which has nails around its edge was used as a mesh frame. The reinforcement were wound into four different patterns for experimental use. These are called square, diamond, triangle and laddered diamond patterns respectively. The detail dimensions are given in *Fig. 3-12*. The vol% or wt% of reinforcements incorporated into sparsely reinforced TPU sheet in the four different patterns are calculated in Table 3-5.

3.4.2. Experimental Thermoforming Procedures for Developing Sparsely Reinforced TPU Elastomer Sheets

Thermoforming was conducted as follows:

(a) Preheat the furnace. The furnace was turned on and set for a temperature of 90-100°C. This hastened the later heating stage.

(b) Put the mesh frame into the mold and adjust the air redistribution plate position below the mesh. The position of plate should be in a distance below the reinforcement meshes but above the vacuum holes so that the fibres are able to tighten down under vacuum force, and are able to contact the air redistribution plate perfectly.

(c) Clamp the sheet tightly between the top mold frames.

(d) Move the furnace to the mold station, locate the mold in the centre part of heating area, adjust the distance from the centre of heating elements to sheet about 26 cm.

(e) Heat the sheet to the thermoforming temperature.

(f) Turn on the vacuum pump, and open the valves fully until the sheet is sucked down to the air redistribution plate. Turn off the vacuum pump, and heat the sheet a few minutes more, apply vacuum again. Then turn off the vacuum and furnace to allow cooling.

(g) Cut the reinforcements holding the thermoformed sheet to the mesh frame. Flip the thermoformed sheet over, and put the sheet between the insert plate and the mesh frame. Reassemble the mold, but with the vacuum ports above the mesh frame (*Fig. 3-6b*), and repeat above procedure (b) to (f).

(h) Trim the thermoformed sheets.

3.5. Discussion

Figure 3-13 is an experimental result of thickness distribution of thermoformed TPU sheets. It shows that the sheet created by the current thermoforming method has a relatively uniform thickness. In a thermoforming process, it is expected that the final thermoformed materials have a uniform thickness, good bonding between the TPU sheets and reinforcements, and repeatable results. These are affected by many factors such as uniform heating, proper forming temperature, and proper application of vacuum pressure.

3.5.1. Uniform Heating

Uniform heating will result a uniform temperature distribution over the surface of TPU sheet. This will lead to a uniform sheet stretching as air is evacuating. To obtain a uniform heating, the current run through the three heating element groups, and the distance between the heating elements and TPU sheets have to be adjusted properly. The rate of heating is another factor. If the current is turned up too quickly, a crack may initiate over the TPU surface, causing the thermoforming process to fail. There are many other aspects that influence the TPU sheet heating. These include the thickness of the sheet, thermal conductivity of the material, specific heat of the material, moisture content of the material, and IR absorbtion properties of the material. Heating is a very complex process.

3.5.2. Proper Forming Temperature

Thermoplastic sheet at the forming temperature can be considered as a rubbery elastic solid, a highly viscous fluid or as something in between. Once the plastic sheet is at the appropriate forming temperature, it can be stretched properly. At a given temperature the extent to which the sheet can be stretched limits the way in which it can be thermoformed. The amount of deformation depends upon sheet temperature, level of applied force, level of molecular order and orientation, and general material stress-strain behaviour. At a low forming temperature, the plastic sheet is not quite soft, does not stretch easily down along the mold wall, and does not faithfully replicate the mold details. Under these conditions, it is easy to create a non-uniform thickness distribution. It also

requires high forming forces. At a higher forming temperature, the sheet is quite limp, is easy to stretch and replicates well at very modest forming pressure. However, if the sheet temperature is too high, it will start to flow quickly down the sag. There is insufficient time to apply vacuum pressure and the sheet will be thick at the centre.

3.5.3. Effect of Vacuum on Thermoforming

The quality of the sparsely reinforced TPU sheet relies on the vacuum pressure applied to some extent. First of all, good sealing between the layers of the mold and sheet must be established. Otherwise, it is not only a waste of energy but can be detrimental to the quality of forming. As soon as the vacuum is applied, the rushing air movement created by the suction could cause local chilling of the heated thermoplastic sheet. Any premature actuation of the vacuum prior to reaching forming temperature would affect sheet stretching and ultimately the forming results. TPU sheet itself will tend to go back to its original position due to its viscoelasticity and memory function, and can not draw uniformly into the bottom surface of the mold to form close contact with the reinforcements. In thermoforming sparsely reinforced materials, it is also necessary to maintain a sufficiently high vacuum. For forming the first layer of the sheet, the application of vacuum should be repeated one time to form a composite having good bonding between the TPU sheet and reinforcements. It is very important in thermoforming that the vacuum should remain on the part until it has cooled to the heat distortion temperature. The rate of vacuum application also affects the forming results. The faster the vacuum the better the part forms. Sheet will draw more uniformly, and

stick to each other better. This will also improve the cycle time by causing a more intimate contact with air redistribution plate.

3.5.4. Uniformity of Thickness Reduction

Non-uniform thinning of the drawn sheet is the limiting factor of straight vacuum forming. It depends on the ratio of the overall mold height to width (H/W), as well as on the shape, angle, and radii of the mold. The smaller the H/W ratio, the more uniform the drawing. A more uniform thinning is obtainable by differentiated vacuum draw, i.e., intensified suction in corners and less suction on flat surfaces.

Another variable which influences the uniformity in thickness reduction is the speed of drawing, affected by the speed of evacuation of the motion air. Slow drawing may result in crazing owing to early cooling. Very fast drawing may result in too much thinning on the corners or undercuts, because the material did not flow fast enough.

3.5.5. Clamping

Clamping is very important in whole thermoforming process. It is known that all thermoplastic sheet materials have a tendency to soften and lose their self-supportiveness. They also distort and may sag when exposed to the heat cycle. When heated, thermoplastic sheet will react and yield to natural thermal expansion, loss of crystallinity, and relief of molecular orientation, all of which tend to cause sheet movement and distortion. So, in a heating cycle, if insufficient clamping force is provided to the thermoplastic sheet along its four sides, the unheld and unsupported side will usually

distort and will often pull away from the clamping area. This causes a shift in material thickness and material gathering, with thickening and gathering that concentrates toward the centre of the sheet.[Ref. 3-9]

3.6. Summary

Sparsely reinforced flexible TPU elastomer sheets were developed successfully and economically using a special designed thermoforming processing technique in a laboratory scale. In order to get good thermoformed samples, many parameters must be carefully controlled such as heating rate, forming temperature, vacuum pressure. If a surge vacuum tank had been used in this experiment, a better TPU composite would probably be obtained.

CHAPTER 4

INVESTIGATION OF TEAR BEHAVIOUR OF SPARSELY REINFORCED TPU ELASTOMER SHEETS

4.1. Tear

Tearing can be considered as a rupture propagating from a stress raiser. Tearing is one of the methods of testing the strength of rubbers. The most common strength test method is tensile testing as reported in Chapter 6.

Tear tests have been developed for flexible materials to obtain an indication of the toughness of film and sheeting which may develop cracks during handling. In a tear test, a stress concentration is attained before testing by specially incising the specimen. The place of the cut determines the source of the tear of the specimen during deformation.

According to the theory of the tearing of rubbers,[150] the tearing of elastomer occurs in two stages. In the first stage, only deformation of the specimen takes place with increasing distance between the grips, and there is no noticeable growth of the cut. In the second stage, tearing begins. The cut grows in length, but only after the distance between the grips reaches some critical value at $l=l_k$, and then rapid growth of the cut across the whole specimen takes place at a speed near the speed of sound in rubber. In other words, there is no sub-critical slow crack slow growth of the cut during testing.

4.1.1. Tear Test

In the current work, tear tests were conducted using a modified ASTM D624-86, Die C type and ASTM D1004-90 tests.[151, 152] The modified Die for the test specimens is shown in *Fig. 4-1*. The details of the dimensions of the enlarged die are indicated in Table 4-1. The dimensions were chosen to allow a reasonable measure of the effect of the reinforcement webs in the gage section.

The tear samples were Die-cut in a hydraulic press to insure a good finish. The samples of the single TPU sheet were cut both in parallel and transverse to the direction of extrusion of the film. The thermoformed double sheet with no reinforcement and sparsely reinforced TPU sheets were cut parallel to the extruded direction.

In the tear test, the thickness of the sample was measured first by a low pressure digimatic indicator, and then the tear sample was clamped on the Instron testing machine. Tearing experiments were carried out by pulling apart the clamps of the testing machine under tensile force. The Instron machine recorded the maximum force and displacement. The chart on the Instron tester was used to trace the whole process of the tearing test and to display a tearing curve of the force vs displacement throughout the tests.

4.1.2. Tear Resistance

The tearing resistance is expressed in maximum force in Newtons to rupture a specimen. It can be calculated as follows:

$$T_s = F/t \tag{4-1}$$

where T_s is the tear resistance [KN/m], F is the maximum force [N] and t is the specimen

thickness [mm].

The tear resistance of a polymeric film or sheeting is a complex function of its ultimate resistance to rupture. The resistance to tearing is partly dependent upon thickness and may be affected to a large degree by mechanical fibering of the rubber under stress, as well as by stress distribution, strain rate, and size of specimen. In the present case, when testing reinforced sheet, it is also affected by the load gathering effect of the reinforcement, and reinforcement's ability to act as a crack arrestor.

4.1.3. Materials

The materials tested include unreinforced TPU sheets. It has been tested in both single thickness (0.3 mm) and thermoformed double thickness (0.54 mm), and also as reinforced thermoformed double sheets. The reinforcement materials tested were carbon fiber with either 1K or 3K (3000 fibers/strand). An elastomer TPU-rod reinforcement has been used also. For comparative purposes, a commercially available polyester scrim material coated on both sides with urethane was also tested. In fairness to the producers of this material, its properties have been developed for other applications and certainly do not represent the optimum capability of this type of material in this type of application. However, it is a type developed for related purposes and is used for comparison here because design engineers may be familiar with it.

Among the major differences between the material developed in this work and the commercial scrim is the size and spacing of the reinforcement. The commercial material has a fine screen of reinforcement about 0.12-0.13 mm in diameter spaced in a square

grid of 0.5 x 0.5 mm. The sparsely reinforced material has reinforcements in the order of 1 mm in diameter with a reinforcement spacing of about 1 cm for both the TPU-rod and the carbon fiber reinforcements in a variety of patterns.

4.1.4. Annealing

4.1.4.1. Purpose of Annealing

The behaviour of a fiber-reinforced polymer is governed, primarily, by properties of (i) the reinforcing fiber, (ii) the polymer matrix and, (iii) the efficacy with which stress is transferred across the resin-fiber interface. The failure of any one of these components could lead to failure of the composite. The most desirable interphase, it should be noted, is not the one that provides the strongest chemical bonding. Too strong an interphase will tend to drive a crack normal to the fiber. The composite could be considered to behave as a homogeneous material and crack propagation would be unstable. Poor bonding at the interface would mean crack propagation along the interface. So too strong an interphase results in high shear strength but low fracture toughness, while too weak an interphase results low energy shear failure. This implies high toughness. Thus, the ideal interface for optimized composites would have to lie between these two extremes.[153]

Carbon fiber reinforced polymers usually have low interlaminar shear strength. Advancing their development was subject to improvement of their interfacial properties. The poor shear strength of carbon fibers reinforced composites is attributed to a "lack of bonding" between matrix and filaments.[154]

In the vacuum thermoforming process, a good intimate contact between TPU sheet

and carbon fibers may not be formed due to factors such as forming temperature, vacuum pressure, or the time the vacuum is applied. Therefore, an annealing process was developed to obtain better bonding for some of the thermoformed sheets having triangle and diamond patterns reinforced with 1K and 3K carbon fibers.

On the other hand, annealing will induce the morphological changes in segmented elastomers. At the annealing temperature, the soft segments and the hard segments have high enough mobility to rearrange themselves into a more ordered structure. So the short-range ordering of the soft and the hard segments will be improved by annealing,[155-159] which will promote the enhancement of the tear resistance.

4.1.4.2. Device for Annealing

The device used in annealing is shown in *Fig. 4-2*. It is composed of heating elements, a press, and clamps. The press is made from two thin aluminum plates with the approximate dimensions of 40 cm by 30 cm. A 2.5 cm thick aluminum block with the dimension 25 x 25 cm is welded on each side of the aluminum plate, and eight cartridge heaters were embedded uniformly in each side of the aluminum blocks. The aluminum plates were heated by cartridge heaters. The press was covered with an alumina fiber insulation blanket to reduce the heat losses to the environment. A thermocouple was inserted between the aluminum plates to measure the annealing temperature. The temperature of the aluminum plates was indicated and controlled by a temperature controller and the current was adjusted by the variacs.

4.1.4.3. Annealing Procedure

The sheet for annealing was laid up between the two heated aluminum plates. The compressive force was applied through the C-clamps. Annealing was performed under heating and pressure for a holding time of 30 minutes at temperatures 120°C and 135°C. The annealing temperature determined from the DSC curve in *Fig. 3-7*, was chosen to where the hard segments begin to soften.

4.2. Tear Test Results

4.2.1. The Characteristic Tearing Curves of Sparsely Reinforced TPU Sheets

Characteristic tearing curves of the TPU elastomer sheets sparsely reinforced with TPU-rod, 1K and 3K carbon fiber, and the polyester scrim are shown in *Figs. 4-3* to *4-6*. The TPU sheets reinforced with TPU-rod give a quite smooth increasing tear resistance curve with increasing elongation. The TPU sheets reinforced with 1K or 3K carbon fibers exhibit a serrated curve. The individual serrations represent the processes of debonding, pulling-out or breaking of the carbon fibers. The plots of tear resistance versus elongation for carbon fiber reinforced materials show the initial stiffness is high, followed by load drop serrations where fibers break or debond. The maximum force occurs either at an early stage or near the end of the tearing stage, depending on the reinforcement patterns. In each peak, debonding of the fiber initiates and propagates rapidly to cause complete local debonding of the interface; then the peak force drops suddenly to a force required to extract the debonded fiber from the matrix. The force sustained by friction gradually decreases as the fiber is progressively pulled out. The cut in the tear sample will not

grow unless the higher load is sufficient to debond the fibers.

4.2.2. Tear Test Results of Single TPU Sheets

Figure 4-7 shows the tear test results of single TPU sheet. It shows that the tear resistance parallel to the extruded direction is higher than that transverse to the extruded direction, but the elongation results are opposite. The elongation in the transverse direction is greater than that parallel to the extruded direction. The tear resistance of single TPU sheet is lower than the thermoformed double TPU sheet.

4.2.3. Tear Test Results of Sparsely Reinforced TPU Sheets

Table 4-2 summarizes the results of the tear tests. The trends can be seen more clearly in the bar charts as shown in *Figs 4-9, 4-10. Figures 4-9* and *4-10* show the tear resistance and elongation of reinforced TPU elastomeric sheet with all types reinforcement and web patterns, compared with unreinforced thermoformed double sheet. The tear resistance is calculated on the basis of the sheet thickness only, ignoring the reinforcement. The salient results are that, compared with unreinforced material, all types of reinforcement increase the load required to cause failure, as expected. Somewhat surprising is that all types of reinforcement also increase the sample extension required to cause failure. This latter result is in contradiction to the general principles of fiber reinforcement of composites, which ordinarily require a minimum critical volume of reinforcement as given in Eq. (1-1). According to this body of theory, reinforcement below V_{min} will decrease strength and ductility. Later in this chapter an explanation is

given for why the theory does not hold for reinforced elastomers.

The poorest tear strength was found in the unreinforced TPU sheet. Adding a stiff reinforcement, whether it be polyester scrim, or 1K or 3K carbon fibers, stiffened the material to about the same extent. The tear strength of the commercial scrim was higher than TPU with no reinforcement, and was about equal to the carbon fiber reinforced TPU. These were all significantly lower than TPU-rod reinforced sheet. Summarizing the results in *Fig. 4-8*, the best tear resistance and elongation to failure was given by the TPU-rod reinforced TPU sheet. With this reinforcement, the elastomeric composite exhibits a very large increase in tear resistance.

As shown in *Figs. 4-8* and *4-9*, the unreinforced thermoformed double-sheet extended about 134% of the initial grip separation before failure at about 212 N/mm. The 1K carbon fiber reinforced sheets required a higher load to failure (between 243 to 333 N/mm) and the tear resistance is increased 15 to 57% depending on the reinforcement web patterns. In the 3K carbon fiber case, the higher load required to failure ranges from 250 to 310 N/mm and so the tear resistance increased between 18 to 46%, compared with the 212 N/mm value for the unreinforced sheet. Surprisingly, an equal or greater extension to cause failure of 1K and 3K carbon fiber reinforcement was found (up to 214%), compared with 134% for the unreinforced material. The samples reinforced with TPU-rod extended between 274% and 308%, depending on the web pattern. The loads required increased to between 458 and 623 N/mm compared with the unreinforced material at 212 N/mm so that the tear resistance increased from 116 to 194%.

The reinforcement mesh arrangement has a influence on the final tear resistance

and elongation. Comparing different reinforcement patterns, the triangle pattern has the highest contribution to increasing tear resistance (except the diamond ladder in 1K case) and the diamond pattern exhibits the highest extension. The reinforments in all patterns contributed to the increase of the tear resistance.

4.2.4. Tear Test Results from Annealing

The results of annealing are presented in Table 4-3 and *Fig. 4-10.* For TPU sheet reinforced with 3K carbon fiber in the triangle pattern, the tear resistance was increased about 50% for an annealing temperature of 135°C, and 14% at 120°C, when compared with no annealing. Compared with thermoformed double sheet with no reinforcements, the tear resistance of 3K carbon fiber material was increased about 122% at an annealing temperature 135°C, and 67% at 120°C. For the diamond pattern, at both temperatures, the tear resistance increased 30% compared with no annealing, and the tear resistance increased 62% compared with thermoformed double sheet with no reinforcements. In the case of TPU sheet reinforced with 1K carbon fiber, no improvement after annealing was observed, which has been interpreted to mean the thermoforming process had already produced a good contact condition between the fibers and matrix. As shown in *Fig. 4-11* the close contact surfaces between the 3K carbon fibers and TPU sheet is increased after annealing. In this case, the bonding between the fibers and TPU matrix was improved by annealing, and so the reinforcement effect of 3K carbon fiber was significantly enhanced. *Figure 4-12* also demonstrates the effect of improvement in bonding after annealing in the 3K carbon fiber case. Comparing the tear curves for 3K carbon fiber

after annealing, an ideal annealing condition was found at around the 135°C, *Fig. 4-12c*. The first peak in the curve as shown in *Fig. 4-12* was the highest, and all the serrated curves were maintained at a higher force level. *Figure 4-13* shows X-ray difraction patterns for the TPU samples. The intensity of the peaks at 9.5°, 20°, 28.5° of 2θ for the samples annealed were enhanced, and the peaks at 9.5° and 28.5° of 2θ became more sharp, compared with samples not annealing.

4.3. Discussion

4.3.1. Theoretical Background on Tearing of Elastomers

In the tearing of an elastomer, the elastic energy (W) of a sample in a tear test is a function of two variables; its length and the depth of the cut c:[150]

$$dW = \left(\frac{\partial W}{\partial l}\right)_c dl + \left(\frac{\partial W}{\partial c}\right)_l dc \qquad (4-2)$$

This equation means that the elastic energy of the specimen W increases due to the strain strengthening work of the external force F (first member), and it decreases as a result of the formation of new surfaces with the growth of the cut as the elastic energy is released (the second term is negative).

According to Rivlin and Thomas,[160] following the Griffith model,[161] $(\partial W/\partial c)_{lc}$ is the work of formation of two surfaces with an area 2t cm^2 (where t is the thickness of the sample) during the growth of the cut along a path 1 cm in length. At the critical stress to initiate crack growth, the work which is expended in the formation of an area of the new surface for a unit length advancement of the crack is

$$T_{ch.e} = (\partial W/\partial c)_{lc}/2t \qquad (4\text{-}3)$$

and this is called the characteristic energy of tearing. It is a constant of the material and consists in the free surface energy created and the energy dissipated per 1 cm^2 of the surface of the tear. The energy dissipated depends on the speed of the process, but at a constant critical speed of tearing, it is a constant of the material. If a crack now propagates through the specimen this energy will be dissipated in the formation of the new surface, in the kinetic energy of motion of the crack edges, and in the heat required for molecular motion of the chain as the specimen retracts. For a rigid specimen which will crack at small strains, the latter two contributions are negligible and the stored energy is primarily spent in creating new surface area. For an elastomer all considerations of the energy disspation will have to be considered. In either case, however, if the criterion for tear is assumed to be the existence of a critical energy of dissipation, then a specimen cannot tear until this amount of energy has been stored in the specimen.[162]

It is important to note that the tearing energy of an elastomer does not relate directly to its tensile strength. The tearing energy is the energy required to extend the rubber to its maximum elongation before the tear begins to propagate. This depends on the shape of the stress-strain curve together with the viscoelastic nature of the elastomer.[163]

4.3.2. Effect of Orientation on Tear Resistance

From the single sheet tear test results (*Fig. 4-7*), it is observed that the tear resistance is higher in the direction parallel to extrusion. Because the TPU sheet used in

the tearing test was made by an extrusion process, the molecular chains were highly oriented along the extrusion direction, and so will behave as an ordered crystalline structure. Generally, the crystalline structure is much stronger than random molecular structure. Molecular orientation is one of the most important factors affecting fracture resistance. In an unoriented state, polymer molecules are distributed randomly within the samples. On the application of strain, the molecules tend to align with the direction of strain. The greater the strain, the higher the degree of alignment of the molecules, and the higher the tear resistance. The major factors influencing anisotropy are:[104] (a) molecular chain structure; (b) degree of orientation; (c) thermally activated relaxation process.

From the single TPU sheet tear test results (*Fig. 4-7*), the elongation is higher in the direction transverse to extrusion. The reason for this higher transverse elongation is that on stretching the previously oriented material in the direction perpendicular to the applied load, the molecule chains are first disoriented, and then reoriented in the direction of the applied force. Molecular chains in the deoriented state are much easier to stretch, and to rearrange because of their visco-elasticity under the applied load. Therefore, the tear test results show that a greater elongation occurs in the transverse direction.

4.3.3. Effect of Reinforcements on Tear Resistance

4.3.3.1. Effect of TPU-rod Reinforcements on Tearing

Figure 4-14 shows the tear process of TPU elastomer sheets reinforced by TPU-rod with different patterns. The crack growth of the TPU elastomer sheets reinforced

with TPU-rod or carbon fibers was slowed down effectively or arrested completely. It is observed that the initiator crack present at the start of the die-C tear test started to grow until it reached a reinforcement, the strongest point of crack resistance being fiber junctions. Then its propagation was stopped by the reinforcements until much higher elongations and load were applied. These results were as expected, given the natural extendability of the TPU fibres. Generally speaking, the extruded polymer fibers have a highly oriented molecular structure, from which they are greatly strengthened and stiffened. So the extendable reinforcement of TPU rod in the tear test was able to continue to gather the load to itself during extension. The overall effect is that the TPU reinforcing rods acted as very effective crack arresters, as demonstrated in *Fig. 4-15*, without reducing the extendability of the sheet material. These phenomena help to explain the higher tear strength and elongation in the TPU rod reinforced material.

4.3.3.2. Effect of Carbon Fiber Reinforcements of Tearing

Figure 4-16 shows the tear testing sequence of carbon fiber reinforced TPU elastomer sheets. As can readily be seen, the sample still continued to deform a certain amount after crack growth was obvious. To understand how carbon fibers can increase the tear resistance and extension of a tear test sample, consider the following.

The toughness of a composite has been found[165-168] to be higher than that of the fiber or the matrix. One or more energy absorption processes which are not present in conventional materials must, therefore, exist in composite systems. The increase in tear resistance has been attributed to several fracture mechanisms. It is proposed that work

done against pull-out is a major contributor. Other researchers consider the energy required to debond the fiber from the matrix to be a major factor.[169] Important energy absorption mechanisms active during the longitudinal tensile loading of a unidirectional continuous fiber lamina[170] are listed below:

1. Stress relaxation energy (energy dissipated owing to reduction in stresses at the ends of a broken fiber[165]

$$E_r = \frac{v_f \sigma_{fu}^2 l_c}{6 E_f} \qquad (4-4)$$

2. Stored elastic energy in a partially debonded fiber[169]

$$E_s = \frac{v_f \sigma_{fu}^2 y}{4 E_f} \qquad (4-5)$$

(where y = debonded length of the fiber when it breaks)

3. Fiber pull-out energy[166]

$$\begin{aligned} E_p &= \frac{v_f \sigma_{fu} l_c^2}{24 L_f} && \text{for} \quad l_f > l_c \\ &= \frac{v_f \sigma_{fu} l_c^2}{24 l_c} && \text{for} \quad l_f < l_c \end{aligned} \qquad (4-6)$$

where σ_{fu} is the ultimate fiber strength, l_c is the minimum fiber length required for the fiber stress to be equal to the fiber ultimate strength at its midlength, l_f is the fiber length, v_f is the volume fraction of the fibers, E_f is Young's modulus of the fiber.

These equations imply:

1. All energy expressions are on the basis of unit fracture surface area.

2. Debonding of fibers ahead of a crack tip or behind a crack tip is an important

energy absorption mechanism. However, no suitable energy expression is available for this mechanism.

3. Energy may also be absorbed by the yielding of fibers or matrix if either of these constituents is ductile in nature.

Based on the above concepts, fibers play an important role in the increasing tearing resistance and elongation in the composite. Most methods for increasing the toughness are based on promoting the occurrence of the fiber pull-out process. For example,[171] fibers have been coated intermittently to produce alternating strong and weak bonding. The strong bonding maintains the required strength while the weak bonding assists crack blunting by the Cook-Gordon[172] debonding mechanism and increases the fiber pull-out length. Fiber pull-out was by far the largest factor contributing to the fracture toughness of a fibrous composite.

In a tear test, the greatest stress concentration is located by specially incising the specimen. The placement of the cut determines the location of the tear of the specimen during deformation. The fiber is a main load bearing element. The stress is transmitted to the fiber by shear stresses along the fiber direction through the matrix. The force loaded onto a tearing specimen will be redistributed along the fiber directions around the tip of the cut, depending on the pattern of the reinforcement web. In the tear test, the strain is localized regardless of the material by the shape of the sample. This is not like the case for an initially uniform strain field where the failure of a given fiber will lead to strain localization of the sort that one would expect to occur when a fiber breaks in a tensile test sample. In the Die C tear test, the strain gradients are severe enough that

localization is not governed by the details of individual fiber failures. But this on its own does not explain the increase in extension to failure for carbon fiber reinforced tear test samples. In fact what happened was that the carbon fibres broke in many places before the die-cut notch began to propagate as a tear. At the end of the broken fibers, the elastomer is more free to extend, pulling with itself the material surrounding the broken end of the fiber. This leads to local debonding at the torn fiber end which spreads back further along the fiber. Depending on the fiber/matrix interfacial strength, these stress components are capable of completely debonding the fibers from the surrounding matrix even before they fail in tension. Partial fiber-matrix debonding ahead of the main crack tip has the effect of blunting the crack front, as the fibers still carry some of the load. The ends of broken fibers redistribute the high strain regions in the ligaments ahead of the crack tip, thereby reducing the notch sensitivity of the TPU elastomeric sheet. High fiber strength and low interfacial strength promote debonding over fiber tensile failure. In the presence of broken fibers, the notch sensitivity and the stress concentration of the notch in tear samples was dispersed over a larger region, so that the matrix could be deformed more under the higher force. The fibers which were in a direction perpendicular to the direction of propagation of fracture can arrest or deflect the advancing tear, thereby delaying the failure.

With increasing load, the fibers continue to break at various locations. Because of statistical distribution of surface flaws, the fiber failure does not necessarily occur in the crack plane. Therefore, the opening of the matrix crack may cause broken fibers to pull out from the surrounding matrix as indicated in *Fig. 4-17a*. This is resisted by the

friction at the fiber/matrix interface. If the interfacial strength is high or the broken fiber lengths are greater than $l_c/2$, the fiber pull out is preceded by either debonding or fiber failure, ahead of and even behind the crack front. In the latter case, broken fibers act as a bridge between the two faces of the matrix crack.

Once the tear has started to grow, it then encounters moderately long fibre segments that have to be dragged through the matrix in order for the crack to advance. In *Fig. 4-17b*, for the case of 1K fiber reinforcement, the carbon fibers are deformed into a wavy pattern. A probable explanation is as follows (see arrows in *Fig. 4-17b*). During tension, the fibers debond and slip in the surrounding matrix tube. On unloading, they buckle into wavy patterns as the elastomer contracts significantly more than the fibers, applying a shear that leads to compression in the fibers. Note that the cut ends of the fibers in *Fig. 4-17b* which have obviously pulled in from the edge of the sample during loading. Unable to contract back along the elastomer jacket during unloading, the fibres buckle to produce the wavy patterns.

4.3.4. Effect Adhesion on Tear Resistance

The nature of the interface has a large influence on the mode of failure and the toughness of the composite. A strong interface would promote crack propagation across the fibers, whilst a weak interface would promote failure by fiber debonding and pull-out. In the case of "good" adhesion between matrix and fiber the maximum stress that can be transmitted from the matrix to the fiber is equal to the shear yield point of the matrix, τ_m for a plastic matrix, and equal to the shear strength of the matrix for a brittle material.

In the case of "poor" adhesion the maximum stress transmissible from the matrix to the fiber will be smaller than τ_m and equal to the shear strength of adhesion.[173]

In continuous fiber-reinforced composites the resistance to shear between matrix and fiber has a relative small effect on the composite strength under tension along the fibers. In practice, it does have a certain effect at stresses close to the ultimate stress, when the "weaker" fibers begin to break and stress transmission through the matrix begins to play an important role.

Two key phenomena occurring during bonding are intimate contact and healing[174] Intimate contact characterizes the amount of physical contact that has been established between two surfaces after they are brought together. In reality, materials never have a perfectly smooth surface; they contain many surface asperities. Because of these asperities, perfect contact in not established by merely bringing the two surfaces together. Upon the application of pressure and/or temperature, the asperities can be deformed by increasing the relative amount of area in contact. The degree of intimate contact is a measure of the relative amount of surface area in contact at any time. It is a function of the applied temperature and pressure, the duration of the application, and the relative surface roughness which characterizes the asperities.

In the annealing process, the application of pressure causes the elements to deform and spread along the interface. In the case of thermoplastics which have a high viscosity, a large pressure is needed to cause the asperities to flow. Because of the temperature dependence of the viscosity, the application of temperature facilitates the flow allowing for greater contact area as pictured in *Fig. 4-11b.*

As shown in *Fig. 4-12*, the size of each peak is dependent on the interfacial parameters of the composite system. A system with a high interfacial shear strength τ_i will have a plot with a steeper slope and a larger initial tear force. A composite system in which the frictional shear stress (stress between the debonded fiber and the matrix during fiber extraction) is only slightly lower than τ_i will exhibit a very small drop. The higher the load at which the serration peak occurs, the better the adhesion between the carbon fibers and TPU matrix, and the more the energy required to pull out the fibers.

On the other hand, an increase in the intensity and sharpness of the peaks in the X-ray difraction patterns as shown in *Fig. 4-13* indicates that the short-range ordering of the soft segments and hard segments in the TPU elastomer sheets was improved through annealing, which clearly helps to increase the tear resistance. Therefore, the annealing process developed in the present study is quite an efficient way to enhance the intimate contact and hence the tear resistance.

4.3.5. Fracture Morphology of Tearing

In a tearing process, molecular chains must be broken. The surfaces of tear cracks are rough on a molecular scale since the tear follows a path of least resistance to minimize the number of chains that are broken. The first chains to be broken are those in a taut configuration; as the tearing proceeds, other chains become taut and break.[175]

The fracture surfaces of selected torn samples were analyzed using scanning electron microscopy (SEM). *Figure 4-18* shows SEM photomicrographs of the failed samples from tearing tests. Two distinct morphologies are observed. First in *Fig. 4-18a*

is a mostly relatively flat shiny featureless fracture surface on a sample of the thermoformed TPU double sheet with no reinforcement. Secondly, in *Fig. 4-18b and 4-18c*, there is a rich tear zone characterized by a rough dull undulate fracture surface representitive of the samples of the TPU sheets reinforced with TPU-rod or carbon fibers. The appearance of the torn surface depends on the tear speed, being characterized by a transition from a smooth to a rough surface. The rough surface tearing was described as "stick-slip" by analogy to a sliding friction response,[162] which occurred at a slow tear speed.

From the pictures of the fracture surface, it can be seen that the crack growth rate was changed by incorporating reinforcements. It is thought that the flat featureless zones of thermoformed TPU double sheets (*Fig. 4-18a*) correspond to relatively fast crack growth and the rough wavelike region of the reinforced TPU sheets *(Fig. 4-18b, 18c)* correspond to apparent slow crack growth.[176] The deformation process of polymers is not simple. Microstructurally it involves lamellar tilting, slip and twist and leads to a microfibrillar morphology. The lamellar thickness in the drawn region may or may not correspond with that in the undrawn region. When it is the same, the deformation process involves pulling out blocks of lamellae and orienting them in the draw direction. When the lamellae thickness is different in the drawn and undrawn regions, it probably means that local melting and recrystallization or annealing has occurred during drawing. The higher the force applied, the more the deformation of the blocks of lamellae will occur in the draw direction, which will cause a change in surface morphology.

As discussed in the above section, the TPU sheets reinforced with TPU-rod or

carbon fibers demonstrated an increase in both tear resistance and elongation. This implies that the growth rate of the crack is clearly slowed down because the crack is either arrested, hindered or deflected by encountering the reinforcements. The matrix materials could then be stretched more under a higher load that causes a rough dull wavelike fracture surface.

4.4. Summary

(1) TPU elastomer sheets sparsely reinforced with either TPU-rod or carbon fibers show an evidently increase in the tear resistance and the elongation in a Die C type tear test. The highest tear resistance and elongation was provided by the TPU-rod reinforcement. The TPU elastomer rod is a very effective crack arrestor.

(2) In the presence of carbon fibers, the notch sensitivity of the crack front was reduced in the tear test. The carbon fibers absorb the extra energy required to pull them out of the matrix during crack propagation. Fiber pull-out both raised the load and increased the extension required of the samples to complete the fracture. Debonding of fibers ahead of a crack tip or behind a crack tip is an important energy absorption mechanism.

(3) Annealing process developed in the present study is quite an efficient way to enhance the intimate contact and hence the tear resistance.

(4) Sparsely incorporated reinforcement in the TPU elastomer sheet changed the fracture morphology of the torn samples from a shiny flat surface into a rough wavelike surface. It is recognized from fracture morphology that the flat

featureless regions in unreinforced TPU sheet corresponds to relatively fast crack growth whereas a rough wavelike regions in the reinforced TPU sheets corresponds to slow crack growth.

CHAPTER 5

SNAGGING RESISTANCE OF SPARSELY REINFORCED ELASTOMER SHEETS

5.1. Introduction

Snagging is the glancing penetration of a sheet material by sharp objects. Failures due to snagging hazards occur in a variety of end uses, including industrial bags, liners, and tarpaulins. One example of a liner is for road vehicles or rail cars hauling hazardous liquids. Should the single shell of the tank break, or be punctured, the resulting spillage could affect people as well as the environment with the potential for high liability. Snagging resistance is one of the properties that would be required in a liner sheet material.

A snagging resistance test method should determine the dynamic tear resistance of plastic film and thin sheeting subjected to end-use snagging-type hazards. The dynamic tear test chosen measures the resistance of a material to dynamic puncture by a sharp point, and the propagation of that puncture resulting in a tear. The ASTM D2582-90 Standard Test Method for puncture-propagation tear resistance of plastic film and thin sheeting was followed.[177]

In this chapter, we are concerned with the investigation of the toughness of a sparsely reinforced TPU elastomer sheet facing a snagging-type failure.

5.2. Snagging Tests

5.2.1. Snag Tester

A snag test apparatus conforming to ASTM D2582-90 has been built, as shown in *Fig. 5-1*. The main units of this apparatus are the test carriage, test stand, and specimen holder.

The test carriage is composed of a weight carriage, probe, and additional weights. The weight carriage drawing can be exploded into parts as shown in *Fig. 5-2*. The weight carriage rides on the two 6.4 mm (1/4") diameter rods that are 915 mm (3 feet) in length and it falls freely along guide channel rods down to a padded drop base on the test stand. To attach the weights to the main carriage body, a 6.35 mm diameter threaded nylon rod was used with a standard wing nut. To prevent the rods from swaying, a brace is used. This brace is anchored to the base of the tester and attached to an aluminum rectangular bar that holds the rod vertical and also maintains the centre to centre distance between the rods. Attached to one of the rods is the release mechanism. The release mechanism is totally adjustable so the carriage can be dropped from any desired height. The carriage has built into it a sharp horizontal test probe (sharpened drill rod) which contacts the test sheet material clamped in an arc across a vertical clearance groove on the sample holder. The latter is essentially a piece of curved sheet metal with a vertical tear slot in the centre to accommodate the probe, and the clamps to hold the sample.

The test stand consists of a large base on which everything else is mounted. The base has adjustable feet in each corner so that the tester can be levelled before tests are performed.

5.2.2. Snagging Test

Before any testing, it is necessary to measure and record the thickness of the samples, then cut the samples to 152.4 mm (6.0 in.) by 406.4 mm (16.0 in.), clamp the edges of the sample on both sides and along the top to the holder. To secure the specimen to the holder drape the specimen against the holder, and then use the clamps to fasten the perimeter of the specimen to the holder. It is then ready for testing.

With the specimen clamped in place, the carriage is brought down until the probe point touches but does not indent the specimen (*Fig. 5-3*) and locked in a place. The height (h_o) of the carriage probe is measured from the base of the tester. From the point of contact, the carriage was raised 508 mm (20 in.) within ± 2.0 mm. Confirming that the carriage had the appropriate weight, the carriage was released.

The carriage dropped vertically along guides, using a controlled release mechanism. The probe will at first contact the sheet specimen held taut over an arc of sheet metal, then it snags and drags the sheet specimen to tear, or to the arrest of the carriage. The probe was a 3.18 mm diameter drill rod having on one end a truncated cone (short base 0.40 mm in diameter with a 30° included angle) so that most of the tear is propagated against the body of this rod. The carriage was be dropped from different heights and could be loaded with different weights to accommodate materials with widely different snag resistance. After the carriage had been arrested, the height of the carriage from the base was read again and this value was recorded to the nearest 0.5 mm. The position of h_o (initial height without snagging) and h (final height after snagging) were indicated as shown in *Fig. 5-4*. The carriage was then raised back to the release

mechanism and the mechanism was re-cocked. The clamps were releaseed and the specimen was relocateed for the next test. The procedure was repeated for a minimum of five trials for each sample tested.

In this snag test, the ASTM carriage drop was performed with 0.1134 kg mass increments for the first four weights, then increments of 0.2268 kg up to 0.9072 kg in total under a standard drop height of 508 mm. The carriage itself weighs 0.1134 kg, and so an additional seven 0.1134 weights, made of lead, were required for the test procedure.

5.2.3. Dynamic Tear Resistance

The average dynamic tear resistance was derived from an energy balance equation. The potential energy of carriage before release Wg(H+L) is equal to the work done by the sample in bringing carriage to a stop, where W is the mass of the carriage and added weights (kg), g is the acceleration of gravity, H is the height the carriage falls before contacting the sheet (mm), L is the vertical distance over which the sheet is torn (mm). The work done cn the sample film in propagating the tear (effective tear resistance force times the distance over which tearing occurs) is assumed to be equal to the potential energy given above. Therefore, the mean dynamic tear resistance F, in Newtons, of the material can be calculated as follows:

$$F=9.8065\,W\left(1+\frac{H}{L}\right) \qquad (5\text{-}1)$$

where 9.8065 is the conversion factor g for Newtons. To determine the dynamic tear resistance, a standard drop height H=508 ± 2 mm is employed. The desirable results for

a snag test are a high F (dynamic tear resistance) and a low L (tear length) value.

5.2.4. Materials

The materials tested include an unreinforced TPU sheet both in single thickness (0.3 mm) and thermoformed double thickness (0.54 mm), and also as reinforced thermoformed double sheets. The reinforcement materials tested have been carbon fiber with either 1000 (1K) or 3000 (3K) fibers per strand, and 1 mm diameter extruded TPU-rod. For comparative purposes, a commercially available polyester scrim material coated on both sides with urethane and polyethylene (PE) film were also tested. The details of snag test results are summarized in *Table 5-1,2.*

5.3. Results and Discussion

5.3.1. Snagging Tear Type

There exist two types of tear observed in a snagging test, namely the slit and the "V" type tear; the type observed depends on the material tested. Here, a slit tear means a single tear parallel to the direction of the falling carriage, whereas a "V" tear which has two individual tear legs which radiate approximately ±45° from the point the tear was initiated. The two legs make a "V" but are not necessarily of equal length. All TPU sheets exhibit a V-shape tear. With the falling direction parallel to extrusion a 90° tear angle was produced, but when in the transverse direction the "V"-type tear angle was closer to 50°, as seen *Fig. 5-5a.* TPU sheet reinforced with polyester (the commercial scrim) exhibited a single slit tear when the falling direction was parallel to the fiber grid

orientation, and V-shape tear when the falling direction was 45° to the fiber grid orientation (*Fig. 5-5b*). Polyethylene film had a slit tear in the parallel to extrusion orientation, and V-shape tear in the transverse to extrusion direction.

It is thought that the V-shape tear angle which occurred in TPU sheet may be due to its particular two phase structures. The hard segments will act as reinforcing particles dispersed in the soft segment matrix. When the impact force between the carriage and the sheet acts on the TPU sheet, then the hard segments will hinder the motion of carriage, and the flexible soft segment chains will provide rebound resilience and deflect the force outward at an angle to the carriage drop direction. The force of the carriage will first try to break the weaker bonds that are between the chains rather than break the chains themselves. So if a material tested is tough and could provide some recoil, the colliding force, a "V"-type tear will be formed. If the material could not resist the initial impact force (inelastic collision), the carriage will cut through the specimen, and a slit-type tear will be produced, seen *Fig. 5-5b*.

To understand the mechanics of the snag test failure modes, the author has observed that when the carriage is lowered carefully to the contact position on the sheet, the probe point snags the sheet at the contact point. If it is then gently pushed a little further into a soft elastomer like the TPU, the material just above the contact point is stretched and thinned, while material just below the contact point is gathered and buckled so that a supportive bulge of elastomer develops extending along the probe toward the carriage. The effect of this bulge is to redistribute some of the force supporting the carriage to the sheet material in a butterfly wing pattern extending outside of the sample

holder groove and above the probe point. As the probe point moves down further it eventually punctures the sheet at the probe point, but the tear then extends roughly perpendicularly to the main normal stress direction. The latter is along the roots of the butterfly wings, so the tear direction is outward and downward from the probe contact point. The stiffer commercial scrim material does not resist tear initiation long enough to develop a similar bulge below the probe, and so it is simply cut by the point of the probe.

These observations could imply that the details of the dynamic tear resistance are governed by the dimensions of the tear slot and probe angle. While this may have some effect on the results, we believe that this tests apparatus gives a reproducible means of mimicking a glancing blow snag type incident like that which would be encountered by a polymer sheet in service. Most snags would result in a similar bulge being developed by a soft elastomer, but not by a stiffer sheet material. At present, the author is unaware of any detailed discussion of the effects of the test stand dimensions on snag test results, although this must have been discussed by the appropriate ASTM committee when this standard was proposed and evaluated.

It is suggested that the "V"-shape tear represents a ductile fracture with better dynamic tear resistance, and slit-shape tear represents a brittle fracture with weaker dynamic tear resistance. The tougher the material is then the larger is the "V" tear angle.

5.3.2. Effect of Orientation on Dynamic Tear Resistance

Figure 5-6 shows the results of TPU single sheet tested parallel and transverse to

extrusion directions. There is a higher resistance to tear in the parallel-to-extrusion direction than in the transverse direction. The dynamic tear resistance in the parallel-to-extrusion direction is 8 to 35% higher than in transverse-to-extrusion direction, depending on the weight of carriage.

During extrusion, forces exerted on the polymer liquid cause the molecules to partially align. If this is followed rapidly by cooling, before the long molecules have time to wriggle back to random conformations, the cold solid polymer is left with a frozen-in molecular orientation, which remains when the stress is removed.[178] Because the TPU sheet used in snagging tests was made by an extrusion process, the molecular chains were highly oriented along the extruded direction, and so will behave as an ordered crystalline structure. Molecular orientation is one of the most important factors affecting the fracture toughness. In principle, a polymer will show a high strength, tear resistance and moduli in the direction parallel to the orientation because the applied loads are carried largely by the strong covalent bonds of the polymer chains. The properties are poor in the direction perpendicular to the orientation because the loads are carried primarily by the weak Van der Waals' bonds.[179] The covalent bond strength (50-100 kCal/mole) is much greater than Van der Waals forces (10-20 kCal/mole). Also, if there are small cracks or other imperfections in the polymer, they become oriented parallel to the orientation direction. These oriented cracks are strong stress concentrators for loads applied perpendicular to the orientation direction. Therefore, the dynamic tear resistance is higher in the parallel to extrusion direction than in the transverse to extrusion direction. From the results of the tests on the TPU sheet, it is clear that some of the extrusion orientation remains in

the sheet, and this causes a directional difference in the dynamic tear resistance. However, whatever the direction of loading, the TPU material has a high enough ductility that it tears in a V mode rather than a slit tear regardless of orientation.

5.3.3. Effect of Thickness on Dynamic Tear Resistance

Figure 5-7 shows that as the thickness of the TPU increases, the dynamic tear resistance increases. Comparing thermoformed double TPU sheet (of thickness t=0.54 mm) with a single layer of TPU sheet (t=0.3 mm), there is a 20 to 47% increase in the dynamic tear resistance depending on the weight of carriage. During a tear test, it was considered that a specimen of volume V and initial thickness t stretched but not torn by the probe, to have an elastic stored energy per unit volume W. If a crack now propagates through the specimen, this energy will be dissipated in the formation of the new surface, in the kinetic energy of motion of the crack edges, and in the heat required for molecular motion of the chain as the specimen retracts. For a rigid specimen, which will crack at small strains, the latter two contributions are negligible and the stored energy is primarily spent in creating new surface area. For an elastomer all the mechanisms will have to be considered. In either case, however, if the criterion for tearing is assumed to be the existence of a critical energy of dissipation, then a specimen cannot tear until this amount of energy has been stored in the specimen.[180] The significant empirical result from these tests is that the snagging resistance of unreinforced TPU increases as the thickness is increased.

5.3.4. Effect of Reinforcements on Dynamic Tear Resistance

Figure 5-8 illustrates the effect of reinforcements on dynamic tear resistance. All types of sparse reinforcement added to TPU elastomer sheets increase the dynamic tear resistance. The best performance was from TPU-rod strengthened materials with an equilateral triangle reinforcement pattern. Going from the thermoformed unreinforced TPU double sheet to the TPU-rod reinforced sheet, the enhancement in dynamic tear resistance is from 48 to 87% depending upon the weight of carriage. When the TPU-rod reinforced sheet is compared with a single sheet of TPU, dynamic tear resistance is improved 150% on average and the tear length is decreased by 127-160%. Carbon fibers sparsely reinforcing the TPU sheet also improved the dynamic tear resistance. Compared with thermoformed unreinforced TPU double sheet, the dynamic tear resistance is increased 8 to 20%, or 11 to 36% for the 1K and 3K carbon fiber reinforcements respectively, depending on the carriage weight.

It was observed that for the samples of TPU elastomer sheet reinforced with TPU-rod, the tear path mostly was constrained to the initial probe contact point within the perimeter of the nearest reinforcements. That is, the TPU-rod reinforcement deflected, rebounded, and/or absorbed the impact energy of the carriage through their elastically deforming reinforcement webs, and effectively served as a barrier to stop the tear and the motion of the test carriage when the probe reached the first TPU-rod reinforcement, except at the highest applied load. In the standard weight range, even if a TPU-rod was broken through, most of the energy was consumed in work done to break the TPU-rod reinforcement so that the further descent of the weight carriage was prevented. The

growth of a crack was effectively restrained to a very limited length, and crack propagation was eventually arrested either along the TPU-rod reinforcement or at a junction of the webs. The increase in snagging resistance is therefore mainly attributed to the extruded TPU-rod reinforcement. It is known that these extruded polymer rods have a highly oriented molecular structure from the forming process, and the fiber strength increases directly with the draw ratio.[181]

For carbon fiber reinforced material, the fibers also play a major role in bearing the impact energy of the carriage. As soon as the probe encounters the fiber, the carriage has to spend energy debonding, dragging, and breaking fibers before the probe can descend and the crack can propagate. The carriage impact forces were transmitted into the carbon fibers, and redistributed through the webs. It was observed that some carbon fibers were in a wavy pattern near the tear regions. The fibers sometimes broke near where the probe had contacted the sheet, but at other times it had broken several web junctions away from the probe contact point. The wavy patterns reveal the way that stiff carbon fibers in an elastomer matrix can improve dynamic tear resistance. The wavy patterns are observed in fibers that have been broken and debonded. Following the fracture of the carbon fibers, the adjacent elastomer sheath around the fibers is stretched further along the fiber direction. At first it transmits load between the broken ends of the carbon fiber, but with debonding spreading back along the fibers from the broken ends, the sheath stretches more than the broken segments of the carbon fiber all along the debonded length. The tensile stress acting on the sheath in the direction of the fiber would cause it to contract around the debonded fiber. On unloading, the tensile stress is

released in the elastomer. As the elastomer recoils, it exerts (through shear) a compressive stress on the fiber, causing it to buckle into the wavy pattern observed. The significance of the wavy pattern is that it shows that there was relative shear on the interface between the fibers and there surrounding elastomer sheaths which continued after the carbon fibers had broken. So even after failure, the carbon web continues to support some of the load. Part of the energy of the carriage is thus used up in breaking the fibers, in debonding the fiber from the elastomer, and in shearing the sheath along the fiber. The amount of energy consumption is a function of the number of strands in the carbon fiber, and the adhesion between carbon fiber and TPU sheet matrix.

It is seen from *Fig. 5-8* that 3K carbon fiber reinforced TPU sheet has better snagging resistance than the 1K carbon fiber case because the fibers are stronger and so more friction work is needed to break the fibers initially. They also have a larger contact area between the fibers and the surrounding elastomer sheath. Although a carbon fiber has quite a high modulus and strength, its graphitic structure determines its brittle nature.[182] These PAN-based carbon fibers have poorer impact resistance in the direction transverse to the fiber axis direction than along the fiber direction. In spite of their brittleness, the carbon fibers arrested the tear at the first fiber strand or after only one fiber strand had broken. TPU sheets reinforced with carbon fiber were tougher than unreinforced materials, but they have a lower dynamic tear resistance than the TPU-rod reinforced TPU sheets.

As is evident in *Fig. 5-9*, commercial polyester scrim with the reinforcements aligned in the horizontal and vertical directions both produced a low energy tear

separating along the cloth thread direction. With the carriage direction parallel to the fibers, tear resistance is very poor, which is 21 to 94% smaller than TPU single sheet. When the scrim sheet was rotated 45° in the snag test, the failure changed into a V-shape failure with significantly improved tear resistance approximately matching unreinforced thermoformed TPU double sheet, but it is still far lower than the TPU elastomer sheet reinforced with TPU-rod (*Fig. 5-10*), or the carbon fiber reinforced TPU. The dynamic tear resistance of TPU elastomer sheet reinforced with TPU-rod is 186-389% higher than polyester scrim in the parallel to cloth thread direction, and is 44-105% higher than polyester scrim in the 45° to cloth thread direction. It is proposed that the lower dynamic tear resistance of TPU reinforced with polyester scrim is due to the polyester scrim reinforcement stiffening the material sufficiently that there is no mechanism to redistribute the concentrated point load of the sharp probe.

5.4. Summary

Sparsely reinforced TPU sheet materials have very high dynamic tear resistance. The best toughness occurs when the sparse reinforcement is extruded TPU-rod, but carbon fibers also contribute significantly to snagging resistance. In contrast, the closely spaced stiff fiber, polyester scrim coated with TPU had poor snagging resistance in the ASTM Standard test for snag resistance. In tough materials, the tear extends roughly perpendicular to the main normal stress direction to give the sheets a "V"-shape tear. It is suggested that the typical two phase structures of the TPU material assists the TPU elastomer sheets to form "V"-shape tear in the snagging tests. The dynamic tear

resistance is affected by TPU sheet orientation and thickness, and is increased most when TPU sheet is sparsely reinforced with TPU-rod or carbon fibers. The dynamic tear resistance is higher in parallel to extrusion direction than in the transverse to extrusion direction. Thicker sheet has a higher dynamic tear resistance.

CHAPTER 6

UNIAXIAL TENSION DEFORMATION BEHAVIOUR OF SPARSELY REINFORCED TPU ELASTOMER SHEETS

6.1. Rubber-like Elasticity

6.1.1. General Features of Rubber-like Behaviour

The most noticeable and important physical feature of natural rubber and other rubber-like elastomers is the ability to undergo large and reversible elastic deformation under the action of comparatively small stresses. The maximum extension normally lies within the range 500-1000 per cent. The force-extension curve is markedly non-linear (i.e. Hooke's law does not apply). It is not unexpected that stress can cause polymeric molecules to adopt an extended configuration, but at first sight it may seem surprising that on removal of the stress the molecules retract, on average, to their initial coiled form. Simple theories of rubber-like elasticity assume, as an approximation, that both extension and retraction occur instantaneously, and neglect any permanent deformation.[183, 184]

6.1.2. Tension Behaviour of TPU Elastomer

The tensile stress-strain deformation pattern for polyurethane elastomers is similar to those of other elastomers.[185] Typically for elastomers the shape of the curve changes

with increasing deformation so that elastic behaviour over the full stress-strain range cannot be defined simply by Young's modulus. The tensile stress-strain curve for a urethane elastomer at low strain can be described by the general equation:

$$\sigma = G(\lambda - \lambda^{-2}) \qquad (6\text{-}1)$$

where σ = stress calculated on the original undeformed cross-section; G = shear modulus (or modulus of rigidity); λ = ratio of strained to unstrained length, the length being the dimension in the direction of deformation. Also,

$$\text{Young's modulus (E)} = \text{stress/strain} = 3G \qquad (6\text{-}2)$$

where strain is for small strain $(l\text{-}l_o/l_o)$. The above relationships will only apply below the elastic limit. For urethane elastomers (and also all conventional elastomers) the elastic limit is about 2.5%. At larger strains the force-extension relation is non-linear.

6.2. Experimental Method

Tests have been conducted using samples die-cut for tensile tests. The tensile test samples were of a modified ASTM D412 Dumbbell type,[186] made with an oversize gage width to allow a reasonable amount of the reinforcing web to be in the gage section as shown in *Fig. 6-1*. The gage length and width of the die are 102 mm and 45 mm respectively.

The tensile tests were performed on a srew-driven Instron universal test machine through pulling the grips apart according to ASTM D412. The force vs displacement was recorded continuously on a chart. The maximum load and displacement were stored in the Instron machine memory. The test materials were unreinforced thermoformed TPU

double sheets, TPU sheets reinforced with TPU-rod, carbon fibers, and polyester scrim.

With the present equipment avaiable, the tensile test samples can only be extended out to about 350%, limited by the extent of screw travel. For the present, all that can be reported are modulus values out to that value.

6.3. Results and Discussion

The tensile test results are shown in *Figs. 6-2* to *6-4* and Table 6-1. The unreinforced thermoformed double TPU samples, as well as most samples reinforced with TPU-rod or carbon fibers stretched out to the limit (350 %) of the tensile tester without failure.

6.3.1. Effect of TPU-rod Reinforcements on Tension Deformation

The uniaxial tensile deformation behaviour of the TPU-rod reinforced sheets generally follow a path similar to the unreinforced TPU sheets as shown in *Fig. 6-2*. There was a 43% increase in initial stiffness at low displacement (~3 cm) for square, diamond, and triangle patterns, compared with unreinforced thermoformed TPU double sheets. It is believed that this increase in initial stiffness is due to the incorporation of of the extruded TPU reinforcement with higher hardness. As well there is the extra volume of the reinforcements to support the load. As extension continued, TPU sheets reinforced with different reinforcement patterns produced different enhancement in load bearing ability for a given amount of displacement, and almost kept this difference constant as the load continued to increase. The TPU elastomer sheets with a triangle

pattern showed the highest increase in strength, and the square pattern the lowest increase. At a displacement of 20 cm, compared with unreinforced thermoformed double sheet, the amount of increase in load is 29%, 48%, and 61% for square, diamond, and triangular patterns respectively, as seen in *Fig. 6-2e*. The differences in the load enhancement is mainly controlled by the reinforcements mass incorporated with different patterns.

6.3.2. Effect of Stiff Reinforcements on Tensile Deformation

Carbon Fibers. For the carbon fiber reinforced TPU sheets, the force-displacement curves are different from unreinforced TPU elastomer sheet. Generally, the curves have three distinct regions: (i) the load increases linearly up to a maximum value, (ii) the load sharply drops to a restrained force, followed by oscillations, then (iii) the load essentially traced out the deformation behaviour of unreinforced TPU materials: the force continued to increase until failure occured, as shown in *Figs. 6-3 and 6-4*. In region (i), the carbon fibers play the major load bearing role under a tensile force. So the initial stiffness was high during the very early stages of deformation until the fibres were debonded or broken. From that point on the load either suddenly dropped or levelled off. In region (ii) the fibers continued to break into shorter lengths under increasing strain and the load remained more or less constant. Region (ii) is a transition region where the maximum force decreases to a value required to extract the debonded fibers from the matrix. The small oscillations are due to the continuing process where fibers debond, slip, drag, and break in local regions until the fibers and matrix cease to interact.[187] Beyond that strain level, the load-displacement curve followed that of the unreinforced

TPU material. In the region (iii), the TPU matrix becomes the main load bearing support.

From Table 6-2, it is clear that the carbon fiber reinforced sheets bear a higher force than the unreinforced TPU sheet when the displacement was less than 20 cm except for the square pattern in the 3K carbon fiber case. After the displacement reached 30 cm, the force borne was either slightly higher or lower than the unreinforced TPU sheet behaviour.

The initial stiffness of TPU sheets reinforced with 3K carbon fiber is higher than the sheets reinforced with 1K carbon fibers except for the diamond laddered pattern. In the 1K carbon fiber case, the diamond laddered pattern gives a high load value in regions (i) and (ii), followed by triangle, diamond, and square. In the 3K carbon fiber case, the triangle pattern shows the highest and longest load holding at region (ii). The strain range over which the serrations occurred depended on the adhesion between the TPU matrix and carbon fibers, fiber strand, and reinforcement patterns. Increase of bonding, fibers/strand, and amount of fibers added in will promote a longer serrated period of strain.

A few of the reinforced samples failed during the test (marked by X at the end of the path) but most samples pulled out to the end of the beam travel. When failure did occur, it was at the edge of the grip rather than in the gage section.

Polyester Scrim Reinforcements. The main results, shown in Table 6-1 and in *Fig. 6-4e* are that the commercial polyester scrim material has a much higher initial strength (at a cross-head displacement of 5 cm) than the materials produced by author, but at that point the scrim strength drops significantly as the first fibers tear. In contrast, the coarse carbon fiber reinforced materials, after suffering an early drop in strength, later

recover and eventually exceed their initial strength as the urethane stretches out to the limit of the tensile test machine crosshead travel. The commercial scrim material has by far the poorest elongation to complete failure.

6.4. Summary

The reinforcements provide some strengthening at small displacements, but not much at moderate to large displacements. Incorporated of reinforcements may some decrease in elongation though all samples stretched out at least 300%. At the early stage of displacement, the carbon fibers can support higher loads than TPU-rod. The highest strengths at high displacement among the local materials is achieved by the TPU rod reinforced sheets with the TPU-rod in an equilateral triangular pattern.

CHAPTER 7

BIAXIAL TENSION DEFORMATION BEHAVIOUR OF SPARSELY REINFORCED ELASTOMER SHEETS

7.1. Introduction

Bulge testing can be used to obtain the biaxial tensile material properties up to large values of strain. The membranes used in the bulge test usually are elastomeric materials, which often exhibit viscoelastic behaviour. The purpose of the bulge investigation is to characterize the bursting characteristics under biaxial tension deformation for the sparsely reinforced elastomer sheets. The bursting strength of elastomer sheet can be measured as the hydraulic diaphragm bulge strength. Important information for bulge-out strength design includes: the relationship between pressure and the deflection of the polymer sheets; the time needed to blow out the sheet; the deformation to failure, and the fracture phenomena characteristics of the elastomeric sheet under large deformation.

7.2. Bulge of a Plane Circular Membrane

In equi-biaxial tension (inflation), the strain was produced by the inflation of a circular sheet clamped around its circumference by the means of a bulge test. Under equi-biaxial extension, the rubber is stretched by equal amounts in two orthogonal

directions in the sheet. Such a strain occurs in the inflation of a spherical balloon. The state of strain corresponds exactly with that produced by frictionless uniaxial compression, the only difference being in the nature of the applied stress.[188] In equi-biaxial extension all lines in the plane of the extension are changed in the same ratio, and the stress is the same on all sections normal to this plane.

The inflation of a plane circular membrane was first studied experimentally by Treloar[189] and analytically by Adkins and Rivlin,[190] who employed the Taylor's series approach to calculate the deformation of a neo-Hookean membrane. The general theory of nonlinear membranes has been presented in tensor form by Green and Adkins.[191] To date, very few problems pertaining to nonlinear viscoelastic membranes have been investigated because of the inherent complexities associated with nonlinearity , both in geometry and in material.[192] The strain in the sheet is, of course, not uniform over the entire surface, but it is very nearly uniform over a region in the neighbourhood of the centre of the sheet, or 'pole' of the spheroidal balloon, to which the measurements of strain are usually confined.[188]

The problems examined here consider only thin sheets in which the through-thickness stress σ_3 will be taken as approximately zero, i.e. plane stress.[193] As the sheets are thin it will be further assumed that they are incapable of supporting shear stresses. As a result, a biaxial system of membrane stresses σ_1 and σ_2 will be present as described in *Fig. 7-1*. The extensions will be given in terms of the extension ratios λ_1, λ_2 and the through-thickness λ_3 value is determined from the further assumption of constant volume: The extension ratios may be written as:

$$\lambda_1\lambda_2\lambda_3 = 1; \qquad \lambda_3 = \frac{1}{\lambda_1\lambda_2} \tag{7-1}$$

$$\lambda_1 = \frac{\delta l}{\delta r_o}$$

$$\lambda_2 = \frac{r}{r_o} \tag{7-2}$$

$$\lambda_3 = \frac{t}{t_o}$$

The meridional extension ratio λ_1 is the local value (taken along a line from the centre of the dome to the rim) where δr_o is the unstrained length of that segment and δl is the inflated length of a segment of a radial line. The circumferential extension ratio λ_2 is for the change in length of a circular segment of the membrane originally at some radius r from the centre to the original circumference C_o. Because of symmetry, the ratio of its new circumference length C to the original circumference C_o will be r/r_o. λ_3 is the extension ratio through the thickness.

If the bulging sheet problem is considered then it is not an unreasonable assumption to consider the section as the cap of a sphere for the early stages of inflation. At any instant, the central portion of the bulging specimen is equivalent to part of a thin spherical shell yielding under internal pressure as shown in *Fig. 7-2*. Thus the shape of the bulged specimen may be taken as:

$$r = R \sin\beta \tag{7-3}$$

where R is the radius of the sphere. A displacement transducer measures the height change h in the centre portion, and the radius can be calculated from this reading. If a is the radius of the clamp, then from the geometry we have

$$R = \frac{a^2 + h^2}{2h} \tag{7-4}$$

The strain at all points is assumed to equal:

$$\lambda_1 = \lambda_2$$

The pressure is related to the tensile force F per unit length of section by the equation

$$P = \frac{2F}{R}$$
$$F = \sigma_2 \lambda_3 t_o \tag{7-5}$$

A pressure transducer measures the bulge pressure and the membrane stress is given by:

$$\sigma_1 = \sigma_2 = \frac{PR}{2t} = \left(\frac{PR}{2t_o}\right)\lambda_1^2 \tag{7-6}$$

These equation strictly apply only at the pole of the bulge. The method of analysis of the stresses is generally applicable for any curved membrane.[194] If the membrane is not spherical in the segment considered, the equation becomes:

$$\frac{\sigma_1}{r_1} + \frac{\sigma_2}{r_2} = \frac{P}{t} \tag{7-7}$$

where t is the membrane thickness and r_1 and r_2 are principal curvature directions at the point in question. The lines in the membrane along which these radii are measured are always orthogonal, and represent a minimum or a maximum at the point in question. For the case of a spherical membrane, this reduces to Equation (7-6).

7.3. Hydraulic Bulge Tests

7.3.1. Bulge Testing Apparatus

The bulge testing apparatus for this investigation has been designed and

constructed as shown in *Fig. 7-3*. The basic elements are a hydraulic system, pressure vessel and signal-processing unit.

The hydraulic unit consists of a pump (positive displacement rotary gear pump: TEEL-7P041), an in line flowmeter (FL-505), regulator valves, and connecting pipes. The capacity of the pump can run up to 689.5 KPa (100 psi). The flowmeter has an accuracy ±5% full scale and can directly read flow rate for water to 1.89-18.9 LPM (0.5-5 GPM) at 1724 KPa (250 psig).

The pressure vessel unit includes a pressure gage, clamping rings, pressure chamber, air and water release valves, protective cover, and support table. The detailed diagram of the pressure chamber is given in *Fig. 7-4*. The clamping ring is 28 cm in diameter and is attached to the pressure chamber with an airtight gasket. The pressure chamber was connected through a pipe line to the pump which supplied hydraulic pressure. The whole protective cover was completely sealed with clear silicon to prevent water from leaking and splashing at the time the sheet is bulged out.

The signal-processing unit is composed of a data acquisition system , sensors, and computer. The data acquisition system is an adapted Sciemetric Instruments Inc.'s Gen200 system. It consists of a Model 294 Wall mount system chassis, Model 294P-40 power supply for Model 294 Chassis, Model 802 interface card, Model 231 integrating A/D converter module, Model 252 32 channel analog expansion module, Model 206A bridge/strain gauge conditional module, and Gen200 software package (Ver 3.5).

The Model 231 is an Analog to Digital converter module. It is designed to be used with an analog channel expansion unit to provide a multi-channel A/D conversion

system. It is capable of measuring voltage, resistance, current and frequency signals, on any channel, with multiple ranges.

The Model 252 is a 32 channel analog expansion module designed to be used with an analog-to-digital (A/D) module such as the Model 231. This module provides 32 analog channels, and can be daisy chained with other such expansion modules to accommodate up to 256 (differential) or 512 analog channels per A/D module.

The Model 206A bridge conditioning module is designed to interface and simplify the connections of various bridge-type sensors to the SYSTEM 200, such as load cell, pressure sensors, LVDT's, strain gauges, etc.

The analogue signals have a range of ±5~±10 V and a variety of signals such as pressure, strain, voltage, resistance can be selected. In this apparatus, a pressure transducer sensor (PX302-100GV) and an ultrasonic position sensor (940-A4V-2E-1C0) were used to track the pressure-distance-time data through the data acquisition system. The data in the tests was continuously monitored, displayed and recorded in the computer.

The ultrasonic position sensor is positioned on the centre of the top of the protective cover (*Fig. 7-3*). It is protected by a cone-type box to reduce water splashing. The height of the cone is designed to be just the distance of the ultrasonic sensor's dead zone. The ultrasonic sensor has a maximum sensing distance of 1200 mm. The operating principle of the ultrasonic sensor can described as follows:

Ultrasonic sensors have an acoustic transducer which is vibrating at ultrasonic frequencies. The pulses are emitted in a cone-shaped beam and aimed at a target object. Pulses reflected by the target to the sensor are detected as echoes. The device measures

the time delay between each emitted and echo pulse to determine the sensor-to-target distance. Ultrasonic sensors have a "dead" zone in which they cannot accurately detect the target. This is the distance between the sensing face and the minimum sensing range.

In present case, the minimum distance is 150 mm. The main parameters of ultrasonic sensor are listed in Table 7-1. A 10 V excitation voltage is needed when the ultrasonic sensor is connected with the data acquisition system. The Model 253-32 channel analog expansion module is linked to the ultrasonic sensor to accept the input signal. The pressure transducer sensor has a bridge type millivolt output, which is connected with Model 206A bridge/strain gauge conditioning module.

7.3.2. Bulge Testing

Bulge tests were performed under hydraulic pressure supplied by the hydraulic system. The procedure was as follows. Water was put into pressure vessel until it was full. The specimen was then clamped tightly between the rings, and any air trapped in pressure vessel was fully evacuated through the air release valves. Then the sheet was subjected to a uniform pressure causing a biaxial strain bulge in the material driven by the hydraulic system, and was gradually bulged out. The bulging rate was controlled through the flowmeter and the regulator valves at the flow rate range of 2.2 litres per minute. The pressure-deflection characteristics of a circular membrane clamped at the edge will depend on the diameter of clamps. Here, a fixed diameter ring of 28 cm only was used.

Pressure-distance-time data from starting test to failure were measured by a

pressure transducer sensor and an ultrasonic position sensor through the data acquisition system. The deflection of the specimen during the membrane inflation is defined as the height of the centre of the bulge. The pressure vs the vertical displacement of the middle of the membrane is measured to failure; the latter is defined as leakage through the membrane. The burst strength of an elastomer sheet is the pressure required to rupture the sheet.

The central part of the bulge is very nearly spherical and the spherical region increases with the bulge height. Since no membrane solution is expected to be sufficiently accurate near the clamped edge, it is reasonable to assume the bulge to be entirely spherical when large strains are considered.[195] Strength-deflection response provides an indication of the capacity of sheet to absorb energy. Strain and current thickness can be derived from the measured height, and stress can be computed from pressure, radius of curvature, and thickness as discussed above.

7.3.3. Materials

The materials tested include unreinforced TPU both in single thickness (0.3 mm) and thermoformed double thickness (0.54 mm), and the reinforced thermoformed TPU double sheets with carbon fibres (1K and 3K), or TPU elastomer rod. For comparative purposes, a commercially available polyester scrim material coated on both sides with urethane was also tested. Two other commercially available sheet materials, polyethylene film (0.1 mm in thickness), and high impact polystyrene (0.77 mm in thickness) were also tested for comparative purposes.

7.4. Results and Discussion

7.4.1. Sequence of Bulging Deformation Process

The bulge test process of the TPU sheets sparsely reinforced with either TPU-rod or carbon fibres can be visualized by the sequence profiles as shown in *Fig. 7-5*. It was observed that the unreinforced TPU sheets can undergo very large deformation. When the reinforcements are incorporated, the amount of deformation was constrained to some extent depending on the reinforcement types, but they still can experience relatively large deformations, especially compared with commercially available scrim. The deflection of the scrim was 91 mm, but for sparsely reinforced TPU sheets, the deflection was in the range of 205 to 378 mm at the time of failure. The advantage of the sparsely reinforced TPU sheets are that they are not only able to support a high pressure but they also able to undergo a large deformation before failure.

7.4.2. Characteristic Curves of Bulge Tests

The bulge test results of the unreinforced and reinforced TPU sheets are displayed in *Figs. 7-7 to 7-10*. The biaxial tension deformation behaviour for the unreinforced TPU elastomer sheets and the TPU sheets sparsely reinforced with TPU-rod and carbon fibres are similar to the behaviour in uniaxial tension as mentioned in Chapter 6. Typically, the shape of the curves changes with increasing deformation such that the elastic behaviour over the full stress-strain range cannot be defined simply by Young's modulus. Generally, it is noticed from the bulging curves that the pressure required to bulge reaches a maximum first, then the materials will continue to extend symmetrically under falling

pressure to failure. However, in the case of the unreinforced TPU sheets, the falling pressure will settles out to a constant value, and eventually the pressure may rise again until fracture intervenes.

It is also observed from the bulge tests that the deformation curves for the TPU-rod reinforced sheets display smooth curves like these of the unreinforced TPU sheet as revealed in *Fig. 7-6, 7-9*, but the TPU sheets reinforced with carbon give the serrated curves seen *Fig. 7-7, 7-8*. The individual serrations on the pressure vs deflection curves are due to carbon fibres debonding, breaking and pulling-out. The peak height reached depends on carbon fibre strand, and the adhesion between the carbon fibres and the matrix. The deformation curves followed the thermoformed TPU double sheet after the fibres on the dome surface area were broken.

7.4.3. Effect of Thickness of TPU on the Bursting Strength

The effect of the thickness of the TPU on bursting strength was also studied. Interestingly, the burst strength for the unreinforced TPU sheet is roughly proportional to the sheet thickness. The thickness of the three sheets shown in *Fig. 9* are 0.3, 0.53 and 2 mm. The maximum pressures were 17.7, 29 and 119 KPa, giving pressure/thickness ratios of 59, 54.7, and 59.5 [KPa/mm] respectively. In the 2 mm case, the sheet could not be tested to failure due to the limit of the protective box size, but the comparison is given at maximum pressure.

7.4.4. Effect of Reinforcements on the Maximum Bursting Strength

As summarized in Table 7-2, the pressure required to bulge unreinforced TPU or TPU-rod reinforced materials reached a maximum after a central vertical deflection in the

105-120 mm range. Note that a vertical deflection of 140 mm would represent an ideal hemisphere. The TPU sheets reinforced with TPU-rod have approximately the same or higher deflection than the unreinforced TPU materials before reaching the maximum pressure. There is a difference in the behaviour of the 3K carbon fibre reinforcement (seen *Fig. 7-10*). The amount of deflection at maximum burst strength is significantly reduced. The pressure build-up is very fast, and quickly reaches a maximum at a deflection of around 60-90 mm. Then, as soon as the fibres have been debonded or broken the deformation behaviour approaches that of unreinforced thermoformed TPU double sheet. So, as expected, the initial stiffness of the material reinforced with 3K carbon fibre shows an increase, compared with unreinforced thermoformed double sheet, but the early local failure of the fibres is not followed by immediate rupture.

7.4.5. Effects of Reinforcements on Burst-Deflection Characteristics

7.4.5.1. Effect of Flexible Reinforcements

Generally, the TPU reinforced sheets can bear a higher maximum pressure and pressure at failure than unreinforced thermoformed double TPU sheets as shown in *Fig. 7-6* and in Table 7-3. The amount of increase is dependent on the arrangement of the web patterns and reinforcements. The triangle pattern displays the highest load bearing ability, compared to the square or diamond patterns. For the triangular web, the bulge strength was 35% higher than for unreinforced thermoformed double sheets, and is 116% higher than a single sheet of the TPU. For both unreinforced and TPU reinforced materials, the maximum pressure reached is approximately proportional to the total

mass/unit area of polyurethane. This implies that an equivalent bulge strengthening could be obtained by simply using thicker material rather than by isolated reinforcing webs. However, using a TPU reinforcement web does produce a material with a much higher tear strength. The TPU sheets reinforced with the TPU-rod, either in solid or hollow form, were also examined. The results in *Fig. 7-11* show that the solid TPU-rod performs a better reinforcing role, which supported a higher bursting pressure and larger deflection.

7.4.5.2. Effect of Stiff Reinforcements

When carbon fibre reinforcements are incorporated, the initial stiffness is increased in the bulging tests. The TPU sheets reinforced with 3K carbon fibre increase the load bearing ability between 22 and 160% at the maximum pressure reached, depending on the reinforcement patterns. As shown in *Fig. 7-7*, the composite made with the 3K carbon fibre with a triangular pattern has the highest burst strength. The maximum pressure reached is 160% higher than the unreinforced TPU double sheet, 330% higher than TPU single sheet, and 95% higher than the triangle pattern reinforced sheet with TPU-rod. In the 1K carbon fibre case (*Fig. 7-8*), the load bearing ability is lower than 3K carbon fibre but still is 11.4 to 23.3% higher than unreinforced TPU double sheet. In summary, for carbon fibre reinforced TPU sheet, the maximum burst strength is a function of the strand size, bonding, and web pattern. The amount of load enhancement is affected by the web patterns. The highest reinforcement effect is given by the triangle pattern and the square pattern has lowest reinforcement effect.

The commercial polyester scrim is very stiff, and it has a brittle fracture character

as shown in *Fig. 7-12*. This reinforced material could not withstand large deformation like that of the 3K carbon fibre material. As soon as the highest pressure was reached, the first polyester fibres broke and failure occurred immediately. But the maximum pressure required was twice as high as the TPU sheet reinforced with 3K carbon fibre of triangle pattern.

7.4.6. Effect of Different Materials on Burst-Deflection Characteristics

Figure 7-13 illustrates the bulge test results for polystyrene, polyethylene and polyurethane sheets. The high impact PS has a very poor bulge behaviour. It can withstand a relative high pressure but the deflection was very small and the time to failure was short. *Figure 7-14* compares the time needed to bulge the sheets to failure for different materials, reinforcements, and patterns. For sparsely reinforced materials, the bulging out time is the shortest for the triangular pattern (*Fig. 7-14a*). It is thought that the deflection and the time to failure are affected by the maximum pressure reached by the sparsely reinforced materials. Compared to the other materials (*Fig. 7-14b*), the time to failure for the polystyrene is the shortest, less than 50 seconds. The longest bulge time is given by single TPU sheet. This good bulging characteristic of the TPU materials may result from the fact that the TPU chains contain a large number of polar groups and, since the chains are not bound closely together by short covalent chemical bonds, these polar groups are free to align themselves and form relatively strong physical-chemical bonds. The large number of these polar groups prevents the chains sliding over each other under an applied stress, and this effect results in TPU of very high elongation.[19]

7.4.7. Formation of Craze II under Bulging Tests

7.4.7.1. Classification of Craze

According to Kausch, crazes exist in two different forms:[197, 198]

- Conventional or extrinsic crazes (crazes I) which are preferentially formed at sample surfaces and under the influence of defects acting as stress concentrators.
- Intrinsic crazes (crazes II) which are formed after notable stretching in the whole sample volume and as a consequence of the breakdown of the entanglement network; intrinsically crazed samples appear thoroughly whitened.

Typically, extrinsic crazes (crazes I) are initiated at an early stage of deformation, well below the yield point. They start growing from surface defects. At high stresses and strains, well above the yield point, numerous crazes (crazes II) are initiated throughout the sample volume. The large number of crazes II give rise to the phenomenon of stress-whitening.

7.4.7.2. Formation of Craze for TPU Materials under Bulging Deformation

For all the TPU sheet materials, it was noticed that a craze phenomena appeared when the height of the deflection approached about 240 mm as shown in *Fig. 7-5*. The time required for the formation of crazes is an inherent characteristic. The craze first occurred around the top pole point where the strain is a maximum, and is equi-biaxial. The area of the craze surface propagated as the height of the deflection was increased. The failure of the bulge occurred after a significant part of the dome had turned colour from transparent to an opaque bright white.

7.4.7.3. Clarification of Crazes Occurring under Bulging Deformation

It is suggested that the crazes which occurred in bulge test are intrinsic crazes because the crazes were seen after the maximum pressure was reached. Crazing is a mechanical separation of polymer chains or groups of chains under tensile stress. According to Kausch,[197, 198] craze initiation occurs preferentially in regions where chains were oriented transversely to direction of stress. The development of craze surfaces is at right angles to the principal tensile stress direction, and is clearly linked to the dilatational (hydrostatic) component of the applied stress. Once craze is initiated, crazes can grow under continued stress. In the case of the present bulge tests, near the pole of the bulge, the stresses are close to equi-biaxial with in-plane shear close to negligible. This means that for any two arbitrarily chosen orthogonal directions in the plane of the sheet, the tensile stresses will be high and close to equal in both directions. If, for any reason there is local molecular alignment, then the tensile stress transverse to this alignment will be high. This is the condition that will favour Craze II initiation.

7.4.8. Effect of Reinforcements on the Failure Mode under Bulging Deformation.

Another interesting phenomena observed is that the incorporation of reinforcements can prevent sheet materials from failing by simultaneous multiple crack paths, as shown in *Fig. 7-15*. Failure of the reinforced sheets in bulging starts around the pole position on the top surface of the dome. Then, a crack propagates rapidly along the path of a reinforcement, and eventually arrests at a reinforcement fibre, the strongest point of resistance being fibre junctions.

In contrast to this, unreinforced single sheet failure has simultaneous multiple crack growth radiating out from the central craze. Generally, failure starts at the top surface of the centre pole point, then cracks quickly grow along many directions to the clamp rim at very high speed. This "explosion" produces many broken segments of sheet as shown in *Fig. 7-15a.*

7.4.9. Effect of Bulging on the Microstructures of the Materials

Figure 7-16 shows microstructural pictures of the single TPU sheet before and after bulge testing. It is seen the appearance of the bulged out TPU sheet changed from a uniform flat sheet to a bubble type of sheet. The large deformation behaviour of TPU can be explained by the TPU structures. As mentioned Chapter 2.1.2., urethane elastomers are generally accepted to have a two-phase structure in which rigid segments separate to form discrete domains in a matrix of soft segments. Van der Waals and hydrogen-bonded interaction are considered to hold together the individual discrete domains of the rigid segments. It is thought that the bubble type deformation was caused by permanently deformed hard segments and soft segments. The molecular chains of hard segments and soft segments were stretched upon loading to higher strain, but the relaxation of the soft segment chains and hard segment chains would be different when the load was removed. Craze also plays an important role. So internal curved surfaces were formed as in *Fig. 7-16b.*

Figure 7-17 is an acoustic C-scan image of the high impact PS after bulge test, examined by wide field pulse ultrasonic microscopy. A few nodes (butterfly-shape) are

noticed in the image. It is proposed these nodes are probably a high stress concentration locations where the failure occurred, between the PS and its rubber microconstituents. This explains the many short seam type cracks which developed during the bulging failure.

7.5. Summary

Elastomer TPU sheet sparsely reinforced with carbon fibre or with TPU-rod can bear a high load and undergo relatively large deformation in bulge tests. The triangular pattern shows the highest load support ability among the three web patterns. The maximum pressure is increased proportionally with the thickness of unreinforced TPU sheet. Incorporating reinforcements into TPU sheet changes the fracture mode. Reinforcements act as an effective barrier to hinder crack propagation and to prevent the bulged TPU sheets from breaking simultaneously into multiple pieces. Formation of intrinsic crazes (Craze II) in TPU sheets in the biaxial strain region occurs after a deflection of about 240 mm , and is manifested by whitening of the sheet. Failure of the sheet follows shortly thereafter. High impact PS and Polyester scrim show brittle fracture under biaxial tension testing.

CHAPTER 8

PUNCTURE BEHAVIOUR OF SPARSELY REINFORCED TPU ELASTOMER SHEETS

8.1. Penetration Resistance

Penetration Resistance is the ability of a flexible sheet material to withstand elongation and /or puncture by a probe driven perpendicular to a clamped sheet surface.

Penetration resistance is an important end-use performance parameter of thin flexible materials where a sharp-edged product can destroy the integrity of a barrier wrap. This will permit package entry/exit of gases, odours, and unwanted contaminates, causing potential harm to the product and reducing shelf-life. In the transportation of the liquids, if an accident happens, some sharp broken edges or spikes of the crashed tank may pierce inward onto the membrane of the tank to cause leakage. So the slow rate penetration test is one of the representative tests for sparsely reinforced TPU elastomer sheet potentially used as a liner materials in tank cars. Material response to penetration will vary with numerous factors, such as film thickness, elastic modulus, rate of penetration, temperature, shape and type of probe.

8.2. Slow Penetration Tests

8.2.1. Apparatus

Slow penetration tests were conducted according to the ASTM F1306-90 on an

Instron universal testing machine.[199] The apparatus for slow rate penetration tests comprises a specimen clamping fixture, compression load cell, and a support shaft for the penetration probe.

The specimen clamping fixture is shown in *Fig. 8-1*. The bottom plate of the fixture is screwed down onto the movable beam of the Instron machine, where the grip is usually installed. The specimen is clamped in a ring-shape holder with a 35 mm through hole on the top of the fixture. Tightening force is applied by the four screw knobs on the top of the fixture.

The penetration probes were designed as the two types shown in *Fig. 8-2*: (a) a relatively sharp pointed indentor; (b) a screwdriver-like indentor which allows the probe to engage a reinforcement to examine the effect of the fibers. This latter probe was specially designed for this study. Therefore, the slow rate penetration tests are refered to as the "sharp point slow puncture test" or "dull edge slow puncture test" depending on the probe type. The dimension and shape of the two penetration probes are displayed in *Figs. 8-3, 8-4*.

The connecting support shaft is used to link the compressive load cell and the penetration probe. The apparatus of the penetration test is shown in *Fig. 8-5*.

8.2.2. Slow Rate Penetration Tests

In the slow rate penetration test, the sample holder is directly placed and centred under the crosshead probe. The crosshead probe should be as close as possible to the test specimen possible without making direct contact. The clamping fixture sitting on the movable beam is driven upwards, and the sharp-pointed or screwdriver-like penetration

indentor is pushed into a membrane which is tightly clamped in the ring-shaped holder. For the dull edge slow rate test, the screw-like indentor should aim at either a fiber or a joint of a reinforcement if possible. The resistance force as a function of penetration depth is recorded on a chart of the Instron machine.

The distance the probe travels from sheet contact to an instantaneous drop in load as observed on testing equipment recorded is defined as probe penetration to failure. The energy stored in the sheet at failure can also be found by integrating the force-distance curve. A higher force and depth of penetration to failure contribute to better penetration resistance.

8.3. Results and Discussion

Generally, the curves for both sharp-point and dull-edge slow rate tests have the features shown in *Fig. 8-6*, but for stiff fiber reinforced sheet materials, a serrated type curve replaces the smooth curve. The summarized results of the slow rate penetration tests are given in Table 8-1 and 8-2.

8.3.1. Sharp Point Slow Rate Tests

In this test, Table 8-1 shows that the TPU unreinforced double-sheet had the best penetration resistance as judged by a combined resistance force, penetration depth and energy criterion. The commercial polyester scrim had the poorest properties. The TPU material reinforced with carbon fiber or TPU rod all gave good results though not quite as high as the unreinforced material. As the thickness of the TPU sheet increases from single sheet to thermoformed double sheet, the penetration force and stored energy

required to puncture the TPU sheets is proportionally increased: see Table 8-1.

8.3.2. Dull-edge Slow Rate Tests

A modified test in which a screwdriver-like indentor (*Figure 8-2*) was pushed into the materials using the same clamping device gave slightly different results (Table 8-2). In these tests, the performance of the reinforcements resisting the penetration force of the dull-edge indentor is different. The carbon fiber supported the load before it was broken. Then the matrix became the main load supportor. In contrast, the TPU-rod was able to bear the load until failure occurred. Therefore, the TPU rod reinforced material gave both the highest resistance force and the largest stored energy. Adding carbon fibres to unreinforced TPU generally slightly decreased the peak force attained, and decreased the penetration depth, but had little effect on the stored energy compared with unreinforced sheet because the resistance force built up more quickly as a function of penetration depth when the carbon fibers were added. The commercial polyester scrim material had a better resistance force than the unreinforced TPU sheet, but failed after a low penetration distance so that it had the lowest energy to failure.

8.3.3. Effect of Reinforcements on Puncture Resistance

Generally, fibers added into the matrix will increase the stiffness of the material. This means that in the slow rate penetration tests, the reinforcements will constrain the deformation behaviour of the matrix material to some extent. When the sharp indentor pushes into a reinforced sheet, the area of the deformation in the reinforced sheet will be restricted by the size of the spacing in the fiber meshes instead of the clamping hole size.

In this way, the stress concentration factor in this small area causes the local stress to build up to a much higher level than unreinforced material, which has a more unrestricted deformation area 35 mm in diameter. Increase in the stress concentration caused a reduction in the force level for penetration to failure in the reinforced TPU materilas. The smaller the mesh size is, the less the penetration depth will be, as is shown in the case of the TPU reinforced by polyester scrim. It is seen in Tables 8-1 and 8-2 that the polyester scrim has the smallest penetration depth, followed by 3K and 1K carbon fiber respectively. *Figure 8-7* is the photographs of failure samples after slow rate tests. It is clear that the deformation of the reinforced materials was restricted by fiber webs. The deformation area of double sheet is larger than that reinforced sheets, which were limited by the fiber webs as seen in *Fig. 8-7b* to *8-7d*. The penetration of the polyester scrim reinforced materials is concentrated on a small area (*Fig. 8-7d*). The flexible TPU-rod is extendable under the penetration force so the material possesses high energy to puncture and a larger deformation area.

On the other hand, increase of fiber strand and diameter and fiber volume fraction will reduce the depth of penetration of the reinforced sheets due to the increase of the stiffness. In both of these slow rate tests, the penetration depth of the sheets reinforced with 3K carbon fiber are less than that with 1K carbon fiber.

8.4. Summary

The puncture resistance of the sparsely reinforced TPU elastomer sheets approximately matches these of the unreinforced thermoformed TPU double sheets. The polyester scrim reinforced material shows the poorest penetration resistance. The penetration resistance is decreased as the the stiffness of film material is increased.

CHAPTER 9

CONCLUSIONS AND RECOMMENDATIONS FOR FUTURE WORK

9.1. Conclusions

The following conclusions can be made from the present work on the "Development of Sparsely Reinforced Elastomer Sheets":

(1) A specially designed thermoforming processing technique has been successfully used in developing sparsely reinforced TPU elastomer sheets on a laboratory scale. Pretreatment of the carbon fibers is an important step to get good sparsely reinforced thermoformed samples. Also, parameters such as heating rate, forming temperature, vacuum pressure must be carefully controlled to obtain satisfactory thermoformed materials.

(2) Sparsely reinforced elastomers provide a material which is very tough and strong with respect to both tear initiation and tear propagation. TPU elastomer sheets sparsely reinforced either with TPU-rod or carbon fibers show an evident increase in the tear resistance, without compromising their elongation properties in a Die C type tear test. The reinforcing webs serve as an effective barrier to hinder the crack growth.

If the sparse reinforcement is itself an elastomer, then both the junctions of the reinforcement and the reinforcement itself act as crack arrestors, thus providing a very effective way to improve the tear resistance and elongation of the elastomer sheets.

If the sparse reinforcement is carbon fiber, the notch sensitivity of the crack front was reduced in the tear test. Then crack propagation was hindered by fiber pull-out forces. Fiber pull-out both raised the load and increased the extension required of the samples to complete the fracture. Debonding of fibers ahead of a crack tip or behind a crack tip is an important energy absorption mechanism. Use of an annealing process is an effective way to improve the close contact between the carbon fiber and TPU matrix and to increase the tear resistance.

If the stiff reinforcements are spaced closely together, then the initial stiffness of the composites is increased, but the tear resistance is decreased.

(3) Sparsely incorporated reinforcement in the TPU elastomer sheet changed the fracture morphology of the torn samples from a shiny flat surface into a rough wavelike surface. It is recognized from the fracture morphology that the flat featureless regions in unreinforced TPU sheet correspond to relatively fast crack growth whereas rough wavelike regions in the reinforced TPU sheets apparently correspond to slow crack growth.

(4) Sparsely reinforced TPU sheet materials have very high dynamic tear resistance. The best toughness occurs when the sparse reinforcement is extruded TPU-rod, but carbon fibers also contribute significantly to snagging resistance. In contrast, the closely spaced stiff fiber in commercial polyester scrim coated with TPU had poor snagging resistance in the ASTM Standard test for snag resistance.

In tough materials such as TPU elastomer sheets, the tear extends roughly perpendicular to the main normal stress direction to give a "V"-shape tear, otherwise the

tear path shows a "slit"-shape tear in a low dynamic tear resistance material.

The dynamic tear resistance is affected by TPU sheet orientation and thickness. The dynamic tear resistance is higher in parallel to extrusion direction than in the transverse to extrusion direction, and is increased most when TPU sheet is sparsely reinforced with TPU-rod or carbon fibers.

(5) In the tension tests (unaxial and biaxial tension), carbon fibers (1K and 3K) increase the initial stiffness of the TPU elastomer sheets. After the carbon fiber is pulled out or broken, the elastomer sheet behaves like the thermoformed TPU double sheet. Elastomer TPU sheet sparsely reinforced with carbon fiber can bear a high load and undergo relatively large deformation in the bulge tests.

For the TPU-rod sparsely reinforced TPU elastomer sheets, the load bearing ability is increased. The amount of strength increase is roughly proportional to the wt% amount TPU-rod fiber incorporated. The same strength could be achieved by using a thicker sheet with the same weight/m^2. Sparse flexible elastomer webs are not a cost effective reinforcement to improve the tensile or biaxial strength of elastomers. It is less expensive to just use a thicker material.

Incorporating reinforcements into TPU sheet changes the fracture mode in the biaxial tension tests. Reinforcements act as an effective barrier to hinder crack propagation and to prevent the bulged TPU sheets from breaking simultaneously into multiple pieces. The triangular pattern shows the highest load support ability among the three web patterns.

It is suggested that the crazing occurring in the TPU sheets in the near biaxial

strain region after deflections of about 240 mm are intrinsic crazes (Crazes II).

(6) The puncture resistance of the sparsely reinforced TPU elastomer sheets approximately matches these of the unreinforced thermoformed TPU double sheets. The polyester scrim reinforced material shows the poorest penetration resistance. The penetration resistance will be decreased as the stiffness of film material is increased.

9.2. Recommendations For Future Work

The current project "Development of Sparsely Reinforced Elastomer Sheets" just finished its initial stage of development in the lab scale. To form a large scale production, more work needs to be done. The following suggestions are proposed for future work.

1). Develop a continuous production process to produce the sparsely reinforced TPU elastomer sheets. If thermoforming technique is to be adapted, a surge vacuum tank should be used in the thermoforming process.

2). Incorporate different reinforcements such as Kevlar aramid fiber or glass fibers for comparison of reinforcement effects with TPU-rod and carbon fiber in sparsely reinforced TPU materials.

3). Complete the impact test, and permeability test of the sparsely reinforced TPU elastomer sheet.

4). Model the bulge behaviour of the sparsely reinforced TPU elastomer sheet under hydraulic bulging test to better understand the biaxial tension deformation at large strain.

References:

1. E. Nalder, Tankers Full of Trouble, Grove Press, New York, 1994.

2. L. Krten, "Statistics Concerning the Transport of Dangerous Goods", Work Term Report, (1993).

3. Canada. Statistics Canada, Rail In Canada 1989, Queen's Printer, Ottawa, p.161-173, (1991).

4. Competition Policy and the Deregulation of Road Transport, Orrganization for Economic and Cooperative Development (OECD), Paris, P. 15-17, (1990).

5. Road Transport Reseach, Transporting Dangerous Goods by Road, OECD, paris, p. 26-32, 35-41, 94, 95, (1988).

6. Transport Dangerous Goods (TDG), TDG Annual Report 1986-87, Department of Supply and Services (DSS) Canada, Ottawa, p. 9-17, (1987).

7. J. V. Milewski and H. S. Katz, Handbook of Reinforcements for Plastics, Van Nostrand Teinhold Co., New York, p. 7, (1987).

8. Bor Z. Jang, Advanced Polymer Composites, ASM International, Materials Park, Ohio, p. 3, (1994).

9. P. Labossière and K. W. Neale, *Polymer Composites*, Vol. 9, p. 306-317, (1988).

10. B.D. Agarwal and L.T. Broutman, Analysis and Performance of Fiber Composites, Published by John Wiley, p. 26-30, (1980).

11. A. A. Berlin, S. A. Volfson, N. S. Enikolopian and S. S. Negmatov, Principles of Polymer Composites, Springer-Verlag, New York, pp. 15, (1986).

12. H. Z. Katz and J. V. Milewski, ed, Handbook of Fillers and Reinforcements for Plastics, New York, Van Nostrand Reinhold Co., (1978)

13. O. Bayer, H. Rinke, W. Sieken, L. Ortner, H. Schild, (to I. G. Farben), *Ger. Pat.* 728 981, (1937).

14. A. E. Christ, W. E. Handford (to DuPont), *US Pat.* 2333 639, (1940).

15. *Brit. Pat.* 580 524 (1941). (to ICI). Brit. Pat. 574 134, (1942).

16. P. Pinten (to Dynamit AG), *Ger. Pat* 932 633, (1943).

17. K. A. Pigott, J. W. Archer, W. Archer, B. F. Frye, R. J. Cote, and J. H. Saunders, *Ind. Eng. Chem. Prod. Res. Develop.*, Vol. 1, No.1, p. 28, (1962).

18. C. S. Schollenberger, H. Scott, and G. R. Moore, *Rubber World*, Vol. 137, p. 549 (1958).

19. N. R. Legge, G. Holden, and H. E. Schroeder, Thermoplastic Elastomers, Hanser Publishers, New York, p. 16, (1987).

20. C. G. Seefried, jr., J. V. Koleske and F. E. Critchfield, *J. Appl, Polym. Sci.* 19, p. 2493 and 3185, (1975).

21. Becker/Braun, Kunststoffhandbuch, 2. Auflage, VII; 63, Carl Hanser Verlag, (1983).

22. R. Roberts (to Union Carbide), *US Pat.* 4055549, (1976).

23. G. Oertel, *Polyurethane Handbook*, 2nd Ed., Hanser Publishers, New York, p. 17 (1993).

24. Jay Bhattacharyya, Handbook of Polymer Science and Technology, Vol. 2, pp. 557, N. P. Cheremisnoff, ed., Marcel Deker, Inc., New York, (1989).

25. G. Woods, The ICI Polyurethane Book, John Weley & Sons, New York, p. 27, (1987).

26. S. B. Clough, N. S. Schneider, and A. O. King, *J. Macromol. Sci. Phys.*, B2 (4): p. 553-566, (1968).

27. S. B. Clough, N. S. Schneider, and A. O. King, *J. Macromol. Sci. Phys.*, B2 (4): p. 641-848, (1968).

28. J. Blackwell and K. H. Gardner, *Polymer*, 20: 13, (1979).

29. S. L. Cooper and A. V. J. Tobolsky, *J. Appl. Polym. Sci.*, Vol. 10, p. 1837, (1966).

30. A. L. Chang and E. L. Thomas, *Adv. Ser. Chem.* Vol 176, p. 31, (1979).

31. R. Bonart, L Morbitzer, and E. H. Muller, *J. Macromol. Sci. Phys.*, B9(3): p. 447-461, (1974).

32. R. F. Harris, M. D. Joseph, C. Davidson, C. D. Deporter, and V. A. Dais, *J. of Appl. Polym, Sci.*, Vol. 41, p. 487-507, (1990).

33. R. F. Harris, M. D. Joseph, C. Davidson, and C. D. Deporter, *J. of Appl. Polym. Sci.*, Vol. 41, p. 509-525, (1990).

34. R. F. Harris, M. D. Joseph, C. Davidson, and C. D. Deporter, *J. of Appl. Polym. Sci.*, Vol. 42, p. 3241-3253, (1991).

35. M. Xu, W. J. MacKnight, C. H. Y. Chen, and E. L. Thomas, *Polymer*, Vol 24, p. 1327-1332, (1983).

36. C. H. Y. Chen, R.M. Briber, E. L. Thomas, M. Xu, W. J. MacKnight, *Polymer*, Vol 24, p. 1333-1340, (1983).

37. J. L. Hong, C. P. Lilya, and J. C. W. Chien, *Polymer*, Vol. 33, p. 4347-4351, (1992).

38. J. S. Koutsky, N. V. Hein, and S. L. Cooper, *J. Polym. Sci. (B)*, Vol 8, p.353, (1970).

39. N. S. Schneider, C. R. Desper, J. L. Illinger, A. O. King, and D. J. Barr, *J. Macromol. Sci. (B)*, Vol. 11, p. 527, (1975).

40. L. L. Harrell, Jr., *Macromolecules*, Vol. 2, p. 607, (1969).

41. J. Blackwell and M. R. Nagarajan, *Polymer*, Vol 22, p. 202, (1981).

42. J. Blackwell and M. R. Nagarajan, and T. B. Hoitink, *Polymer*, Vol 22, p. 1534, (1981).

43. J. Blackwell, M. R. Nagarajan and T. B. Hoitink, *Polymer*, Vol 23, p. 950, (1982).

44. J. R. Quay, Z. Sun, and J. Blackwell, *Polymer*, Vol 31, June, p. 1003, (1990).

45. S. L. Samuels and G. L. Wikes, *Polymer Lett.*, Vol. 9, p. 761, (1971).

46. S. L. Samuels and G. L. Wikes, *J. Polym Sci. Symp. (D)*, Vol. 43, p. 149, (1973).

47. I. D. Fridman and E. L. Thomas, *Polymer*, Vol. 21, p. 388, (1980).

48. I. D. Fridman and E. L. Thomas, L. J. Lee, and C. W. Macosko, *Polymer*, Vol. 21, p. 393, (1980).

49. I. Kimura, H. Ishihara, d H. Ono, N. Yoshihara, S. Nomura, and H. Kawai, *Macromolecules*, Vol 7, p.355, (1974).

50. Y. J. P. Chang and G. L. Wikes, *J. Polym Sci. Polym. Phy.* Ed,, Vol. 13, p. 455, (1975).

51. Y. Minoura, S. Yamashita, H. Okamoto, and T. Matsuo, *Rubber Chem. Technol*, Vol. 52, p. 920, (1979).

52. R. Bonart, *J. Macromol. Sci. Phys.*, Vol. 2, No. 1, p. 115, (1968).

53. R. Bonart, *Angew. Makromol. Chemie*, Vol 58/59, p.259, (1977).

54. R. D. A. Paulmer, C. S. Shan, M. J. Patni, and M. V. Pandya, *J. of Applied. Polym. Sci.*, Vol. 43, p. 1953, (1991).

55. R. W. Seymour, A. E. Allegrazza, and S. L. Cooper, Jr., *Macromolecules*, Vol 6, p. 896, (1973).

56. A. E. Allegrazza, R. W. Seymour, H. N. Ng, and S. L. Cooper, *Polymer*, Vol. 15, p. 433, (1974).

57. G. M. Estes, R. W. Seymour, S. L. Cooper, *Macromolecules*, Vol. 4, p. 452, (1971).

58. G. M. Estes, R W. Seymour, S. J. Boucher, and S. L. Cooper, in Colloidal and Morphological Behaviour of Block Graft Copolymers, E. M. Gunther, ed., Plenum Press, New York, p. 159-71, (1971).

59. S. B. Lin, K. S. Husang, S.Y. Tsay, and S. L. Cooper, *Colloid Polym. Sci.* Vol. 263, p. 128, (1985).

60. R. W. Seymour, A. E. Allegrezza, and S. L. Cooper, *Macromolecules*, Vol 6, p. 896, (1973).

61. G. M. Ester, R. W. Seymour, and S. L. Cooper, *Macromolecules*, Vol 4, p. 452, (1971).

62. C. F. Wikes and C. S. Yusek, *J. Macromol. Sci.*-Phys., B7, p. 157, (1973).

63. R. Bonart, L. Morbitzer, and G. J. Hentze, *J. Macromol. Sci.* -Phys., B3, p. 337, (1969).

64. R. Bonart, L. Morbitzer, and Z. Z. Kolloid, *Polymer*, Vol 241, p. 909, (1970).

65. A. E. Allegrezza Jr, R. W. Seymour, H. N. Ng and S. L. Cooper, *Polymer*, Vol. 15, p. 433, (1974).

66. C. B. Wang, and S. L. Cooper, *Macromolecules*, Vol. 16, p. 775, (1983).

67. J. A. Miller, S. B. Lin, K. K. S. Hwang, K. S. Wu, P. E. Gibson, and S. L. Cooper, *Macromolecules*, Vol 18, p. 32, (1985).

68. T. L. Smith, *Polym. Eng. Sci.* Vol 17, No. 3, p.129, (1977).

69. H. Hespe, et al, *Colloid Polym. Sci.*, Vol. 250, p. 797, (1972).

70. C. Hepburn, Polyurethane Elastomers, 2nd Ed., Elsevier Applied Science, New York, p. 355, (1992).

71. G. M. Estes, S. L. Cooper, and A. V. Tobolsky, *J. Macromol. Sci.*, Vol 4, No. 2, p. 313, (1970).

72. G. M. Estes, R. W, Seymour, and S. L. Cooper, *ibid.*, p. 516, (1970).

73. G. M. Estes et al., *Polym. Eng. Sci.*, Vol 9, p. 383, (1969).

74. D. Puett, *J. Polym. Sci.* A-2, Vol 5, p. 839, (1967).

75. P. Wright and A. P. C. Cumming, Solid Polyurethane Elastomers, Maclaren & Sons, London, (1969).

76. V. Gajewski, Proc. of 33rd Annual Polyurethane Technical/Marketing Conf., p. 506-515, (1990).

77. U. S. Aithal and T. M. Aminabhavi, *Polymer*, Vol. 31, p. 1757, (1990).

78. N. S. Schneider, L. V. Dusablon, L. A. Spano, H. B. Hopfenberg, and F. Votta, *J. Appl. Polym. Sci.*, Vol. 12, p. 527-532, (1968).

79. T. M. Feng, W. J. MacKnight and N. S. Schneider, *Polymer*, Vol. 32, p. 1493-1503, (1991).

80. B. M Walker and C. P. Rader, Eds, Handbook of Thermoplastic Elastomers, Van Nostrand Reinhold Co., New York, (1988).

81. C. S. Schollenberger and F. D. Stewart, *J. Elastoplast.*, Vol. 3, p. 28, (1971).

82. W. J. Pentz and R. G. Krawiec, *Rubber Age*, Vol. 107, No. 12, p. 39, (1975).

83. J. Delmonte, Technology of Carbon and Graphite Fiber Composites, Van Nostrand Reinhold Co., (1981).

84. E. Fitzer, Carbon Fibers and Their Composites, Springer-Verlag Berlin Heideberg New York Tokyo, (1985).

85. J. B. Donnet and R. C. Bansal, Carbon Fibers, Marcel Dekker, Inc., (1984).

86. J. L. Figueirede, C. A. Bernardo, R. T. K Baker and K. J. Hüttinger, Carbon Fiber Filaments and Composites, Kluwer Academic Publishers, (1990).

87. K. K. Chawla, *Mater. Sci. Eng.*, Vol 48, p. 137, (1981).

88. J. Delmonte, Technology of Carbon and Graphite Fiber Composites, Van Nostrand Reinhold Company, p. 47, (1981).

89. G. D. D'Abate and R. J. Diefendorf, Proc. of the 17th Biennial Conference on Carbon, American Carbon Society, p. 390, (1985).

90. W. Watt, *Proc. R. Soc.* A319, 5, (1970).

91. J. V. Milewski and H. S. Katz, Handbook Reinforcements for Plastics, p. 364 (1987).

92. N. C. W. Judd, Proceedings of the First International Conference on Carbon Fibers, Plastics Institute, p. 258, (1971).

93. A. Y. Lou, T. P. Murtha, J. E. O'Connor and D. G. Brady, Thermoplastic Composite Materials, L. A. Carsson, Ed., Elsevier Sci. Publisher B. V., p. 179, (1991).

94. D. Hull, An Introduction to Composite Materials, Cambridge University Press, p. 9, (1981).

95. D. G. Brady and T. P. Murtha, ANTEC'85, p. 1178, (1985).

96. F. K. Ko, *Textile Structural Composites*, T. W. Chou and F. K. Ko, Ed., Elsevier Science Publishers B. V., Amsterdam, p. 129-171, (1989).

97. K. Fukuta, R. Onooka, E Aoki and Y. Nagatsuka, 15th Text. Res. Symp., S. Kawabata, Ed., The Textile Machinery Soc. of Japan, Osaka, p. 36-38, (1984).

98. M. T. Harvey, Handbook of Engineering: Composites, ASM International, p. 544, (1987).

99. P. K. Mallick, Fiber-Reinforced Composites: Materials, Manufacturing, and Design, Marcel Dekker, Inc. New York and Basel, p. 73, (1988).

100. El. M. Asloun, M. Nardin, J. Schultz, *J. Mater. Sci.*, Vol. 24, p. 1836-1844, (1989).

101. 23. P. Ehrburge and J. B. Donnet, *Philos. Trans. R. Soc. London*, A 294, p. 495, (1980).

102. D. H. Berry, ANTEC'95, p. 4365-4368, (1995).

103. S. K. N. Kutty and G. B. Nando, *Plastics, Rubber and Composites Processing and Application*, Vol. 19, No. 2, p. 105-110, (1993).

104. S. K. N. Kutty and G. B. Nando, *J. of Applied Polymer Sci.*, Vol. 42, p. 1835-1844, (1991).

105. S. K. N. Kutty and G. B. Nando, *J. of Appl. Polym. Sci.*, Vol. 43, p. 1913-192, (1991).

106. R. D. A. Paulmer, C.S. Shan, M.J. Patni, and M.V. Pandya, *J. of Applied Polymer Sci.*, Vol. 43, p. 1953-1959, (1991).

107. A. Mateen, A. Shamim, "Thermal Expansion of rigid Polyurethane, Reinforced by Hammer-milled Glass Fiber", *J. of Mater. Sci.*, (1989).

108. J. L. Cawse and J.L. Stanford, *Polymer*, Vol. 28, March, p. 356-367, (1987).

109. H. G. Kia, *Polymer Composite*, June, Vol. 9, No. 3, 237-241, (1988).

110. S.G. Damani, and L. James Lee, *Polymer Composites*, Vol. 11, No. 3, p. 174-183, (1990).

111. J. J. Zwinselman and U. Tribelhorn, Polyurethane 88, p. 61-67, (1988).

112. M. Begemann, G. Menges and W. Michaeli, Polyurethane 88, p. 56-60, (1988).

113. U. E. Younes, 33rd Annual Polyurethane Technical/Marketing Conf., Sept. 30-Oct.3, p. 610-615, (1990).

114. S. Arenz and D. Lausberg, "Glass Fiber Reinforced Thermoplastic Polyurethanes: A New Material for Exterior Body Parts", *SAE Paper: 900079.*

115. H. J. Kogelnik and R. G. Eiben, 32nd Annual Polyurethane Technical/ Marketing Conf., Oct. p. 1-4, 134-138, (1989).

116. R. J. Cavalier and A. J. Dumont, 31st Annual Polyurethane Technical/ Marketing Conf., p. 311-313, (1988).

117. A. G. Andreopoulos, A. V. Konstantinidou, and H. J. Petsalas, *J. Appl. Polym. Sci.*, p. 2073-2078, (1989).

118. J. Harry DuBois, Plastic History, USA, p. 38-51, (1972).

119. W. McConnell, "The Oldest Infant", in P. F. Bruins, Ed., Basic Principles of Thermoforming, Gordon and Breach, p. 3, (1971)

120. Anonymous, "Plastics' Junior Giant," *Modern Plastic*, Vol. 32, 8, p. 87, (1955).

121. Anonymous, "Shape a Sheet," *Modern Plastics*, Vol. 31, 9, p. 87, (1954).

122. J. L. Throne, Thermo Forming, Hanser Publishers, New York, (1986).

123. E. S. Childs, "Thermoforming - Trends and Prospects", in P. F. Bruins, Eds., Basic Principles of Thermoforming, Gordon and Breach, p. 37, (1971).

124. N. Plazer, "Sheet Forming", Processing of Thermoplastic Materials, E. C. Berhardt, Ed., p. 447, (1959).

125. G. Gruenwald, Thermoforming: A Plastic Processing Guide, Technomic Publishing Co., Inc., Lancaster, (1987).

126. J. Florian, Practical Thermoforming: Principles and Applications, Marcel Dekker, Inc., New York, p. 93, (1987).

127. C. S. Schollenberger, Handbook of Elastomers, Anil K. Bhowmick and H. L. Stephens, Eds., Marcle Dekker, Inc., New York, p. 385, (1988).

128. C. S. Schollenberger, H. Scott and G. R. Moore, *Rubber World*, Vol. 137, p. 549, (1958).

129. C. S. Schollenberger, H. Scott and G. R. Moore, *Rubber Chem. Technol.*, Vol. 35, p. 742, (1962).

130. W. K. McConnell, Jr., Thermoforming Technology, Notes from Thermoforming Seminar od SPE, (1992).

131. J. McMurry, Organic Chemistry, 2nd Edition, Brooks/Cole Publishing Co., California, p. 392, (1988).

132. J. B. Lambert, H. F. Shurvell, D. A. Lightner, and R. G.. Cooks, Introduction to Organic Spectroscopy, Macmillan Publishing Co., New York, p. 135, (1987).

133. F. P. Incropera and D. P. Dewitt, Fundamentals of Heat Transfer, John Wiley & Sons, New York, p. 579, (1981).

134. R. Gardon, *J. of American Ceram. Soc.*, Vol. 44, No. 7, p. 305-312, (1961).

135. D. O. Hummel, Infrared Spectra of Polymers: in the medium and long wavelength regions", Interscience Publishers, New York, p. 3.

136. C. Hepburn, Polyurethane Elastomers, 2nd Edition, Elsevier Applied Sci, New, York, p. 311, (1991).

137. V. V. Zharkov, A. G. Strikovsky and T. E. Verteletskaya, *Polymer*, Vol 34, No.5, p. 938-941, (1993).

138. D. A. C. Compton etc., Structure-Property Relations in Polymers, by Marek W. Urban and Clara D. Craver, Editor.

139. R. F. Harris, *J. Appl. Polym. Sci.*, Vol. 41, p. 509-525, (1990).

140. R. D. A. Paulmer, C. S. Shan, *J. Appl. Polym. Sci.*, Vol. 43, p. 1953-1959, (1991).

141. J. Bhattacharyya, Handbook of Polymer Science and Technology, N. P. Cheremisinoff, Ed., Vol. 2, p. 575, (1989).

142. D. Randall, S. Cook, P. Goodall, and R. Sayers, 34th Annual Polyurethane Tech./Marketing Conf., p. 612, (1992).

143. Y. Eckstein and R. L. Jackson, 35th Annual Polyurethane Tech./Marketing Conf., p. 68, (1994).

144. S. Dinda, S. P. Keeler, K. F. James, P. A. Stine, J. P. Orlan, and V. L. Viel, How to Use Circle Grid Analysis for Die Tryout, American Soc. for Metals, Metals Park, Ohio, (1981).

145. G. E. Dieter, Mechanical Metallurgy, 3rd Ed., McGraw-Hill, Inc., New York, p. 75, (1986).

146. ASM International, Engineered Materials Handbook, *Vol. 1: Composites*, Metals Park, Ohio, p. 148, (1988).

147. W. Meckel, W. Goyert, and W. Wieder, Thermoplastic Elastomers, N. R. Legge, G. Holden and H. E. Schroeder, Ed., Hanser Publishers, p. 38, (1987).

148. J. P. Bell, J. Chang, H. W. Rhee, and R. Joseph, *Polymer Composites*, Vol. 8, No. 1, p. 46-52, (1987).

149. A. Sengupta and H. P. Schreiber, *Adhesion Sci. Technol.*, Vol 5, No 11, p. 947-957, (1991).

150. G. M. Bartenev and Yu. S. Zuyev, Strength and Failure of Visco-Elastic Materials, Pergamon Press, p. 235, (1968).

151. ASTM D 624-86, "Standard Test Method for Rubber Property - Tear Resistance".

152. ASTM D 1004-90, "Standard Test Method for Initial Tear Resistance of Plastic Film and Sheeting".

153. S. G. Damani, *Polymer Composites*, Vol. 11, No.3, p. 174-183, (1990).

154. J. L. Figueirdo, C. A. Bernardo, R. T. K. Baker, and K. J. Hüttinger, Carbon Fibers Filaments and Composites, Kluwer Academic Publishers, p. 147, (1990).

155. J. W. C. Van Bogart, D. A. Bluemke, and S. L. Cooper, *Polymer*, Vol. 22, p. 1428-1438, (1981).

156. W. C. Hu and J. T. Koberstein, *J. Polym. Sci., Part B: Polym. Phys.*, Vol. 32, p. 437-446, (1994).

157. T. M. Don, W. Y. Chiu, and K. H. Hsien, *J. Appl. Polym. Sci.*, Vol. 43, p. 2193-2199, (1991).

158. C. Li and S. L. Cooper, *Polymer*, Vol. 31, p. 3-7, (1990).

159. H. N. Ng, A. E. Allegrezza, R. W. Seymour, and S. L. Cooper, *Polymer*, Vol. 14, p. 255-261, (1973).

160. R. S. Rivlin and A. G. Thomas, *J. Polymer Sci.*, Vol 10, p. 29, (1953).

161. A. A. Griffith, *Phil. Trans. Roy. Soc. London*, A221, p. 163, (1920).

162. B. Rosen, Fracture Processes in Polymeric Solids: Phenomena and Theory, p. 463, (1964).

163. I. M. Ward, Mechanical Properties of Solid Polymers, John Wiley & Sons, p. 449, (1983).

164. P. L. Soli, Crystallization and Mechanical Behaviour of Polymers, Seminar Notes from SPE, p. 34, (1992).

165. D. C. Philips, "The Fracture Energy of Carbon Fibre Reinforced Glass", *J. Mater. Sci.* Vol. 7, (1972).

166. A. Kelly, "Interface Effects and the Work of Fracture of a Fibrous Composite", Proc. Roy. Soc. Lond., A319:95, (1970).

167. D. H. Kaelble, *J. Adhesion*, Vol. 5, p. 245, (1973).

168. J. N. Kirk, M. Munro, and P. W. R. Beaumont, *J. Mater. Sci.*, Vol. 13, p. 2197, (1970).

169. J. O. Outwater and M. C. Murphy, "The Fracture Energy of Unidirectional Laminates", Proc. 24th Annual Technical Conf., SPI, Paper 11C, (1969).

170. P. K. Mallick, Fiber Reinforced Composites, Marcel Dekker, Inc., New York, p. 73, (1988).

171. A. G. Atkins, *J. Mater. Sci.*, Vol. 10, p.819, (1975).

172. J. Cook and J. E. Gordon, *Proc. R. Soc.*, A282, p. 508, (1964).

173. A. A. Berlin, S. A. Volfson, N. S. Enikolopian, and S. S. Negmatov, Principles of Polymer Composites, Springer-Verlag, New York, p. 10, (1986).

174. C. A. Butler, R. Pitchumani, and J. W. Gillespie, Jr., Proc. of the 10th Annual ASM/ESD Advanced Composites Conf., p. 596, (1994).

175. L. E. Nielsen, Mechanical Properties of Polymers and Composites, Vol. 2, Marcel Deker, Inc., New York, p. 321, (1974).

176. E. K. Rodriguez, R. Basar, E. G. Kolycheck, and H. S. Tseng, 34th Annual Polyurethane Technical/Marketing Conf., p. 629-638, (1992).

177. "Standard Test Method for Puncture-Propagation Tear Resistance of Plastic Film and Thin Sheeting", ASTM D2582-90, (1990).

178. N. G. McCrum, C. P. Buckley, and C. B. Bucknall, Principles of Polymer Engineering, Oxford University Press, New York, p. 60 (1988).

179. L. E. Nielsen, Mechanical Properties of Polymers and Composites, Vol 2, Marble Dekker, Inc., New York and Basel, p. 288, (1974).

180. G. M. Bartenev and Yu. S. Zuyev, Strength and Failure of Visco-Elastic Materials, Pergamon Press, New York, (1968).

181. J. B. Donnet and R. C. Bansal, Carbon Fibers, Marcel Dekker, Inc., New York and Basel (1984).

182. W. Brostow and R. Corneliussen, eds, Fracture of Plastics, Hanser Publishers, New York, p. 430, (1986).

183. A. N. Gent, "Rubber and Rubber Elasticity: A Review", *J. Ploym. Sci. Symposium*, No. 48., p. 1-17, (1974).

184. I. M. Ward and D. W. Hadley, An Introduction to the Mechanical Properties of Solid Polymers, John Wiley and Sons, p. 29 (1993).

185. C. Hepburn, Polyurethane Elastomers, Elsevier Applied Science, New York, p. 357, (1992).

186. "Standard Test Methods for Rubber Properties in Tension", ASTM D 412-87, (1987).

187. Y. Yue, *J. of Mater. Sci.*, Vol. 27, p. 3843-3855, (1992).

188. L. R. G. Treloar, The Physical of Rubber Elasticity, 3rd Edition, Clarendon Press, Oxford, p. 80-100, (1975).

189. L. R. G. Treloar, *Inst. Rubber Ind. Trans.*, Vol. 19, p. 201, (1944).

190. J. E. Adkins and R. S. Rivlin, *Phil. Trans Royal Soc., London*, A244, p. 505, (1952).

191. A. E. Green and J. E. Adkins, Large Elastic Deformations, The Clarendon, Oxford, (1960).

192. W. W. Feng, *J. Applied Mechanics*, Vol. 59, p. S29-S34, (1992).

193. J. G. Williams, *J. Strain Analysis*, Vol. 5, p. 49-57, (1970).

194. R. G, Budynas, Advanced Strength and Applied Stress Analysis, McGraw_Hill Book Company, New York, pp. 63-66, (1977).

195. J. Chakrabarty and J. M. Alexander, *J. Strain Analysis*, Vol. 5, p. 155-161, (1970).

196. C. Hepburn, Polyurethane Elastomers, Elsevier Applied Science, New York, p. 355, (1991).

197. H. H. Kausch, Polymer Fracture, 2nd ed., Sringer-Verlag Berlin Heidelberg, New York, p. 332-365, (1987).

198. H. H. Kausch, Crazing in Polymers, Springer-Verlag, New York, p. 57, (1983).

199. "Slow Rate Penetration Resistance of Flexible Barrier Films and Laminates", ASTM F1305-90, (1990).

TABLES

Table 1-1. 1989 Modal Profile of U.S.-Canadian Trade.[2]

(1) Overall international trade modal splits.[2]

Motor Carrier	34.0%
Rail	19.7%
Marine	30.7%
Air	0.2%
Other*	15.4%

* Other is mainly thought to be pipeline.

(2) Provincial trade modal splits (in percentage).[2]

PROVINCE	Motor Car	Railroad	Marine	Air-Other
Ontario	47.5	16.2	33.7	0.32.3
Quebec	43.1	21.9	34.1	0.40.5
British Columbia	35.2	30.9	31.2	0.22.5
Alberta	8.7	18.9	1.4	0.170.9
New Brunswick	41.1	8.6	46.2	0.33.8
Saskatchewan	18.6	44.4	5.03	0.032.0
Manitoba	50.1	27.3	2.0	0.419.8
Nova Scotia	6.16	5.07	88.3	0.23.01
P. E. I.	88.3	2.4	9.0	0.30.0
Newfoundland	1.6	0.4	97.4	0.00.6

Table 1-1. Continued.

(3) Percentages of a) petroleum or coal products and (b) chemicals or allied products to the total goods movements between provinces and the U.S.[2]

Province		Petroleum/Coal Products	Chemicals/Allied Products
Ontario	North-bound	4.8	7.1
	South-bound	8.4	7.8
Quebec	North-bound	2.4	6.1
	South-bound	6.8	9.5
British Columbia	North-bound	-	5.5
	South-bound	-	4.0
Alberta	North-bound	-	13.1
	South-bound	11.2	19.3
New Brunswick	North-bound	-	4.0
	South-bound	9.1	-
Saskatchewan	North-bound	11.3	9.8
	South-bound	10.8	70.0
Manitoba	North-bound	-	12.5
	South-bound	11.1	6.7
Nova Scotia	North-bound	-	14.5
	South-bound	-	-
Prince Ed. Island	North-bound	72.0	-
	South-bound	-	0.4
Newfoundland	North-bound	-	-
	South-bound	-	-

Table 1-2. Classifications of Dangerous Goods.[3]

Classifications	Definition
Class 1	Explosive, including explosives within the meaning of the Explosives Act;
Class 2	Gases: compressed, deeply refrigerated, liquified or dissolved under pressure;
Class 3	Flammable and combustible liquids;
Class 4	Flammable solids; substances liable to spontaneous combustion; substances that on contact with water emit flammable gases;
Class 5	Oxidizing substances; organic peroxides;
Class 6	Poisonous (toxic) and infectious substances;
Class 7	Radioactive materials and prescribed substances within the meaning of the Atomic Energy Control Act;
Class 8	Corrosives; and
Class 9	Miscellaneous products, substances or organisms considered by the Governor in Council to be dangerous to life, health, property or the environment when handled, offered for transport or transported and prescribed to be included in this class.

Table 1-3. Accidents handled by CANUTEC 1986-1987.[6]

Mode	Number of Accidents	Class	Number of Accidents
Road	250	1	7
Rail	39	2	60
Marine	8	3	93
Air	14	4	14
Facilities	151	5	21
		6	57
		7	12
		8	119
		9	58
		NR	71

Table 2-1. Properties of carbon fiber types.[98]

Fiber type	Density g/cm³	Young's modulus GPa	Young's modulus 10^6 psi	Tensile strength GPa	Tensile strength 10^3 psi	Electric resistivity ohm · m	Thermal conductivity W/m K	Thermal conductivity BTU in./h ft² °F
High-strength (PAN)	1.7-1.8	230-250	33-36	2.8-4.0	0.41-0.58	12-30	7-10	50-70
Ultrahigh strength (PAN)	1.7-1.8	260-290	38-42	4.1-5.7	0.59-0.83	14-20	7-9	50-60
High-modulus (PAN, mesophase pitch)	1.8-2.0	350-550	50-80	1.7-3.5	0.25-0.50	5-10	60-200	420-1400
Ultrahigh-modulus (mesophase pitch)	2.0-2.2	600-900	90-130	2.1-2.5	0.30-0.36	1-4	400-2500	2800-17 300
Low-modulus (rayon, pitch)	1.5-1.7	40-60	6-9	0.6-1.0	0.085-0.145	30-100	7-28	50-190

Table 2-2. Classified textile structure of fiber reinforcements.[97]

Dimension \ Axis	0 NON - AXIAL	1 MONO - AXIAL	2 BIAXIAL	3 TRIAXIAL	4 ~ MULTI - AXIAL
1 D		ROVING - YARN			
2 D	CHOPPED STRAND MAT	PRE-IMPREG-NATION SHEET	PLANE WEAVE	TRIAXIAL WEAVE 1)-3)	MULTI-AXIAL WEAVE, KNIT
3 D Linear Element	Z, X, Y	3-D BRAID	MULTI-PLY WEAVE	Z, X, Y TRIAXIAL 3-D WEAVE	(MULTI-AXIAL 3-D WEAVE) 4)~n, 12)~14)
3 D Plane Element	Z, X, Y	LAMINATE TYPE	H or I BEAM	HONEY-COMB TYPE	

Table 3-1. Chronology of thermoforming.[118, 119]

Period	Event
Prehistory (Egypt)	Heating tortoise shell (Keratin) in hot oil, then shaping (Food Containers)
Prehistory (Micronesia)	Heating tortoise shell (Keratin) in hot water, then shaping (bowls)
Prehistory (Americas)	Heating treebark (natural cellulose) in hot water, then shaping (Bowls, Boats)
1845	Extrusion process commercialized for plastics
1850's	Gutta-Percha replace ivory for billiard balls
1856	First moldable plastic (fibrous cellulosic pulp and gum shellac)- peck
1862	Cellulose nitrate solvated with camphor (Parkesine)- Alexander Parkes
1868	Celluloid, molding grade pyroxylin - John Wesley Hyatt
1870's	Hydraulic planer for cutting thin sheets - Charles Burroughs Co., NJ
1870's	Celluloid tubes steam-heated, placed in form, inflated (Blow Molding)
1910	"Sharps" piano keys drape-formed over captive wooden core
1930	Bottle formed from two thermoformed halves - Fernplas Corp.
1930's	Relief Maps for US coast & geodetic survey
1938	Blister pack of cellulose acetate (CA)
1938	Rollfed automatic thermoformer - Clauss B. Strauch Co.
1938	Cigarette tips, ice-cube trays automatically thermoformed
1942	Cast PMMA (acrylic) thermoformed for fighter.bomber windows, windshields
1948	Cast PMMA (acrylic) thermoformed for bathtubs (Troman Bros., England)
1954	Skin-package products - Hardware Manufacturers Association, Chicago
1970	ABS automobile body - Borg-Warner

Table 3-2. Examples of applications of thermoformed parts.[123]

Packaging and Related Items
Blister Packs, Point-of-Purchase
Bubble Packs, Slip Sleeve, Vacuum Carded
Electronics, Audio/Video Cassette Holders
Tools, Hand, Power
Cosmetics, Cases, Packages
Foams, Meat, Poultry Trays
Unit Serving, Foodstuffs
Convenience, Carryout, Co[illegible]-in-Box
Convertible-Oven Food Serving
Wide-Mouth Jars
Vending Machine Hot Cup
Egg Cartons, Wine Bottle Protectors
Produce Separators (Apples, Grapefruit)
Portion, Unit Dose Drugs
Form-Fill-Seal (Jelly, Crackers)
Vehicular
Automotive Door Innerliners
Automotive Utility Shelves, Liners
Snow-Mobile Shrouds, Windshields
Motorcycle Windshields, Scooter Shrouds, Mudguards
All-Terrain Vehicle Exterior Components
Golf Cart Shrouds, Seats, Trays
Tractor Shrouds, Door Fascia
Camper Hardtops, Interior Components (Doors, etc.)
Truck Cab Door Fascia, Instrument Cluster Fascia
Recreational Vehicle Interior Components, Window Blisters
Industrial
Tote Bins
Pallets
Parts Trays, Transport Trays
Equipment Cases
Building Products
Shutters, Window Fascia
Skylights, Translucent Domes
Exterior Lighting Shrouds
Storage Modules, Bath, Kitchen, Pantry
Bath and Shower Surrounds (GR-UPE backed)
Soaking Tubs (GR-UPE Backed)
Retrofit Shower Components, Shower Trays
Others
Exterior Signs
Advertising Signs, Lighted Indoor Signs
Swimming and Wading Pools
Trays, Baskets, Hampers, Carrying Cases
Luggage
Boat Hulls, Surf-Boards (with PUR Foams)
Animal Containers
Prototype Concepts for Other Plastic Processes

Table 3-3. Common polyurethane Infra-red absorption wavelengths.[136]

Functional group	*Wavelength of the most intense bands (μm)*
—NCO	4·4
—N=C=N—	4·7
—C=O in uretidione	5·61–5·63
—C=O in isocyanurate	5·85–5·92 7·0–7·1 confirmation band
—C=O in urethane	5·75 (films and elastomers) 5·75–5·85 (solutions)
—C=O in uretoneimine	5·75
—C=O in urea	5·9–6·1
—C=O in allophanate and biuret[a]	5·71–5·85, 6·85–7·06
—C=O in esters	5·71–5·83
—C=N in carbodiimide dimer	5·96
—C=N in carbodiimide trimer	5·98, 8·1–8·3
Amide II band (NH)	6·5
—NH stretching band	3·0
C—O in aliphatic ether	9·3
C—O, stretch and/or OH deformation	8·1
C=C, skeletal stretch of benzene ring	6·2
C—CH_3 (symmetrical) deformation	7·25

[a] Cannot be distinguished in mixture.

Table 3-4. Physical properties of TPU and carbon fibers.

a. Physical properties of Elastollan 1100 series TPU:

TPU Type	Density (g/cc)	Hardness (Shore A)	Tensile strength		Tear Strength (KN/m)	Tensile Strength (MPa)	Elongation (%)
			@ 100% (MPa)	@ 300% (MPa)			
1185	1.12	85	7.6	12	105	32	640
1195	1.14	95	14.1	26.7	144	37	441

b. Physical properties of THORNEL® pan based carbon fibers.

T-300	Yield (g/m)	Density (g/cc)	Fiber Area in Yarn (cm^2x10^{-3})	Tensile strength (GPa)	Young's Modulus (GPa)	Elongation (%)	Sizing (wt.%)
1K	0.0660	1.770	0.3742	3.88	236.3	1.6	1.20
3K	0.2006	1.753	1.129	3.70	222.5	1.7	1.35

Table 3-5. Percentage of reinforcements incorporated in the TPU sheets for four different fiber patterns.

Fiber weight: (g/m)

TPF (d=1mm):	0.974		
	Uncoated	Coated	CF-area ($cm^2 \times 10^{-3}$)
CF-1K:	0.0678	0.0715	37.42
CF-3K:	0.1949	0.2143	1.129

Sheet Size:	1698.39 (cm^2)
Sheet Weight:	92.09 (g)
	542.34 (g/m^2)
Sheet Volume:	85.85 (cm^3)
Sheet Thickness:	0.05055 (cm)

Patterns	Number of Fibers		Total-TPF (g/sheet)	Total-TPF (g/m^2)	Total-CF (g/sheet)		TPF (wt%/sheet)	CF (wt%/sheet)		TPF (vol%/sheet)	CF (vol%/sheet)	
	Length (cm)	Fibers			(1K)	(3K)		(1K)	(3K)		(1K)	(3K)
Square	length: 48.3 width: 34.3	28 38	25.85	152	1.90	5.69	28.08	2.06	6.18	24.26	1.16	3.49
Diamond	60° length: 41.9	80	32.64	192	2.40	7.18	35.45	2.61	7.80	30.66	1.46	4.41
Triangle	60° length: 41.9 length: 48.3	80 28	45.80	270	3.37	10.08	49.74	3.66	10.95	43.02	2.05	6.19
Laddered Diamond	26° length: 38.7 length: 48.3	80 53	55.07	324	4.05	12.12	59.81	4.39	13.16	52.24	2.47	7.44

Table 3-5. Continued.

Patterns	Total-TPF (g/sheet)	TPU-Rod (g/m^2)	TPU-Rod + TPU (g/m^2)	Total Carbon Fiber (g/sheet)		Carbon Fiber (g/m^2)		Carbon Fiber+TPU (g/m^2)	
				(1K)	(3K)	(1K)	(3K)	(1K)	(3K)
Square	25.85	152	694	1.90	5.69	11.19	33.51	553.5	575.9
Diamond	32.64	192	734	2.40	7.18	14.13	42.29	556.5	584.6
Triangle	45.80	270	812	3.37	10.08	19.85	59.39	562.2	601.7
Laddered Diamond	55.07	324	866	4.05	12.12	23.85	71.38	566.2	613.7

Table 4-1. The details of the dimensions of the enlarged die.

Dimension	Standard Die C (mm)	Modified Die C (mm)	Ratio
A	102	215.9	2.12
B	19	44.5	2.34
C	19	57.1	3.00
D	12.7	38.1	3.00
E	25	44.5	1.78
F	27	57.1	2.11
G (Angle cut)	90°	90°	

Table 4-2. Tear Test Results.

Samples		Thickness	Tear Resistance	Elongation
Patterns	Reinforcements	(mm)	(N/mm)	(%)
Single Sheet Transverse	None	0.321	178.5	122
Single Sheet		0.302	197.2	98
Double sheet		0.547	212.5	134
Polyester Scrim	Polyester	0.419	278.1	62
Square	1K Carbon Fiber	0.535	243.2	181
Diamond		0.491	243.5	203
Diamond Transverse		0.526	237.2	210
Triangle		0.503	262.8	145
Laddered Diamond		0.492	300.5	159
Laddered Diamond Transverse		0.452	332.9	214
Square	3K Carbon Fiber	0.544	249.5	170
Diamond		0.533	266.9	194
Triangle		0.499	310.0	134
Square	TPU-rod	0.489	457.9	274
Diamond		0.487	513.8	320
Diamond Transverse		0.471	284.5	208
Triangle		0.454	623.0	308

Table 4-3. Comparison of the tear resistance of the samples annealed at 393 and 408K with those with no annealing.

Samples	Temperature (K)	Tear Resistance (KN/m)	Elongation (%)
CF1KDm	room	245.5	186.8
	393	246.6	165.3
	408	247.1	205.7
CF3KDm	room	266.9	193.8
	393	353.3	124.1
	408	343.6	146.1
CF3KTri	room	309.9	133.6
	393	353.0	137.5
	403	472.0	108.7

Table 5-1. Snag test results.

Samples	Thickness (mm)	Drop Height (mm)	Carriage Weight (kg)	Tear Length (mm)	Tear Resistance F (N)
Single Sheet Parallel	0.28	508	0.1134	6.1	93.7
			0.2268	9.9	116.4
			0.3402	11.6	149.4
			0.4536	16.0	145.7
			0.6804	19.8	177.9
			0.9072	27.8	171.5
Single Sheet Transverse	0.28	508	0.1134	6.6	86.7
			0.2268	11.5	100.5
			0.3402	15.7	111.3
			0.4536	19.2	122.1
			0.6804	27.1	131.8
			0.9072	34.8	138.8
Double Sheet Parallel	0.54	508	0.1134	4.5	126.7
			0.2268	6.7	170.9
			0.3402	9.6	179.9
			0.4536	11.3	204.4
			0.6804	16.1	217.2
			0.9072	19.7	238.3
TPU Triangle Reinforced	0.55	508	0.1134	2.4	236.5
			0.2268	4.5	253.3
			0.3402	5.1	335.7
			0.4536	6.2	368.9
			0.6804	8.7	396.3
			0.9072	10.7	431.3

Table 5-1. Continued (I).

Samples	Thickness (mm)	Drop Height (mm)	Carriage Weight (kg)	Tear Length (mm)	Tear Resistance F (N)
TPU Polyester Scrim Parallel	0.412	508	0.1134	7.4	77.5
			0.2268	13.1	88.5
			0.3402	17.8	98.6
			0.4536	24.1	98.2
			0.6897	37.5	97.1
			0.9072	57.0	88.2
TPU Polyester Scrim (45°)	0.412	508	0.1134	4.2	135.6
			0.2268	6.5	176.1
			0.3402	8.4	205.1
			0.4536	10.9	211.8
			0.6804	16.0	218.5
			0.9072	22.5	209.8
Polyethylene Sheet Parallel	0.063	508	0.1134	17.0	34.3
			0.2268	32.3	37.2
			0.3402	47.5	39.0
			0.4536	53.9	46.4
			0.6804	74.4	52.2
			0.9072	94.8	56.6
Polyethylene Sheet Transverse	0.063	508	0.1134	14.9	39.0
			0.2268	26.9	44.2
			0.3402	37.5	48.5
			0.4536	47.8	51.7
			0.6804	62.0	61.3
			0.9072	72.3	71.4

Table 5-1. Continued (II).

Samples	Thickness (mm)	Drop Height (mm)	Carriage Weight (kg)	Tear Length (mm)	Tear Resistance F (N)
CF-1K Triangle Reinforced	0.538	508	0.1134	3.8	149.78
			0.2268	6.2	184.5
			0.3402	8.9	193.8
			0.4536	10.0	230.4
			0.6804	13.4	259.6
			0.9072	17.0	274.7
CF-3K Triangle Reinforced	0.485	508	0.1134	3.3	172.3
			0.2268	6.0	190.5
			0.3402	7.5	229.3
			0.4536	9.3	247.4
			0.6804	12.3	282.3
			0.9072	14.9	312.2

Table 5-2. Comparison of snag test results for various cases.

Carriage Weight (Kg)	Comparison of Dynamic Tear Resistance Increase (%) in Various Cases										
	SH // vs SH ⊥ to Extrusion Direction	PE ⊥ vs PE // to Extrusion Direction	PEs 45° vs PEs // to Grid Direction	TPUDSH vs TPUSH	TPUTri vs TPUDSH	CF1KTri vs TPUDSH	CF3KTri vs TPUDSH	CF3KTri vs CF1KTri	TPUTri vs PEs //	TPUTri vs PEs 45°	TPUSH vs PEs //
0.1134	8.08	13.66	75.11	35.14	86.74	17.65	36.04	15.04	205.36	74.38	21.01
0.2268	15.81	18.90	98.99	46.85	48.25	7.98	11.49	3.25	186.31	43.88	31.51
0.3402	34.29	24.37	108.12	20.37	86.60	7.70	27.47	18.32	248.14	63.65	51.64
0.4536	19.27	11.54	115.62	40.32	80.47	12.71	21.03	7.38	275.64	74.22	48.34
0.6804	35.00	17.44	125.14	22.12	82.45	19.52	29.97	8.74	308.28	81.35	83.25
0.9072	23.57	26.23	137.88	38.99	80.97	15.27	31.01	13.65	389.08	105.60	94.44
Average:	22.67	18.69	110.14	33.97	77.58	13.47	26.17	11.06	268.80	73.85	55.03

Table 6-1. Tensile test results.

Fiber Patterns	Fibers	Thickness (mm)	Force (N)		Displacement (mm)	Comments
			at 1st Peak	at Stop		
DSH	None	0.558	/	433.0	535.7	not break
Square	TPU rod	0.448	/	450.5	514.0	"
Diamond		0.501	/	523.0	535.1	"
Triangle		0.442	/	490.5	517.0	break
Square	1K Carbon Fiber	0.485	81.0	419.0	538.5	not break
Diamond		0.554	152.0	493.0	541.8	"
Triangle		0.454	189.0	369.0	538.2	"
Diamond Laddered		0.527	260.0	400.0	486.9	break
Square	3K Carbon Fiber	0.489	320.0	341.0	536.7	not break
Diamond		0.473	200.5	371.5	538.2	"
Triangle		0.447	239.0	325.5	536.3	"
Square	Polyester Scrim	0.409	648.0	376.5	121.4	break, short elongation

Table 6-2. Comparison tension load bearing ability of carbon fiber sparsely reinforced TPU sheets with different patterns composed with thermoformed double TPU sheets at a given cross-head displacement.

Patterns	Fibers	Displacement (cm)				
		10	20	30	40	50
		Force (N)				
DSH	None	110	155	200	265	345
Square	1K Carbon Fiber	120	175	210	275	380
Diamond		155	200	240	305	420
Triangle		160	175	200	250	330
Diamond Laddered		200	205	260	325	-
Square	3K Carbon Fiber	80	115	165	230	330
Diamond		130	165	205	275	380
Triangle		140	170	203	250	340

Table 7-1. The main parameters of the ultrasonic sensor.

Specifications Operating Mode	Analogue
Distance Information	Yes
Linearity (%)	< 0.2
Maximum Sensing Distance (mm)	(R) 1200/ 600 (M)
Minimum Sensing Distance (mm)	150
Carrier Frequency (kHz)	215
Beam Angle (°)	(R) 9/(M) 6
Response Time (ms)	50
Repeatability (mm)	± 1
Analogue Outputs	0,7 ... 10 V - sensitivity: 8 ... 17 mV/mm

Table 7-2. Comparison of the deflection at maximum pressure in the bulge tests.

Samples	Maximum Pressure (KPa)	Deflection @ P_{max} (mm)
TPUSH	17.85	103
TPUDSH	29.63	113
WINDTPU	116.85	123
TPUSQ	31.82	111
TPUDM	34.18	111
TPUTRI	39.57	120
CF1KTRI	36.54	97
CF3KSQ	36.03	80
CF3KDM	44.11	96
CF3KTRI	76.95	61
Polyester Scrim	139.08	91
PS	47.82	21
PE	9.94	79

Table 7-3. Summarized bulge test results.

Samples	Maximum Pressure (KPa)	Deflection @ P_{max} (mm)	Time @ P_{max} (Second)	Deflection @ Failure (mm)	Pressure @ Failure (KPa)	Time @ Failure (Min)
SH	17.85	103	23.95	377	14.14	23.12
DSH	29.63	113	5.33	320	21.38	13.15
WINDTPU	116.85	123.27	4.39	397*	122.41*	22.58*
TPUSQ	31.82	111	49.54	378	20.88	37.08
TPUDM	34.18	111	46.36	332	24.42	18.29
TPUTRO	35.02	119	13.08	263	27.61	4.17
TPUTRI	39.57	120	7.36	342	26.94	9.24
CF1KSQ	33.00	107	3.35	282	19.53	5.41
CF1KDM	35.36	103	21.09	327	22.56	14.15
CF1KTRI	36.54	97	9.78	300	19.02	9.19
CF3KSQ	36.03	80	1.00	285	22.06	12.58
CF3KDM	44.11	96	6.32	245	28.12	6.52
CF3KTRI	76.95	61	1.00	205	24.85	4.17
PEs	139.08	91	-	91	139.08	2.22
PS	47.82	21	-	21	47.82	0.67
PE	9.94	79	20.16	173	7.74	2.64

Table 8-1. Sharp point slow rate penetration test results.

Samples	Thickness [mm]	Force [N]	Preload [mm]	Penetration Depth* [mm]	Energy [J]
SH1	0.302	69.5	3.0	30.5	0.978
DSH1	0.532	122.3	2.2	30.2	1.728
TPUSQ	0.539	111.7	3.0	26.3	1.304
TPUDm	0.528	104.5	2.2	24.2	1.156
TPUTri	0.495	108.5	2.1	25.3	1.257
CF1KSQ	0.440	106.8	3.5	28.8	1.418
CF1KDm	0.559	105.5	2.8	25.9	1.157
CF1KTri	0.465	98.0	2.8	24.1	1.044
CF3KSQ	0.475	108.5	0.9	21.5	1.120
CF3KDm	0.506	104.0	1.9	21.4	1.017
CF3KTri	0.497	122.0	0.6	18.9	1.124
PEs SCRIM	0.406	57.6	2.1	9.2	0.203

* Depth is the depth of penetration at failure.

Table. 8-2. Dull edge slow rate penetration test results.

Samples	Thickness [mm]	Force [N]	Preload [mm]	Penetration Depth* [mm]	Energy [J]	Comments (Compared with DSH)
DSH	0.504	187.0	2.4	42.3	3.70	
CF3KSQ CF3KDm CF3KTri	0.468 0.434 0.511	174.5 159.4 165.8	0.0 0.0 0.0	37.8 33.8 27.8	3.71 2.87 3.48	Force : lower Penetrating depth: lower Energy: lower
CF1KSQ CF1KDm CF1KTR	0.494 0.535 0.447	193.3 193.0 164.8	0.8 1.4 1.1	40.7 40.9 38.3	4.11 3.93 3.36	Force: 2-higher, 1-lower Penetrating depth: approx. same Energy:2 higher,1 lower
TPUSQ TPUDm TPUTri	0.474 0.505 0.481	233.0 220.5 223.5	2.6 2.0 2.0	44.0 42.0 44.3	5.08 4.55 5.31	Force: higher Penetrating depth: higher Energy: higher
PEs SCRIM	0.409	206.0	1.0	15.9	1.43	Force: higher, Penetrating depth: low. Energy: low.

* Depth is the depth of penetration at failure.

FIGURES

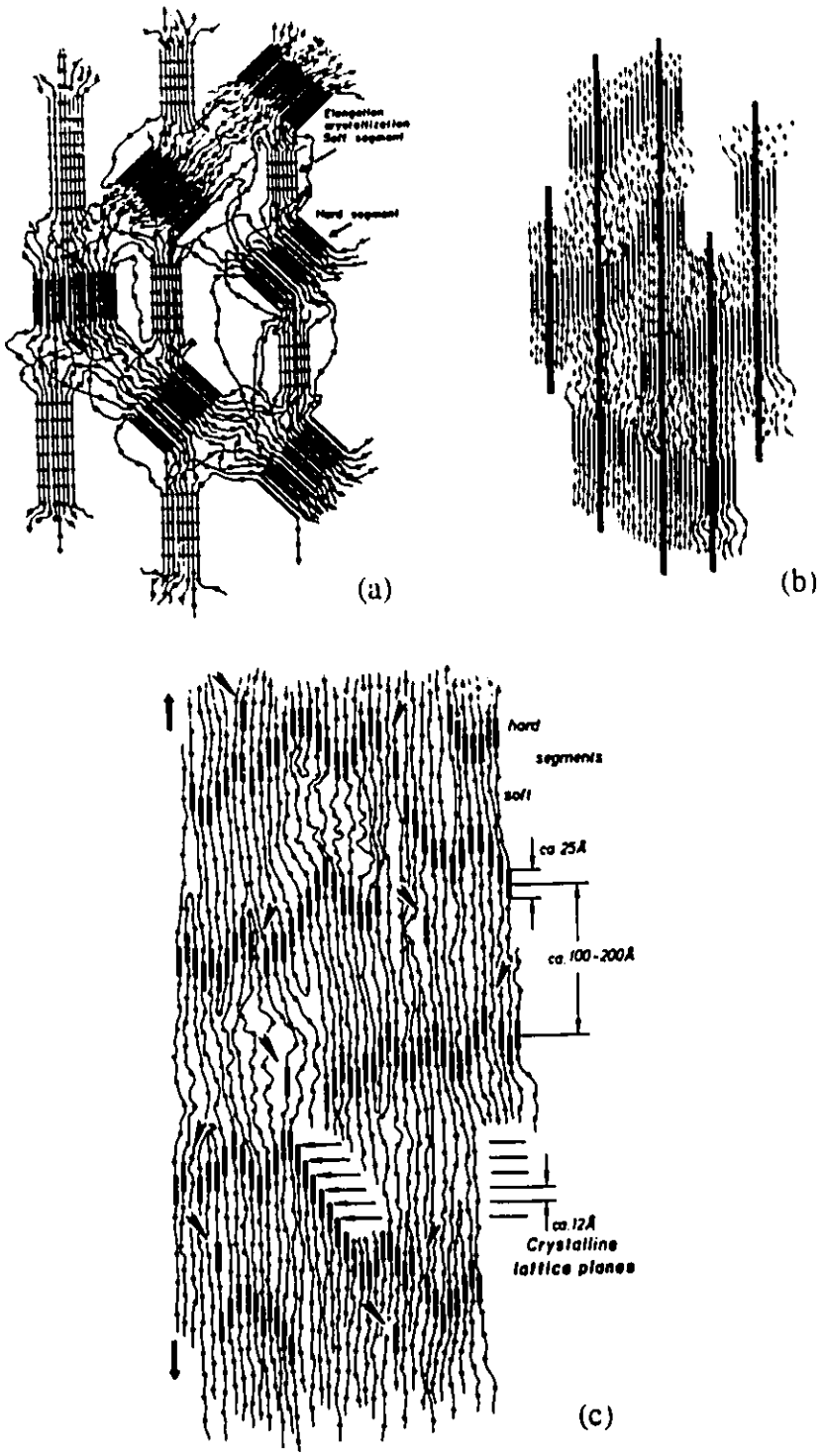

Fig. 2-1. (a) Upon stretching, a portion of the soft segments are stressed by uncoiling; hard segments are oriented in the stress direction; (b) Reorientation after stress and thermofixation;[32] (c) Later proposed structural model for the interrelated position of hard and soft segments subjected to a large stress.[31]

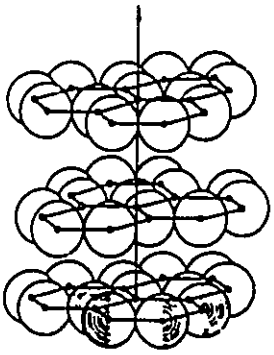

(a)

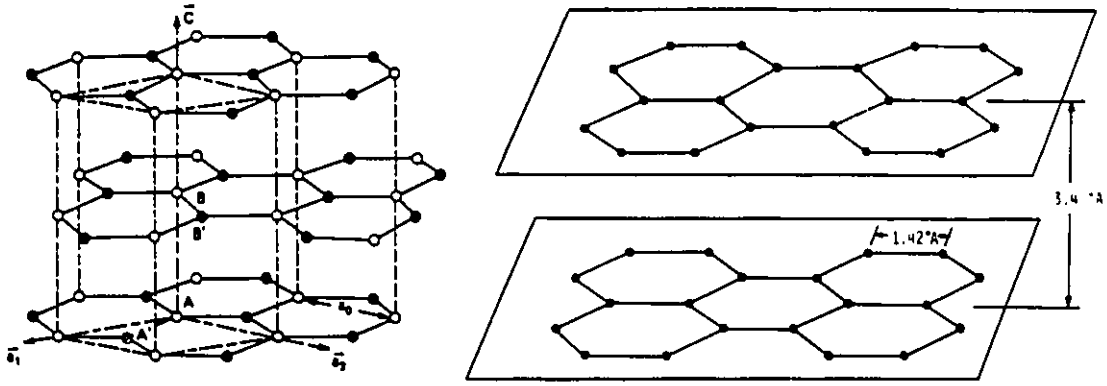

(b)

Fig. 2-2. Structure of graphite. (a) The densely packed graphitic layer structure; (b) Hexagonal structure of crystalline graphite showing ABABA layering

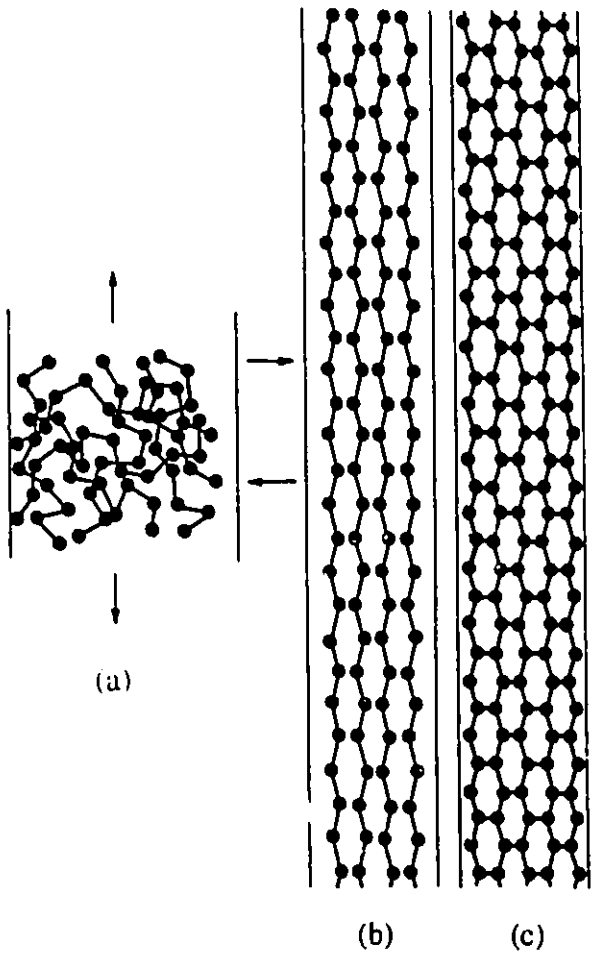

Fig. 2-3. Schematic illustration of the conversion of a polymer into an oriented carbon fiber.[90]

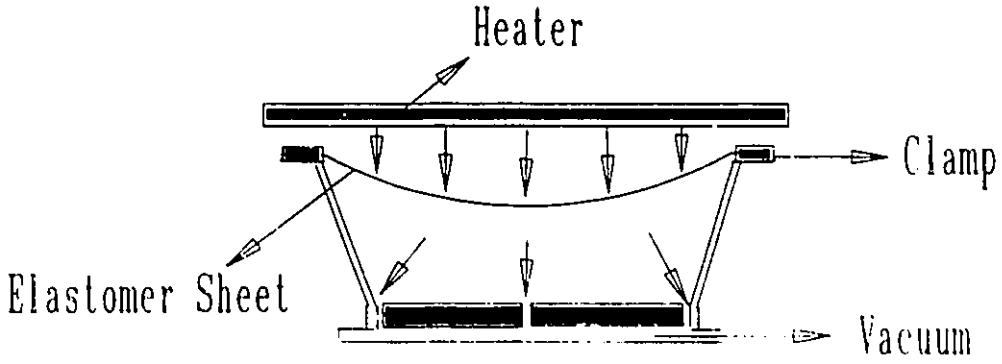

Fig. 3-1. A diagram of the vacuum thermoforming process.

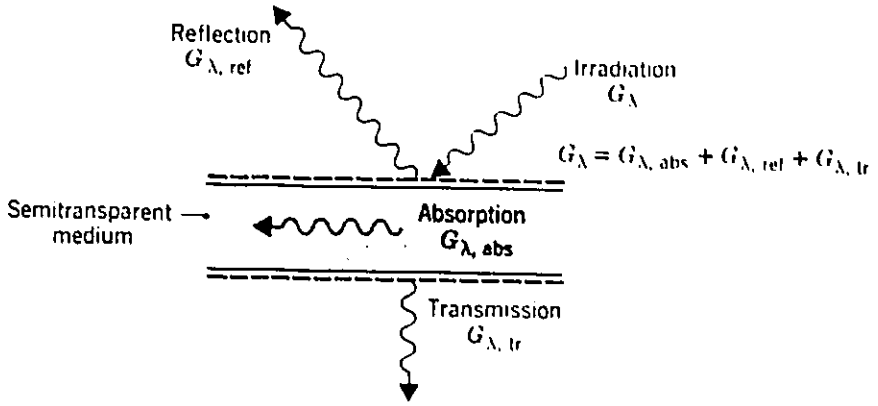

Fig. 3-2. Absorption, reflection, and transmission processes associated with a semi-transparent medium.[1]

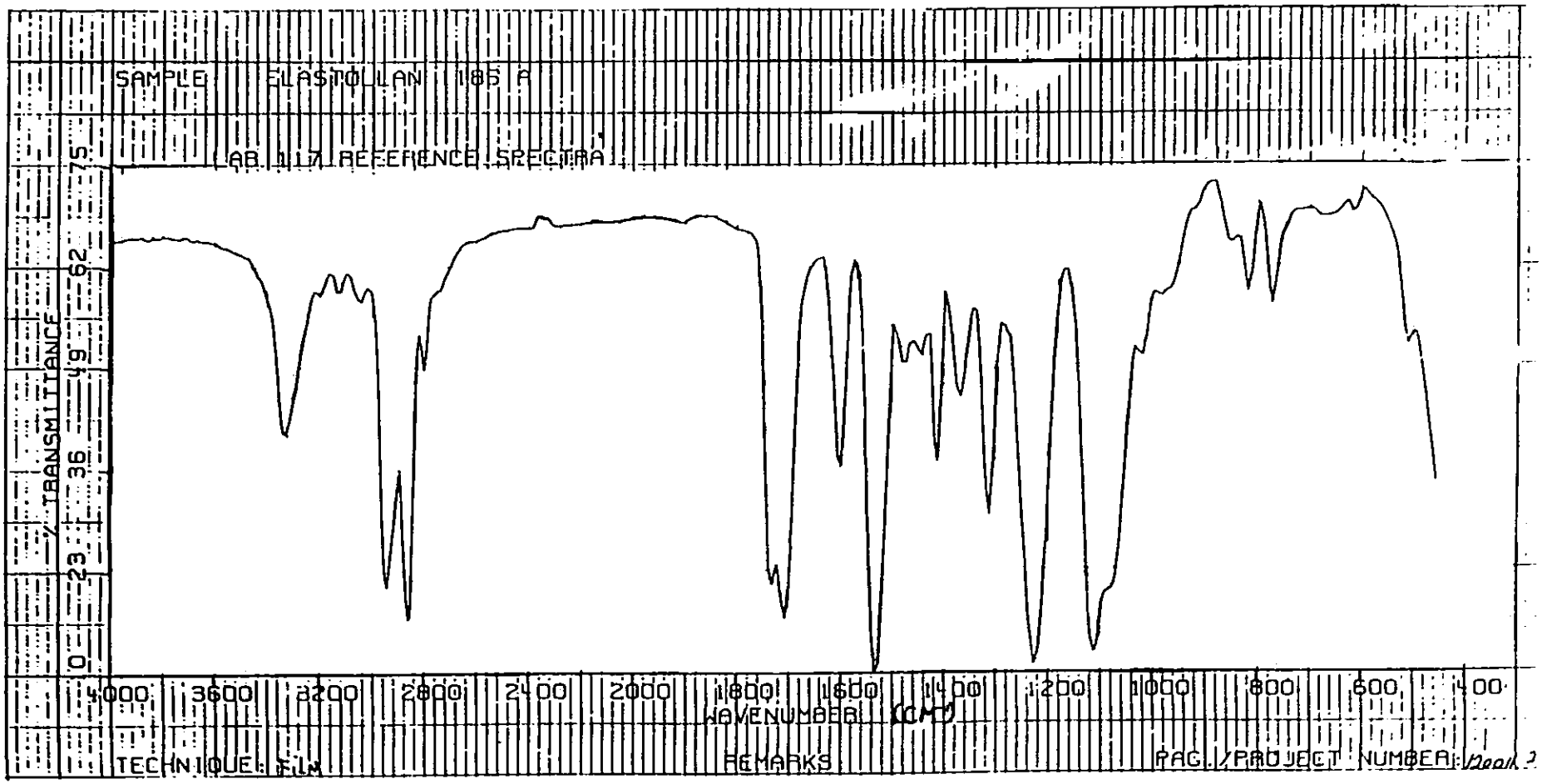

Fig. 3-3. Infrared absorption spectrum of Elastollan 1185A TPU.

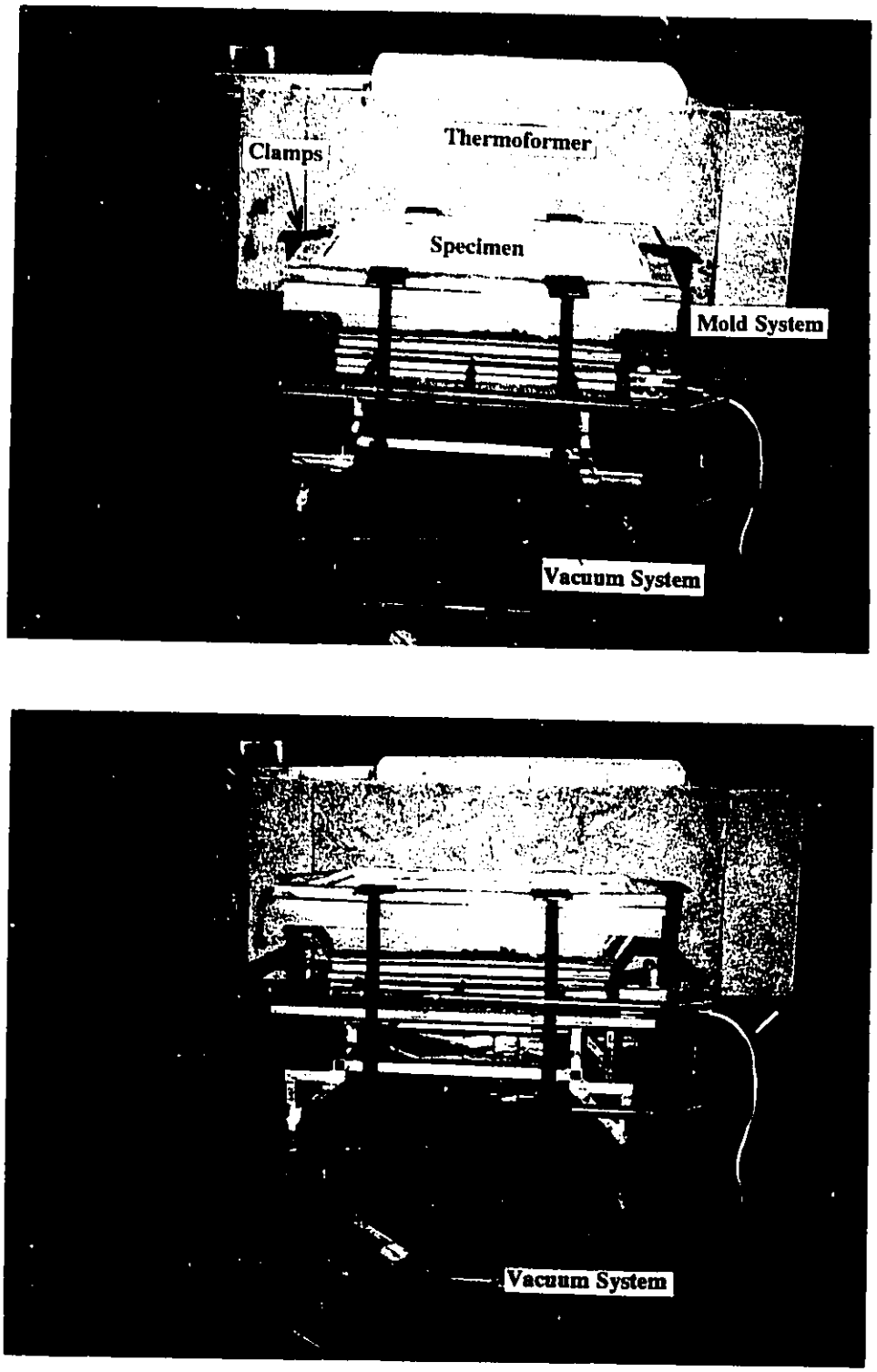

Fig. 3-4. Photographs of the apparatus of the single station thermoforming system.

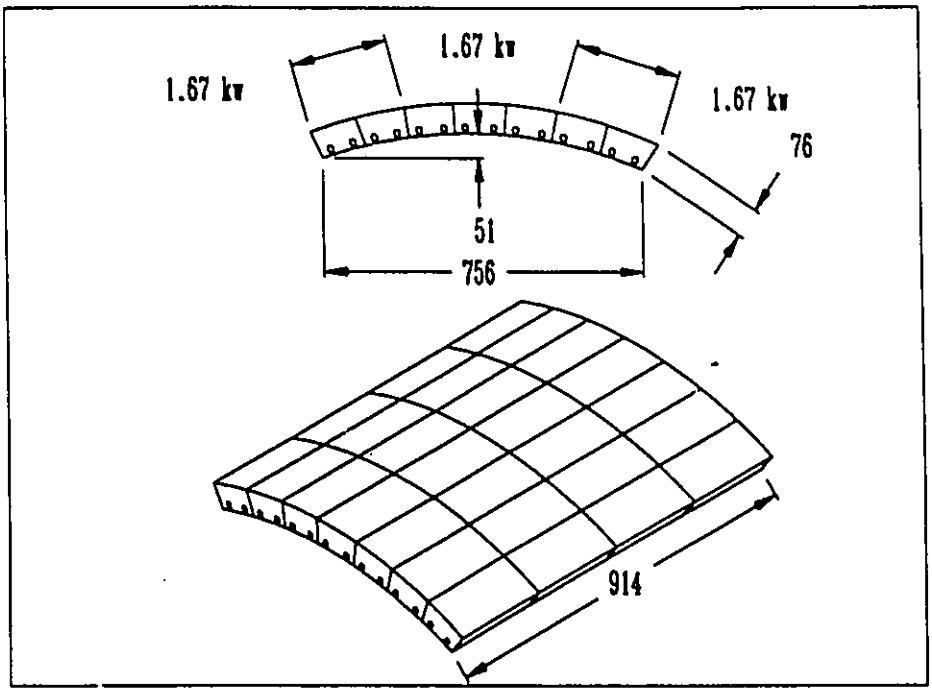

Fig. 3-5. A diagram of the arrangement of the resistance wires in the refractory bricks.

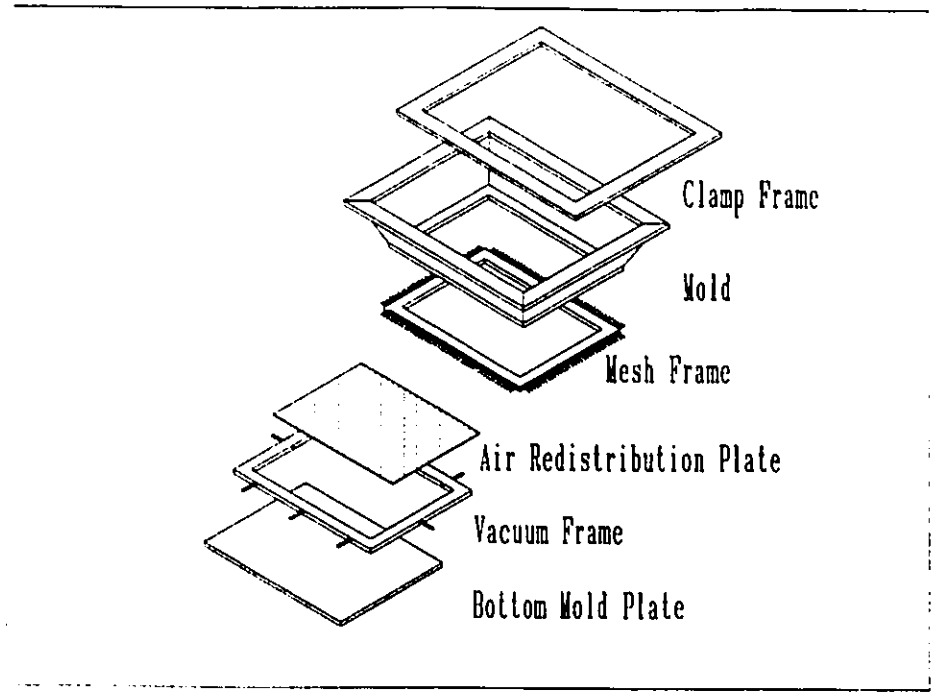

(a)

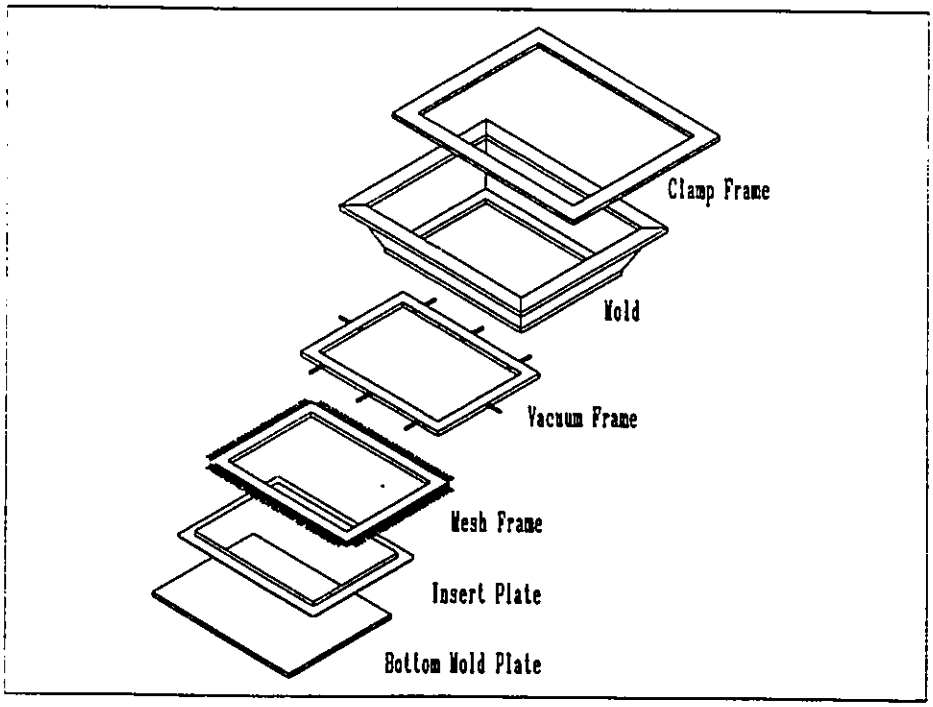

(b)

Fig. 3-6. Mold system design and arrangement; (a) when forming the first side of the sheet; (b) when forming the second side of the sheet.

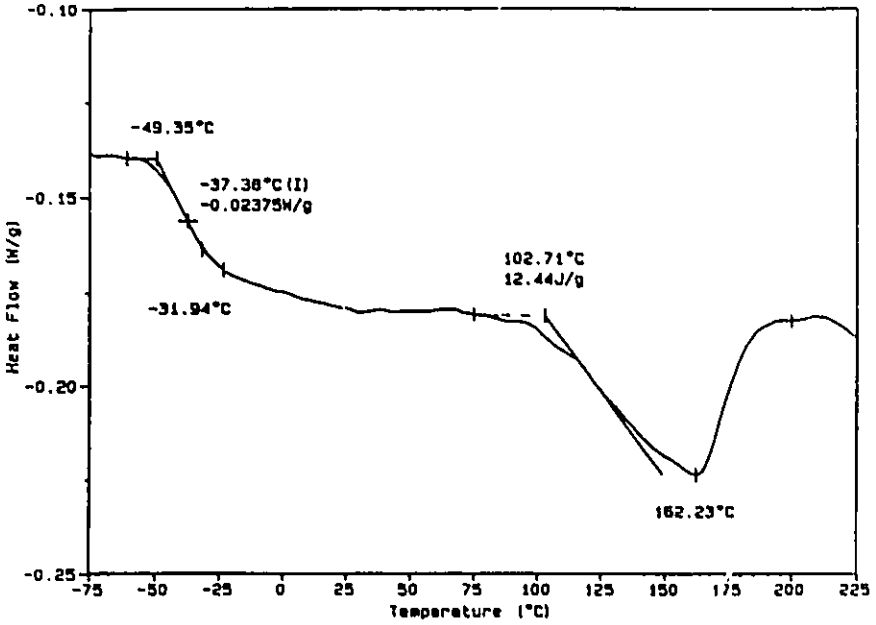

Fig. 3-7. DSC curve of the Elastollan 1185A TPU.

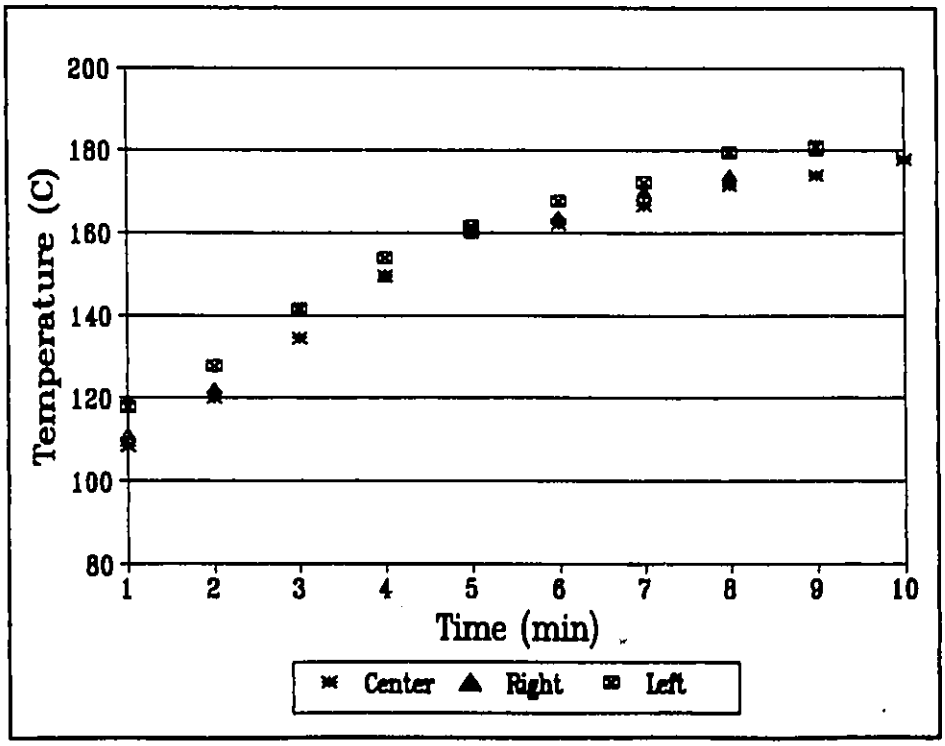

Fig. 3-8. The measurement of the thermoforming temperature of the TPU sheet.

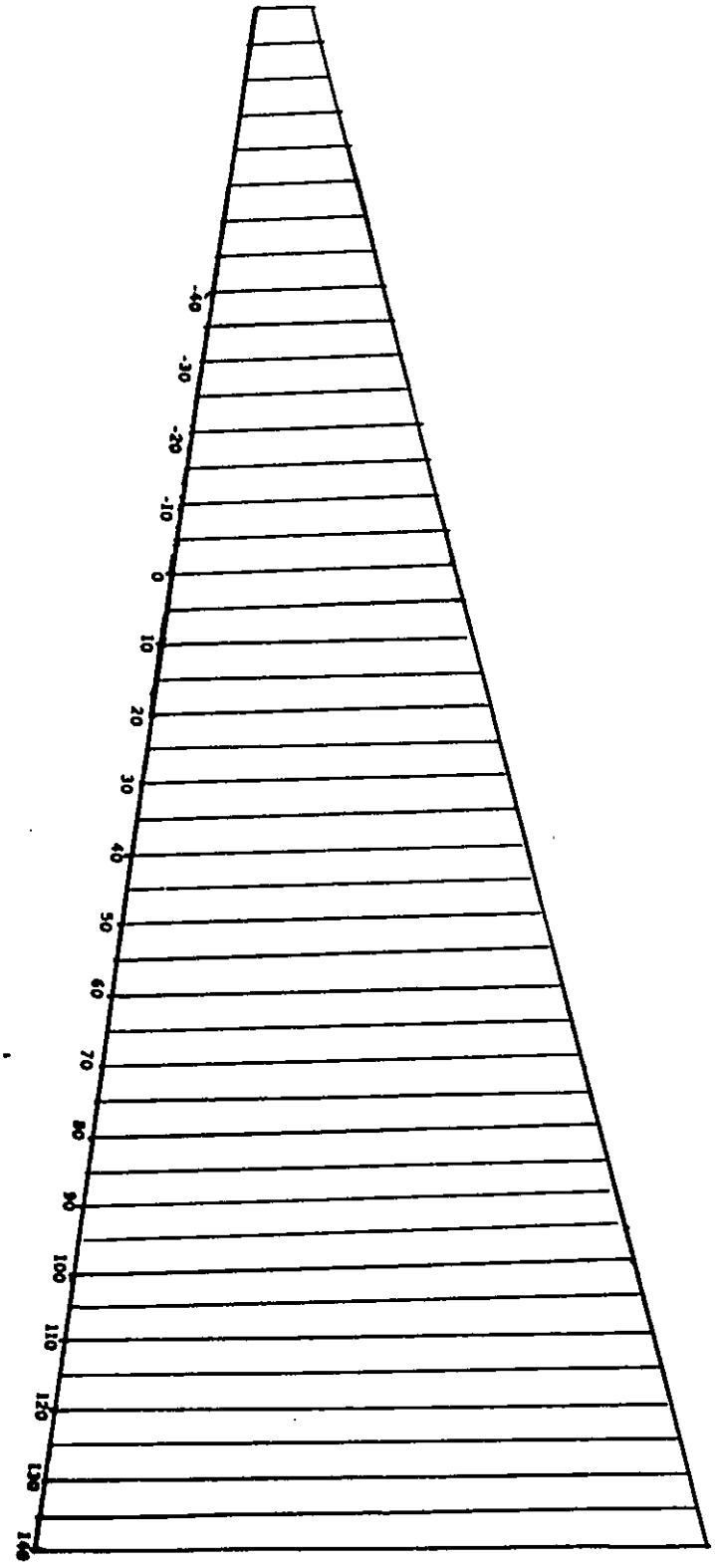

Fig. 3-9. Diagram of a Mylar film with graduated diverging lines.

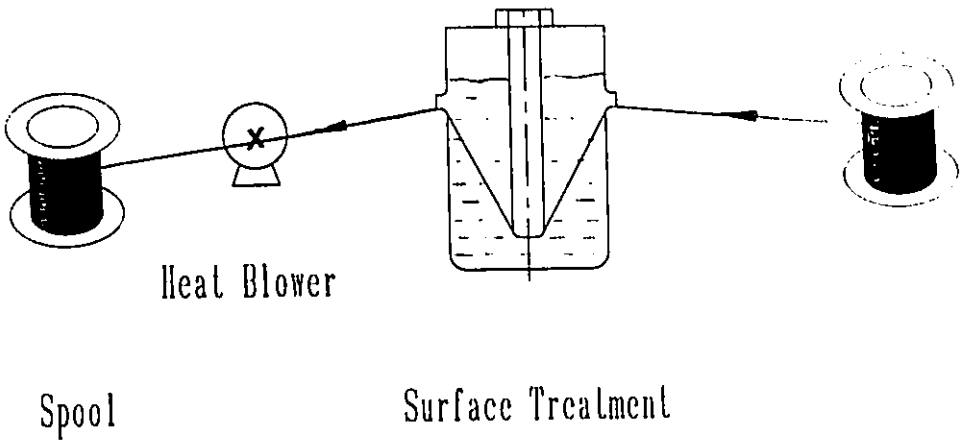

Fig. 3-10. The apparatus used for treating carbon fibers.

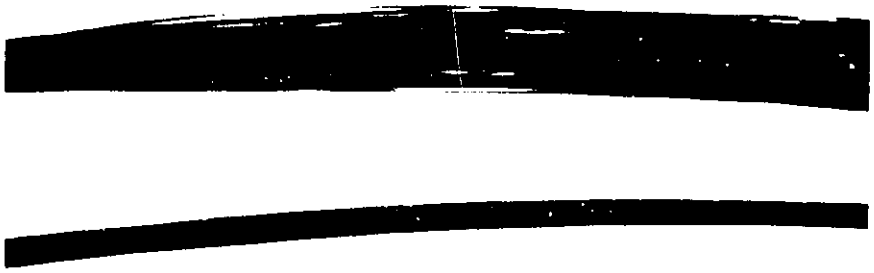

(a)

(b)

Fig. 3-11. Photographs of carbon fibers before coating and after coating. (a) 1K carbon fibers; (b) 3K carbon fibers

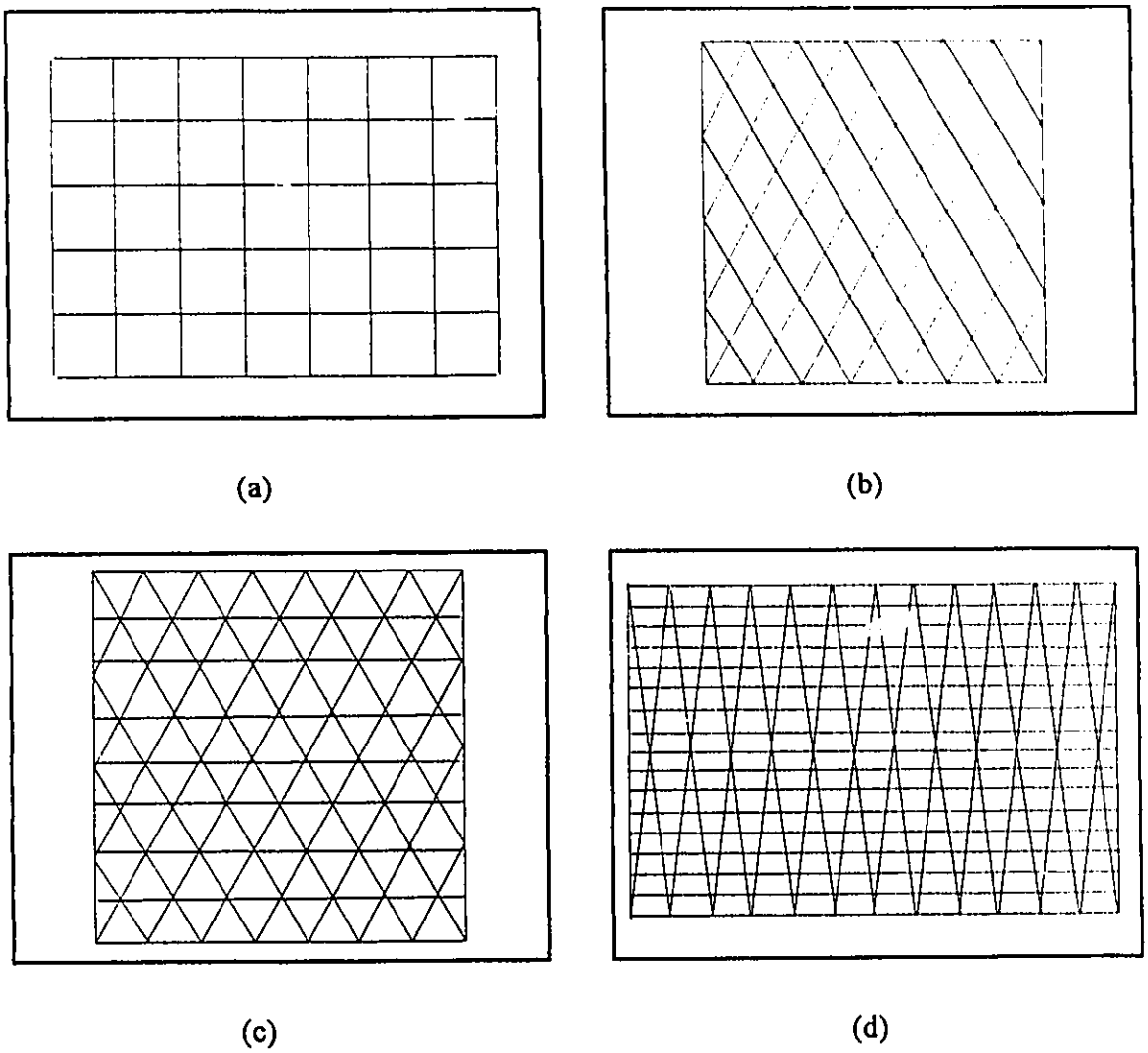

Fig. 3-12. Experimental patterns for the reinforcement. (a) Square (b) Diamond (included angle = 60° (c) Triangle (equilateral) (d) Laddered Diamond (included angle = 26°, ladder spacing = 6.35 mm). For all the patterns, the node spacing along the bottom edge is 12.5 mm.

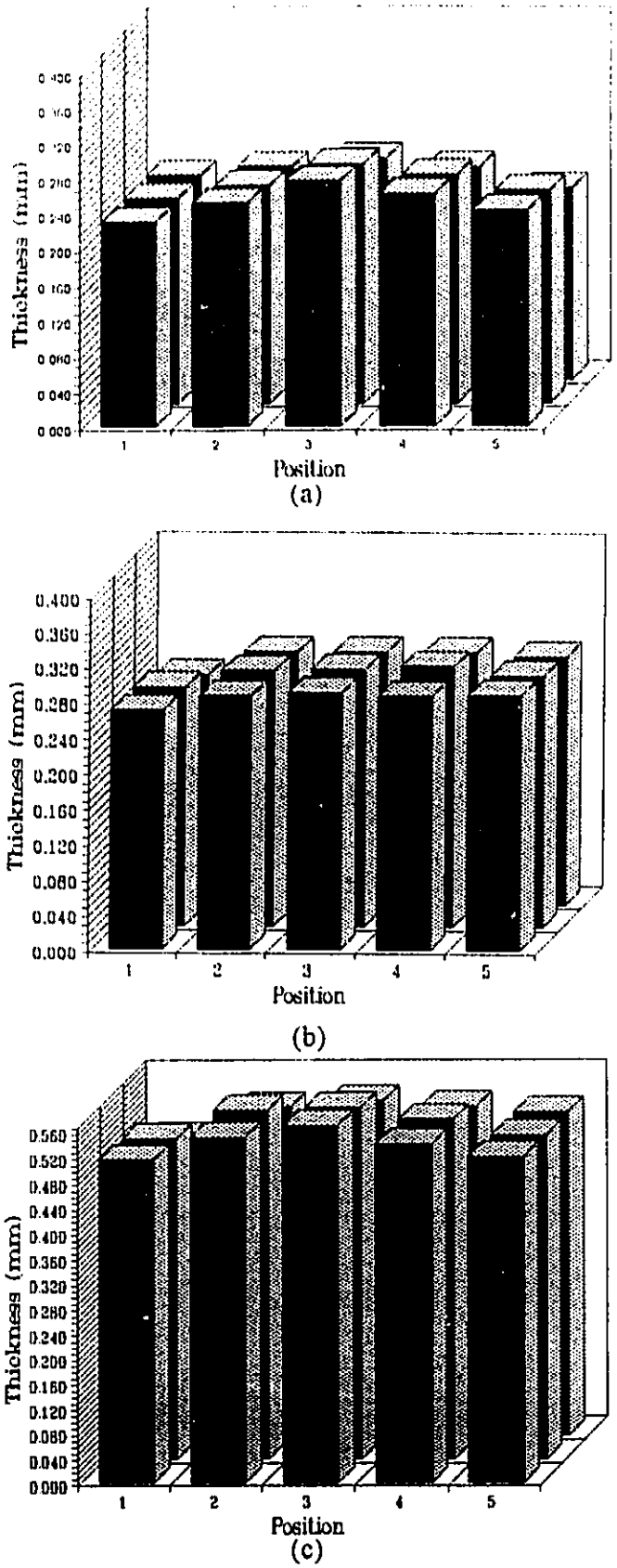

Fig. 3-13. Thickness distribution of the thermoformed TPU sheets. (a) first side of the thermoformed TPU sheet; (b) second layer of the thermoformed TPU sheet; (c) the thermoformed double TPU sheets.

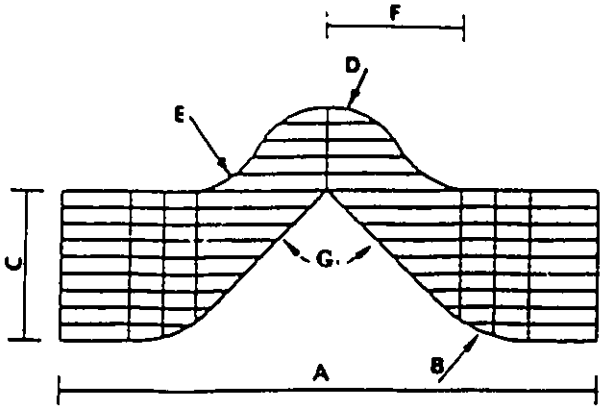

Fig. 4-1. Profile of the tear test specimen.

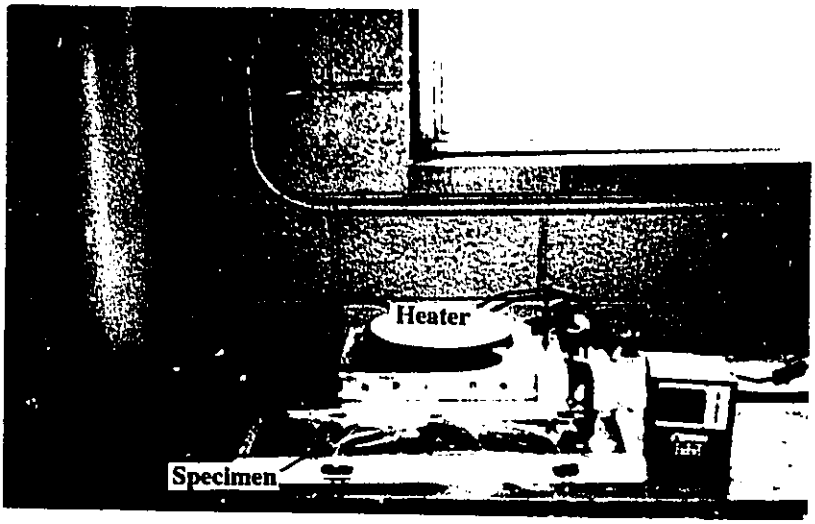

Fig. 4-2. Device for annealing.

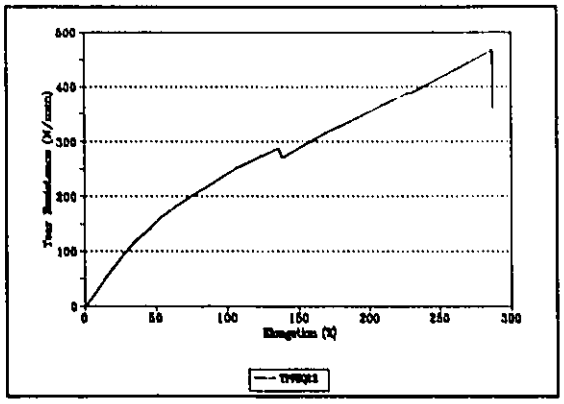

(a) Square

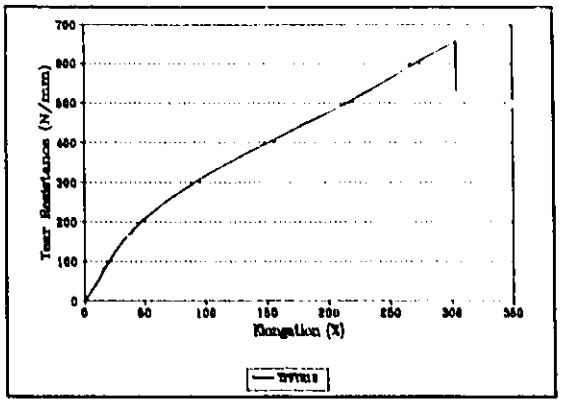

(b) Triangle

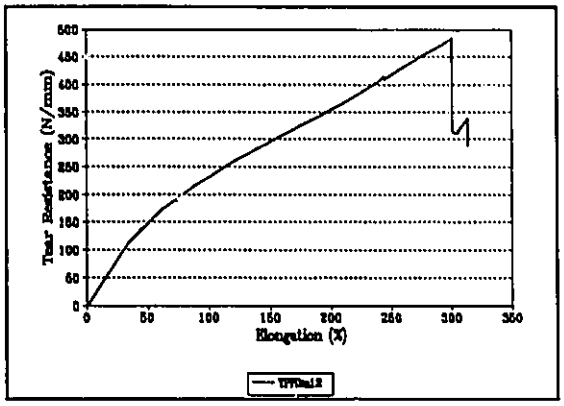

(c) Diamond

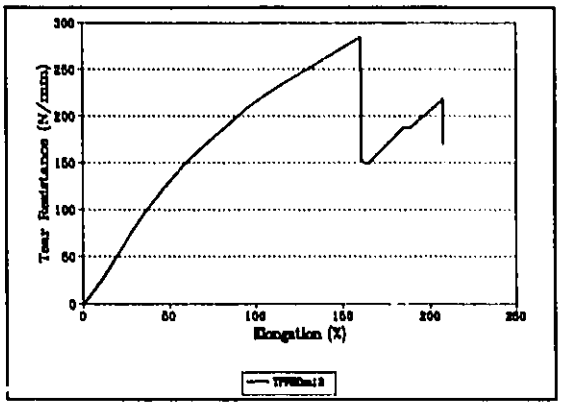

(d) Diamond pattern loaded transversely

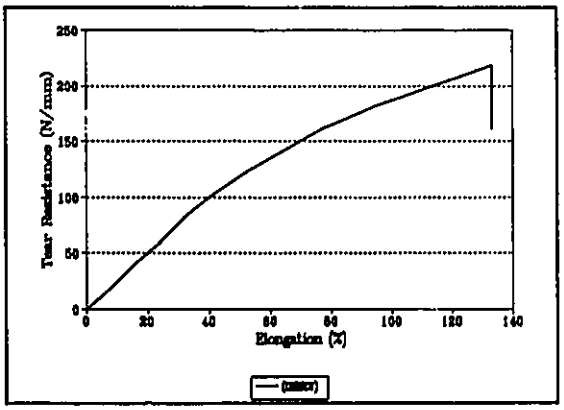

(e) Thermoformed Double Sheet

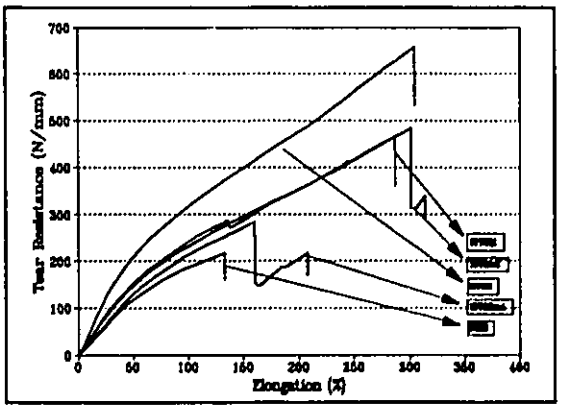

(f) Comparison of the tear test results

Fig. 4-3. The characteristics tearing curves of the unreinforced TPU elastomer sheets and the TPU elastomer sheets reinforced with the TPU-rod.

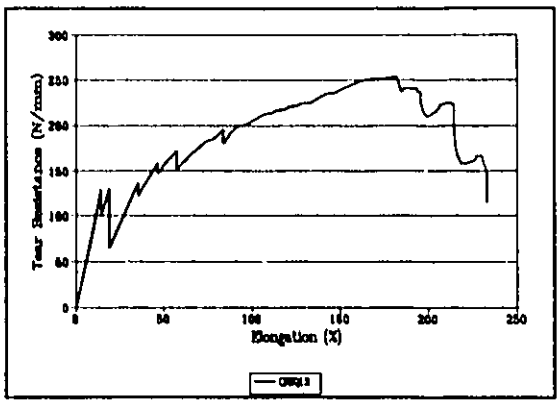

(a) Square

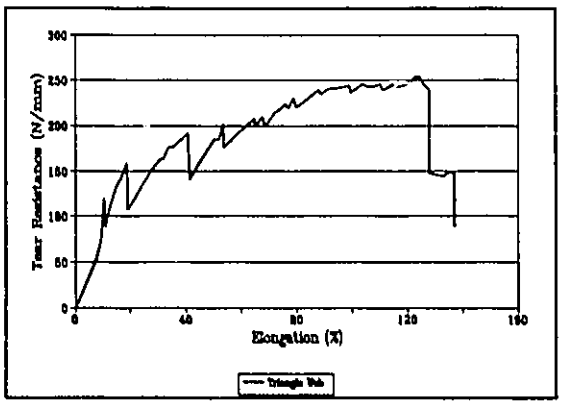

(b) Triangle

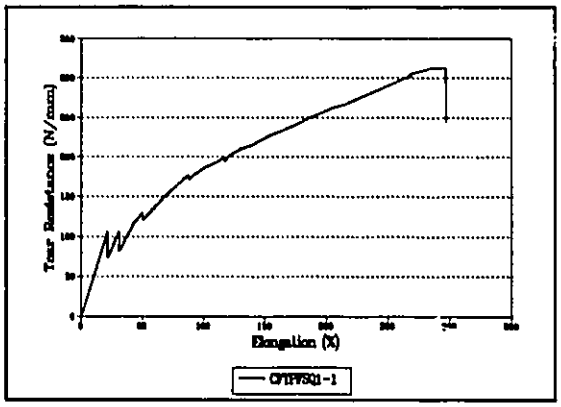

(c) Squares with alternating carbon & TPU fiber

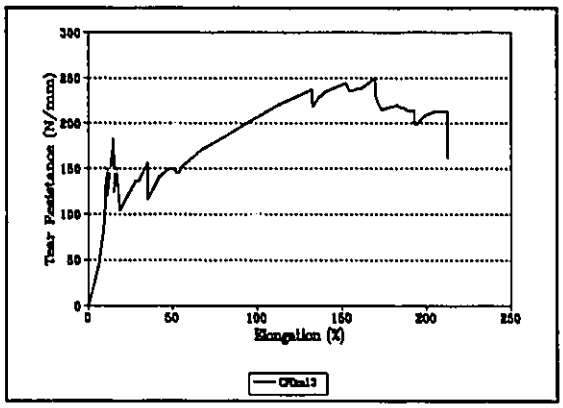

(d) Diamond

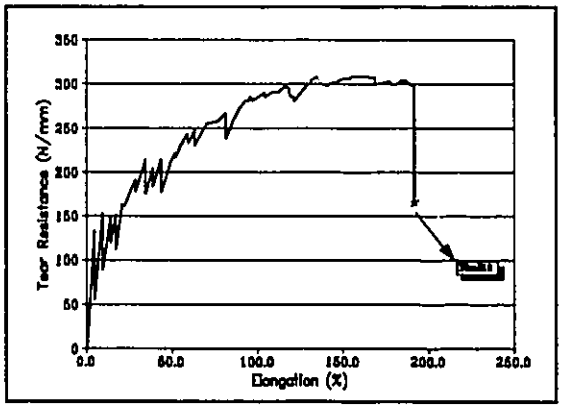

(e) Laddered Diamond

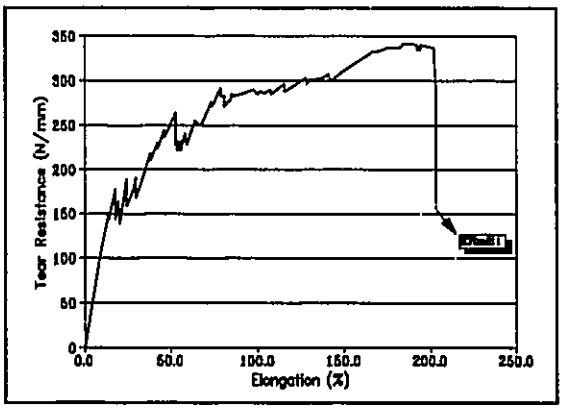

(f) Laddered Diamond loaded laterally

Fig. 4-4. The characteristics tearing curves of the TPU elastomer sheets reinforced with 1K carbon fibers in various patterns.

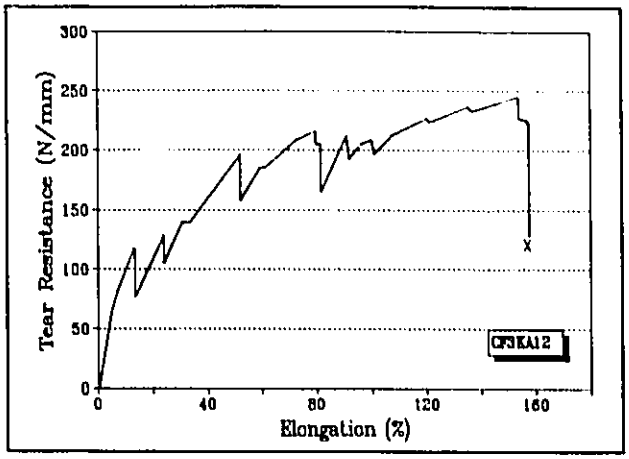

(a) Square

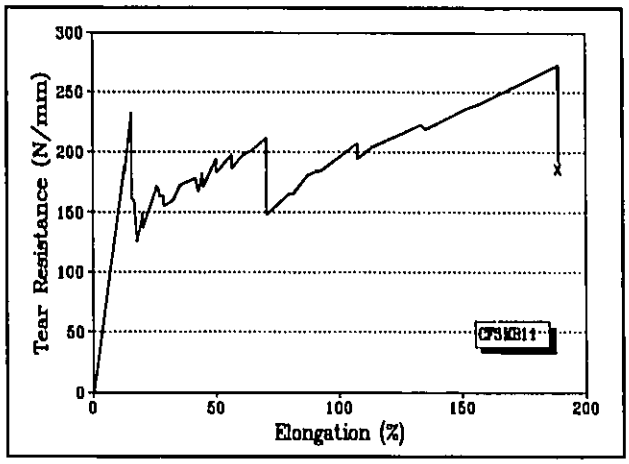

(b) Diamond

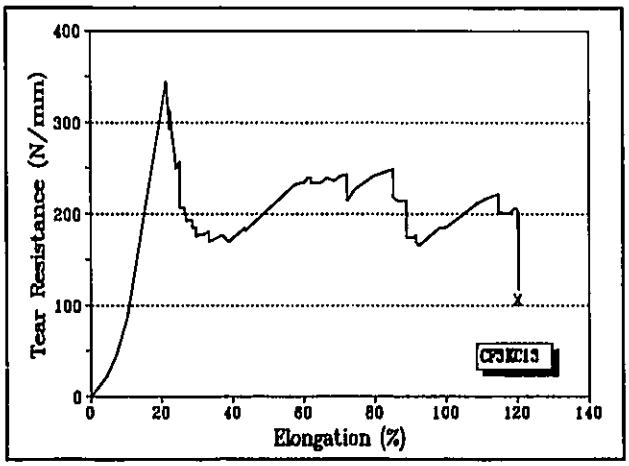

(c) Triangle

Fig. 4-5. The characteristic tearing curves of the TPU elastomer sheets reinforced with the 3K carbon fibers.

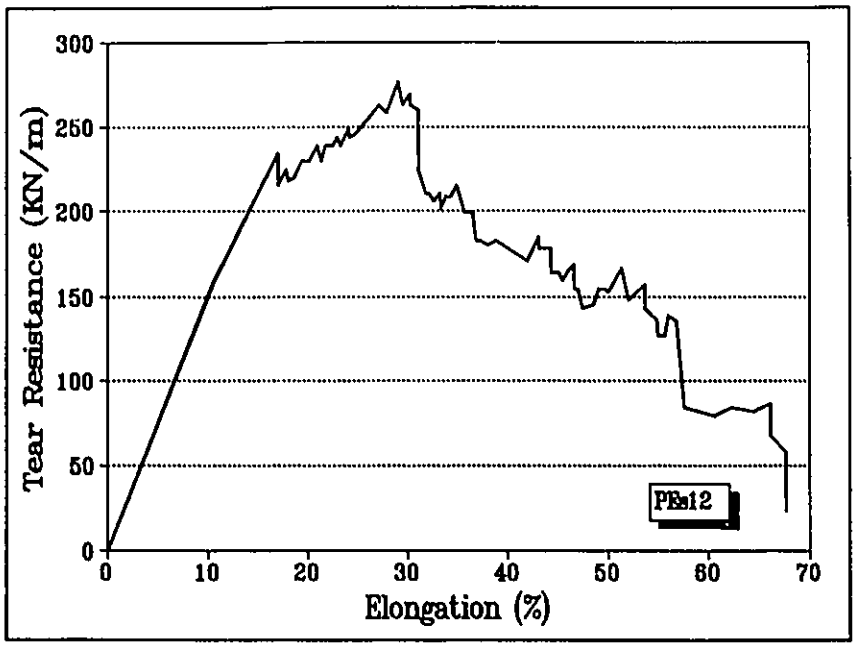

Fig. 4-6. The characteristics tearing curves of the TPU elastomer sheets reinforced with polyester scrim.

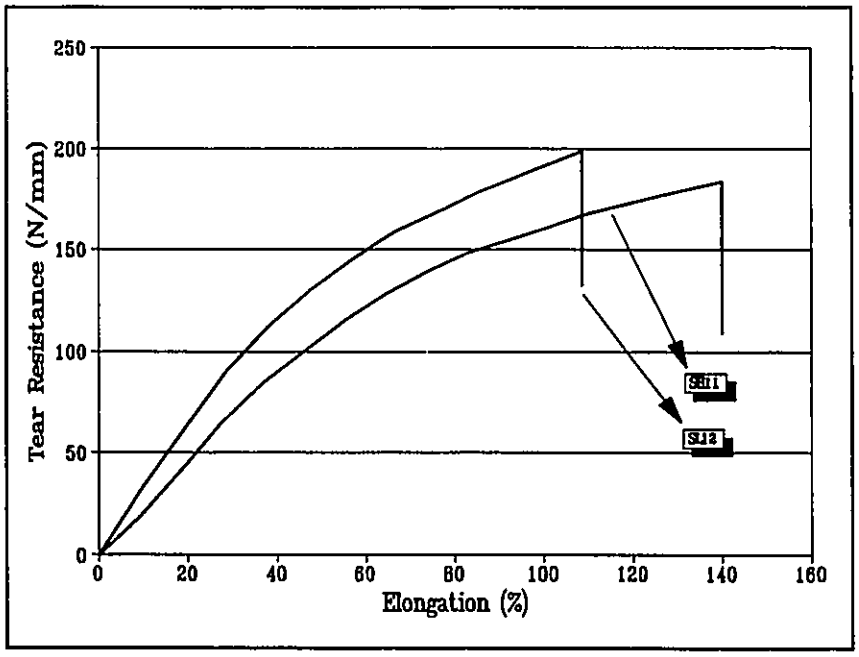

Fig. 4-7. Tear test results of the single TPU sheets under different orientation.

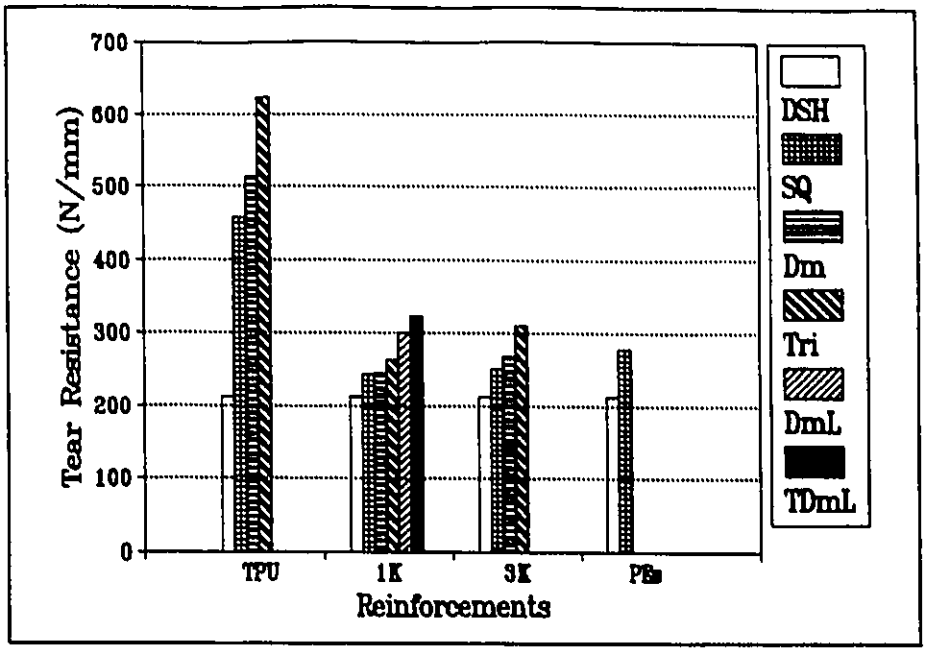

Fig. 4-8.* Comparison of the tear resistance of sparsely reinforced TPU elastomer sheets with unreinforced thermoformed double TPU elastomer sheet.

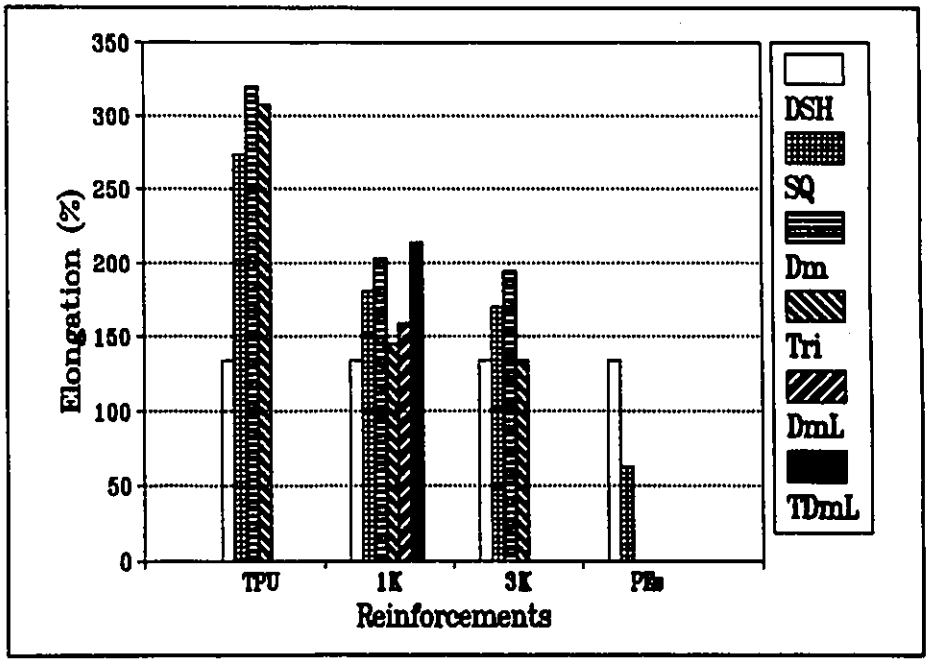

Fig. 4-9.* Comparison of the elongation of sparsely reinforced TPU elastomer sheets with unreinforced thermoformed double TPU elastomer sheet.

* (Reinforcement patterns: DSH thermoformed double sheet with no reinforcement; SQ: square; Dm: diamond; Tri: triangle; DmL: laddered diamond; TDmL: laddered diamond loaded laterally).

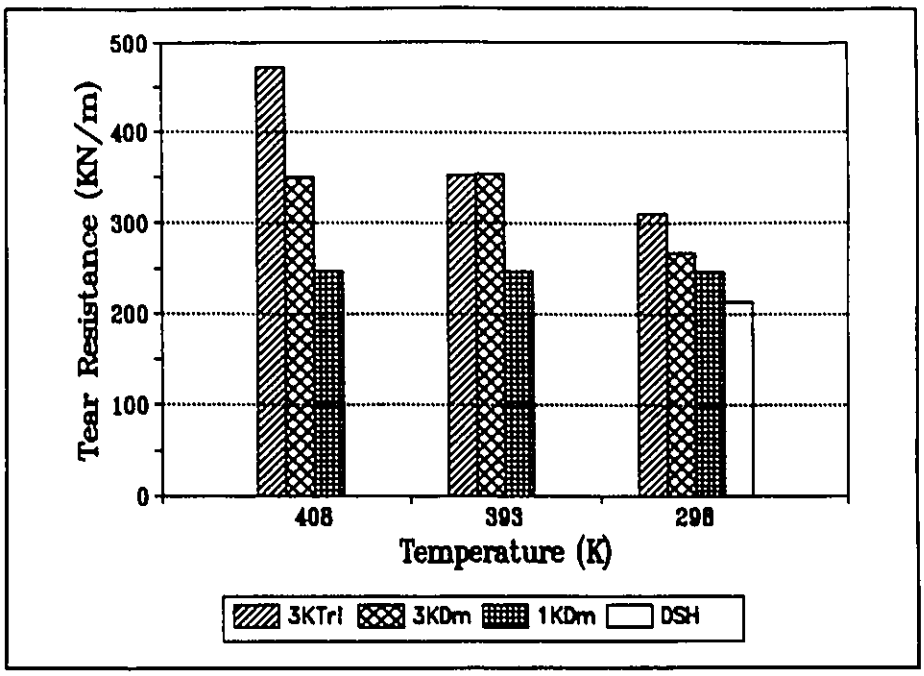

Fig. 4-10. Effect of annealing on the tear resistance of carbon fiber reinforced TPU elastomer sheets (Tri: triangle pattern; Dm: diamond pattern; DSH: thermoformed double sheet with no reinforcement).

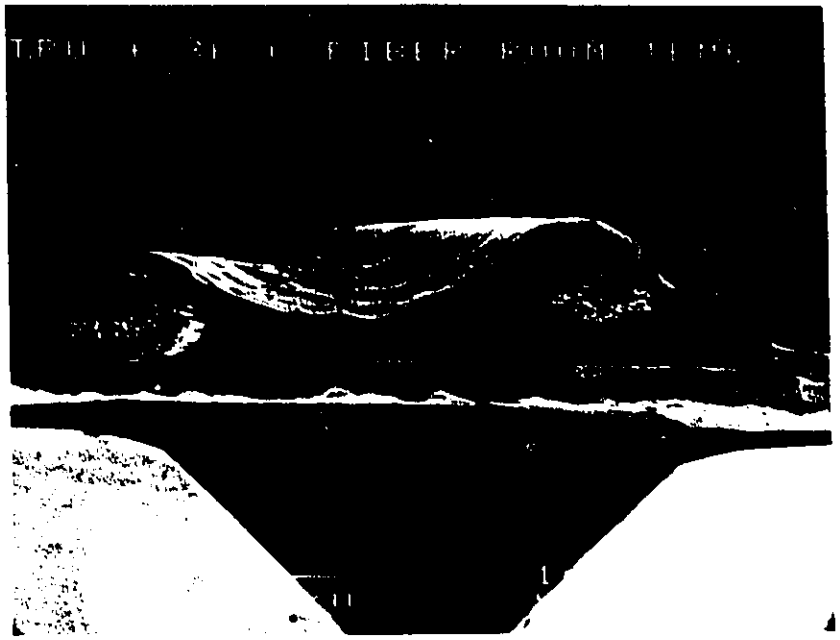

(a)

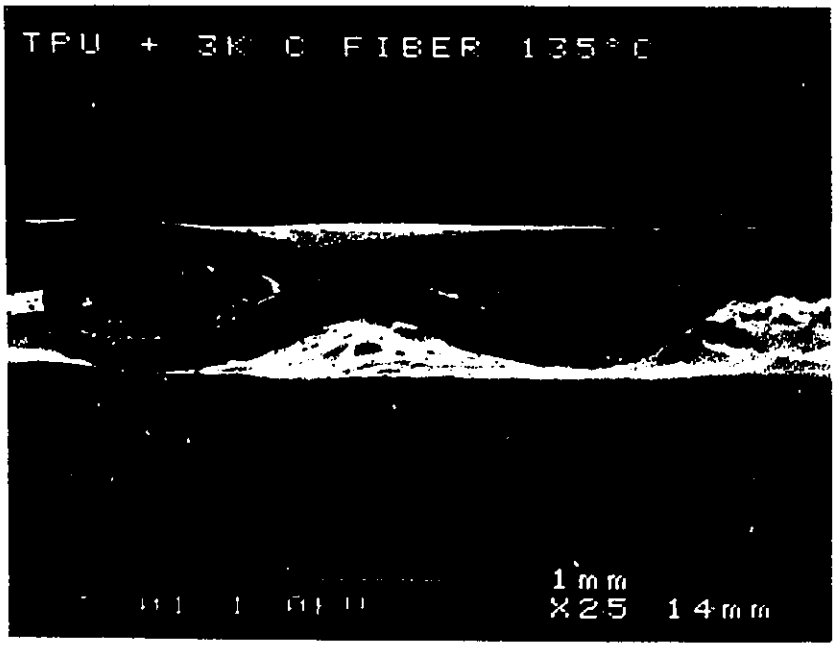

(b)

Fig. 4-11. Effect of annealing on increasing close contact surfaces between the carbon fibers and TPU matrix. (a) before annealing; (b) after annealing. SEM photographs.

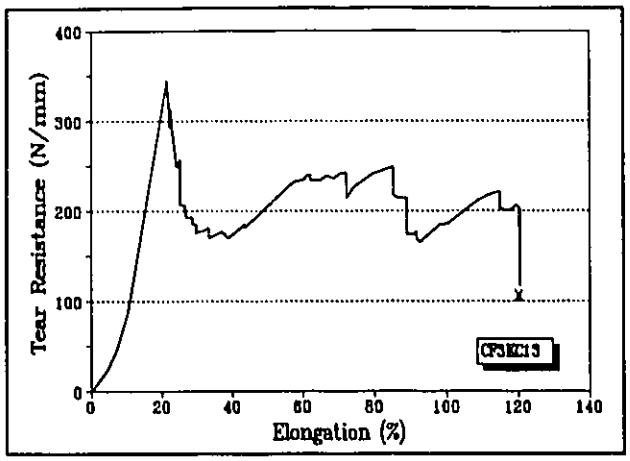

(a) no annealing

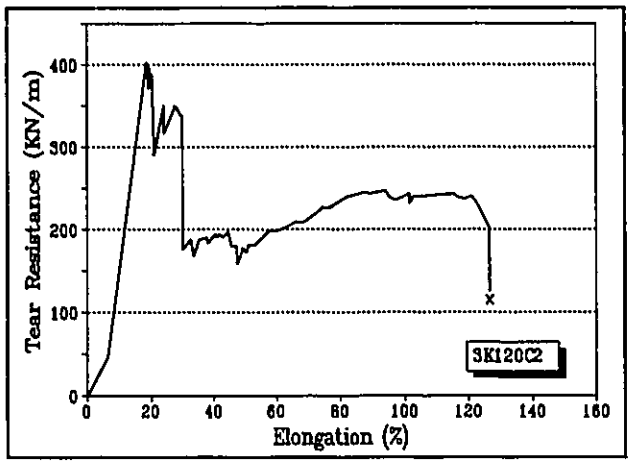

(b) annealed at 120°C

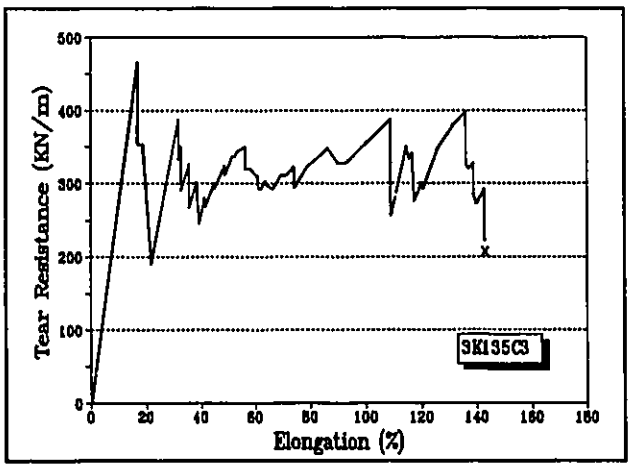

(c) annealed at 135°C

Fig. 4-14. Effect of annealing on the characteristic tearing curves of the TPU elastomer sheets reinforced with the 3K carbon fibers in the triangular pattern.

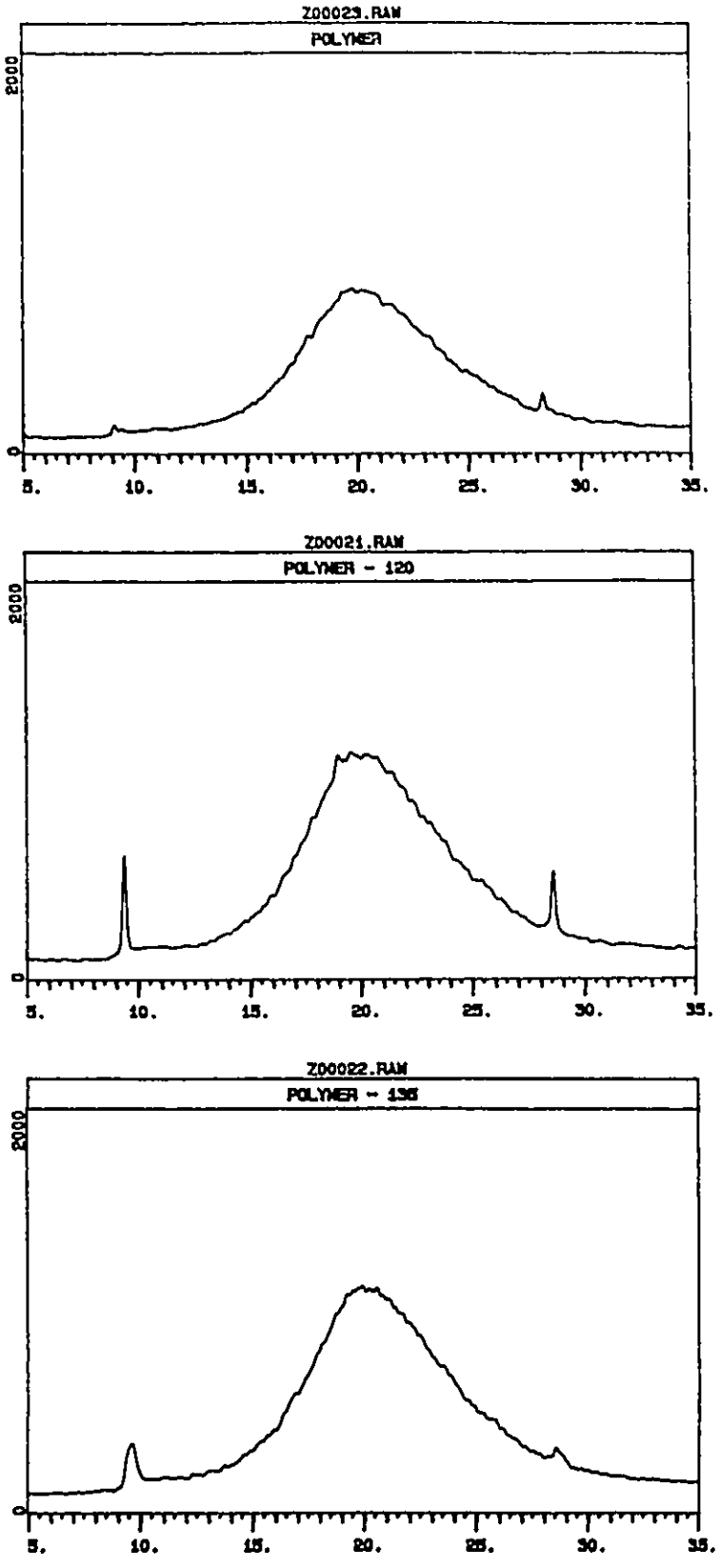

Fig. 4-13. X-ray diffraction patterns of the TPU elastomer sheets; (a) no annealing (b) annealed at 120°C (c) annealed at 135°C.

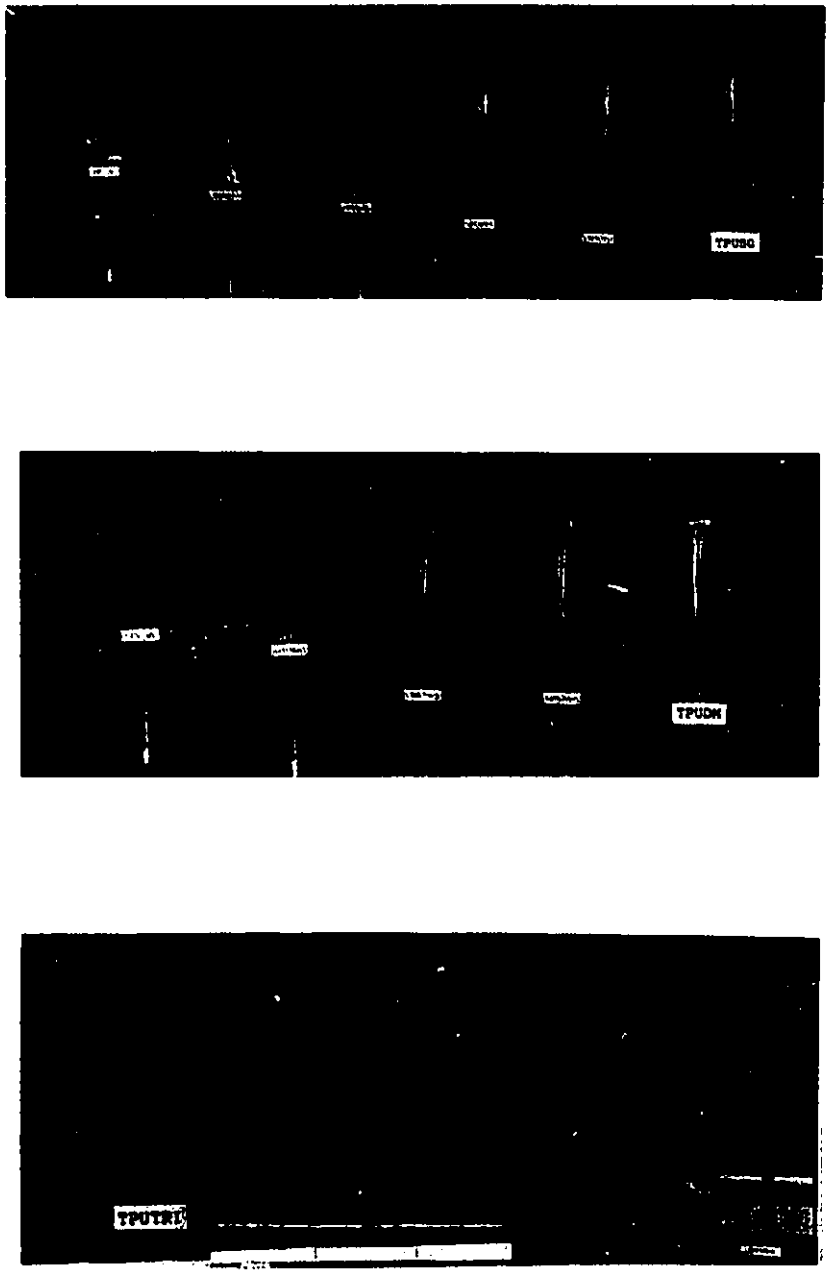

Fig. 4-14. Tear testing sequence of the TPU elastomer sheet reinforced with TPU-rod.

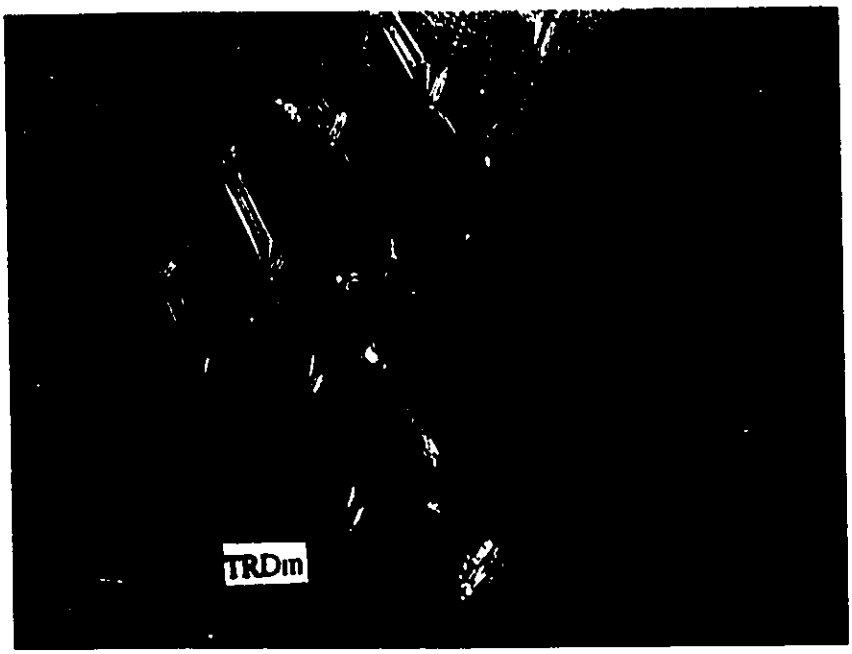

Fig. 4-15. Crack arrested at a fiber junction in a tear sample of TPU elastomer sheet reinforced with TPU-rod.

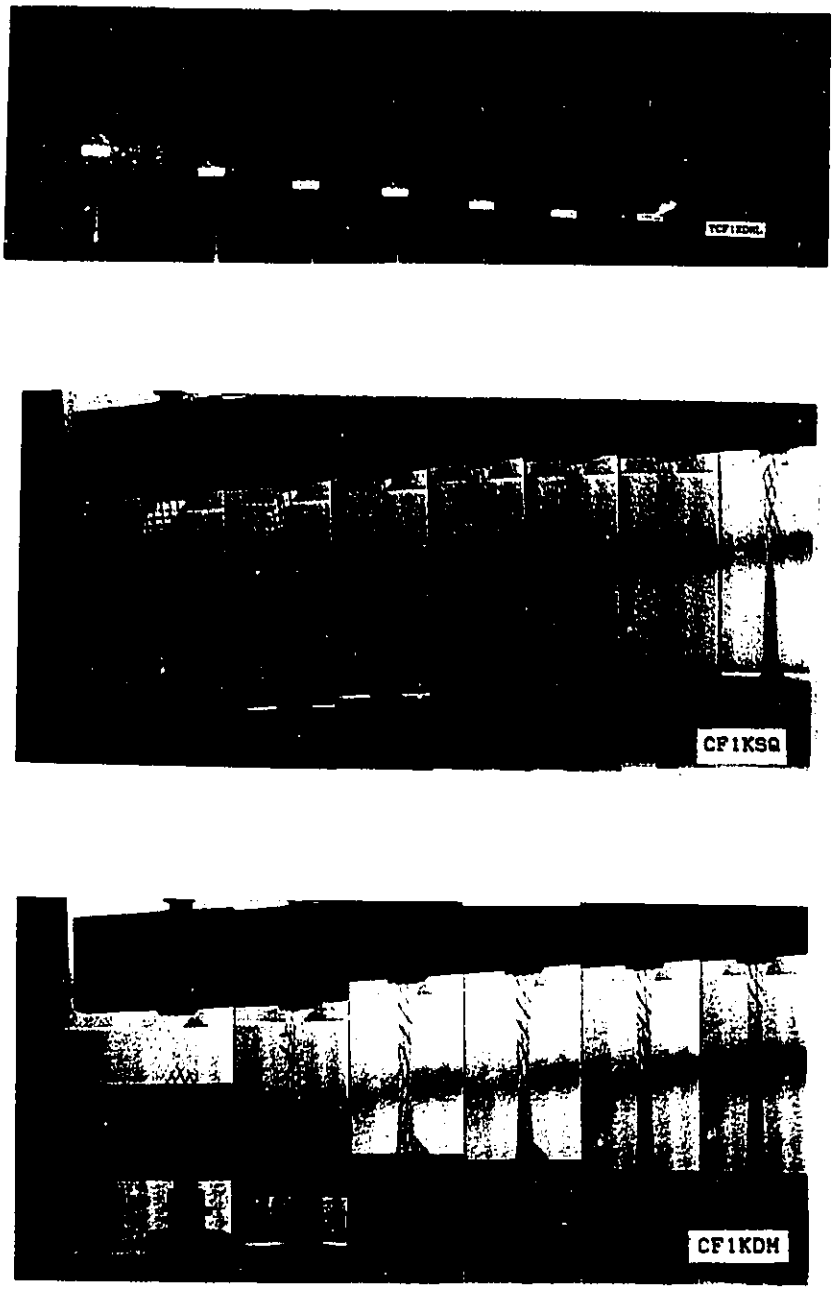

Fig. 4-16. Tear testing sequence of the TPU elastomer sheet reinforced with 1K carbon fibers.

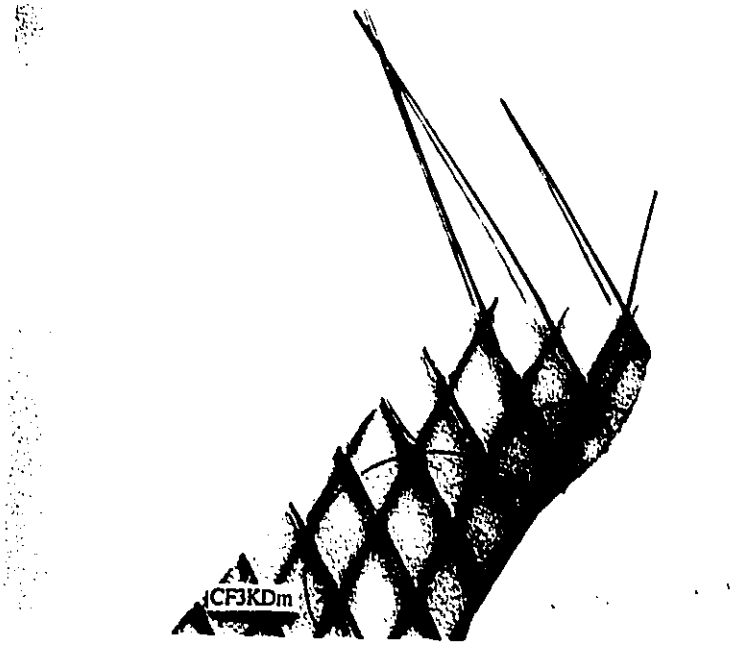

(a)

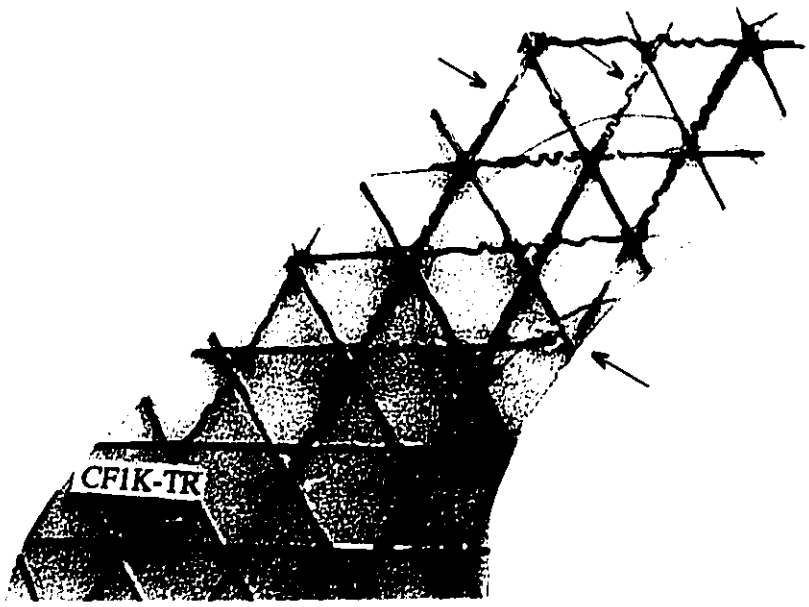

(b)

Fig. 4-17. (a) Fiber pulled out of TPU elastomer sheet reinforced with 3K carbon fibers. (b) Fiber slippage in TPU reinforced by 1K carbon fibers.

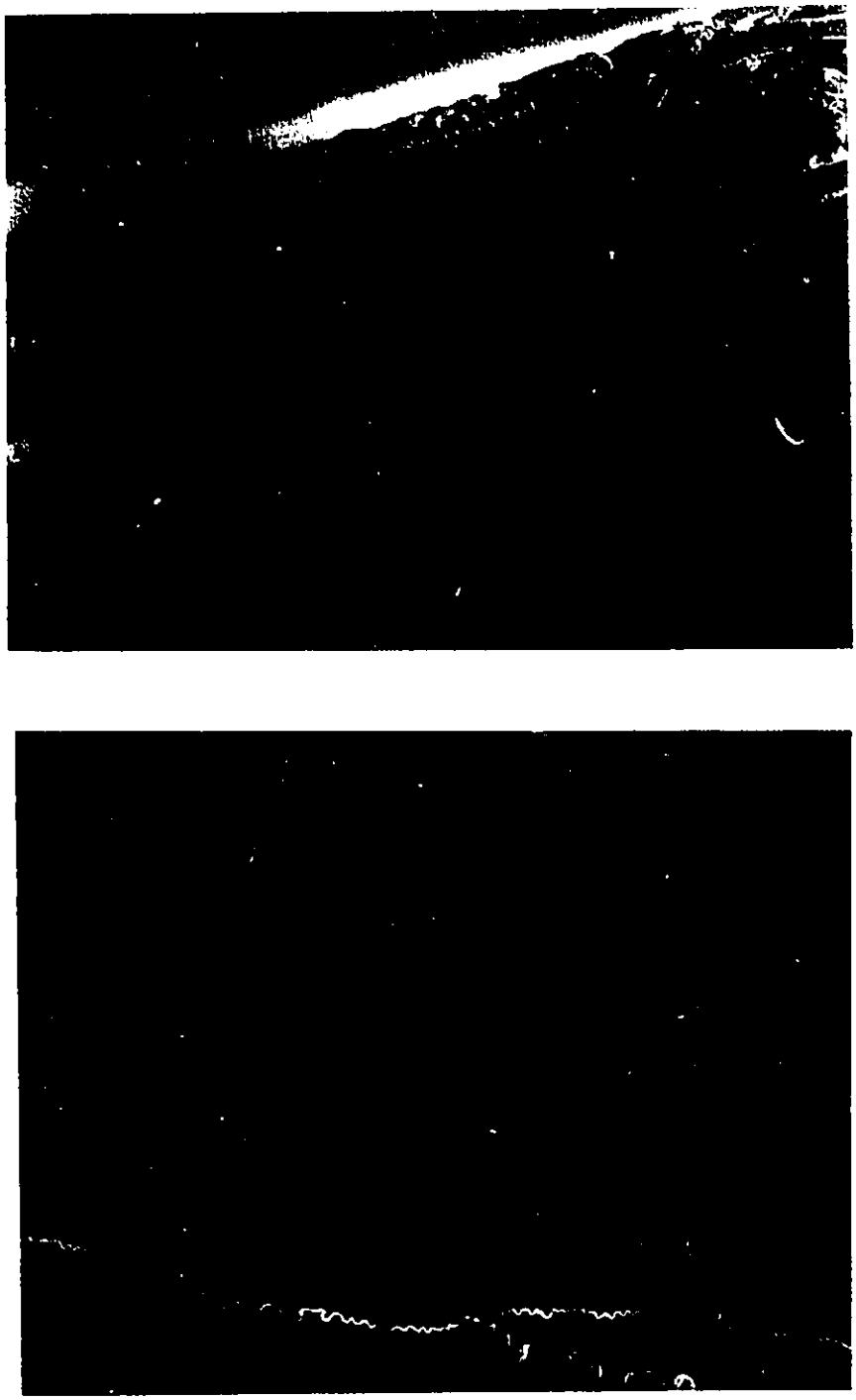

(a)

Fig. 4-18. Fracture morphology of the tearing surfaces of the unreinforced and reinforced TPU elastomer sheets. (a) unreinforced thermoformed double sheets; (b) reinforced with TPU-rod; (c) reinforced with carbon fibers. SEM photograpgs.

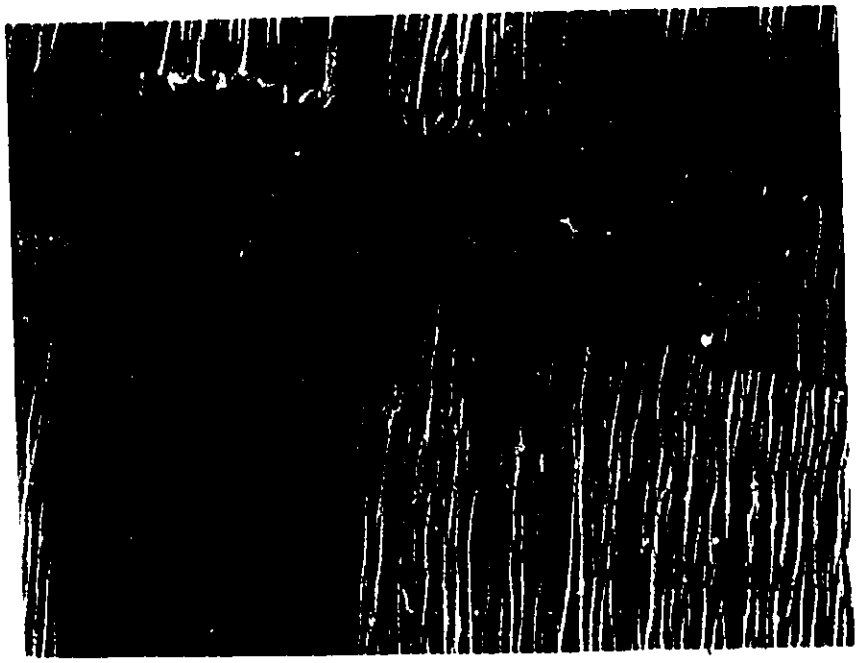

(b-1) TPU-rod with triangle pattern.

(b-2) TPU-rod with square pattern.

Fig. 4-18. Continued (I).

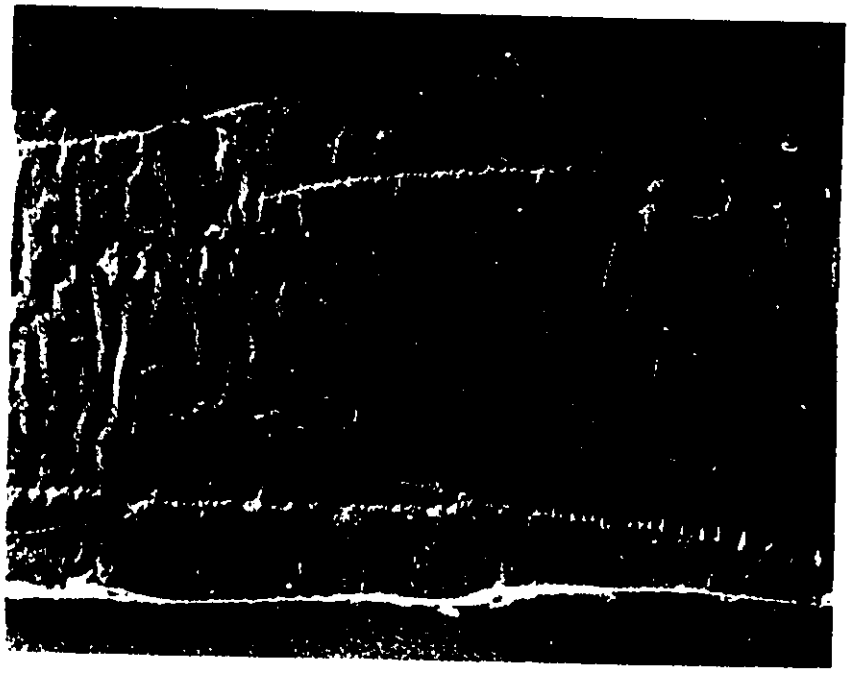

(c-1) Carbon fiber with laddered diamond pattern

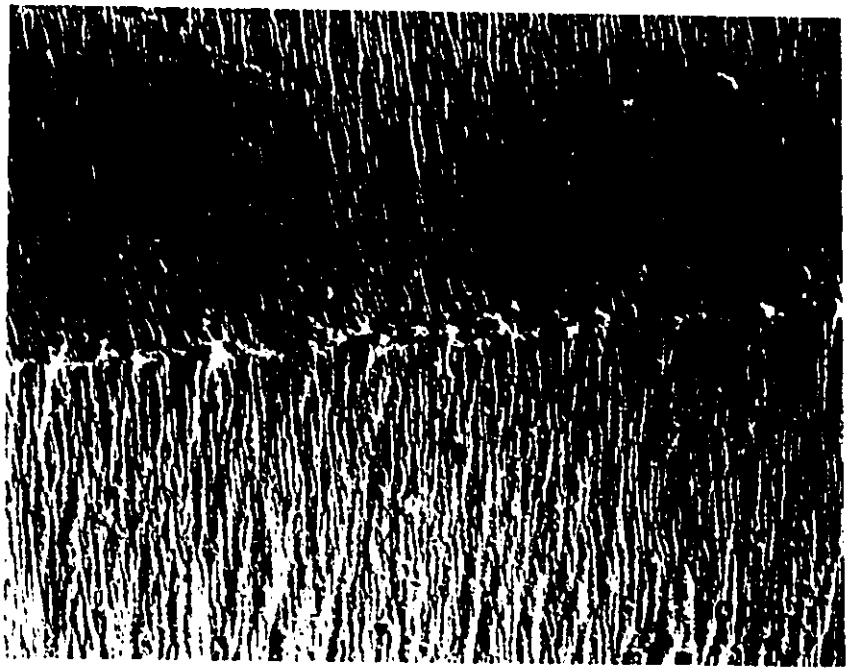

(c-2) Carbon fiber with triangle pattern

Fig. 4-18. Continued (II).

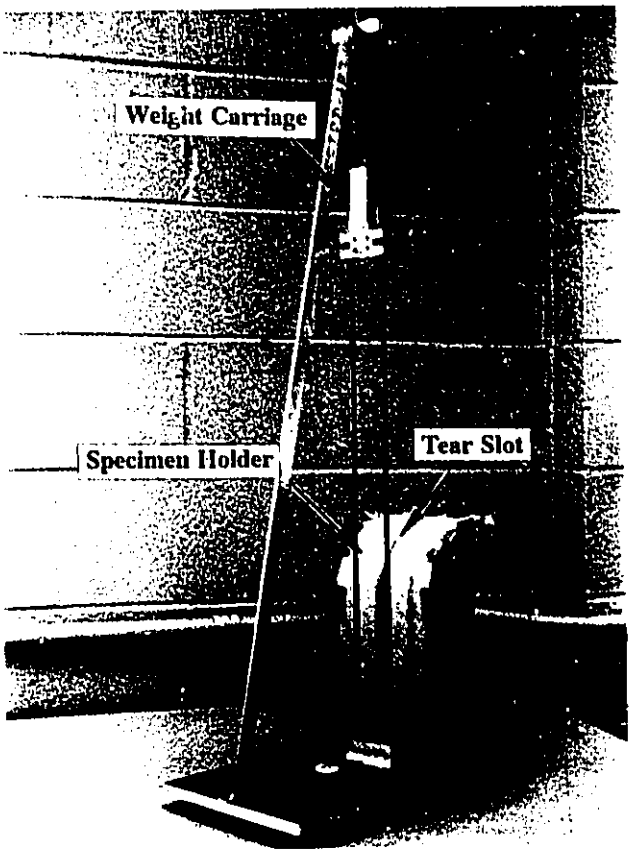

Fig. 5-1. Snag tester.

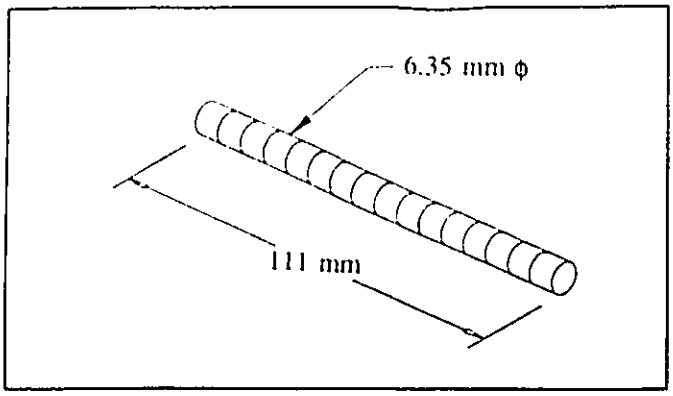

Nylon Threaded Rod

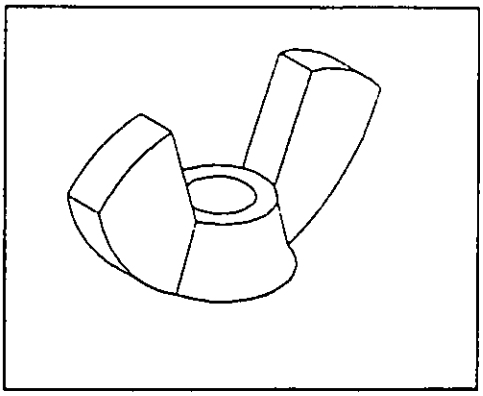

Wing Nut

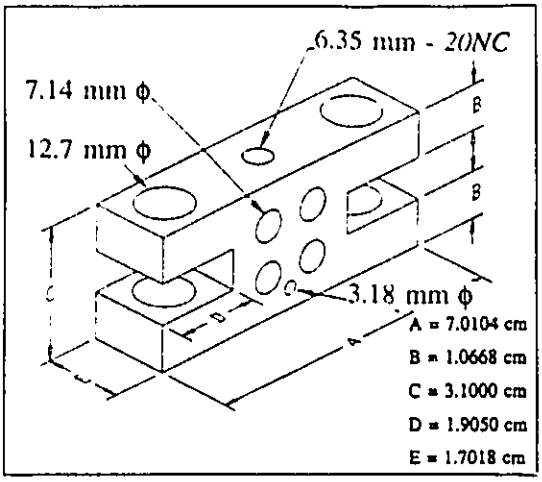

Main Body of Carriage

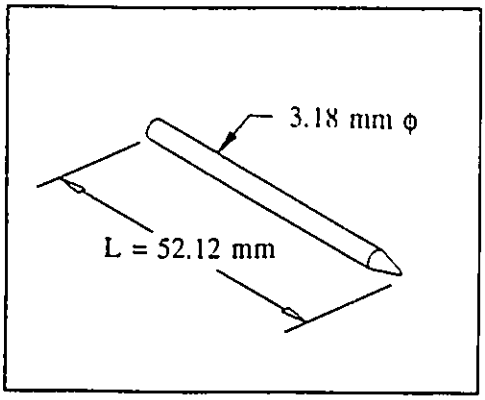

Probe

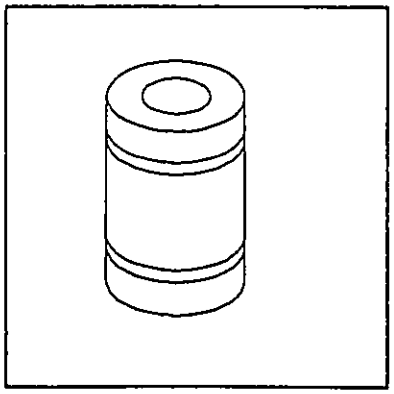

Linear ball

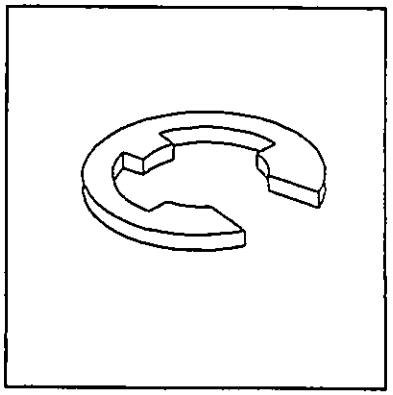

C-Ring

Fig. 5-2. The parts of the weight carriage.

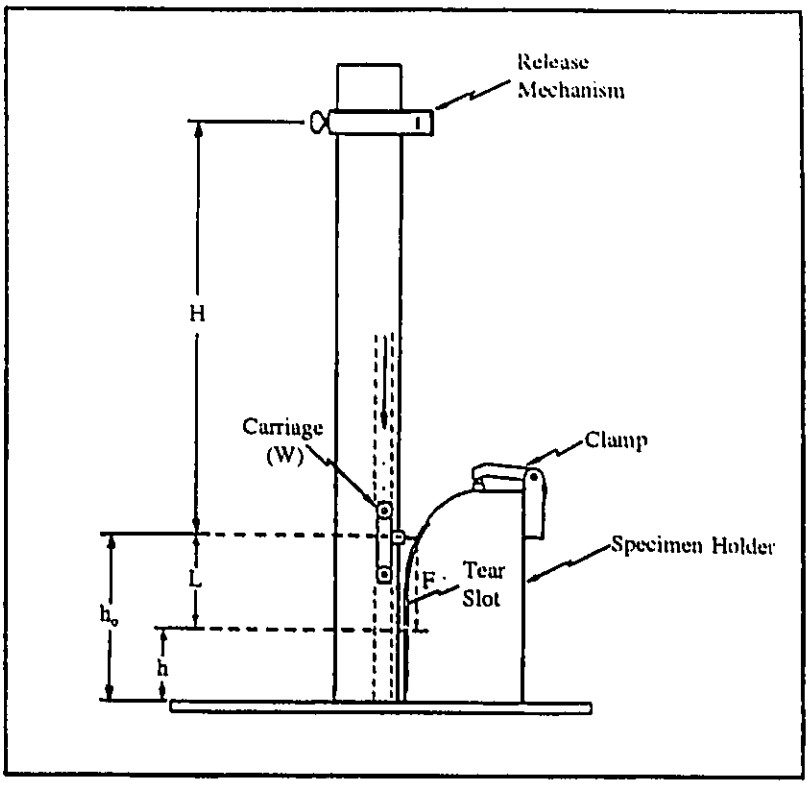

Fig. 5-3. Specimen in the snag test apparatus, showing how the contact height of the probe is determined. The weight carriage is locked at the position where the probe just touches the sheet.

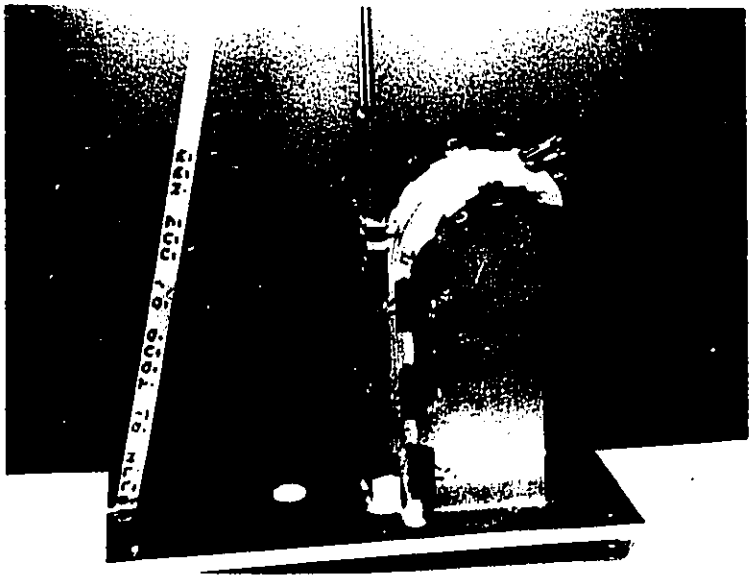

Fig. 5-4. Lateral view of puncture-propagation of tear tester.

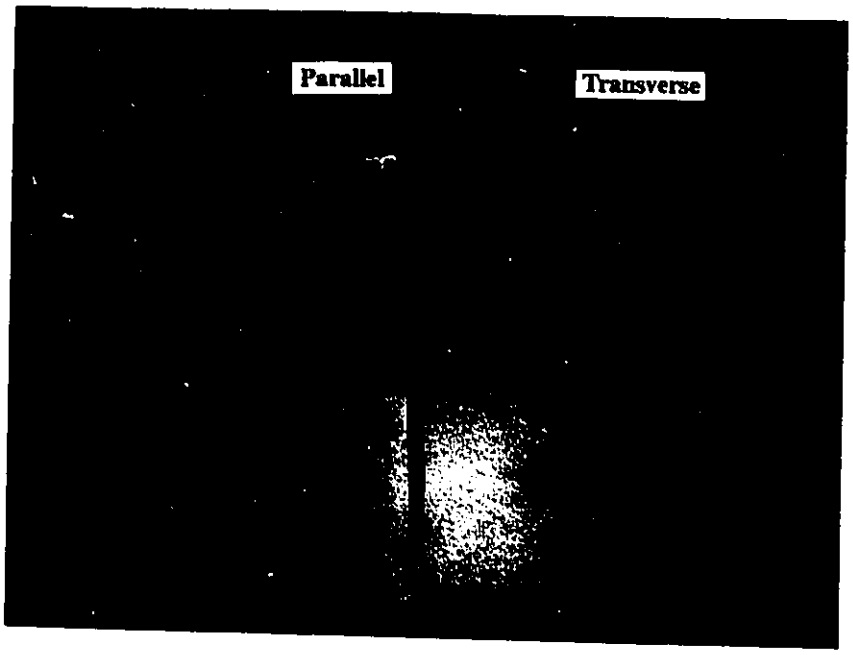

(a)

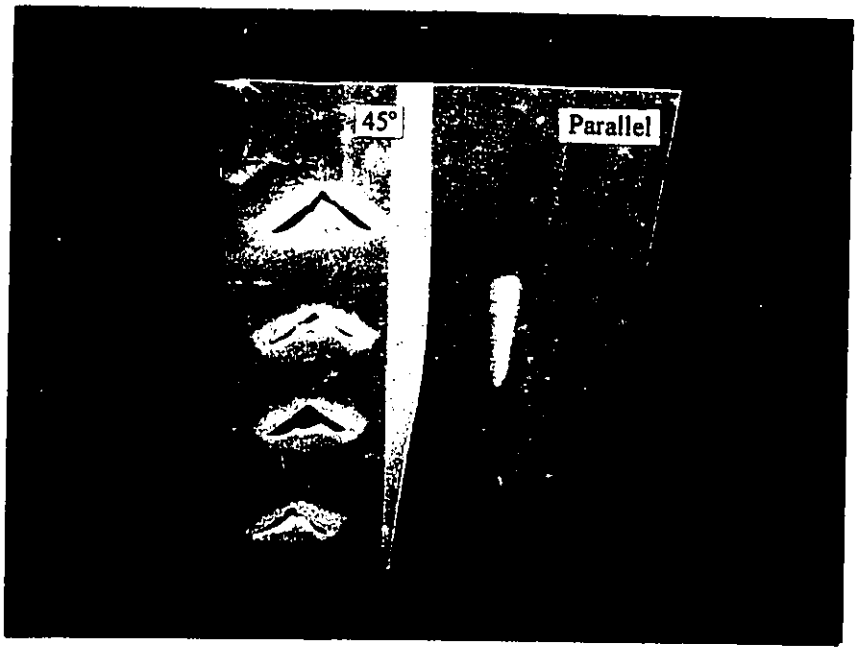

(b)

Fig. 5-5. Snagging tear types: (a) TPU single sheet; (b) Polyester scrim coated TPU.

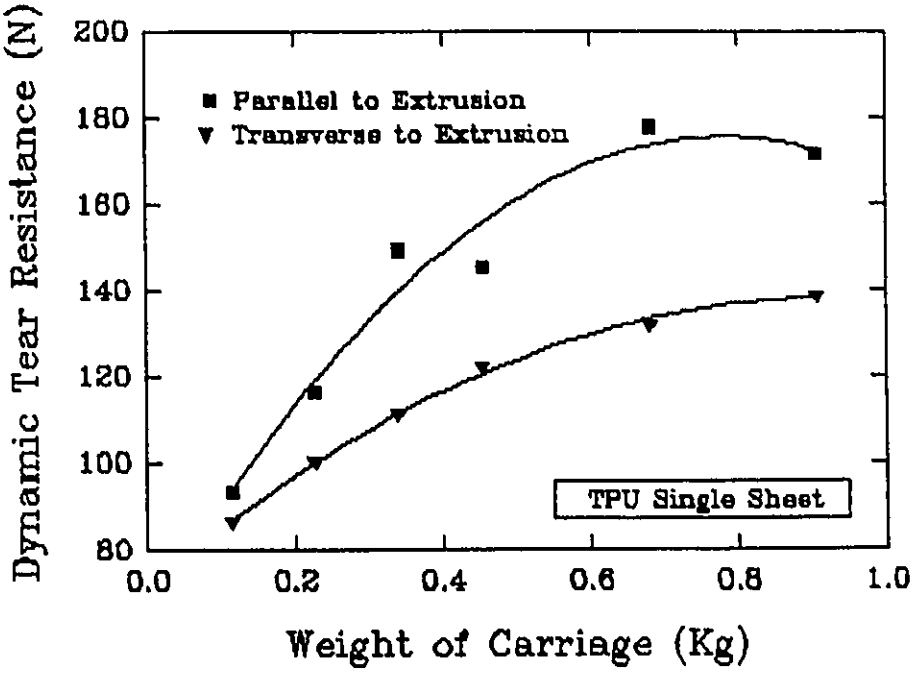

Fig. 5-6. Effect of orientation on dynamic tear resistance of TPU single sheet.

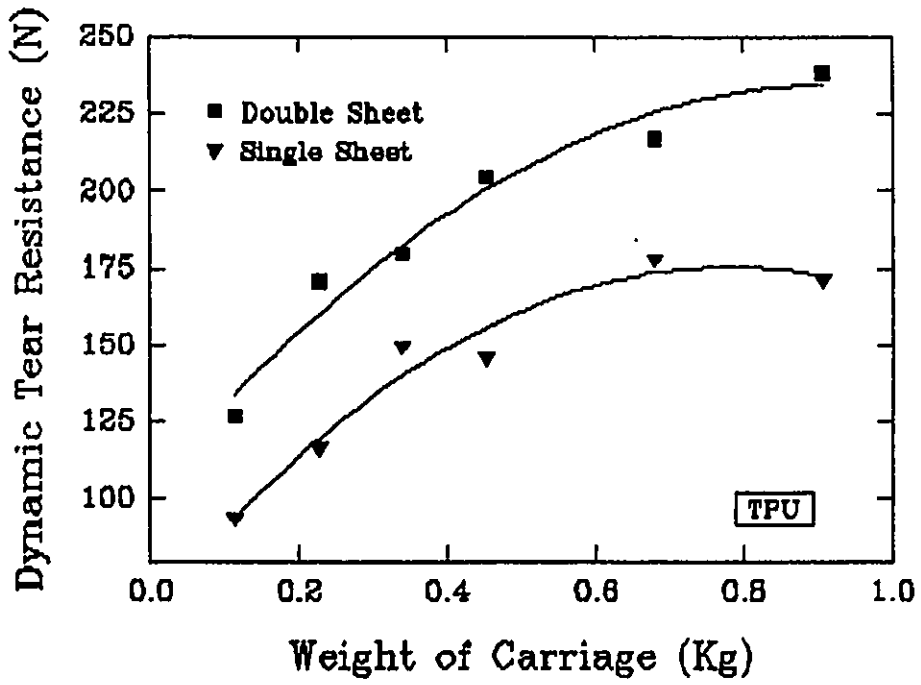

Fig. 5-7. Effect of thickness on dynamic tear resistance of TPU elastomer sheets.

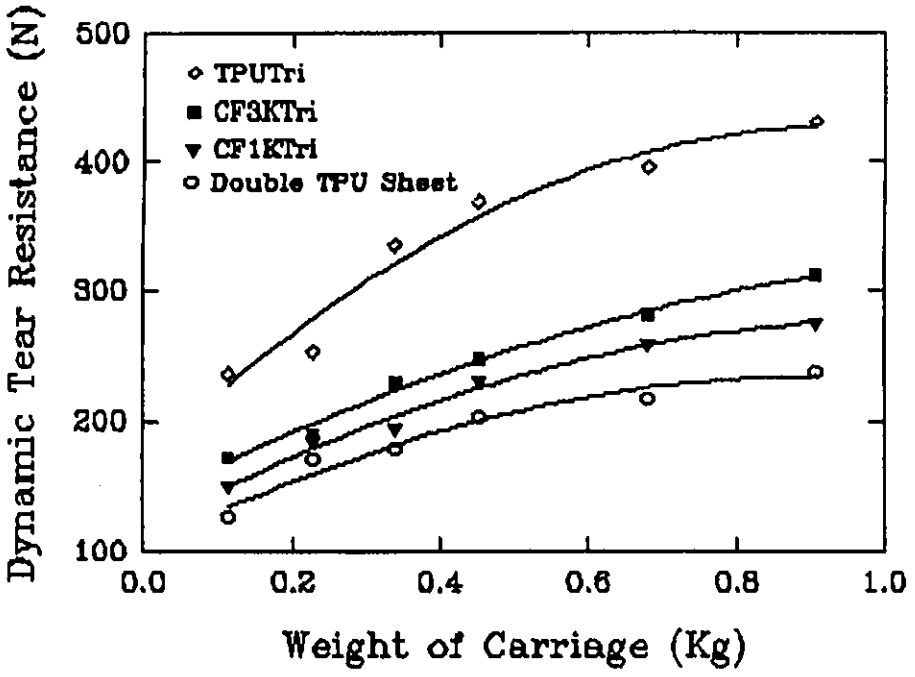

Fig. 5-8. Comparison of dynamic tear resistance of TPU elastomer sheet sparsely reinforced with different reinforcements (Tri: triangle pattern).

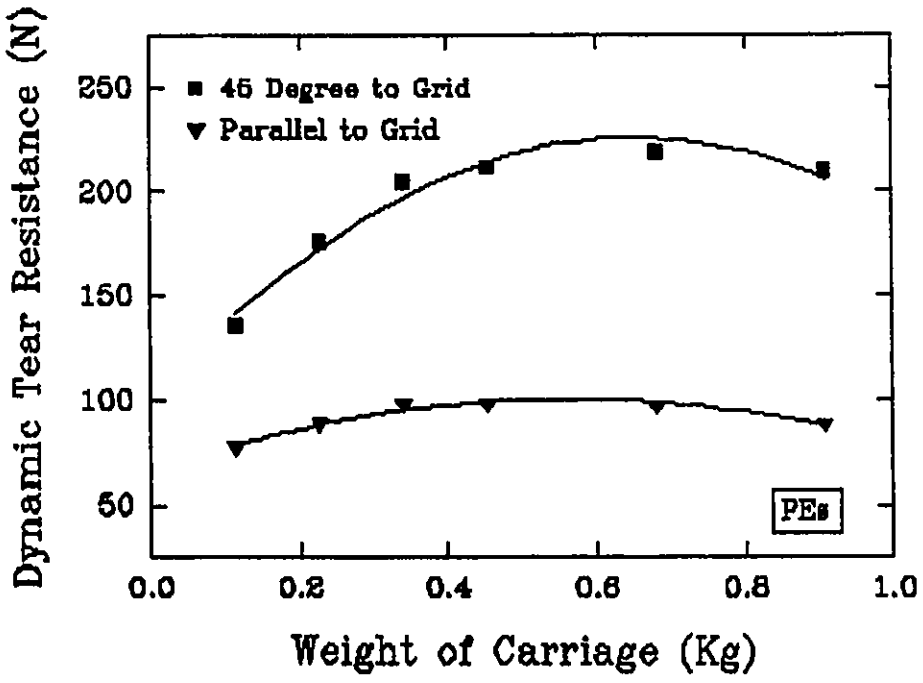

Fig. 5-9. Dynamic tear resistance of polyester scrim (PEs) coated with TPU in different fiber orientations.

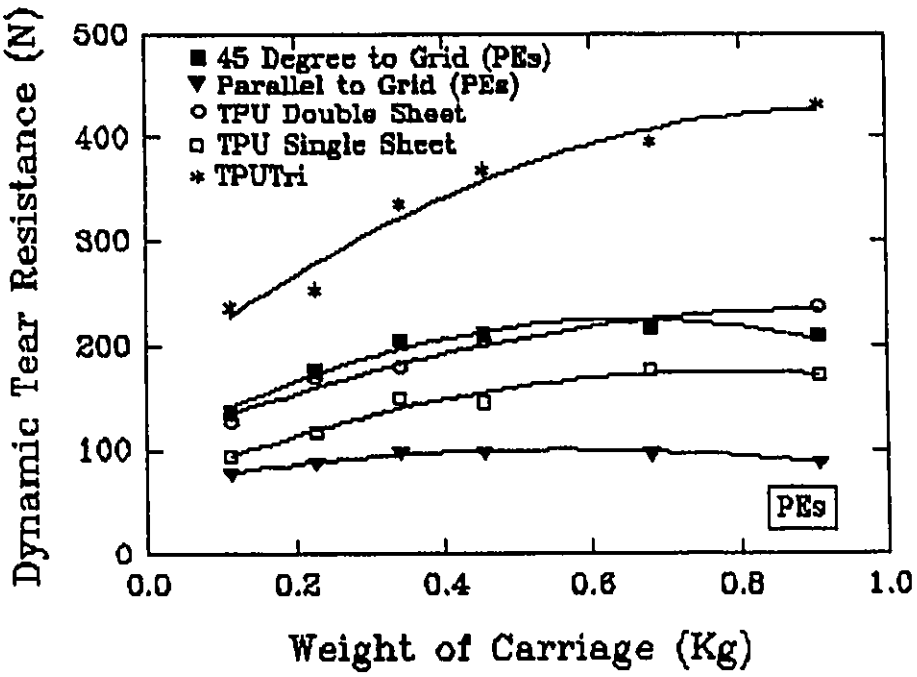

Fig. 5-10. Dynamic tear resistance of polyester scrim (PEs) coated with TPU, compared with unreinforced TPU elastomer sheets and TPU elastomer sheet reinforced with TPU-rod.

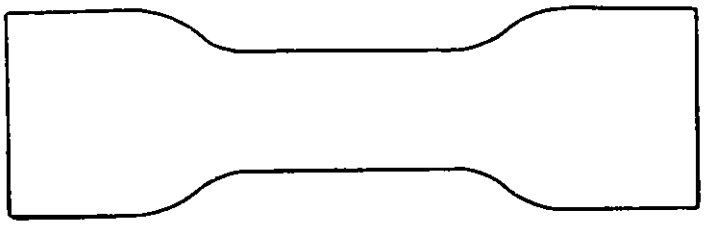

Fig. 6-1. Profile of the tensile test specimens. The gage length is 102 mm, the gage width is 45 mm, and the overall length is 277 mm.

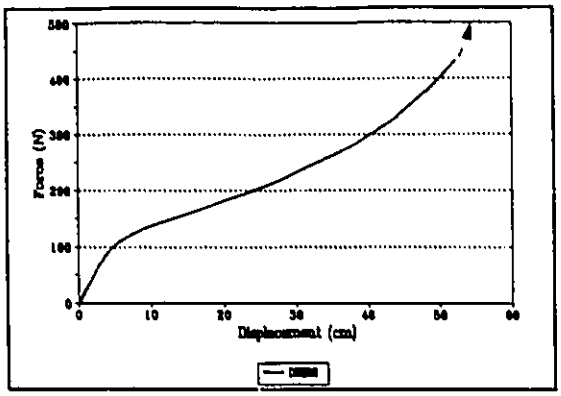

(a) Thermoformed double-sheet

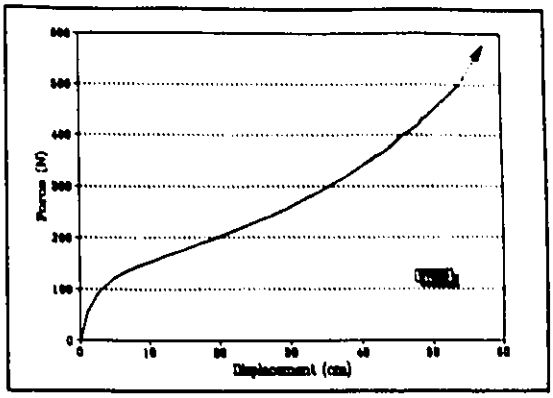

(b) Square

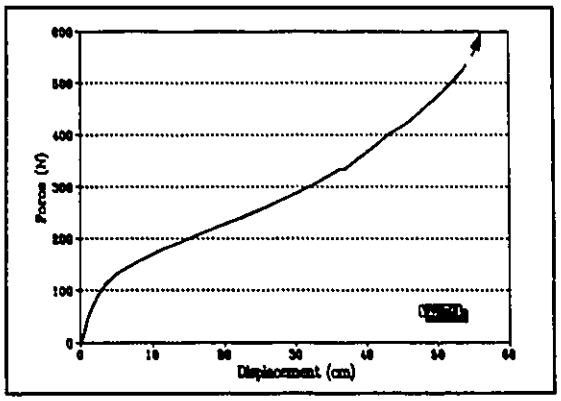

(c) Diamond

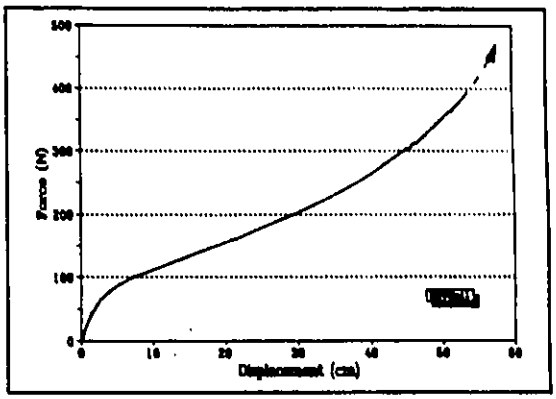

(d) Diamond loaded transversely

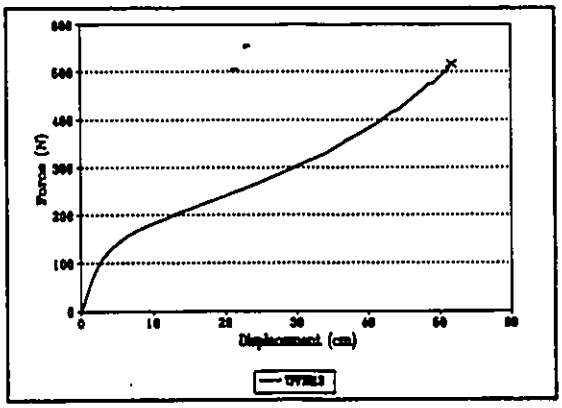

(e) Triangle

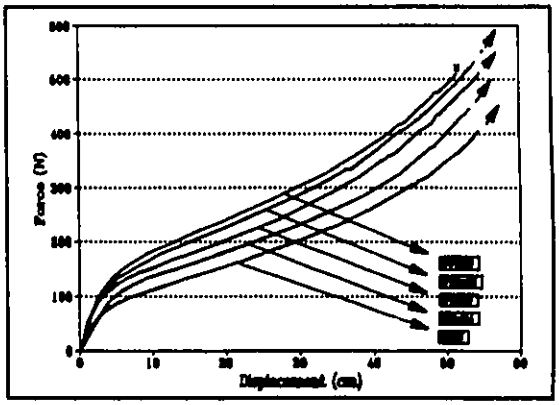

(f) Comparisonof test results

Fig. 6-2. The uniaxial tension deformation behaviour of the unreinforced thermoformed TPU double sheet and the TPU sheets reinforced with TPU-rod.

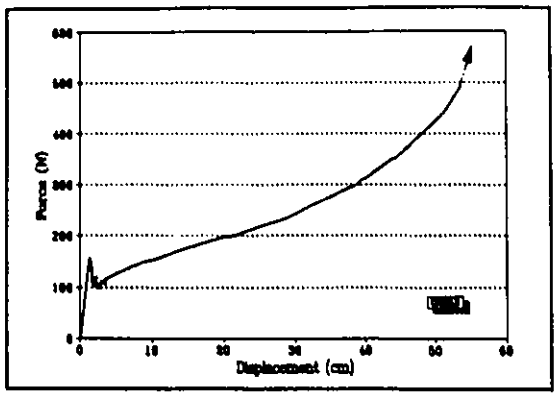

(a) Diamond

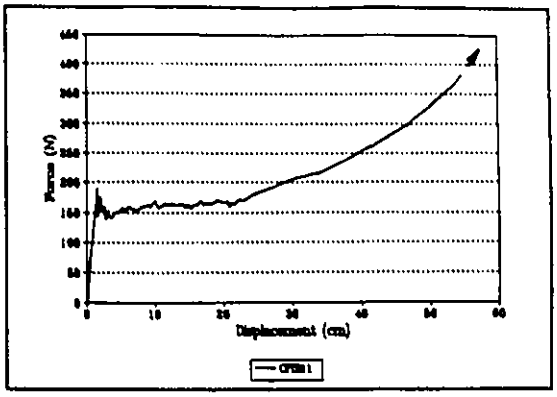

(b) Triangle

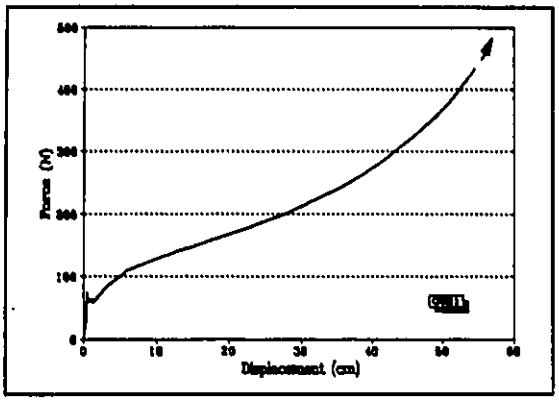

(c) Square

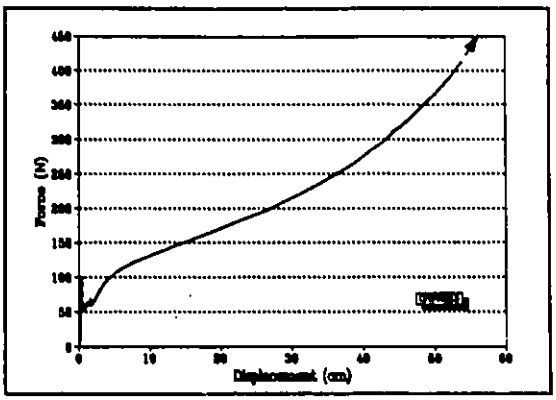

(d) Alternating carbon fiber and TPU Squares

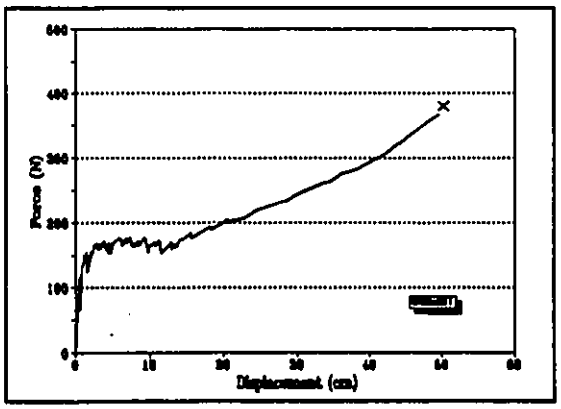

(e) Ladder Diamond loaded Laterally

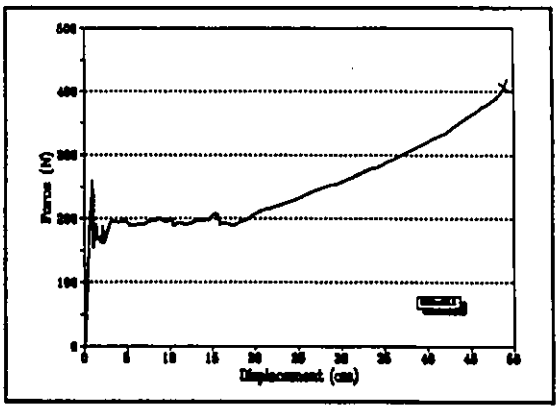

(f) Ladder Diamond

Fig. 6-3. The uniaxial tension deformation behaviour of the TPU sheets reinforced with 1K carbon fibers in various patterns.

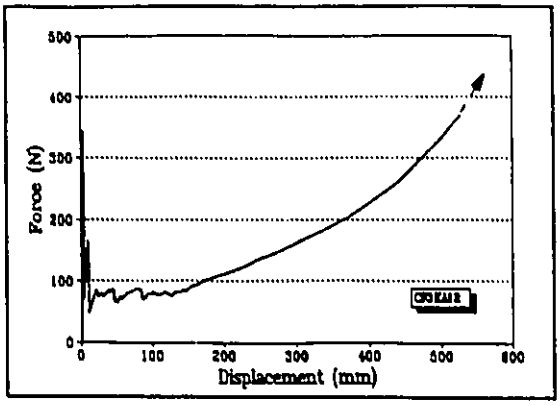

(a) Square

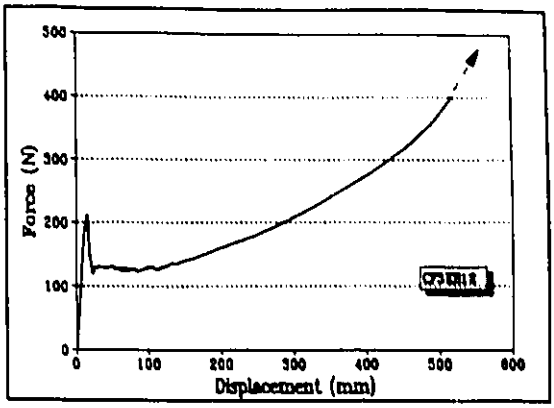

(b) Diamond

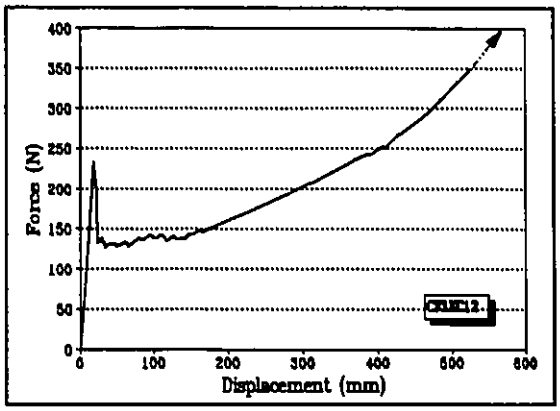

(c) Triangle

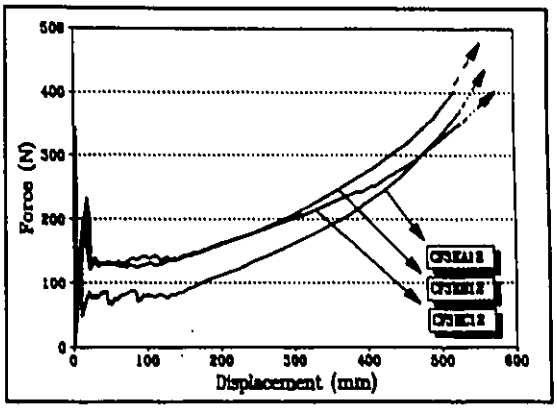

(d) Comparison of three patterns

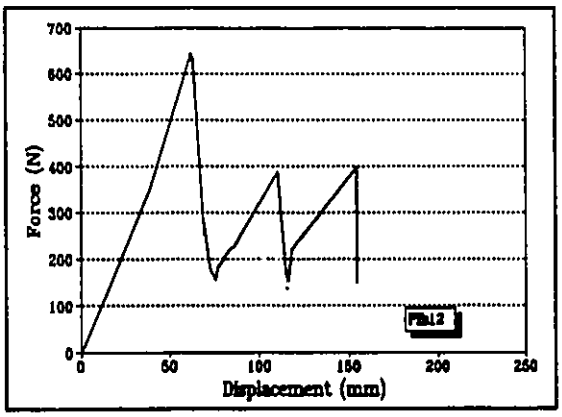

(e) Reinforced with polyester scrim

Fig. 6-4. The uniaxial tension behaviour of the TPU sheets reinforced with 3K carbon fibers and polyester scrim in various patterns.

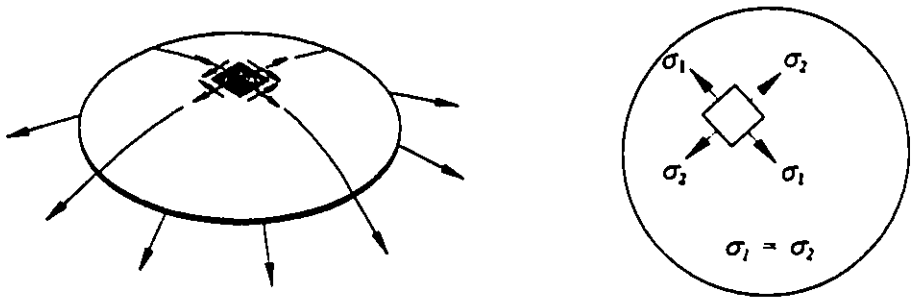

Fig. 7-1. Stress state for a thin sheet in a bulge test.

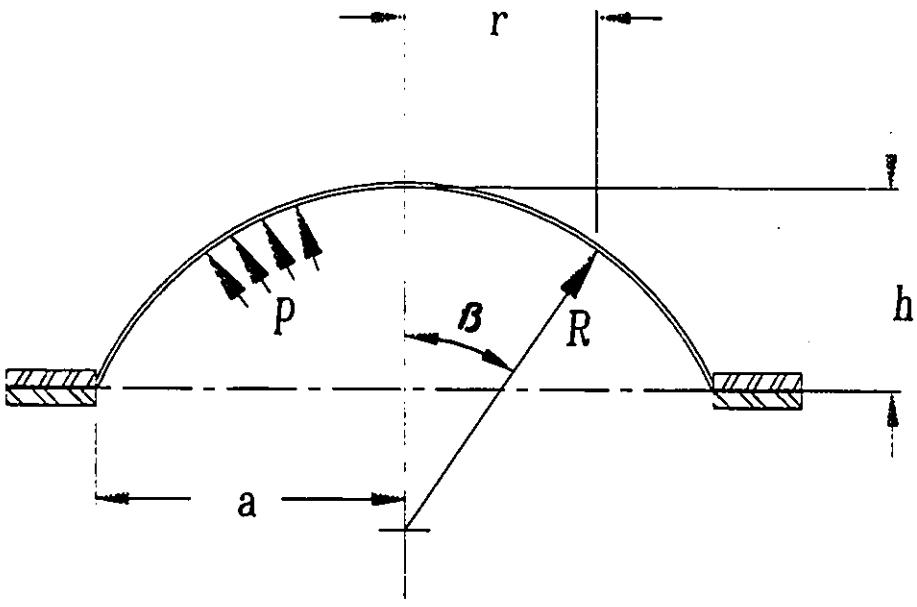

Fig. 7-2. Geometry of a bulging specimen.

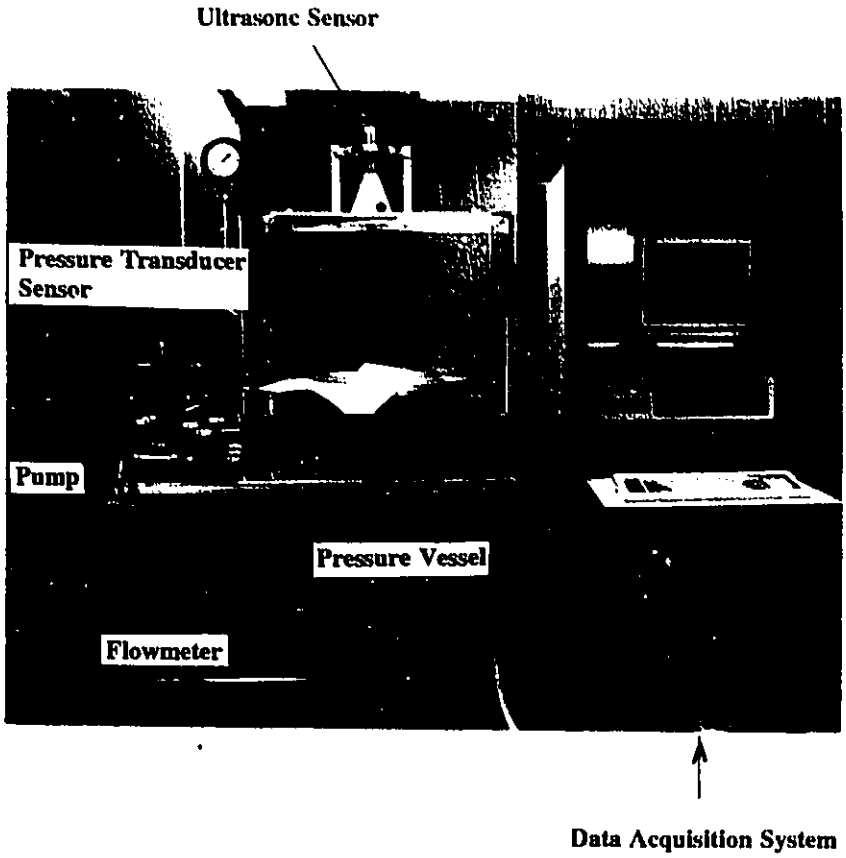

Fig. 7-3. The hydraulic bulge testing apparatus.

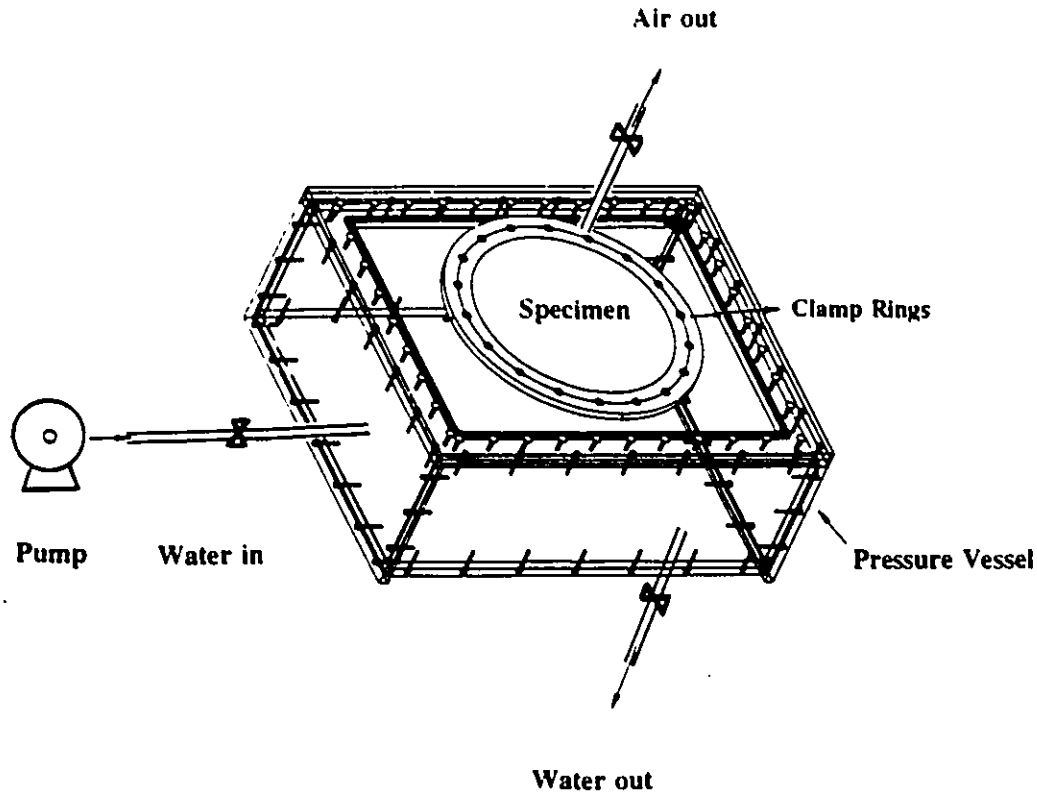

Fig. 7-4. Pressure chamber

Fig. 7-5. The sequences of the profiles of the unreinforced and reinforced TPU sheets in a bulge testing process: (a) TPU single sheet; (b) reinforced with the 3K carbon fiber in triangle pattern [TR]; (c) reinforced with TPU-rod in square [SQ], diamond [Dm], and triangle patterns; (d) reinforced with the 1K carbon fiber in diamond and triangle patterns.

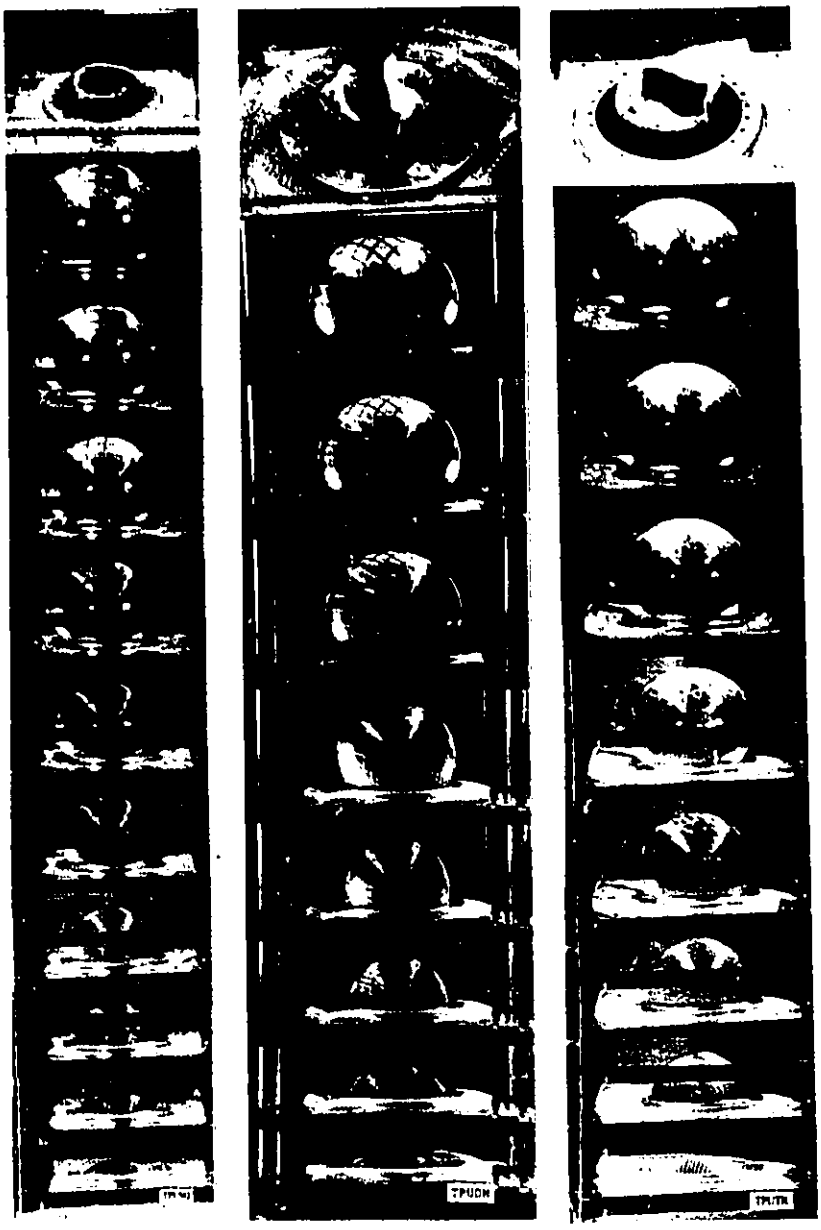

c

Fig. 7-5. Continued (I).

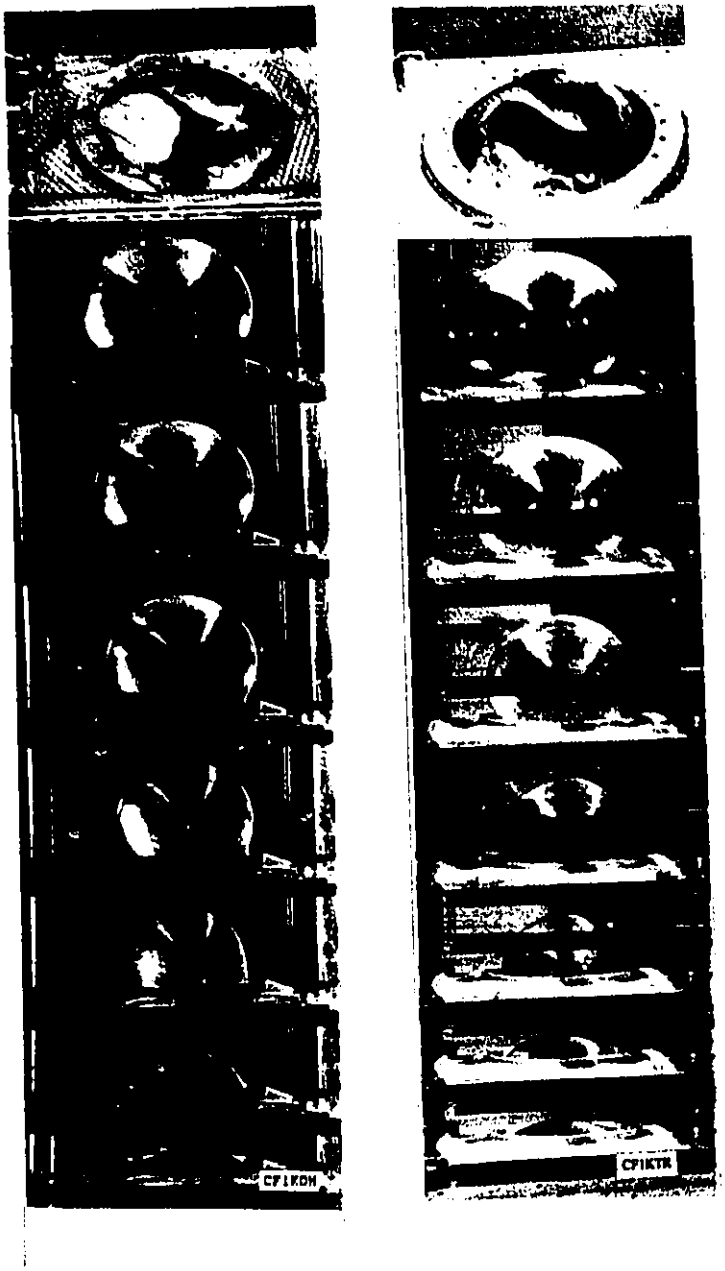

d

Fig. 7-5. Continued (II).

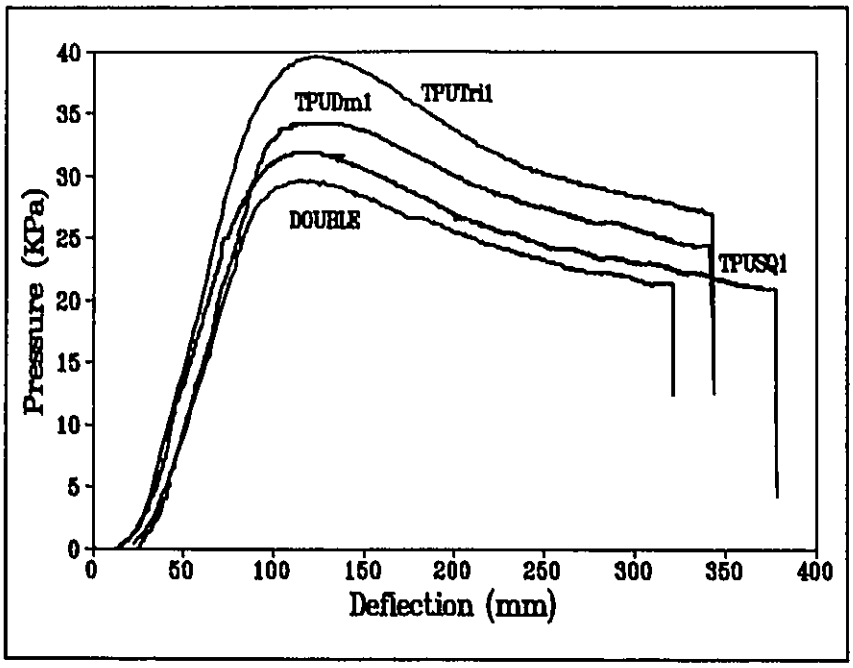

Fig. 7-6. Bulge test results of the TPU elastomer sheets reinforced with TPU-rod in different web patterns (SQ: square pattern; Dm: diamond pattern; Tri: triangle pattern; Double: thermoformed unreinforced TPU double sheet).

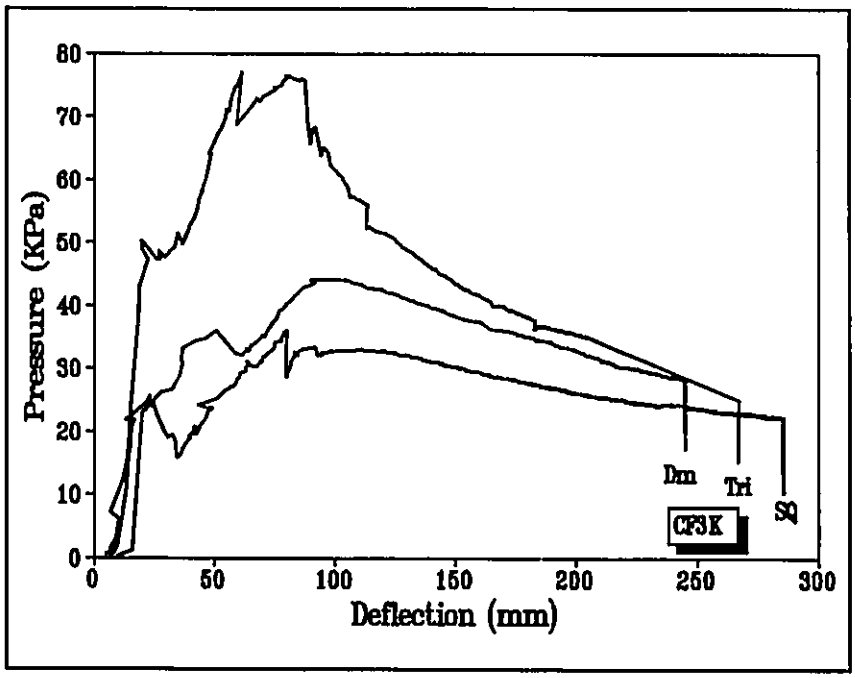

Fig. 7-7. Bulge test results of the TPU elastomer sheets reinforced with 3K carbon fibers in different web patterns (SQ: square pattern; Dm: diamond pattern; Tri: triangle pattern; double: thermoformed unreinforced TPU double sheet).

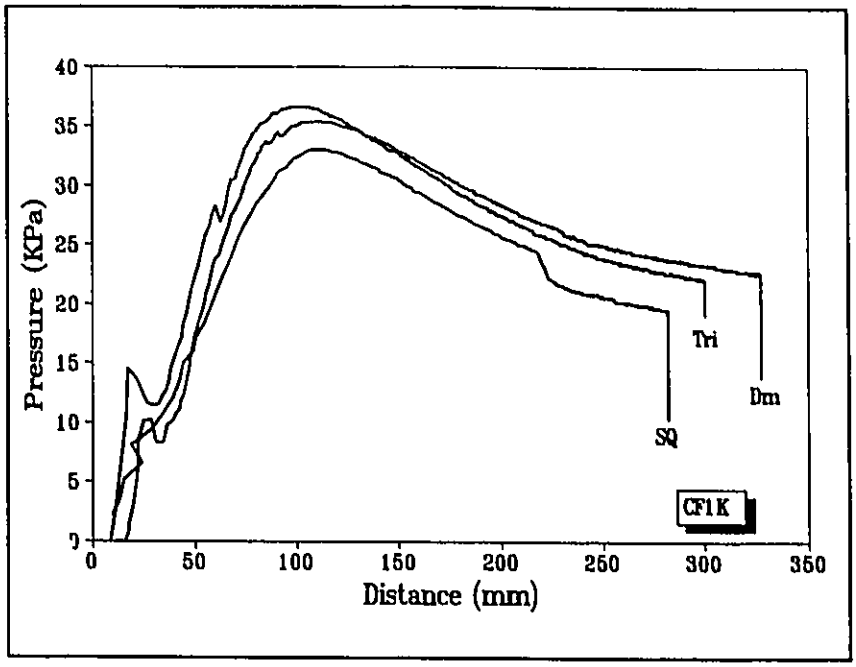

Fig. 7-8. Bulge test results of the TPU elastomer sheets reinforced with 1K carbon fibers in different web patterns (SQ: square pattern; Dm: diamond pattern; Tri: triangle pattern; Double: thermoformed unreinforced TPU double sheet)

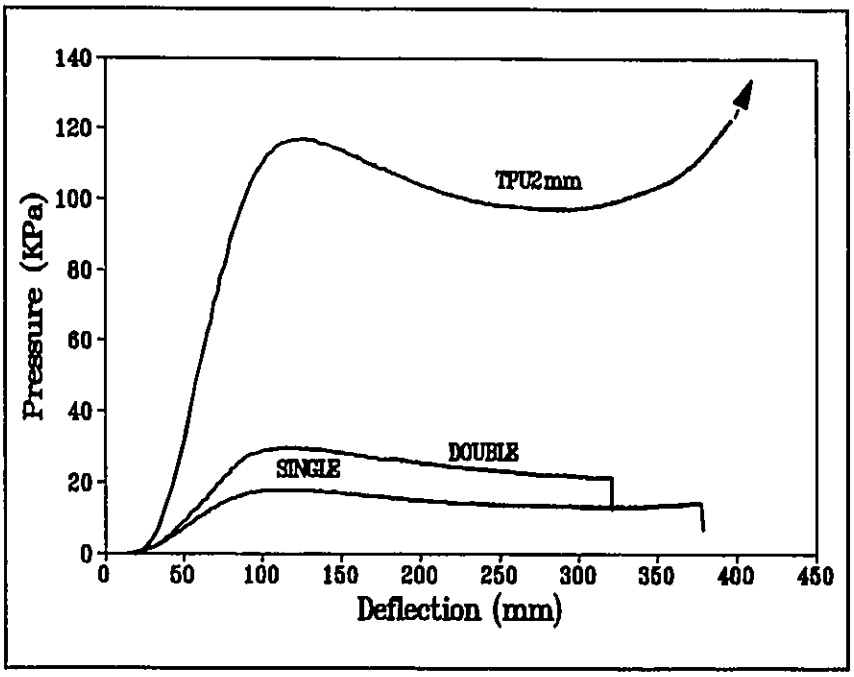

Fig. 7-9. The effect of the thickness of unreinforced TPU sheet on the burst strength.

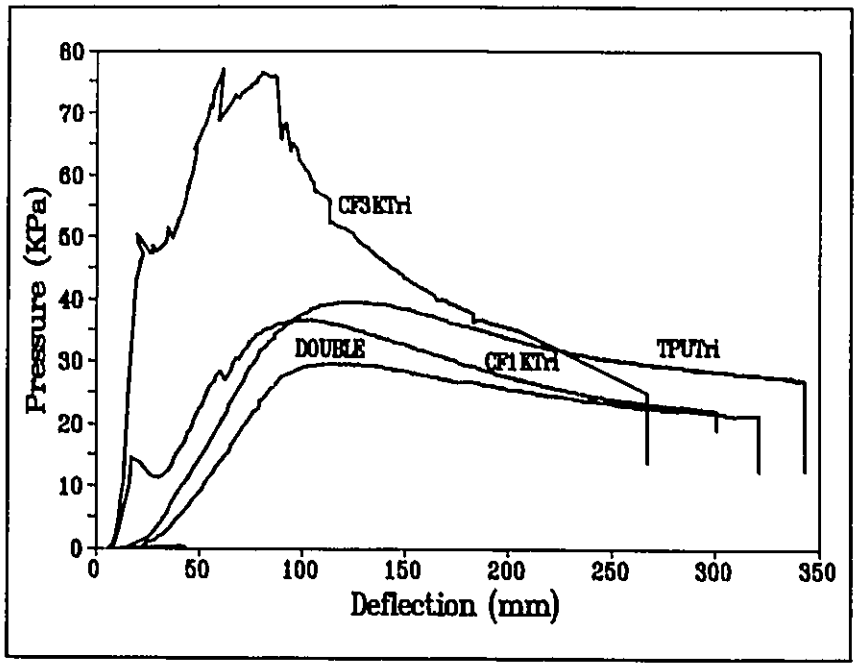

Fig. 7-10. Comparison of bulge test results of flexible TPU elastomer sheets sparsely reinforced with different reinforcements in the triangle pattern (Double: thermoformed unreinforced TPU double sheet; CF: carbon fiber).

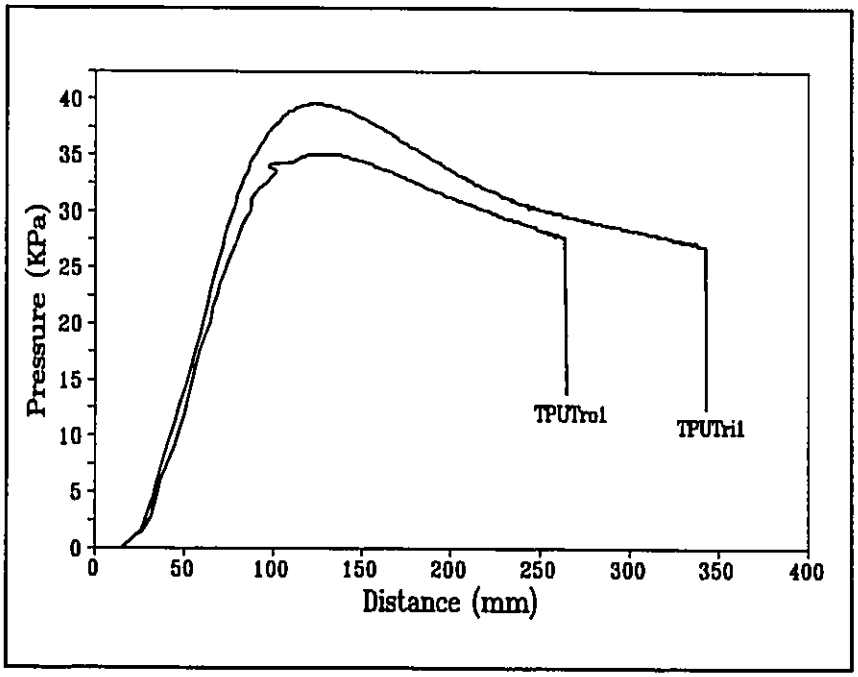

Fig. 7-11. Bulge results of the TPU elastomer sheets reinforced with solid or hollow TPU-rod.

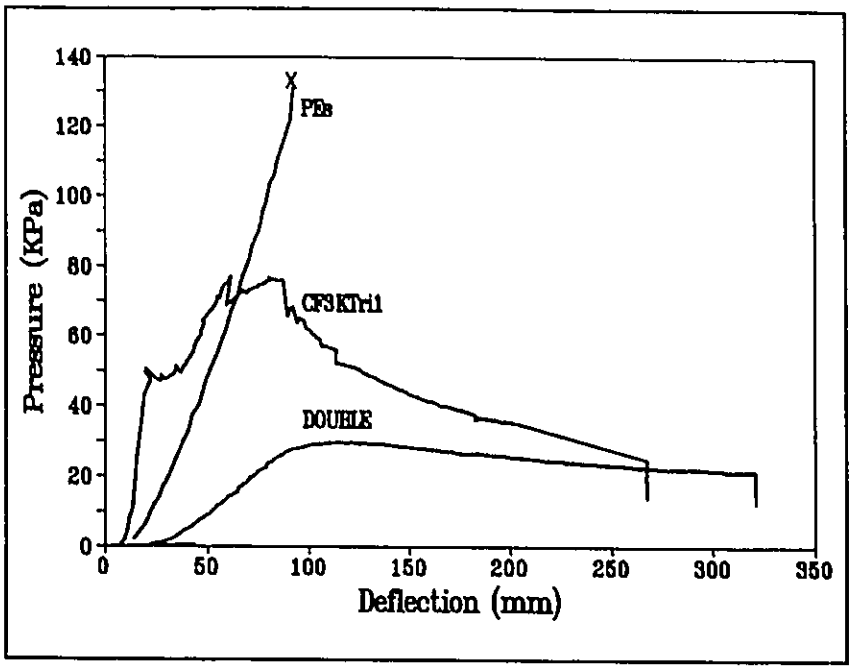

Fig. 7-12. Comparison of the bulge test results of commercial polyester scrim (PEs) for flexible TPU elastomer sheet reinforced with 3K carbon fiber in the triangle pattern.

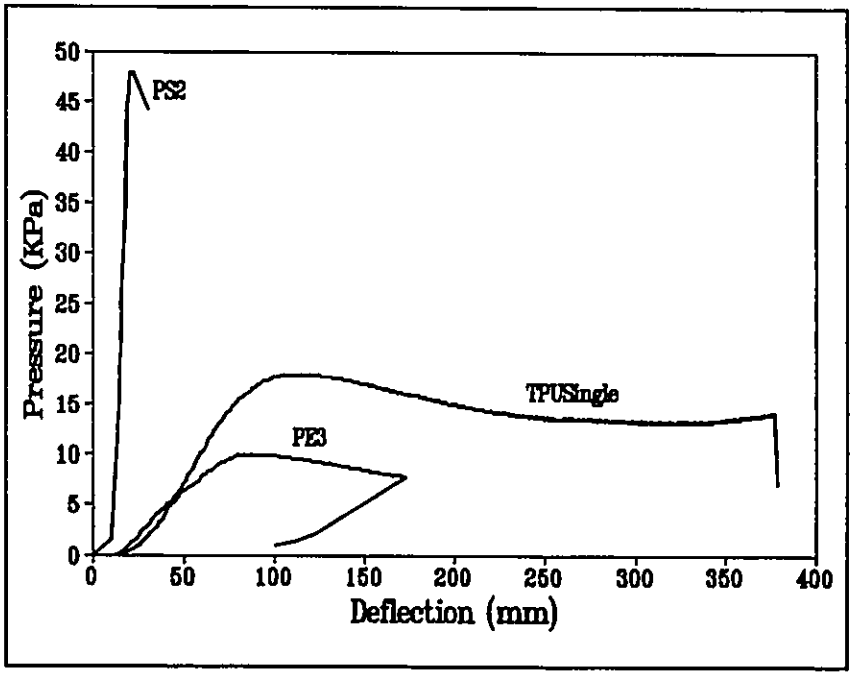

Fig. 7-13. Bulge test results of high impact polystyrene (PS), TPU single sheet and polyethylene film (PE).

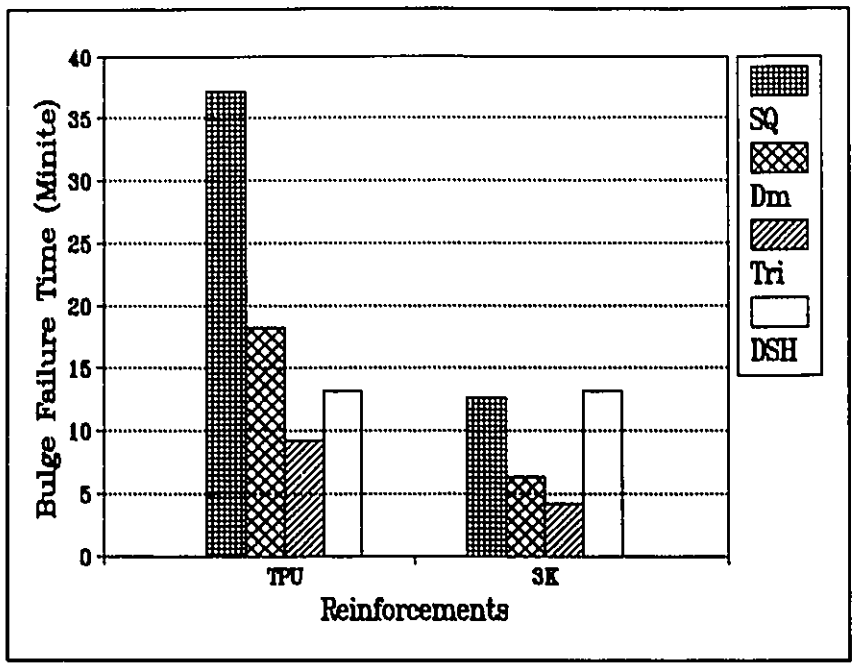

(a)

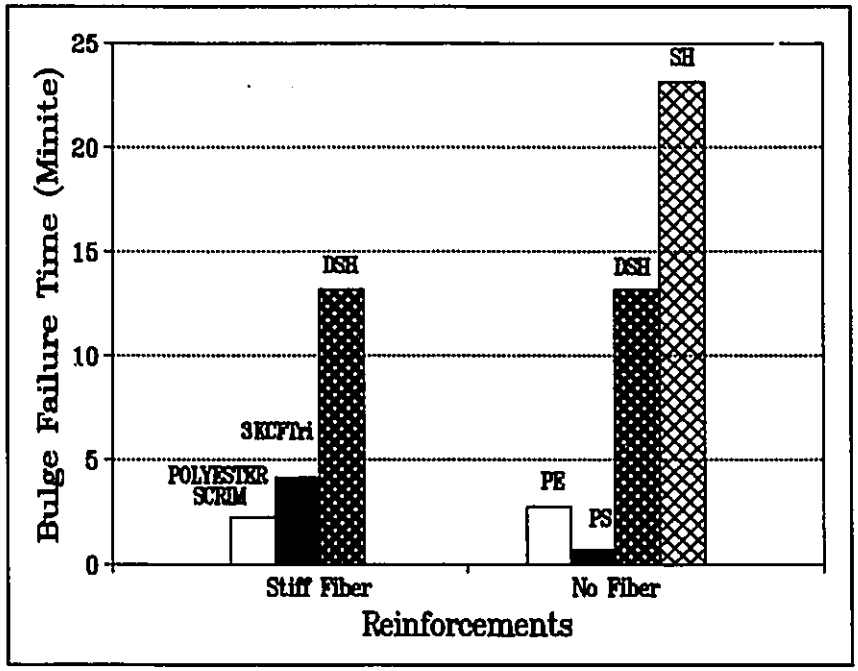

(b)

Fig. 7-14. Comparison of bulging failure time with different materials; (a) sparsely reinforced TPU sheets (b) different materials; (SQ: square pattern; Dm: diamond pattern; Tri: triangle pattern; SH: TPU single sheet; DSH: thermoformed unreinforced TPU double sheet).

Fig. 7-15. Fractured specimens from the bulge tests.

(a)

(b)

Fig. 7-16. The microstructure of the TPU single sheet: (a) before bulge test; (b) after bulge test. Optical micrograph. Magnification 100X.

Fig. 7-17. The ultrasonic microscopy image of high impact PS after bulge test. Magnification 60X.

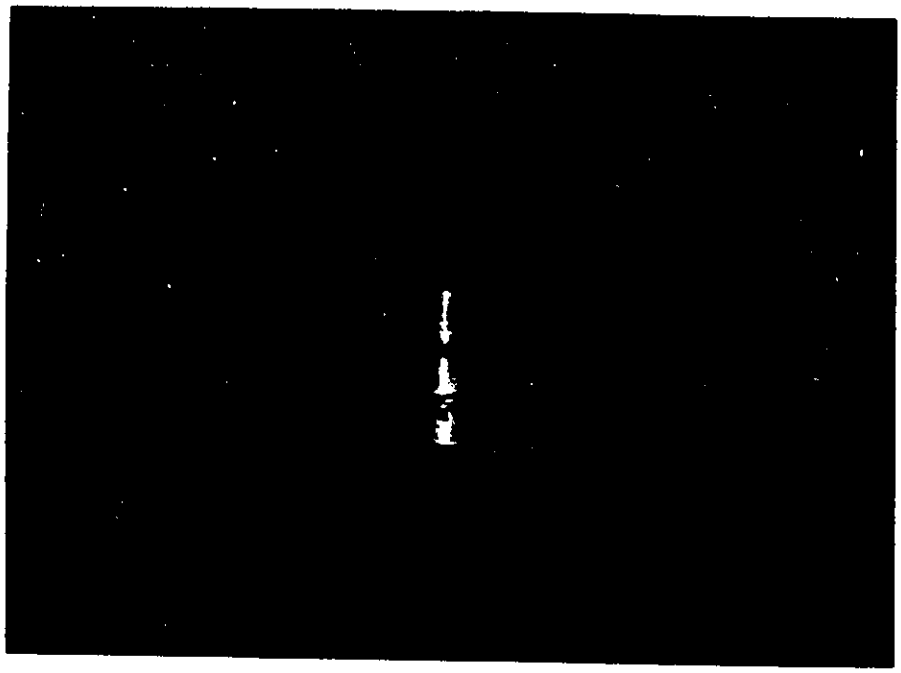

Fig. 8-1. The specimen clamping fixture for slow rate penetration tests.

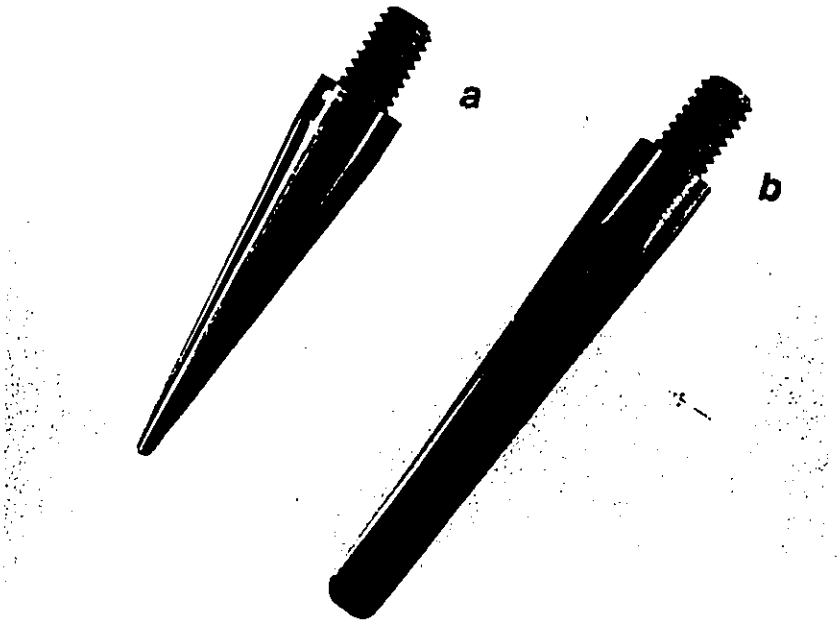

Fig. 8-2. Two types of penetration probes; (a) a relatively sharp pointed indentor; (b) a screwdriver-like indentor.

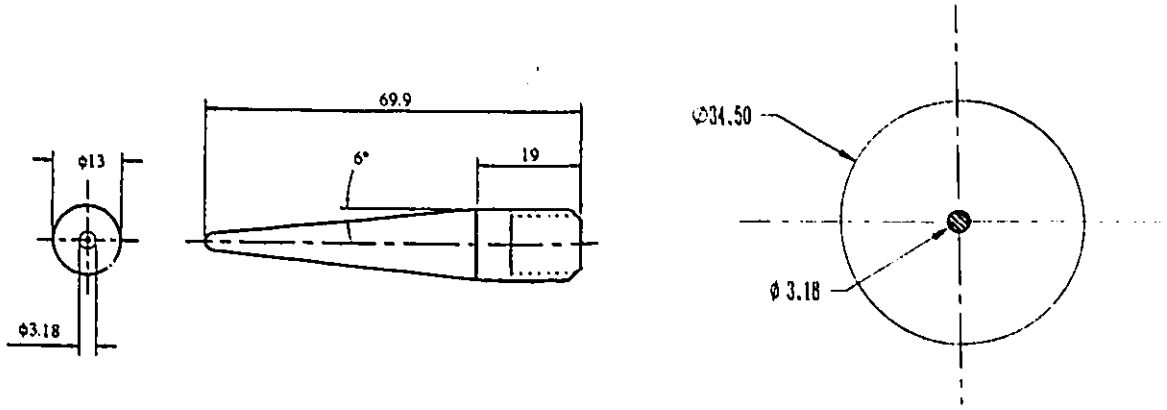

Fig. 8-3. (a) The shape of the indentor; (b) The outer circle is the inner edge of the clamping ring, the inner circle is the area of the tip of the indentor at the end of the cone.

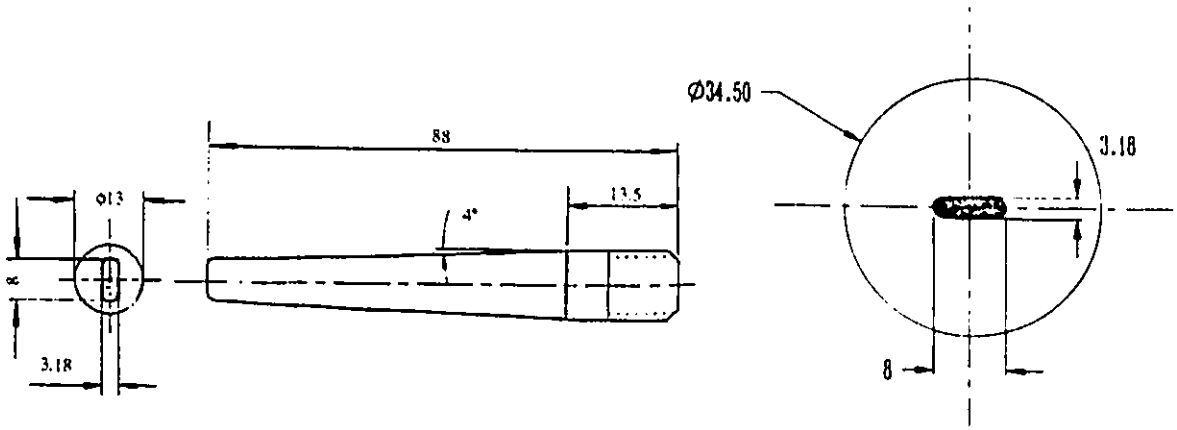

Fig. 8-4. (a) The shape of the dull-edge indentor; (b) The outer circle is the inner edge of the clamping ring, the inner area is the tip of the indentor at the end of the dull-edge.

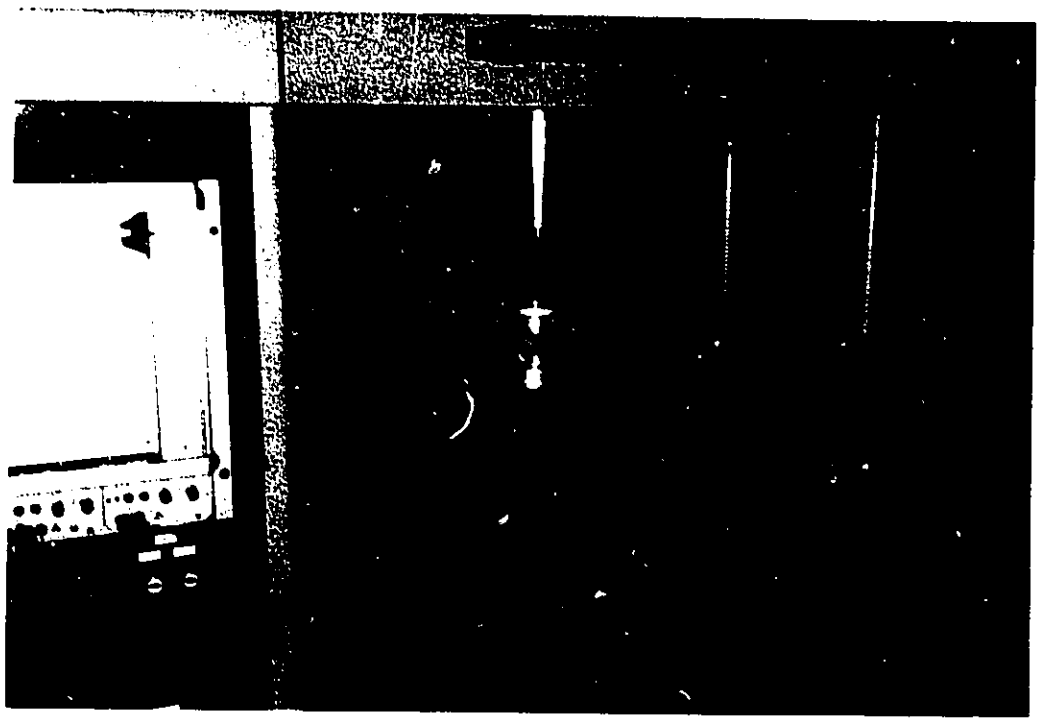

Fig. 8-5. The penetration testing apparatus.

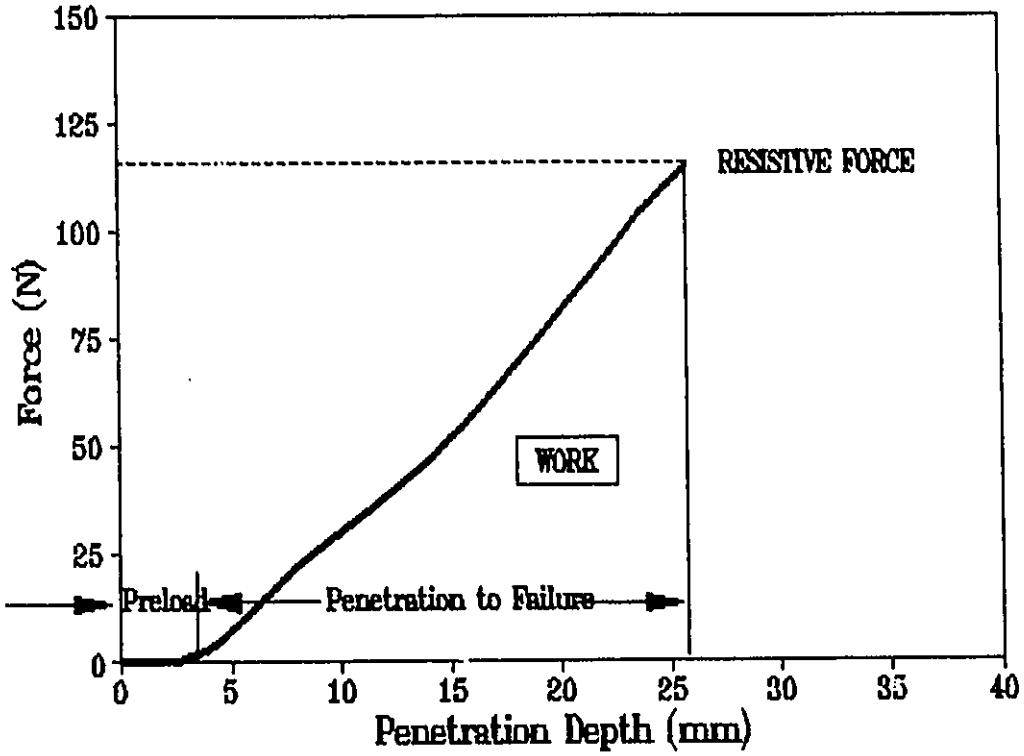

Fig. 8-6. The characteristic curves of the slow rate penetration test.

(a)

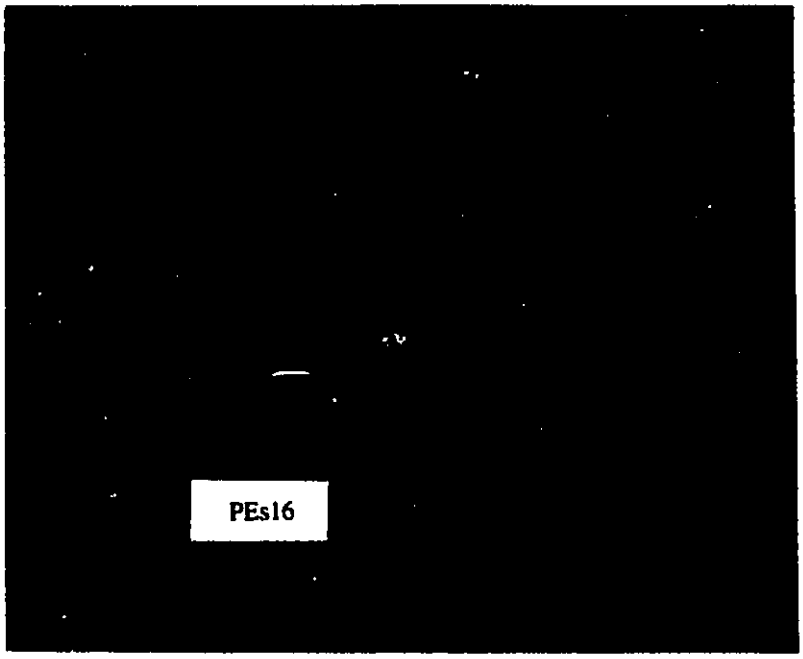

(b)

Fig. 8-7. Photographs of failure TPU elastomer sheets after slow rate tests. (a) unreinforced thermoformed TPU double sheet; (b) polyester scrim coated with TPU; (c) reinforced with carbon fiber in diamond and triangle patterns; (d) reinforced with TPU-rod in diamond and triangle patterns.

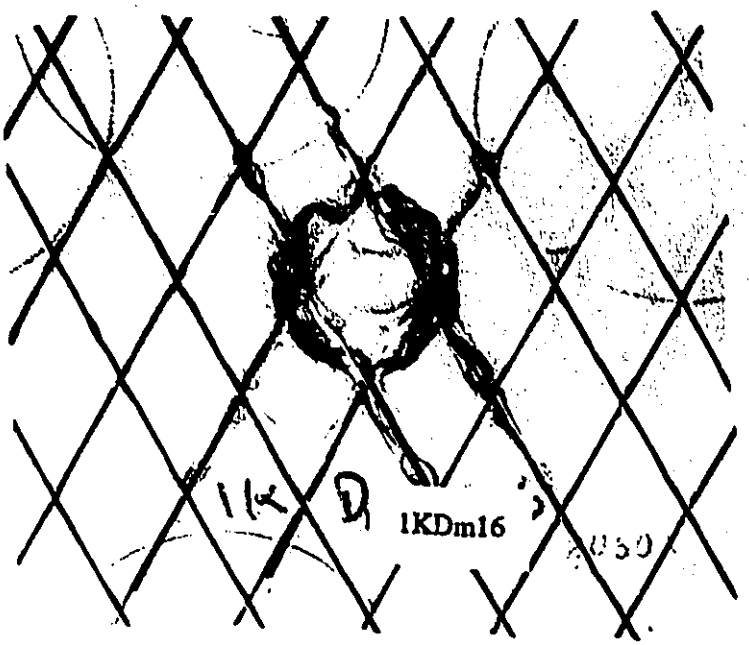

(c-1)

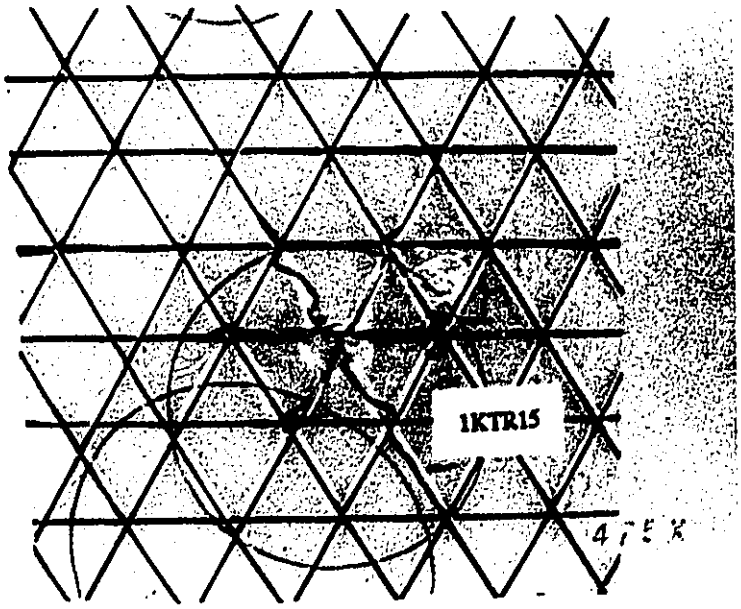

(c-2)

Fig. 8-7. Continued (I).

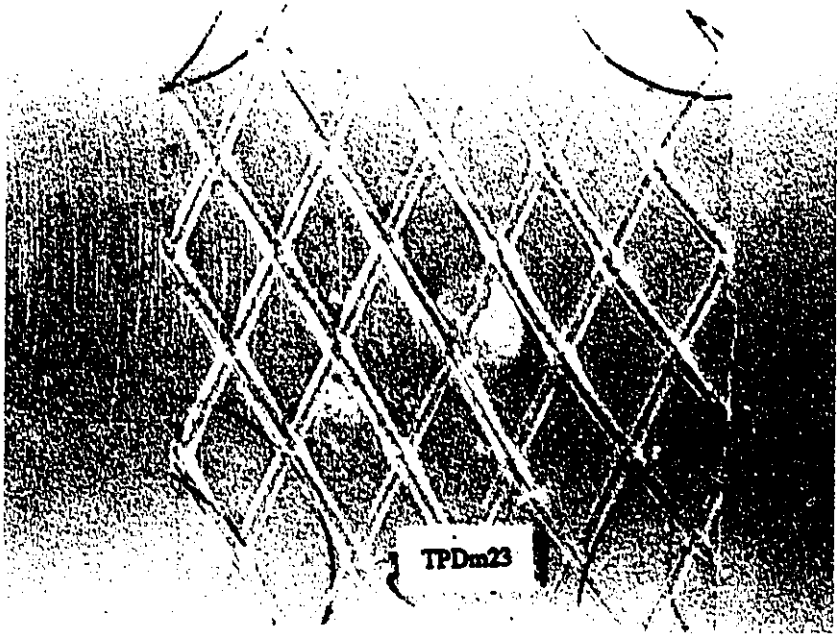

(d-1)

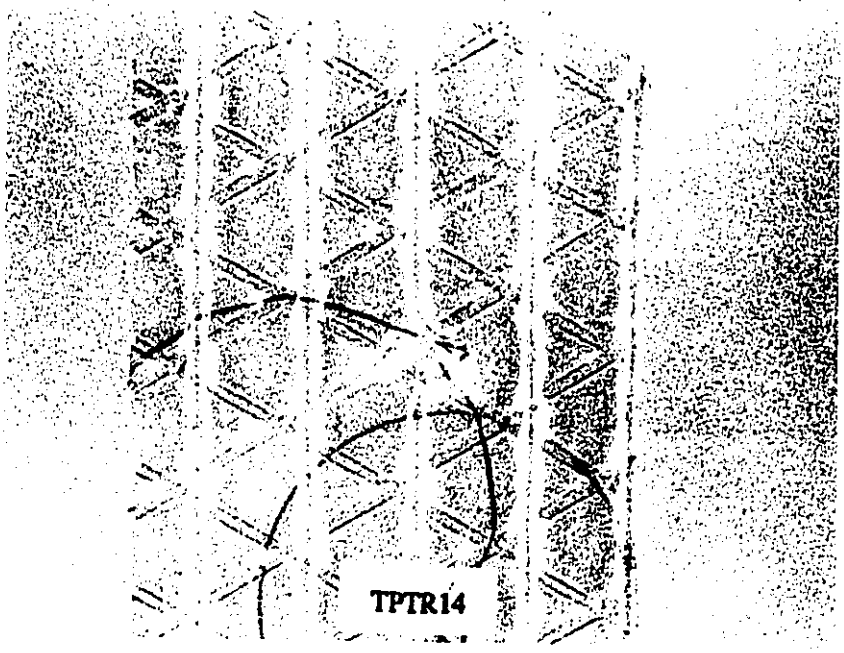

(d-2)

Fig. 8-7. Continued (II).

SIGNIFICANT CONTRIBUTIONS OF THIS RESEARCH

In the course of this research, the author of this disseration has done the following unique work:

1). Designed and made a productive special thermoforming process for developing continuous fiber reinforced elastomer sheet.

2). Developed a new type of reinforced polymer composite: sparsely reinforced elastomer sheet.

3). Examined the deformation behaviour of the sparsely reinforced elastomer sheets by the means of tensile tests, tear tests, snagging tests, puncture tests, and the bulge tests.

PUBLICATIONS RELATED TO THIS WORK

1. D. F. Watt and R. Pan, "Use of Fail-safe Elastomer Liners in Liquid Hauling", ***PPR'95*** International Conference Proceddings, Oct. 31 - Nov. 3, Toronto, Canada, p. 289-298, 1995.

2. R. Pan and D. F. Watt, "Biaxial Tension Deformation Behaviour of Sparsely Reinforced Elastomer Sheets", paper accepted by ***Plastics, Rubber & Composite Proccssing and Application***, Oct., 1995.

3. R. Pan and D. F. Watt, "Snagging Resistance of Sparsely Reinforced Elastomer Sheets", paper submitted to ***Polymer Composites***, June, 1995.

4. R. Pan and D. F. Watt, "Tear Resistance of Sparsely Reinforced Elastomer Sheets", paper accepted by ***Polymer Composites***, May, 1995.

5. R. Pan and D. F. Watt, "Use of Flexible Reinforcement in Elastomers", ***SPE ANTEC Tech Papers, 1995***, Boston, p. 4078-4082, 1995.

6. D. F. Watt and R. Pan, "Fail-Safe Liquid Containment Materials", ***ASM/ESD 10th Advanced Composites Conference***, Detroit, Nov. 7-10, p. 31-40, 1994.

7. D. F. Watt and R. Pan, "Development of Sparsely Reinforced Elastomer Sheet", ***SPE ANTEC Tech. Papers, 1994***, San Francisco, p. 860-864, 1994.

VITA AUCTORIS

The author was born in August, 1957, Beijing, China. She received her B.A.Sc in Engineering Materials from East China University of Chemical Technology, Shanghai, China, in 1982. After working more than seven years as a research engineer on the engineering materials in Shanghai Research Institute of Building Sciences, China, she then came to Windsor, Canada, and started her Masters in Engineering Materials program, Department of Mechanical Engineering at the University of Windsor, Ontario, Canada, in 1989. She received her M.A.Sc. degree in Engineering Materials in Fall, 1991. She continued to pursue her academic career in the Department of Mechanical and Materials Engineering, University of Windsor as a Ph. D. candidate in Fall, 1991 - Fall, 1995. She received her Ph.D. degree at University of Windsor on Dec. 1, 1995.